Brigham Young University
BYU ScholarsArchive

Theses and Dissertations

2009-03-20

Functionalization, Characterization, and Applications of Diamond Particles, Modification of Planar Silicon, and Chemoetrics Analysis of MS Data

Li Yang
Brigham Young University - Provo

Follow this and additional works at: https://scholarsarchive.byu.edu/etd

Part of the Biochemistry Commons, and the Chemistry Commons

BYU ScholarsArchive Citation
Yang, Li, "Functionalization, Characterization, and Applications of Diamond Particles, Modification of Planar Silicon, and Chemoetrics Analysis of MS Data" (2009). *Theses and Dissertations*. 1716.
https://scholarsarchive.byu.edu/etd/1716

This Dissertation is brought to you for free and open access by BYU ScholarsArchive. It has been accepted for inclusion in Theses and Dissertations by an authorized administrator of BYU ScholarsArchive. For more information, please contact scholarsarchive@byu.edu, ellen_amatangelo@byu.edu.

www.manaraa.com

FUNCTIONALIZATION, CHARACTERIZATION, AND APPLICATIONS OF DIAMOND PARTICLES, MODIFICATION OF PLANAR SILICON, AND CHEMOMETRICS ANALYSIS OF MASS SPECTROMETRY DATA

by

Li Yang

A dissertation submitted to the faculty of

Brigham Young University

In partial fulfillment of the requirements for the degree of

Doctor of Philosophy

Department of Chemistry and Biochemistry

Brigham Young University

April 2009

المنارة للاستشارات

www.manaraa.com

BRIGHAM YOUNG UNIVERSITY

GRADUATE COMMITTEE APPROVAL

of a dissertation submitted by

Li Yang

This dissertation has been read by each member of the following graduate committee and by majority vote has been found to be satisfactory.

Date	Matthew R. Linford, Chair
Date	Milton L. Lee
Date	Paul B. Fansworth
Date	Robert C. Davis
Date	Eric T. Sevy

المنارة للاستشارات
www.manaraa.com

BRIGHAM YOUNG UNIVERSITY

As chair of the candidate's graduate committee, I have read the dissertation of Li Yang in its final form and have found that (1) its format, citations and bibliographical style are consistent and acceptable and fulfill university and department style requirements; (2) its illustrative materials including figures, tables, and charts are in place; and (3) the final manuscript is satisfactory to the graduate committee and is ready for submission on to the university library.

Date

Matthew R. Linford
Chair, Graduate Committee

Accepted for the Department

David V. Dearden
Graduate Coordinator

Accepted for the College

Thomas W. Sederberg
Associate Dean, College of Physical and Mathematical Science

المنارة للاستشارات
www.manaraa.com

ABSTRACT

FUNCTIONALIZATION, CHARACTERIZATION, AND APPLICATIONS OF DIAMOND PARTICLES, MODIFICATION OF PLANAR SILICON, AND CHEMOMETRICS ANALYSIS OF MASS SPECTROMETRY DATA

Li Yang

Department of Chemistry and Biochemistry

Doctor of Philosophy

In spite of the stablility (lack of reactivity) of diamond powder, I have developed a method for tethering alkyl chains and polymers to deuterium/hydrogen-terminated diamond. One method is through ether linkages via thermolysis of di-*tert*-amyl peroxide (DTAP). This reaction with DTAP has also been applied to grow polymers on the diamond surface. The other method is atom transfer radical polymerization (ATRP), which was applied to grow polystyrene at the surface of diamond. Both polystyrene-modified diamond and sulfonated polystyrene-modified diamond can be prepared by either method, and can be used for solid phase extraction. Diamond stationary phases are stable under basic conditions, which is not the case for silica-based stationary phases. Surface characterization was performed by X-ray photoelectron spectroscopy (XPS), time-of-flight secondary ion mass spectrometry (ToF-SIMS) and diffuse reflectance Fourier transform infrared spectroscopy (DRIFT).

المنارة للاستشارات

www.manaraa.com

While the main focus of my graduate research has been the surface modification of diamond, I also describe other projects on which I have worked. The use of radical-based processes for modifying diamond is related to a different radical-based synthesis of monolayers or polymers I performed by scribing silicon (Si_{scr}). After preparation of homogeneous olefin-terminated monolayers on scribed silicon made from 1,9-decadiene and chemisorption of Grubbs' catalyst, ring-opening metathesis polymerization (ROMP) of norbornene was demonstrated. These surfaces were characterized by XPS and ToF-SIMS.

I also investigated the extent of PDMS oligomers transfer onto different surfaces with a wide range of hydrophobicities, using an uninked, unpatterned PDMS stamp. The effect of surface free energy on PDMS transfer in microcontact printing was investigated and the relationship between the amount of PDMS in ToF-SIMS spectra and the surface tensions of initial surfaces was revealed. Therefore, PDMS transfer can be applied as a probe of surface free energies using ToF-SIMS, where PDMS preferentially transfers onto more hydrophilic surface features during stamping, with little transfer onto very hydrophobic surface features.

In much of my thesis work, I performed multivariate analysis of my data, especially of my ToF-SIMS data. Such chemometrics methods include principle components analysis (PCA), partial least squares (PLS) cluster analysis, and multivariate curve resolution (MCR). I also applied these tools to analyze electrospray ionization (ESI) mass spectrometry data from a lipidomics study.

المنارة للاستشارات
www.manaraa.com

ACKNOWLEDGEMENTS

The completion of my dissertation and research work was under the guidance of Dr. Matthew R. Linford, the support of graduate committee members, my family and other people. Now I would like to give my sincere appreciation to all of them.

First, I would like to offer my deepest appreciation to my advisor, Dr. Matthew R. Linford, for his guidance, patience, encouragement, and support through these years. I am very grateful to have had the opportunity to work under his supervision. He helped me overcome difficulties in my research and my life.

I also thank my graduate committee members, Dr. Milton L. Lee, Dr. Eric T. Sevy, Dr. Robert C. Davis, and Dr. Paul B. Farnsworth. I sincerely appreciate their instructions, suggestions and revisions to my research and dissertation. I also thank Dr. Steven G. Wood and Dr. Craig D. Thulin for their help and instruction on my tissue analysis project.

I would like to acknowledge all members in our group: Dr. Guilin Jiang, Dr. Yit-Yan Lua, Dr. Michael Lee, Lei Pei, Feng Zhang, Gaurav Sani, David Jensen and Landon Wiest. Thank you all for your friendship and help during my time at BYU.

I would like to give special thanks to my parents and my husband. Their love, support and encouragement were great motivation in my Ph.D. studies.

Finally, I would thank the Department of Chemistry and Biochemistry at Brigham Young University for providing me the opportunity and financial support for my graduate study. Financial support from US Synthetic is also gratefully acknowledged.

المنارة للاستشارات

www.manaraa.com

TABLE OF CONTENTS

PART I Diamond Functionalization and Its Applications 1
Chapter 1 Functionalization of Deuterium- and Hydrogen-Terminated Diamond with Mono- and Multilayers of Di-*tert*-Amyl Peroxide 1
1.1 Abstract 1
1.2 Introduction 2
1.3 Experimental Section 5
1.3.1 Reagents 5
1.3.2 Preparation of Hydrogen-/Deuterium-Terminated Diamond Powder 6
1.3.3 Treatment of Hydrogen-/Deuterium-Terminated Diamond Powder with Di-tert-Amyl Peroxide 6
1.3.4 Multilayers on Deuterium-Terminated Diamond Powder Made with Di-tert-amyl Peroxide 7
1.3.5 Characterization of the Diamond Surfaces 7
1.4 Results and Discussion 8
1.5 Conclusions 16
1.6 References 19
Chapter 2 Direct Polymer Attachment on Hydrogen/Deuterium-Terminated Diamond Particles 22
2.1 Abstract 22
2.2 Introduction 22
2.3 Experimental 25
2.3.1 Reagents 25
2.3.2 Surface Modification and Characterization 25
2.4 Results 27
2.4.1 Reaction of DTD with DTAP and Unsaturated Monomers with and without a Crosslinker 27
2.4.2. Sulfonation of Polystyrene-Functionalized Diamond Powder 32
2.5 Conclusions 35
2.6 References 35
Chapter 3 Direct Polymer Attachment and Growth on Hydrogen-Terminated Diamond Substrates with Atom Transfer Radical Polymerization (ATRP) 38
3.1 Abstract 38
3.2 Introduction 38
3.3 Experimental Section 40
3.3.1 Reagents 40
3.3.2 Surface Modification 40
3.4 Results and Discussion 43
3.4.1 Overview of Atom Transfer Radical Polymerization (ATRP) on Diamond Followed by Sulfonation 43
3.4.2 Immobilization of the ATRP Initiator on the Diamond Powder Surfaces 46
3.4.3 Polymerization on the Diamond Surface by ATRP 50
3.4.4 Sulfonation of Polystyrene Functionalized Diamond Powder 54
3.5 Conclusions 54
3.6 References 56

المنارة للاستشارات
www.manaraa.com

Chapter 4 Phenyl and Sulfonic Acid Stationary Phases on Diamond Substrates for Solid Phase Extraction 58
4.1 Abstract 58
4.2 Introduction 58
4.3 Experimental Section 60
4.3.1 Reagents 60
4.3.2 Stability Test 60
4.3.3 Solid Phase Extraction (SPE) 61
4.4 Results 64
4.4.1 Solid Phase Extraction with Polystyrene-Modified and Sulfonated, Polystyrene-Modified Diamond 64
4.4.2 Stability 69
4.4.3 Column Capacity 72
4.4.4 Percent Recovery 75
4.5 Conclusions 76
4.6 References 76
PART II. Silicon Functionalization 78
Chapter 5 The Chemistry of Olefin-Terminated Homogeneous and Mixed Monolayers on Scribed Silicon* 78
5.1 Abstract 78
5.2 Introduction 79
5.3 Experimental Section 80
5.3.1 Chemicals 80
5.3.2 Preparation for Patterning Silicon Surfaces 82
5.3.3 Preparation of Monolayers 82
5.3.4 Reaction with Bromine 82
5.3.5 Reaction with OsO_4 82
5.3.6 Reaction with Dichlorocarbene 83
5.3.7 Reaction with Grubbs' Catalyst 83
5.3.8 Calculation of Reaction Yields 83
5.3.9 Polymerization 85
5.3.10 Instrumentation 85
5.3.11 PCA Analysis of ToF-SIMS Data 86
5.4 Results and Discussion 87
5.4.1 Chemical Verification of Olefin-Termination at the Monolayer Surface 87
5.4.2 Reaction of Olefin-Terminated Monolayers with Grubbs' Catalyst 92
5.4.3 Polymerization 93
5.4.4 Kinetics of Polynorbornene Growth as Studied by XPS and ToF-SIMS 96
5.5 Conclusions 103
5.6 References 105
PART III.PDMS Transfer in Microcontact Printing 108
Chapter 6 Effect of Surface Free Energy on PDMS Transfer in Microcontact Printing, and its Application to ToF-SIMS to Probe Surface Energies* 108
6.1 Abstract 108
6.2 Introduction 109
6.3 Experimental 115

المنارة للاستشارات
www.manaraa.com

6.3.1 Reagents 115
6.3.2 Solid Surfaces 117
6.3.3 Thin Film Preparation 117
6.3.4 Monolayer Preparation 118
6.3.5 Hexadecyl and Dodecyl Monolayer Preparation (for UV Patterning) 118
6.3.6 Surface Patterning with the Microlens Array 119
6.3.7 Surface Patterning with UV Light 119
6.3.8 PDMS Stamp Preparation 120
6.3.9 Surface Stamping 120
6.3.10 Surface Characterization 120
6.3.11 Surface Tension Calculations 121
6.3.12 Multivariate Statistical Analysis of the ToF-SIMS Data 122
6.4 Results 122
6.4.1 Effect of Surface Free Energy on PDMS Transfer 122
6.4.2 PDMS Transfer to Patterned Surfaces and Probing Surface Energies by Imaging ToF-SIMS 134
6.5 Discussion 141
6.6 Conclusions 144
6.7 References 145
PART IV. Chemometrics 148
Chapter 7 Multivariate Analysis of ToF-SIMS Spectra of Monolayers on Scribed Silicon* 148
7.1 Abstract 148
7.2 Introduction 149
7.3 Experimental 153
7.3.1 Time-of-flight secondary ion mass spectrometry 153
7.3.2 Data Processing 153
7.3.3 Material 154
7.4 Results and Discussion 155
7.4.1 PCA of ToF-SIMS of Homologous Series of Aldehydes and Acid Chlorides on Si_{scr} to Determine the Best Preprocessing Method 155
7.4.2 PCA of ToF-SIMS of 66 Adsorbates on Si_{scr} 163
7.5 Conclusions 172
7.6 References 173
Chapter 8 Screening Phosphatidylcholine Biomarkers in Mouse Liver Extracts from a Hypercholesterolemia Study using ESI/MS and Chemometrics* 175
8.1 Abstract 175
8.2 Introduction 176
8.3 Experimental 179
8.3.1 Materials 179
8.3.2 Instrumentation 179
8.3.3 Animals 180
8.3.4 Plasma and Tissue Collection 181
8.3.5 Extraction Procedure 181
8.3.6 Solution Preparation for Tandem MS 181
8.3.7 Data Processing 181

المنارة للاستشارات
www.manaraa.com

8.3.8 A Brief Overview of Chemometrics Data Analysis Methods 183
8.4 Results 186
8.4.1 MS Data Collection 186
8.4.2 Electrospray MS Analysis of Homogenized Mouse Liver Tissues 187
8.4.3 Principal Components Analysis 190
8.4.4 Hierarchical Cluster Analysis (HCA) 192
8.4.5 Examining the PCA Loadings 192
8.4.6 Identifying the Key Peaks in the Loadings Plots 194
8.4.7 Tandem Mass Spectrometry (MS/MS) and a Literature-Based Identification of the Primary Phosphatidylcholine Biomarkers in the Loadings Plot 197
8.4.8 Multivariate Curve Resolution (MCR) 200
8.4.9 Partial Least Squares (PLS) 200
8.5 Discussion 204
8.6 Conclusions 206
8.7 References 207
PART V. Future work 212
Future Work 212
References 213

المنارة للاستشارات
www.manaraa.com

LIST OF TABLES

Table 2.1. Compositions (atom percentage of elements detected by XPS) of the surfaces of diamond powders..... 34
Table 3.1. Compositions (atom percentage of elements detected by XPS) of the surfaces of diamond powders by XPS. 49
Table 3.2. Ratios of areas of the main peaks (C, O, Br and S) to the sum of all areas of peaks in the negative ion ToF-SIMS spectra. 55
Table 4.1. Stability test results: S2p/C1s ratio from XPS of sulfonated polystyrene (PS) diamonds. 71
Table 5.1 Compositions in mole percent of the mixed solutions used to prepare the surfaces in Figure 5.4. 84
Table 5.2. Ten largest peaks from the loadings plots of PC1 from a PCA analysis of positive ion spectra of samples after different reaction times with norbornene. 100
Table 5.3. Ten largest peaks from the loadings plots of PC1 from a PCA analysis of negative ion spectra of samples after different reaction times with norbornene. 102
Table 6.1. Physical properties of various surfaces before and after stamping. 129
Table 7.1. R^2 values for plots of scores on the PC's vs. the number of carbon atoms in the adsorbate. 156
Table 7.2. The largest peaks from the loadings plots from mean centered positive ion, negative ion, and concatenated positive and negative ion spectra from silicon scribed under different aldehydes. 162
Table 7.3. The largest peaks from the loadings plot of mean centered, positive ion spectra from 66 monolayers. 166
Table 8.1. The ten largest peaks from the loading plot of PC1 in Figure 8.5. 196

المنارة للاستشارات
www.manaraa.com

LIST OF FIGURES

Figure 1.1. The structure of di-tert-amyl peroxide: $(CH_3CH_2C(CH_3)_2O)_2$ 4
Figure 1.2. XPS survey spectra of diamond powders: (a) clean, untreated diamond powder (b) deuterium-terminated diamond powder and (c) deuterium-terminated diamond powder treated with di-tert-amyl peroxide for 1 day at 110ºC. 9
Figure 1.3. DRIFT spectroscopy of diamond powders: (a) raw, untreated diamond powder, (b) diamond powder after deuteration, (c) deuterium-terminated diamond powder treated with di-tert-amyl peroxide for 1 day at 130ºC and (d) the IR absorbance spectrum of neat di-tert-amyl peroxide. 10
Figure 1.4. ToF-SIMS negative ion spectra of (a) clean, untreated diamond powder, (b) deuterium-terminated diamond powder (c) deuterium-terminated diamond powder treated with di-tert-amyl peroxide for 1 day at 110ºC. 12
Figure 1.5. DRIFT spectroscopy for deuterium-terminated diamond powder treated with di-tert-amyl peroxide for 1 day at different temperatures and the IR spectrum of neat di-tert-amyl peroxide. 13
Figure 1.6. DRIFT spectroscopy for a) hydrogen-terminated diamond powder, b) hydrogen-terminated diamond powder treated with di-tert-amyl peroxide for 1 day at 130ºC, c) neat di-tert-amyl peroxide. 15
Figure 1.7. DRIFT spectroscopy (C-H and C-O stretching regions) for deuterium-terminated diamond powder treated with di-tert-amyl peroxide for 1 day at 120ºC for different numbers of exposures to fresh DTAP. 17
Figure 1.8. Area of the C-H stretching region by DRIFT spectroscopy for deuterium-terminated diamond powder treated with di-tert-amyl peroxide for 1 day at 120ºC for different numbers of exposures to fresh DTAP. 18
Figure 2.1. A1 and A2: (a) DRIFT spectrum of deuterium-terminated diamond powder, (b) DRIFT spectrum of a control experiment of deuterium-terminated diamond powder reacted with styrene, without di-tert-amyl peroxide, for 1 day at 110ºC, (c) DRIFT spectrum of deuterium-terminated diamond powder reacted with styrene and di-tert-amyl peroxide for 1 day at 110ºC and (d) IR spectrum of polystyrene. B1 and B2: (a) DRIFT spectrum of deuterium-terminated diamond powder, (b) DRIFT spectrum of a control experiment of deuterium-terminated diamond powder reacted with styrene/DVB, without di-tert-amyl peroxide, for 1 day at 110ºC and (c) DRIFT spectrum of deuterium-terminated diamond powder reacted with styrene/DVB and di-tert-amyl peroxide for 1 day at 110ºC and (d) IR spectrum of polystyrene. 29
Figure 2.2. ToF-SIMS positive ion spectra from 0-100 amu and 100-200 amu: (a) deuterium-terminated diamond powder (b) deuterium-terminated diamond powder reacted with styrene and di-tert-amyl peroxide (c) deuterium-terminated diamond powder reacted with styrene, di-tert-amyl peroxide and DVB, and (d) polystyrene thin film spin-coated onto a silicon surface. 31
Figure 2.3. XPS survey spectra of diamond powders: (a) polystyrene-functionalized diamond powder and (b) sulfonated polystyrene/DVB-fuctionalized diamond powder. 33
Figure 3.1. Mechanism of atom transfer radical polymerization (ATRP) on diamond.

المنارة للاستشارات
www.manaraa.com

..... 44
Figure 3.2. Sulfonation of polystyrene-modified diamond powder. 45
Figure 3.3. XPS of diamond powders. a) hydrogen-terminated diamond, b) piranha treated diamond, used as received diamond that had been cleaned, c) hydrogen-terminated diamond reacted with bromine under light, d) piranha treated diamond reacted with isobromide, e) brominated diamond functionalized with polystyrene by ATRP and f) sulfonated polystyrene diamond powder. 47
Figure 3.4. ToF-SIMS negative ion spectra. A: m/z 0-100 and B: m/z 100-200. a) diamond-brominated by photoreaction, b) diamond-brominated by the nucleophilic addition/elimination reaction, c) diamond functionalized with polystyrene by ATRP (on photoreacted/brominated diamond), d) diamond functionalized with polystyrene by ATRP on 2-bromoisobutyryl bromide modified diamond, e) sulfonated, polystyrene-functionalized diamond (on photoreacted/brominated diamond) and f) sulfonated, polystyrene functionalized diamond made by ATRP on 2-bromoisobutyryl bromide modified diamond.... 48
Figure 3.5. ToF-SIMS positive ion spectra. A: m/z 0-100 and B: m/z 100-200. a) diamond-brominated by photoreaction, b) diamond-brominated by nucleophilic addition/elimination reaction, c) polystyrene functionalized diamond made by ATRP on photoreacted Br_2/diamond, d) polystyrene functionalized diamond made by ATRP on 2-bromoisobutyryl bromide reacted diamond, e) sulfonated polystyrene-functionalized diamond (ATRP, photoreaction) and f) sulfonated polystyrene functionalized diamond (ATRP, 2-bromoisobutyryl bromide)..... 51
Figure 3.6. DRIFT-IR of diamond powders: a) infrared spectrum of neat polystyrene, b) hydrogen-terminated diamond, c) piranha-treated diamond, d) polystyrene functionalized diamond obtained by photoreaction and ATRP, e) polystyrene functionalized diamond obtained by reaction with 2-bromoisobutyryl bromide and ATRP, f) polystyrene-DVB functionalized diamond obtained by 2-bromoisobutyryl bromide and ATRP and g) polystyrene functionalized diamond obtained by di-tert-amyl peroxide and styrene. 53
Figure 4.1. Structure of 1-naphthylamine. 65
Figure 4.2. Positive ion ESI-MS spectra of SPE fractions from polystyrene-modified diamond stationary phases: (a) fraction eluted with water (no analyte present). (b) analyte (1-naphthylamine) eluted with methanol. 66
Figure 4.3. Positive ion ESI-MS spectra of SPE fractions from PS-sulfonated diamond phases: (a) fraction eluted with the phosphate buffer (10 mM, pH=1.9) showing no analyte, (b) the analyte 1-naphthylamine eluted with a higher ionic strength phosphate buffer, which also contained an organic solvent [10 mM, pH=1.9, NaCl, ionic strength 0.2 M): methanol (v/v, 1:1)]. 68
Figure 4.4. IR spectra of polystyrene-functionalized diamond a) before and b) after immersion in solutions of 1M HCl (acid) or 1M NaOH (base). 70
Figure 4.5. Breakthrough curves for 1-naphthylamine on polystyrene (a) and sulfonated polystyrene (b) coated 70 μm diamond particles. Each point represents the peak area of the analyte from the positive ESI-MS spectra..... 73
Figure 4.6. Linear relationship between signal and concentration for the analyte 1-naphthylamine in water (a) and phosphate buffer (pH=1.9) (b) from the positive ion ESI-MS spectra. 74

المنارة للاستشارات
www.manaraa.com

Figure 5.1. Schematic of growing polynorbornene chain on a patterned silicon surface. (Cy = cyclohexyl) 81
Figure 5.2. Schematic of scribing method and olefin-terminated monolayer on a patterned silicon surface. 88
Figure 5.3. Possible arragment of alkyl chains in monolayers on a silicon surface scribed under (a) 50% 1-octene and 50% 1,9-decadiene and (b) 50% 1-decene and 50% 1,9-decadiene. 89
Figure 5.4. XPS (a) Br/Si ratio, (b) Os/Si ratio, (c) Cl /Si ratio and (d) Ru/Si ratio after exposure of monolayers scribed in Table 5.1 to Br_2, OsO_4, CCl_2 and Grubbs' catalyst, respectively. 91
Figure 5.5. XPS Ru/Si ratio measured after adsorption of Grubbs' catalyst onto a homogenous 1,9-decadiene monolayer. 94
Figure 5.6. XPS of silicon scribed in the presence of 1,9-decadiene (functionalized area: 6 mm × 6 mm) before (a) and after (b) the growth of polynorbornene onto the functionalized region. 95
Figure 5.7. XPS C/Si ratio of samples prepared by varying the reaction time of norbornene with 1,9-decadiene monolayers after adsorption of Grubbs' catalyst. Each point represents a different experiment. 97
Figure 5.8. Scores on PC1 from a PCA analysis of TOF-SIMS data showing the combinations of positive and negative ion spectra with two different preprocessing methods (mean-centering and autoscaling): (a) positive ion spectra and mean centering (b) positive ion spectra and autoscaling (c) negative ion spectra and mean centering (d) negative ion spectra and autoscaling. 98
Figure 5.9. Normalized intensity of the ten largest peaks from PC1 loadings plot of a PCA analysis of TOF-SIMS negative ion spectra of samples, the same mean-centered data that were used to make Figure 5.8c. 104
Figure 6.1. Illustration of the PDMS contrast stamping method. A planar PDMS stamp is pressed against a surface. Transfer of unbound PDMS oligomers in the stamp occurs preferentially at hydrophilic regions on the surface, over more hydrophobic regions. 116
Figure 6.2. Structures of C_{60}, THOB and the m/z 207 peak from PDMS. 124
Figure 6.3. Positive ion ToF-SIMS spectra of a C_{60} film before and after stamping with PDMS. 125
Figure 6.4. Positive ion ToF-SIMS spectra of a THOB film before and after stamping with PDMS. 126
Figure 6.5. Positive ion ToF-SIMS spectra of different surfaces after contact with an uninked, unpatterned PDMS stamp. (PDMS is confirmed by the characteristic peaks at m/z 73, 147, 207, and 221.) "Ti" refers to electron beam evaporated titanium on silicon. "Gold" refers to electron beam evaporated Au on Ti on silicon. APTES refers to a layer of 3-aminopropyltriethoxysilane, PEG to a polyethylene glycol monolayer, C16 to a hexadecyl monolayer, PS to polystyrene, perfluoro to a layer of trichloro (3,3,4,4,5,5,6,6,7,7,8,8,8-tridecafluorooctyl)silane, and Teflon to Fluoro Pcl™ PFC M1604V. The Fluoro Pcl™ is a product of Cytonix. 128
Figure 6.6. Change in water contact angle (A), surface tension (B), thickness (C), and percentage of PDMS main peaks in ToF-SIMS spectra (D) after stamping with

المنارة للاستشارات
www.manaraa.com

PDMS for different surfaces. a-k represent clean Si/SiO_2 (a), clean Ti/TiO_2 (b), clean gold (c), dirty Si/SiO_2 (d), SiO_2/PEG monolayer (e), SiO_2/APTES monolayer (f), SiO_2/polystyrene (g), Si/dodecyl monolayer (h), Si/hexadecyl monolayer (i), SiO_2/perfluoro monolayer (j) and Teflon^{TM} (k). 133
Figure 6.7. Relationship between the surface tension at the solid-vapor interface and the percentage of the PDMS main peaks in the ToF-SIMS spectra of various surfaces. 135
Figure 6.8. Positive ion ToF-SIMS images (500×500 μm) for various surfaces before and after stamping with PDMS. SIMS images were collected at m/z 73 and 147 by binning to ±0.3 amu around each integer mass value. 136
Figure 6.9. MCR spectra (loadings plots), associated images (scores plots) and the corresponding percentage of variance in each data set of three grouped MCR components corresponding to the background area, spots and overall area (a) before stamping and (b) after stamping. 139
Figure 7.1. Scores on PC1 of ToF-SIMS positive ion spectra of silicon scribed under aldehydes containing 4 – 11 carbon atoms. Three preprocessing methods were used: a) mean centering, b) autoscaling and c) normalization. 157
Figure 7.2. Scores on PC1 of ToF-SIMS negative ion spectra of silicon scribed under acid chlorides containing 4 – 16 carbon atoms. Three preprocessing methods were used: a) mean centering, b) autoscaling and c) normalization. 158
Figure 7.3. Scores on PC2 of ToF-SIMS positive ion spectra of silicon scribed under aldehydes containing 4 – 11 carbon atoms. Three preprocessing methods were used: a) mean centering, b) autoscaling and c) normalization. 160
Figure 7.4. Plot of the scores on PC1 vs. the number of carbon atoms in the adsorbate. PCA of mean centered a) positive ion scans, b) negative ion scans, and c) combined positive and negative ion scans. 164
Figure 7.5. Plots derived from the positive ion ToF-SIMS spectra of 66 monolayers on Si_{scr}. Φ_{CSi} is the ratio of the area of the speactral regions: 42 ($C_3H_6^+$), 57 ($C_4H_9^+$), 55 ($C_4H_7^+$), 39 ($C_3H_3^+$), 43 ($C_3H_7^+$), 27 ($C_2H_3^+$), 41 ($C_3H_5^+$) by the area of 28 (Si^+), 29 (SiH^+) and 45 ($SiHO^+$). 167
Figure 7.6. Three dimensional plot of scores on PC1, PC2, and PC3 from (mean centered) negative ion data taken from alkyl chloride (RCl), alkyl bromide (RBr), alkyl iodide (RI), acid chloride (RCOCl), aldehyde (RCHO), alkene, and alkyne adsorbates. Ovals are guides to the eye. 169
Figure 7.7. Scores on PC1 for 66 monolayers on silicon from normalized, mean centered a) positive ion scans, b) negative ion scans, and c) combined positive and negative ion scans. 170
Figure 7.8. Partial least squares (with six latent variables) of 66 different monolayers showing the actual and predicted number of carbon atoms in the reactive adsorbates for a) the positive ion spectra, and b) the negative ion spectra. 171
Figure 8.1. Peak areas (a) and normalized peak areas (b) of six peaks of significance from Figure 8.5, showing results from ten dilutions of 50%. [The mouse liver used was obtained at Brigham Young University (BYU). The analysis shown in this Figure was also performed on beef liver (obtained from a local grocery store), which again showed that the ratio of the peak areas of the most significant phosphatidylcholines to the sum of areas remained essentially

المنارة للاستشارات
www.manaraa.com

constant over the same wide range of concentrations.] 188
Figure 8.2. Livers from hypercholesterolemic and normocholesterolemic mice were extracted and analyzed by electrospray mass spectrometry. Shown are representative mass spectra for a normocholesterolemic mouse. (a) Electrospray mass spectrum of mouse 249 in the range from 750 to 850 (b) Whole electrospray mass spectrum of mouse 249 in the range from 100 to 1200..... 189
Figure 8.3. PCA analysis of infusion mass spectrometry data from organic extracts of mouse livers. Samples (red circles) in the red line oval on the left are LDLR-/- mice fed a high fat, high cholesterol diet (HFD) for the entire period. These mice had plasma cholesterol levels between 900 and 1450 mg/dL. Samples in the small dash line ovals on the right are LDLR-/- mice fed chow for the entire period. These mice had plasma cholesterol levels of ca. 250 mg/dL. Samples in the dash-dot line ovals on the right are LDLR-/- mice fed HFD for 21 weeks and then returned to a chow diet. Samples in the dash-dot-dot line oval are C57BL/6 mice fed a chow diet. These are controls in that they are normal mice with the same genetic background as the LDLR-/- mice. Their cholesterol levels were ca. 80 mg/dL. (The samples on the right had plasma cholesterol levels between 60 and 250 mg/dL.) The label numbers indicate individual mice. 191
Figure 8.4. Dendrogram of the K-nearest neighbor (KNN) cluster analysis of all of the electrospray MS data from the mouse liver extracts. The top cluster comes from livers of normocholesterolemic mice and the bottom cluster comes from livers of hypercholesterolemic mice. The y-axis labels are the identification numbers for the original samples. 193
Figure 8.5. Loadings plot of PC1 from the electrospray MS data, where the data were mean-centered. Positive peaks in this loadings plot are more intense in spectra that have positive scores on PC1 (in Figure 8.3), and negative peaks are more intense in spectra that have negative scores on PC1. 195
Figure 8.6. Experimental data and theoretical isotope patterns for two phosphatidylcholines: a) and c) correspond to the m/z 786.60 peak and b) and d) correspond to the m/z 810.60 peak. 198
Figure 8.7. Representative daughter ion spectrum of a phosphatidylcholine. This particular daughter ion spectrum is of the mouse 643 liver tissue extract showing the phosphatidylcholine head group at 184 amu as well as the $(M+1)^+$ ion at 811 amu. 199
Figure 8.8 (a) and (b): Loadings on component 1 and 2 of MCR from the electrospray MS spectra at 700-900 amu, respectively. (c) and (d): Average, normalized electrospray MS spectra of all of the high and low cholesterol mice at 700-900 amu, respectively. 201
Figure 8.9. (a) Root mean square error of the cross validation (RMSECV) and the root mean square error of the calibration (RMSEC) for a partial least squares (PLS) analysis relating plasma cholesterol levels (the Y-block) to mass spectra (the X-block). The RMSECV plot has a minimum at five latent variables. (b) PLS (with five latent variables) of the ESI mass spectra showing the actual and predicted CV total cholesterol levels. 203

المنارة للاستشارات
www.manaraa.com

PART I Diamond Functionalization and Its Applications

Chapter 1 Functionalization of Deuterium- and Hydrogen-Terminated Diamond with Mono- and Multilayers of Di-*tert*-Amyl Peroxide

1.1 Abstract

In spite of an earlier report to the contrary, here I show a method that employs dialkyl peroxides to tether alkyl chains to hydrogen- and deuterium-terminated diamond through ether linkages. In particular, hydrogen-/deuterium-terminated diamond particles were treated with neat di-*tert*-amyl peroxide (DTAP) at elevated temperature. Surface changes were followed by X-ray photoelectron spectroscopy (XPS), diffuse reflectance Fourier transform infrared spectroscopy (DRIFT) and time-of-flight secondary ion mass spectrometry (ToF-SIMS). After these reactions, the oxygen signal in the XPS spectra increased, the deuterium peak in the negative ToF-SIMS spectra decreased, and DRIFT showed C-H stretches, which were not previously present. The threshold for this reaction was determined by DRIFT to be ca. 95ºC. For deuterium-terminated diamond reacted with di-*tert*-amyl peroxide, DRIFT showed that the envelopes of the C-H stretches of the adsorbate and the surfaces were nearly identical. Multilayers of DTAP could be prepared by repeated exposure of the substrate to this reagent.

المنارة للاستشارات
www.manaraa.com

1.2 Introduction

Diamond is an extraordinary material because of its remarkable mechanical, thermal, and electrical properties. It also has tremendous chemical stability and inertness, which makes it an attractive material for many applications, including as a sorbent in separations science.[1, 2]

However diamond's chemical inertness makes its chemical modification challenging. In an effort to enhance and/or take advantage of some of its already remarkable aspects, there has recently been much interest in functionalizing the surface of diamond. For example, chlorinated diamond surfaces react with CHF_3[3] and NH_3[4] in the vapor phase. Fluoro-nanodiamond surfaces react with alkyllithium reagents, diamines and amino acids in the liquid phase, resulting in methyl-, butyl-, hexyl-, ethylenediamino- and glycine-functionalized nanodiamond derivatives.[5] Hydrogen- and deuterium-terminated diamond surfaces can be prepared thermally[6, 7] and by plasma treatment.[8-11] Hydrogen-terminated diamond surfaces have also been modified via UV light. For example, hydrogen-terminated diamond can be covalently modified with molecules bearing a terminal vinyl (C=C) group via a photochemical process using sub-band gap light at 254 nm.[12] Liquid phase reactions are also commonly used. These include the functionalization of diamond (100) by Diels-Alder chemistry.[13] In addition, plasma modification of diamond surfaces,[14, 15] ultrasonic treatment of acid-washed diamond powder[16] and electrochemical methods,[17] such as electrochemical reduction of diazonium salts and photochemical terminations at varying energies, are known.[12, 18-22]

The obvious problem associated with functionalization of hydrogen-terminated (HTD) or deuterium-terminated diamond (DTD) is breaking the strong C-H or C-D bond.

المنارة للاستشارات
www.manaraa.com

One successful approach to this problem has been to use radicals in a two-step, Eley-Rideal type mechanism, where a radical's interaction with HTD or DTD may result in hydrogen or deuterium abstraction from the surface, leaving a carbon-centered radical, and a second radical may then condense with the dangling bond to covalently link this radical to the surface. Tsubota and coworkers have used the thermal decomposition of benzoyl peroxide,[23-27] lauroyl peroxide,[25] diacyl peroxide,[26] dicarboxylic acid[27], a carboxylic acid with benzoyl peroxide[28-30] to functionalize HTD in this manner. They also reported that di-*tert*-amyl peroxide (DTAP, Figure 1.1) *does not* react with HTD.[25] Their reaction conditions for this chemistry were 0.05 g DTAP in toluene on HTD at 85° C for 60 min. Liu[31] subsequently claimed that a low concentration of DTAP (24.5 mg in 50 mL dodecane) would react with HTD (112° C for ca. 2 h). However, the infrared spectrum of his reaction product *does not* confirm that this chemical reaction has occurred. DTAP, and other peroxides, are potentially important reagents for diamond functionalization because of the robust C-O bond (ether linkage) that could be formed to tether DTAP fragments to diamond particles.

In an effort to demonstrate functionalization of hydrogen- and deuterium-terminated diamond with DTAP, and therefore to illustrate that a dialkylperoxide can react with diamond, I have heated HTD and DTD with neat DTAP at higher temperatures or higher concentrations than were previously investigated. This is a one-step modification of hydrogen- and deuterium-terminated diamond using a radical producing species. The reaction mechanism is believed to be as follows: (1) radicals are first created by the thermolysis of DTAP at its weak O-O bond; (2) simple thermodynamics suggests that because the O-H bond is stronger than the C-H bond,[32] these oxygen-centered radicals

المنارة للاستشارات
www.manaraa.com

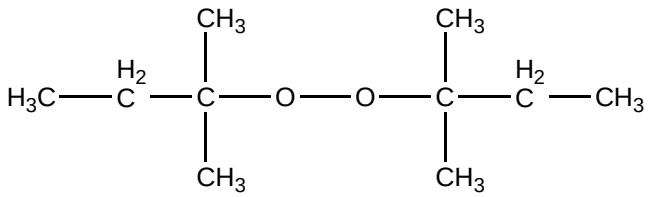

Figure 1.1. The structure of di-tert-amyl peroxide: $(CH_3CH_2C(CH_3)_2O)_2$

المنارة للاستشارات
www.manaraa.com

should abstract hydrogen or deuterium from diamond surfaces, yielding carbon-centered radicals; (3) surface functionalization then takes place by condensation of surface radicals with peroxy radicals. X-ray photoelectron spectroscopy (XPS), diffuse reflectance Fourier transform infrared spectroscopy (DRIFT), and time of flight secondary ion mass spectrometry (ToF-SIMS) provide evidence for this surface reaction.

(1) $(CH_3CH_2(CH_3)_2CO)_2 \xrightarrow{\Delta} 2\ \bullet OC(CH_3)_2CH_2CH_3$

(2) Diamond-(H or D) + $\bullet OC(CH_3)_2CH_2CH_3 \rightarrow$ Diamond• + (H or D)$OC(CH_3)_2CH_2CH_3$

(3) Diamond• + $\bullet OC(CH_3)_2CH_2CH_3 \rightarrow$ Diamond-$OC(CH_3)_2CH_2CH_3$

While this mechanism surely has an element of truth in it, I will argue later that it is an oversimplification of what is probably occurring at the diamond surface. Thus, if peroxy radicals can abstract hydrogen from hydrogen-terminated diamond, they should also be able to abstract it from other chemisorbed peroxy fragments. This leads to the possibility of multilayer growth on diamond using DTAP.

1.3 Experimental Section

1.3.1 Reagents

All chemicals were used as received. Toluene (spectra grade) and di-*tert*-amyl peroxide (97%) were obtained from Sigma-Aldrich (St. Louis, MO). The gas mixtures,

المنارة للاستشارات
www.manaraa.com

including 5% deuterium in argon (99.999%) and 6% hydrogen in argon were purchased from Airgas (Radnor, PA). 1.7 μm diamond powder was provided by U.S. Synthetic (Orem, UT).

1.3.2 Preparation of Hydrogen-/Deuterium-Terminated Diamond Powder

Diamond powder was washed with an acid mixture (90% H_2SO_4+10% HNO_3) at 80° C for 4 h, then rinsed with distilled water.[33] After drying in a Mini-Mite Tube Furnace of Lindberg/Blue M (model number is TF55030A-1), which was purchased from the Thermo Electron (Waltham, MA), clean diamond powder was treated in flowing 5% D_2 (6% H_2) gas at 900° C for 28 h. [*Caution:* Hydrogen and deuterium gas may form explosive mixtures with air. A mixture of 5% D_2 (or 6% H_2) in Ar (or N_2) (forming gas) cannot be ignited and is potentially much safer.] During the reaction, the diamond powder was shaken twice to evenly deuterate (or hydrogenate) the surface and it was cooled in flowing 5% D_2 (or 6% H_2) in Ar. The resulting deuterium (or hydrogen)-terminated diamond powder was used as the starting point for this work.

1.3.3 Treatment of Hydrogen-/Deuterium-Terminated Diamond Powder with Di-tert-Amyl Peroxide

Hydrogen-/deuterium-terminated diamond powder (0.5 g) was suspended in neat di-*tert*-amyl peroxide (25 mL). Nitrogen gas was bubbled through the suspension to remove oxygen. Di-tert-amyl peroxide, $C_2H_5C(CH_3)_2OOC(CH_3)_2C_2H_5$, is a clear, colorless liquid with a half life of 10 h at 123.3°C and 1 h at 143.1°C. Suspensions were then heated to 60, 80, 90, 95, 100, 110, 120, 130 or 150° C for 24 h. An Additional 10 mL

المنارة للاستشارات
www.manaraa.com

of DTAP were added after 10 h reaction to replace the peroxides that were consumed. For the 150° C reaction, 10 mL of DTAP were added two times (every 8 h) during the reaction. The diamond powders were finally washed with toluene and dried in a vacuum dryer. Different reaction temperatures were evaluated in this manner.

1.3.4 Multilayers on Deuterium-Terminated Diamond Powder Made with Di-tert-amyl Peroxide

Deuterium-terminated diamond powder (0.5 g) was heated in neat di-*tert*-amyl peroxide (25 mL) under nitrogen gas at 120°C for 24 h. 10 mL of DTAP was added a second time after 10 h reaction to replace the peroxides that were consumed. The diamond powders were washed with toluene and dried in a vacuum dryer. The entire process above was repeated to build multilayers of DTAP on the surface.

1.3.5 Characterization of the Diamond Surfaces

Time-of-flight secondary ion mass spectrometry (ToF-SIMS) was performed with an ION-TOF ToF-SIMS Ⅳ instrument using monoisotopic 25 keV $^{69}Ga^{+}$ ions. X-ray photoelectron spectroscopy was performed with an SSX-100 X-ray photoelectron spectrometer with a monochromatic Al K_{α} source and a hemispherical analyzer. An electron flood gun was employed for charge compensation. Survey scans as well as narrow scans were recorded with an 800×800 μm spot. The diamond surface was characterized by a Magna-IR 560 spectrometer from Nicolet (Madison, WI). The DRIFT spectra were obtained over the range of 400-4000 cm^{-1}. For each spectrum, 64 scans were collected at a resolution of 4 cm^{-1}. The diffuse reflectance data were plotted with

المنارة للاستشارات
www.manaraa.com

Kubelka-Munk units.

1.4 Results and Discussion

X-ray photoelectron spectroscopy (XPS) was used to study the formation of deuterium-terminated diamond and its subsequent reaction with DTAP. Figure 1.2a shows clean, untreated diamond powder that contains an obvious oxygen signal, (10.1±0.4% oxygen, 89.9±0.4% carbon) presumably due to oxidized carbon at the diamond surface. After the diamond powder is treated in 5% D_2 in Ar, XPS shows a significant reduction in the oxygen signal (See Figure 1.2b) (0.9±0.05% oxygen, 99.1±0.1% carbon).

After deuterium-terminated diamond powder was exposed to heated di-*tert*-amyl peroxide for 1 day, the XPS oxygen signal rose (3.1±0.6% oxygen, 96.9±0.6% carbon), but not to the level found before deuterium termination (See Figure 1.2c). This increase in surface oxygen is consistent with the chemisorption of radical fragments of DTAP, as given in Step 3 of the mechanism (vide supra).

FTIR was also used to characterize diamond powder as it was received, after deuterium termination, and after reaction with DTAP (See Figure 1.3). FTIR of the as-received diamond powder shows evidence of hydrocarbon contamination in the C-H stretching region at ca. 2800 – 3000 cm^{-1} (Figure 1.3a is very similar to that obtained by Liu[31]). After treatment with D_2 gas, these stretches almost entirely disappear, and following treatment with DTAP, a series of stretches reappear in the C-H stretching region. It is of significance that the comparison spectrum of neat DTAP is similar to that of the DTAP-modified diamond, suggesting that DTAP fragments are covalently bonded to the diamond surface.

المنارة للاستشارات
www.manaraa.com

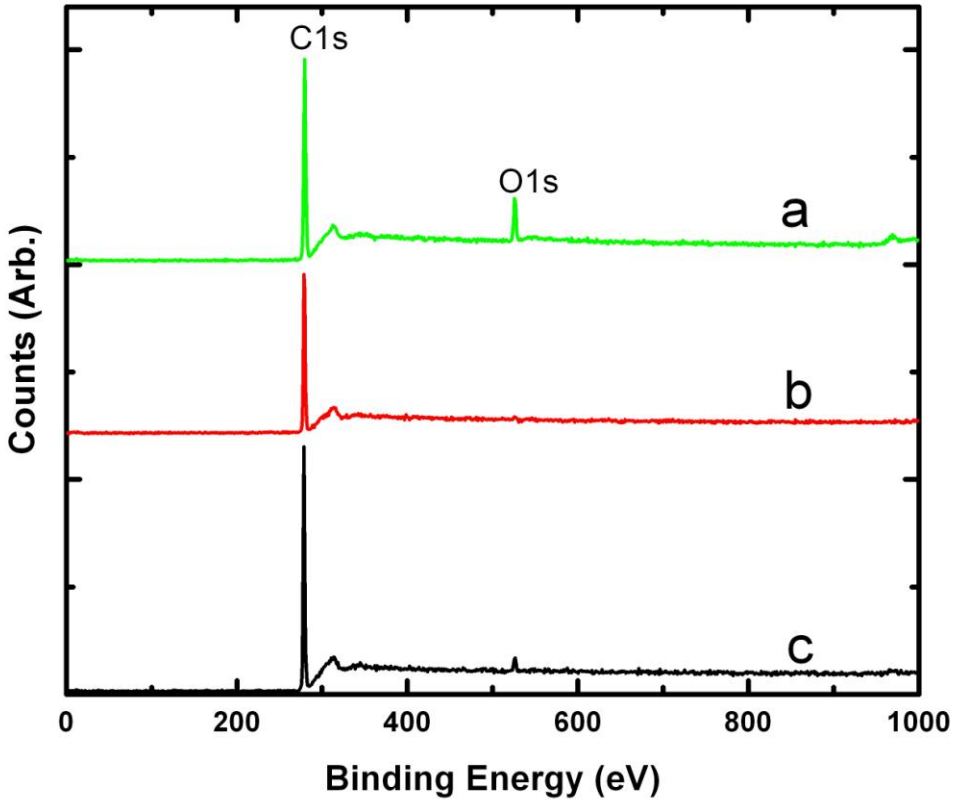

Figure 1.2. XPS survey spectra of diamond powders: (a) clean, untreated diamond powder (b) deuterium-terminated diamond powder and (c) deuterium-terminated diamond powder treated with di-tert-amyl peroxide for 1 day at 110° C.

المنارة للاستشارات
www.manaraa.com

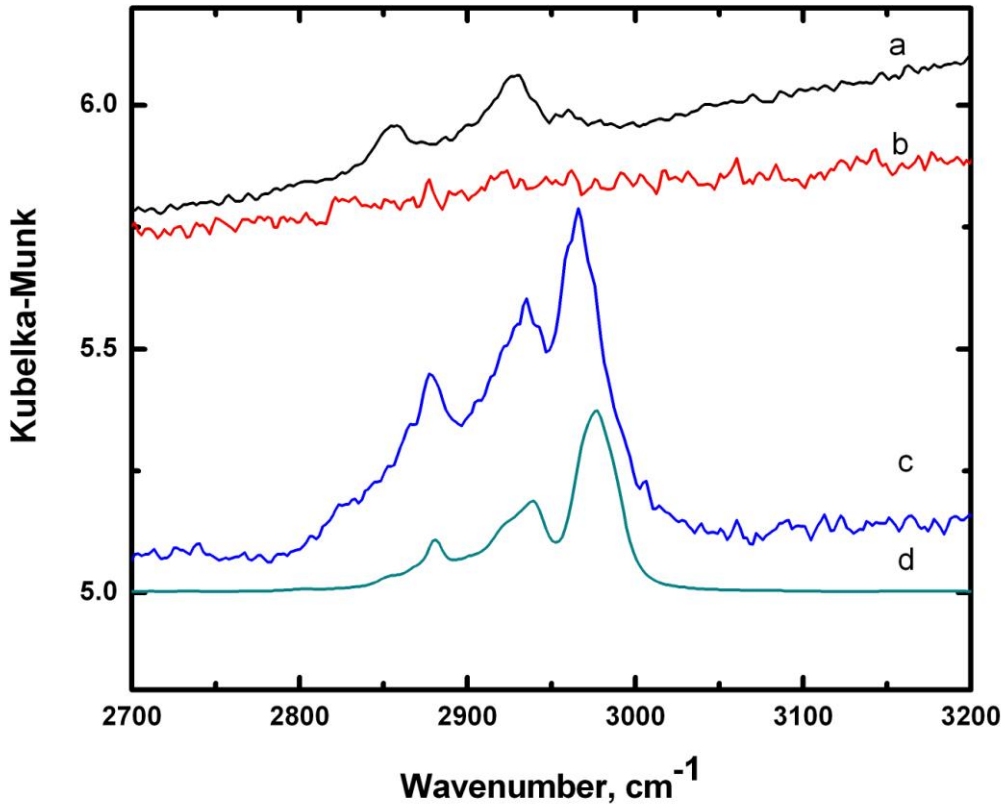

Figure 1.3. DRIFT spectroscopy of diamond powders: (a) raw, untreated diamond powder, (b) diamond powder after deuteration, (c) deuterium-terminated diamond powder treated with di-tert-amyl peroxide for 1 day at 130° C and (d) the IR absorbance spectrum of neat di-tert-amyl peroxide.

المنارة للاستشارات
www.manaraa.com

An advantage of ToF-SIMS is that it can detect every element, while XPS is not sensitive to H (or D). ToF-SIMS provides direct evidence for surface deuteration in both positive and negative ion spectra. In the negative ion ToF-SIMS spectrum, a strong H^- signal is seen in the untreated diamond powder (See Figure 1.4a). This signal is consistent with the C-H stretches in the FTIR spectrum. Following surface deuteration, strong signals due to D^-, CD^-, and C_2D^- appear in the negative ion spectrum (See Figure 1.4b). This spectrum also contains a reasonably large H^- signal, which is consistent with the very low level of C-H stretches that still appears to be in the FTIR spectrum of deuterated diamond (just above the noise level, and presumably due to chemisorption of adventitious hydrocarbons after surface deuteration – hydrocarbons would not survive the conditions of diamond deuteration I employed). Because of its very low penetration depth (*ca.* 2 nm), ToF-SIMS is extremely sensitive to surface contamination. After surface reaction with DTAP, the H^- signal regains its prominence, although some D^- remains, suggesting that the surface reaction was incomplete (See Figure 1.4c).

Because of previous attempts to modify diamond with DTAP (at 85° C or 112° C), it seemed appropriate to understand the relationship between degree of surface functionalization and reaction temperature. Below 90° C, Figure 1.5 a-c shows no obvious spectral changes in the reaction between DTD and DTAP that would suggest surface functionalization. However, at 95° C, the C-H stretching envelope shows a series of low intensity features that begin to resemble those of neat DTAP. The spectrum at 100° C is essentially the same. At 110° C, these features are more pronounced and suggest more effective surface functionalization. Surface functionalization appears to take place even more effectively at 130° C and 150° C.

المنارة للاستشارات
www.manaraa.com

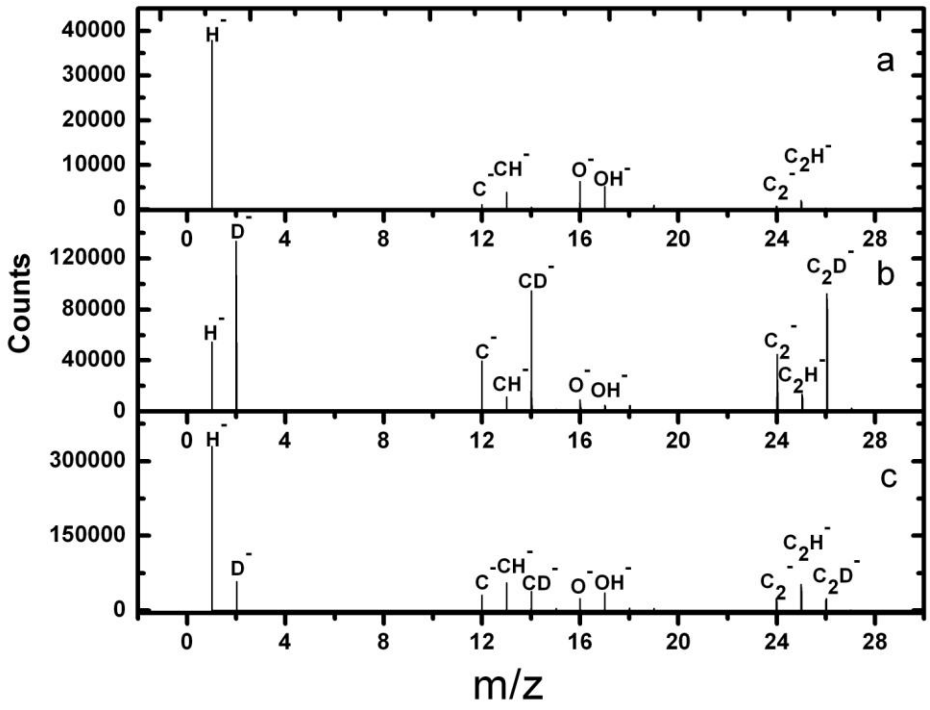

Figure 1.4. ToF-SIMS negative ion spectra of (a) clean, untreated diamond powder, (b) deuterium-terminated diamond powder (c) deuterium-terminated diamond powder treated with di-tert-amyl peroxide for 1 day at 110° C.

المنارة للاستشارات
www.manaraa.com

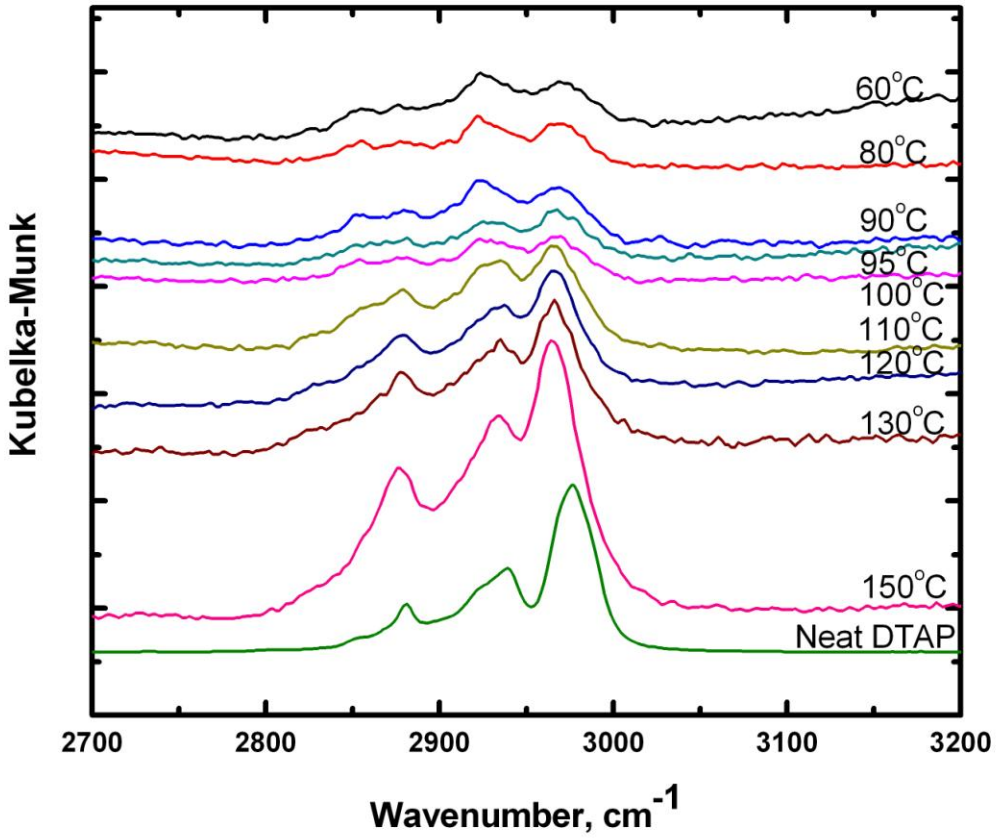

Figure 1.5. DRIFT spectroscopy for deuterium-terminated diamond powder treated with di-tert-amyl peroxide for 1 day at different temperatures and the IR spectrum of neat di-tert-amyl peroxide.

المنارة للاستشارات
www.manaraa.com

I also studied the reaction between hydrogen-terminated diamond and DTAP. Results similar to those obtained with deuterium-terminated diamond are obtained. After hydrogenation, two peaks are present between 2800 and 3000 cm^{-1} (See Figure 1.6 a), which are assigned to the symmetric and asymmetric C-H stretching vibration of the hydrogen-terminated diamond. After the reaction, the C-H stretching vibrations are similar to those of neat DTAP, with added contributions from the HTD surface. These results are consistent with the incomplete surface reaction suggested by the ToF-SIMS results in Figure 1.4.

It is doubtful that the reaction in question could be driven to completion because of steric hindrance of DTAP fragments adjacent to surface C-D or C-H groups. There is also the possibility of H-abstraction from chemisorbed DTAP fragments competing with hydrogen or deuterium abstraction from the surface. Based on the mechanism I already proposed, it should also be possible for peroxy radicals to attack the methylene units of chemisorbed fragments of DTAP. If operative, this procedure could be repeated several times and multilayers could be grown on the diamond surface. This proposed mechanism is as follows:

(4) Diamond-$OC(CH_3)_2CH_2CH_3$ + •$OC(CH_3)_2CH_2CH_3$ → Diamond-$OC(CH_3)_2CH$•(CH_3) + $HOC(CH_3)_2CH_2CH_3$

(5) Diamond-$OC(CH_3)_2CH$•(CH_3) + •$OC(CH_3)_2CH_2CH_3$→ Diamond-$OC(CH_3)_2CH(CH_3)OC(CH_3)_2CH_2CH_3$

etc.

المنارة للاستشارات
www.manaraa.com

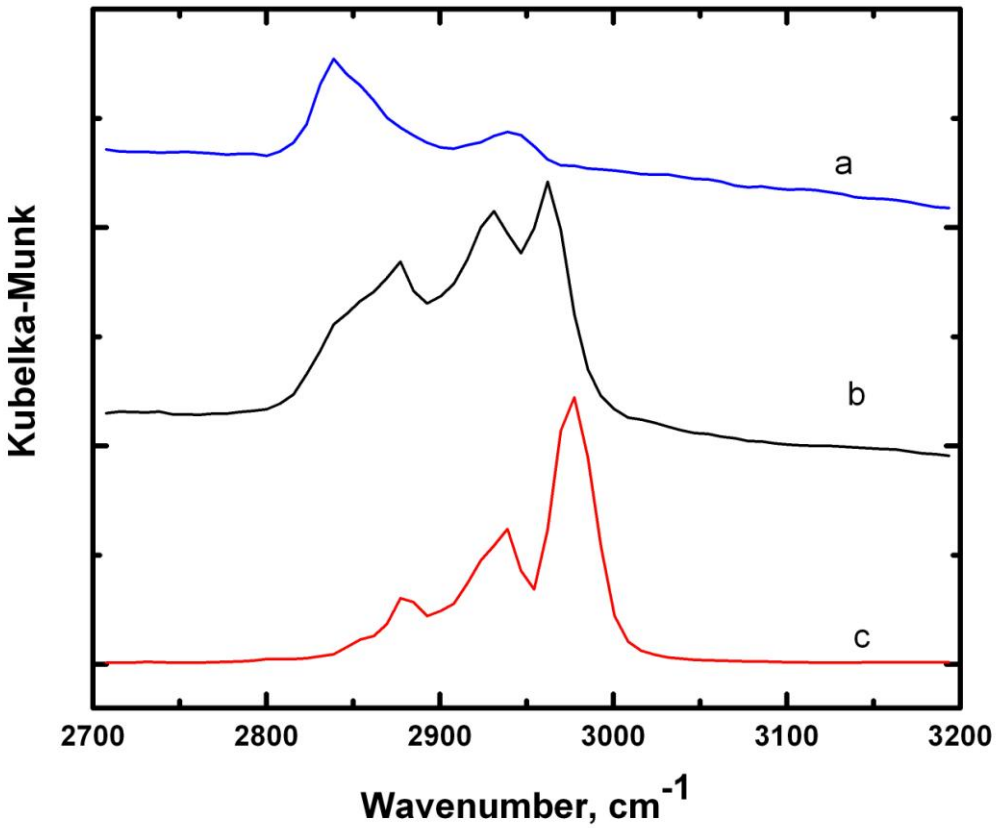

Figure 1.6. DRIFT spectroscopy for a) hydrogen-terminated diamond powder, b) hydrogen-terminated diamond powder treated with di-tert-amyl peroxide for 1 day at 130 ^{o} C, c) neat di-tert-amyl peroxide.

www.manaraa.com

An obvious implication of this mechanism is that polymer brushes of the form: diamond-$(OC(CH_2)_2CH(CH_3))_n$ could be formed, as illustrated in Figure 1.7.

Figure 1.7 shows the C-H and C-O stretching regions of diffuse-reflectance FTIR spectra of diamond treated with neat di-*tert*-amyl peroxide after different numbers of reaction cycles. Bands at 2800-3100 cm^{-1} are assigned to the C-H stretches. Bands at 1350 and 1450 cm^{-1} are due to C-H bends. The band at 1100 cm^{-1} is assigned to the C-O stretch. These peaks increase in intensity with increasing numbers of reaction cycles with DTAP. The spectra also suggest that a small number of carbonyl groups are formed, suggesting additional complexity in the mechanism. Figure 1.8 shows peak areas of the C-H stretches vs. the number of reaction cycles. The peak area increases with increasing number of reaction cycles. The linear fit to this curve is $A= 16.04\times n + 37.13$, where n is the number of layers, with an R^2 value of 0.885. These results are consistent with the hypothesis of multilayer growth on diamond surfaces from DTAP.

1.5 Conclusions

Although there are reports to the contrary, XPS, ToF-SIMS and DRIFT demonstrate the reactivity of DTD and HTD with DTAP at elevated temperature. XPS showed that the oxygen signal increased and deuterium peak in the negative ion ToF-SIMS spectra decreased after the reaction between deuterium-terminated diamond and di-*tert*-amyl peroxide. DRIFT showed that the envelopes of the C-H stretch of the adsorbate and the surfaces were similar after modification. The threshold for the reaction was determined, and multilayer formation was accomplished with several reaction cycles.

المنارة للاستشارات
www.manaraa.com

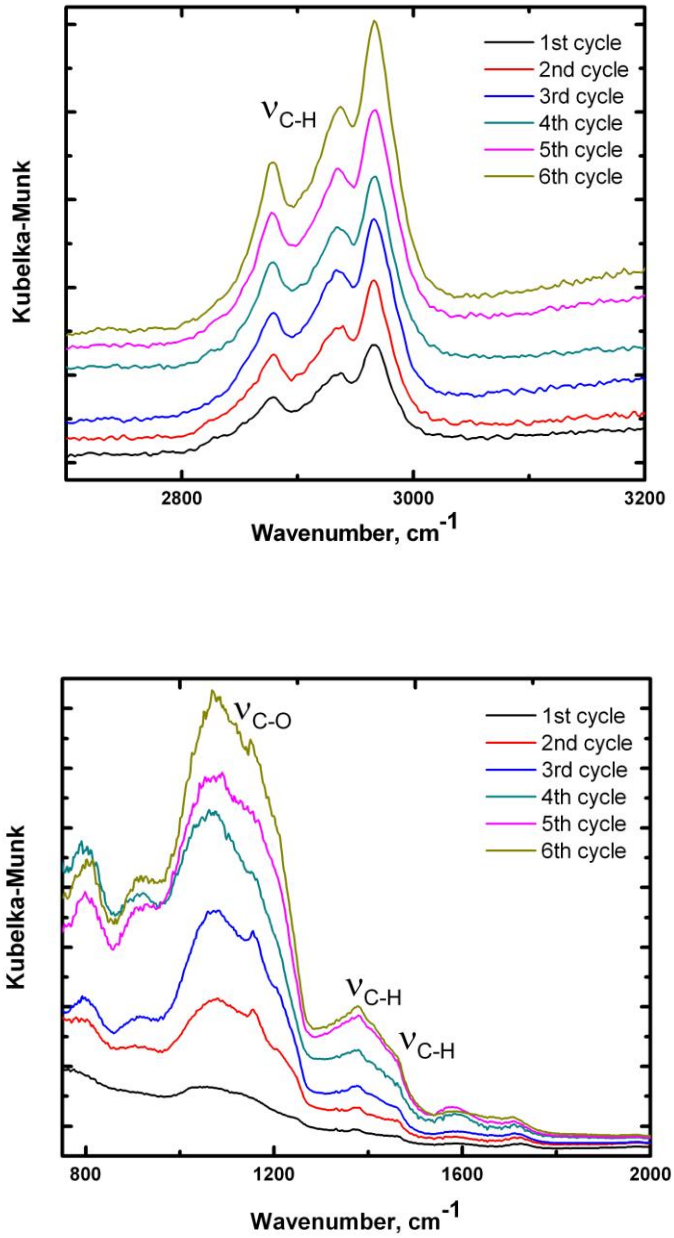

Figure 1.7. DRIFT spectroscopy (C-H and C-O stretching regions) for deuterium-terminated diamond powder treated with di-tert-amyl peroxide for 1 day at 120 ^{o}C for different numbers of exposures to fresh DTAP.

www.manaraa.com

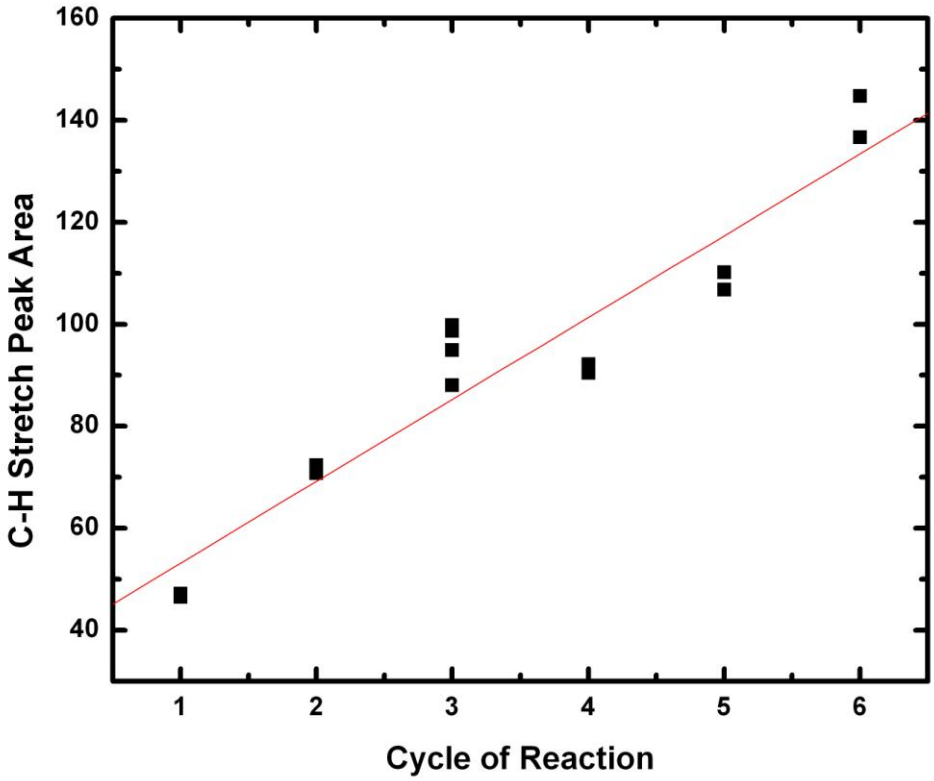

Figure 1.8. Area of the C-H stretching region by DRIFT spectroscopy for deuterium-terminated diamond powder treated with di-tert-amyl peroxide for 1 day at 120 ^{o}C for different numbers of exposures to fresh DTAP.

المنارة للاستشارات
www.manaraa.com

1.6 References

(1) Nesterenko, P. N.; Fedyanina, O. N.; Volgin, Y. V. *Analyst* **2007**, *132*, 403-405.

(2) Nesterenko, P. N.; Fedyanina, O. N.; Volgin, Y. V. *J. Chromatogr.,A* **2007**, *1155*, 2-7.

(3) Ando, T.; Nishitani-Gamo, M.; Rawles, R. E.; Yamamoto, K.; Kamo, M.; Sato, Y. *Diamond and Related Materials* **1996**, *5*, 1136-1142.

(4) Miller, J. B.; Brown, D. W. *Langmuir* **1996**, *12*, 5809-5817.

(5) Liu, Y.; Gu, Z.; Margrave, J. L.; Khabashesku, V. N. *Chem. Mater.* **2004**, *16*, 3924-3930.

(6) Ando, T.; Ishii, M.; Kamo, M.; Sato, Y. *Journal of the Chemical Society, Faraday Transactions* **1993**, *89*, 1783-1789.

(7) Jiang, T.; Xu, K.; Ji, S. *Journal of the Chemical Society, Faraday Transactions* **1996**, *92*, 3401-3406.

(8) Yang, W.; Butler, J. E.; Russell, J. N., Jr.; Hamers, R. J. *Langmuir* **2004**, *20*, 6778-6787.

(9) Tse, K.-Y.; Nichols, B. M.; Yang, W.; Butler, J. E.; Russell, J. N. J.; Hamers, R. J. *Journal of Physical Chemistry B* **2005**, *109*, 8523-8532.

(10) Wang, S.; Swain, G. M. *J. Phys. Chem. C.* **2007**, *111*, 3986-3995.

(11) Kondo, T.; Aoshima, S.; Honda, K.; Einaga, Y.; Fujishima, A.; Kawai, T. *J. Phys. Chem. C.* **2007**, *111*, 12650-12657.

(12) Strother, T.; Knickerbocker, T.; Russell, J. N. J.; Butler, J. E.; Smith, L. M.; Hamers, R. J. *Langmuir* **2002**, *18*, 968-971.

المنارة للاستشارات
www.manaraa.com

(13) Wang, G. T.; Bent, S. F.; Russell, J. N. J.; Butler, J. E.; D'Evelyn, M. P. *Journal of the American Chemical Society* **2000**, *122*, 744-745.

(14) Hahn, M.; Pleu, D.; Nitschke, M.; Frens, G.; Bundel, G.; Prause, S.; Simon, F. *Journal of Adhesion Science and Technology* **2005**, *19*, 1039-1052.

(15) Scruggs, B. E.; Gleason, K. K. *Journal of Physical Chemistry* **1993**, *97*, 9187-9195.

(16) Visbal, H.; Ishizaki, C.; Ishizaki, K. *Journal of the Ceramic Society of Japan* **2004**, *112*, 95-98.

(17) Notsu, H.; Yagi, I.; Tatsuma, T.; Tryk, D. A.; Fujishima, A. *Electrochem. Solid-State Lett.* **1999**, *2*, 522-524.

(18) Ohta, R.; Saito, N.; Inoue, Y.; Sugimura, H.; Takai, O. *J. Vac. Sci. Technol. A* **2004**, *22*, 2005.

(19) Nichols, B. M.; Butler, J. E.; Russell, J. N. J.; Hamers, R. J. *Journal of Physical Chemistry B* **2005**, *109*, 20938-20947.

(20) Nakamura, T.; Ishihara, M.; Ohana, T.; Koga, Y. *Chemical communications (Cambridge, England)* **2003**, *7*, 900-901.

(21) Lasseter, T. L.; Clare, B. H.; Abbott, N. L.; Hamers, R. J. *Journal of the American Chemical Society* **2004**, *126*, 10220-10221.

(22) Nakamura, T.; Suzuki, M.; Ishihara, M.; Ohana, T.; Tanaka, A.; Koga, Y. *Langmuir* **2004**, *20*, 5846-5849.

(23) Tsubota, T.; Hirabayashi, O.; Ida, S.; Nagaoka, S.; Nagata, M.; Matsumoto, Y. *Diamond and Related Materials* **2002**, *11*, 1374-1378.

(24) Tsubota, T.; Hirabayashi, O.; Ida, S.; Nagaoka, S.; Nagata, M.; Matsumoto, Y. *Physical Chemistry Chemical Physics* **2002**, *4*, 806-811.

المنارة للاستشارات
www.manaraa.com

(25) Ida, S.; Tsubota, T.; Hirabayashi, O.; Nagata, M.; Matsumoto, Y.; Fujishima, A. *Diamond and Related Materials* **2003**, *12*, 601-605.

(26) Tsubota, T.; Ida, S.; Hirabayashi, O.; Nagaoka, S.; Nagata, M.; Matsumoto, Y. *Physical Chemistry Chemical Physics* **2002**, *4*, 3881-3886.

(27) Ida, S.; Tsubota, T.; Tanii, S.; Nagata, M.; Matsumoto, Y. *Langmuir* **2003**, *19*, 9693-9698.

(28) Tsubota, T.; Tanii, S.; Ida, S.; Nagata, M.; Matsumoto, Y. *Diamond and Related Materials* **2004**, *13*, 1093-1097.

(29) Tsubota, T.; Tanii, S.; Ida, S.; Nagata, M.; Matsumoto, Y. *Hyomen Gijutsu* **2003**, *54*, 758-763.

(30) Tsubota, T.; Tanii, S.; Ida, S.; Nagata, M.; Matsumoto, Y. *Physical Chemistry Chemical Physics* **2003**, *5*, 1474-1480.

(31) Liu, Y. S., Brigham Young University, Provo, 2007.

(32) *Handbook of Chemistry and Physics*, 81 ed.; CRC Press: Boca Raton, 2000.

(33) Ando, T.; Ishii, M.; Kamo, M.; Sato, Y. *J. Chem. Soc. Faraday Trans.* **1993**, *89*, 1783-1789.

المنارة للاستشارات
www.manaraa.com

Chapter 2 Direct Polymer Attachment on Hydrogen/Deuterium-Terminated Diamond Particles

2.1 Abstract

I describe direct polymer attachment to hydrogen and deuterium-terminated diamond surfaces using a radical initiator (di-*tert*-amyl peroxide), a reactive monomer (styrene) and a crosslinking agent (divinylbenzene) to create polystyrene encapsulated diamond. Chemisorbed polystyrene was sulfonated with sulfuric acid in acetic acid. Surface changes were followed by X-ray photoelectron spectroscopy (XPS), time of flight secondary ion mass spectrometry (ToF-SIMS) and diffuse reflectance Fourier transform infrared spectroscopy (DRIFT).

2.2 Introduction

Although the attachment of various small molecules to diamond has now been reported,[1-9] there has been much less work on polymer modification of diamond surfaces. Gu electropolymerized diamond surfaces with an ultrathin film of a PANI-PAA (polyaniline/polyacrylate) copolymer.[10] In a multistep procedure, Steenackers and coworkers developed functional polymer grafts on oxidized ultrananocrystalline diamond (UNCD) surfaces using UV irradiation.[11] Cheng reported polymer brushes of polystyrene and poly(*t*-butyl methacrylate) (P*t*BMA) on nanodiamond prepared by the reaction between carboxyl and epoxy groups of polymer precursors.[12] Linford and coworkers, showed the adsorption and subsequent crosslinking or curing of poly(allylamine) on

المنارة للاستشارات
www.manaraa.com

oxidized diamond.[13] Oxidized diamond powder can also be noncovalently coated with polylysine.[14] In a study directly related to the present work, Linford and coworkers also demonstrated single-step polymer attachment onto hydrogen-terminated silicon using a radical initiator, an unsaturated monomer, and a crosslinking agent,[15] where the resulting polymer films were 2 – 15 nm thick.

Here, I show a one-step polymerization on hydrogen-terminated diamond (HTD)[16, 17] or deuterium-terminated diamond (DTD) using only saturated monomers and a peroxide initiator. The presence of a crosslinking agent, such as divinylbenzene, appears to enhance polymer growth.

The mechanism by which polymer growth occurs on HTD or DTD is believed to be as follows. Radicals are created by the thermal decomposition of di-*tert*-amyl peroxide at its weak O-O bond. Because the O-H bond is stronger than the C-H bond,[18] these oxygen-centered radicals are believed to abstract hydrogen or deuterium from diamond surfaces, yielding carbon-centered radicals:

(1) $(CH_3CH_2(CH_3)_2CO)_2 \xrightarrow{\Delta} 2\ \bullet OC(CH_3)_2CH_2CH_3$

(2) Diamond-(H or D) + $\bullet OC(CH_3)_2CH_2CH_3 \rightarrow$ Diamond• + (H or D)-$OC(CH_3)_2CH_2CH_3$

The resulting surface radicals could then act as initiation sites for polymerization from the diamond surface.

المنارة للاستشارات
www.manaraa.com

(3) 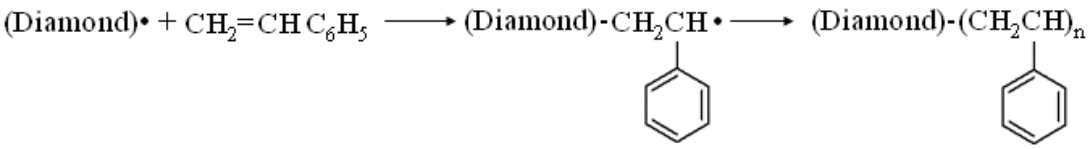

Condensation of surface radicals with peroxy radicals could also take place to terminate reactive surface sites.

(4) Diamond• + •$OC(CH_3)_2CH_2CH_3$ → Diamond-$OC(CH_3)_2CH_2CH_3$

(5) 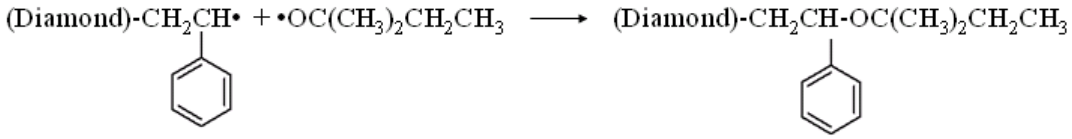

The presence of a bifunctional monomer, a crosslinker, should create additional surface sites for polymer grafting and ultimately lead to tethered polymer films.

In essence, I am demonstrating that the conditions of a typical radical polymerization of unsaturated monomers will produce polymer grafting at HTD or DTD surface in a single chemical step. After surface derivatization, polystyrene functionalized diamond may be sulfonated with sulfuric acid and acetic acid. Surface changes are followed by X-ray photoelectron spectroscopy (XPS), time-of-flight secondary ion mass spectrometry (ToF-SIMS) and diffuse reflectance Fourier transform infrared spectroscopy (DRIFT).

المنارة للاستشارات
www.manaraa.com

2.3 Experimental

2.3.1 Reagents

With the exception that all monomers were passed through an inhibitor-removing column prior to use, all chemicals were used as received as follows: toluene (spectra grade, Aldrich, St. Louis, MO); H_2SO_4 (95-98%, EMD, Gibbstown, NJ), HNO_3 (68-70%, EMD), acetic acid (99%, Mallinckrodt Chemicals, Phillipsburg, NJ), di-*tert*-amyl peroxide (97%, Aldrich); styrene (99%, inhibited with 50 ppm p-*tert*-butylcatechol, Aldrich); divinylbenzene (80%, remainder mostly 3- and 4-ethyl vinyl benzene, inhibited with 1000 ppm p-*tert*-butylcatechol, Aldrich); polystyrene (Aldrich).

The inhibitor-removing sorbent for removing *tert*-butylcatechol were obtained from Aldrich. The mixture gases, including 6% hydrogen in argon (99.999%) and 5% deuterium in argon (99.999%), were purchased from Airgas (Radnor, PA). 1.7 μm diamond powder was provided by U.S. Synthetic (Orem, UT).

2.3.2 Surface Modification and Characterization

Preparation of Deuterium-Terminated Diamond Powder.

Diamond powder was washed with mixed acid (90% H_2SO_4 + 10% HNO_3) at 80° C for 4 h and then rinsed with distilled water.[16] After drying, the clean diamond powder was treated in flowing 5% D_2 (or 6% H_2) in Ar at 900° C (the Mini-Mite Tube Furnace, model number TF55030A-1, Thermo Electron, Waltham, MA) for 28 h. *6% hydrogen or 5% deuterium in argon is not a flammable mixture, and therefore safer to work with than pure H_2 or D_2 gas.* During the hydrogenation/deuteration, the diamond powder was shaken twice to more evenly treat all surfaces of the powders and it was then cooled in

المنارة للاستشارات
www.manaraa.com

flowing 5% D_2 (or 6% H_2) in Ar. The resulting hydrogen/deuterium-terminated diamond powder was used as a starting material.

Treatment of Deuterium-Terminated Diamond Powder with Di-tert-amyl Peroxide, Divinylbenzene (DVB) and Styrene

A solution of di-*tert*-amyl peroxide (0.05 M), styrene (0.75 M), and a crosslinking agent, divinylbenzene (0.025 M), in toluene was bubbled with nitrogen for 30 min prior to addition of hydrogen/deuterium terminated diamond powder (0.5 g). Toluene is a good solvent for radical polymerizations because of its small chain transfer constant.[19] The temperature of the solution was then raised to 110°C. The solution was maintained at this temperature for 24 h with stirring under a reflux condenser, and continuously purged with a gentle stream of nitrogen gas over the surface of the solution. The diamond powder was then removed from solution, sonicated with toluene for 10 min, and filtered. This rinsing procedure was repeated five times. Finally, the diamond powder was dried in a vacuum oven.

Preparation of a Thin Polystyrene Film on Silicon Surfaces

Polystyrene (average Mw ~192,000) was dissolved in toluene at a concentration of 0.5% (w/w). Polystyrene thin films were obtained by spin coating silicon shards with this solution.

Sulfonation of Polystyrene-Functionalized Diamond Powder

The method of polystyrene-divinylbenzene resin sulfonation described by Dumont

المنارة للاستشارات
www.manaraa.com

and Fritz was followed.[20, 21] Polystyrene-functionalized diamond powder (2 g) was slurried in 5 mL acetic acid followed by addition of concentrated sulfuric acid, which had been cooled in an ice bath. The reaction temperature was then set at 90° C for 5 h, after which the slurry was poured over ice to quench the reaction. The diamond powder was filtered and washed with water until the pH of the water was neutral.

Characterization of the Diamond Surfaces

Time-of-flight secondary ion mass spectrometry (ToF-SIMS) was performed with an ION-TOF ToF-SIMS Ⅳ instrument using monoisotopic 25 keV $^{69}Ga^{+}$ ions. X-ray photoelectron spectroscopy was performed with an SSX-100 X-ray photoelectron spectrometer with a monochromatic Al K_{α} source and a hemispherical analyzer. An electron flood gun was employed for charge compensation. Survey scans as well as narrow scans were recorded with an 800×800 μm^2 spot. The diamond surface was characterized by a Magna-IR 560 spectrometer from Nicolet (Madison, WI). The DRIFT spectra were obtained over the range of 400-4000 cm^{-1}. For each spectrum, 64 scans were collected at a resolution of 4 cm^{-1}. Spectra are presented with Kubelka-Munk units.

2.4 Results

2.4.1 Reaction of DTD with DTAP and Unsaturated Monomers with and without a Crosslinker

Figures 2.1 A1 and A2 show the diffuse reflectance Fourier transform infrared (DRIFT) spectra of deuterium-terminated diamond reacted with styrene in the presence

المنارة للاستشارات
www.manaraa.com

and absence of di-*tert*-amyl peroxide. Figures 2.1 B1 and B2 show the infrared spectra of the same reactions with DVB. In both cases, C-H stretches assigned to aromatic rings (3000-3200 cm^{-1}) and alkyl chains (2800-3000 cm^{-1}) appear after the reaction, which are not observed in the deuterium-terminated diamond powder (See Figures 2.1 A1-a and B1-a), the deuterium-terminated diamond powder shows a very clean baseline. The IR spectrum of polystyrene is indicated in Figure 2.1 as a comparision for the functionalized diamond powder (See Figures 2.1 A1-d, A2-d, B1-d and B2-d). In addition to the aromatic and aliphatic C-H stretches, the characteristic ring vibrations of polystyrene at 1450 cm^{-1}, 1500 cm^{-1} and 1600 cm^{-1} appear on DTD after reaction.

For the control reactions of deuterium-terminated diamond powder with styrene or with styrene and DVB without peroxide initiator, DRIFT showed either much smaller or no aromatic C-H stretches (3000-3200 cm^{-1}) and little or no characteristic peaks from polystyrene at 1450 cm^{-1}, 1500 cm^{-1} and 1600 cm^{-1}. These results indicate a small amount of polystyrene adsorption in these control reactions on diamond surfaces. However, these control reactions prove the point that the surface reaction is greatly limited when the radical initiator is absent. These spectra also show that the presence of DVB increases the amount of polystyrene that ends up on the diamond surface. This fact is underscored by the ratio of the aromatic C-H stretches to the aliphatic C-H stretches, which is higher when DVB is present.

المنارة للاستشارات
www.manaraa.com

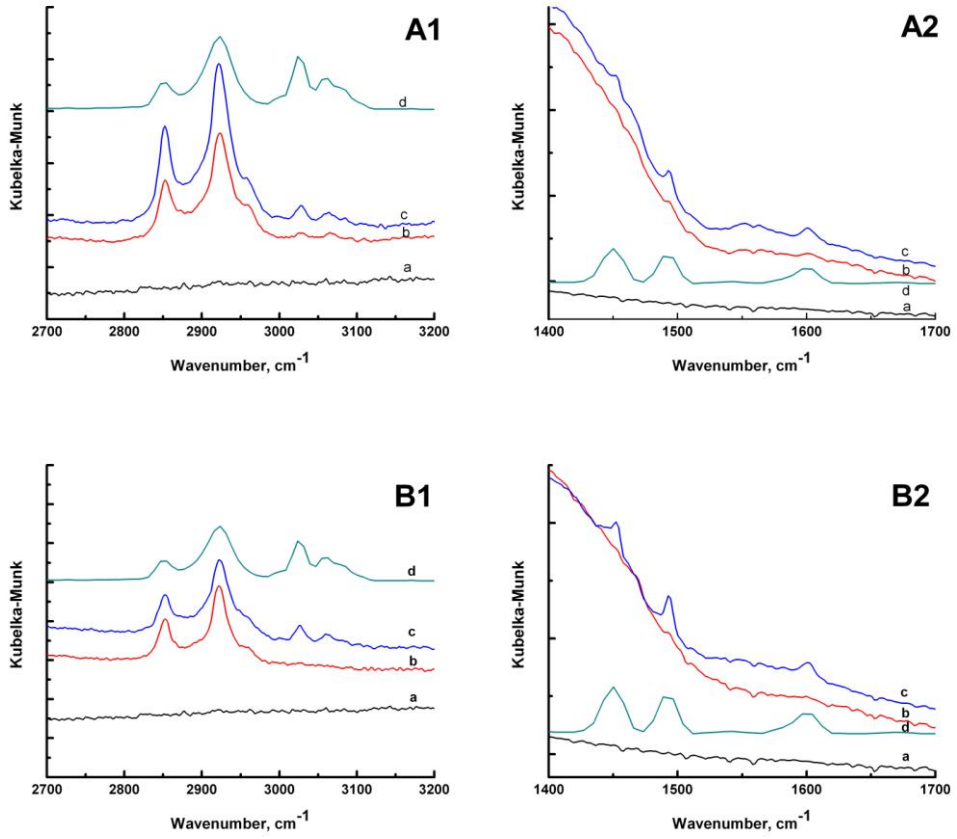

Figure 2.1. A1 and A2: (a) DRIFT spectrum of deuterium-terminated diamond powder, (b) DRIFT spectrum of a control experiment of deuterium-terminated diamond powder reacted with styrene, without di-tert-amyl peroxide, for 1 day at 110° C, (c) DRIFT spectrum of deuterium-terminated diamond powder reacted with styrene and di-tert-amyl peroxide for 1 day at 110° C and (d) IR spectrum of polystyrene. B1 and B2: (a) DRIFT spectrum of deuterium-terminated diamond powder, (b) DRIFT spectrum of a control experiment of deuterium-terminated diamond powder reacted with styrene/DVB, without di-tert-amyl peroxide, for 1 day at 110° C and (c) DRIFT spectrum of deuterium-terminated diamond powder reacted with styrene/DVB and di-tert-amyl peroxide for 1 day at 110° C and (d) IR spectrum of polystyrene.

المنارة للاستشارات
www.manaraa.com

Figure 2.2 shows positive ion ToF-SIMS spectra of deuterium-terminated diamond (DTD) and DTD functionalized by styrene or by styrene/DVB under peroxide initiation. While there are some hydrocarbon peaks in the ToF-SIMS spectra of deuterium-terminated diamond, such hydrocarbon contamination is common on most materials. However, after reaction with styrene and DTAP, a series of hydrocarbon peaks that are characteristic of polystyrene (marked by a red star) appears (See Figures 2.2b and d). The positive ion ToF-SIMS spectra of deuterium-terminated diamond after reaction with styrene/DVB showed these characteristic signals of polystyrene in an even more dominant fashion (See Figures 2.2b and c). The relative intensities of these characteristic peaks are also in quite good agreement with those of the standard polystyrene film well. This is especially true for the highly characteristic higher mass ions at m/z 103, 105, 115, 117 and 128. In contrast, in the spectrum of deuterium-terminated diamond powder, there is little but noise in the high mass region. These SIMS results are in good agreement with the FTIR results shown in Figure 2.1.

In ToF-SIMS negative ion spectra, there is an obvious deuterium peak for the deuterium-terminated diamond. After the reaction with styrene or with styrene/DVB under peroxide initiation, the ratio of H^-/D^- is increased from 0.9 (before) to 2.4-6.6, presumably because deuterium atoms are abstracted by preoxy radicals allowing polystyrene growth on the diamond surfaces. The ratio of C^-/O^- is increased from 2.1 for polystyrene functionalized diamond to 3.0 for polystyrene-DVB fuctionalized diamond, presumably because more carbon is introduced by the functionalization with polystyrene-DVB.

All of these diamond materials were also probed by XPS. The O1s/C1s ratios as

المنارة للاستشارات
www.manaraa.com

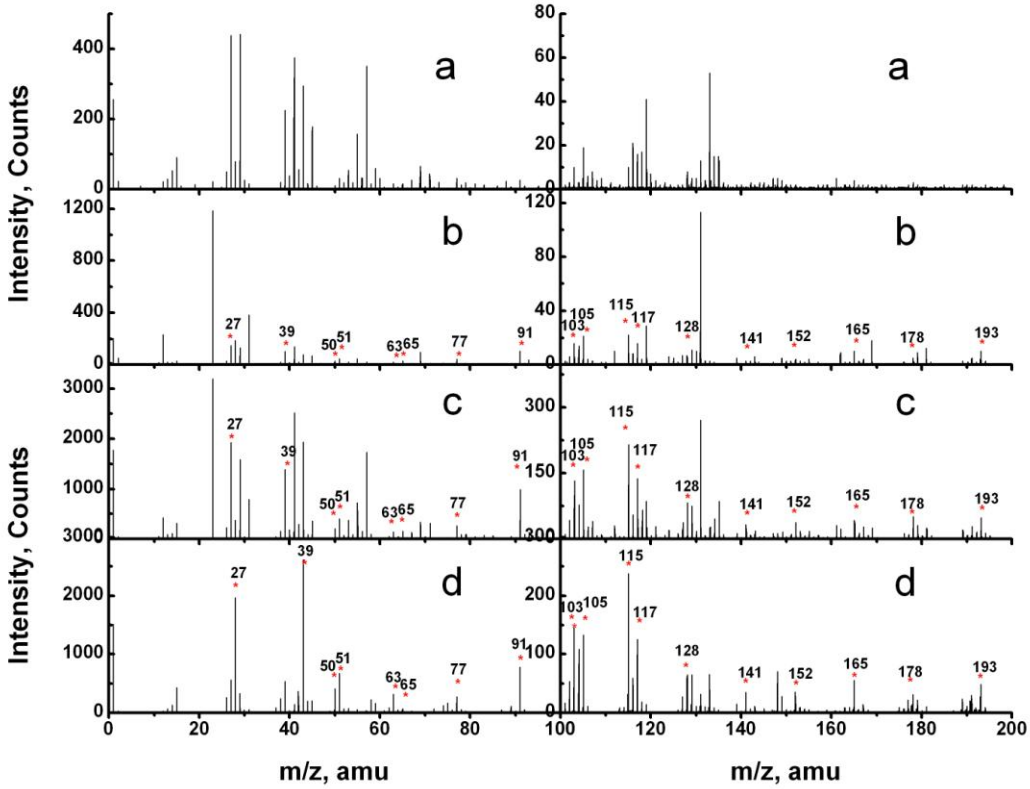

Figure 2.2. ToF-SIMS positive ion spectra from 0-100 amu and 100-200 amu: (a) deuterium-terminated diamond powder (b) deuterium-terminated diamond powder reacted with styrene and di-tert-amyl peroxide (c) deuterium-terminated diamond powder reacted with styrene, di-tert-amyl peroxide and DVB, and (d) polystyrene thin film spin-coated onto a silicon surface.

المنارة للاستشارات
www.manaraa.com

measured in narrow scans decrease from 0.162 for diamond functionalized by polystyrene and DTAP to 0.088 for diamond functionalized with polystyrene/DVB and DTAP. Like the IR and ToF-SIMS characterization, these results are also consistent with a thicker polymer film formed on diamond when DVB is present during the reaction.

Hence, DRIFT, ToF-SIMS and XPS results all suggest that abstraction of deuterium atoms from the diamond surface by the radical species derived from di-*tert*-amyl peroxide in the presence of a monomer, styrene, leads to polymerization on the diamond surface. DVB appears to act as a crosslinker, and as such it can help to increase the thickness of polystyrene on the diamond surface.

2.4.2. Sulfonation of Polystyrene-Functionalized Diamond Powder

I now show that polystyrene (PS) or polystyrene-divinylbenzene (PS-DVB) functionalized diamond powder can be sulfonated by acetic acid and concentrated sulfuric acid heated to 90° C for 5 h.[20, 21] Figure 2.3b shows XPS of sufonated diamond powder that contains an obvious sulfur signal, where no sulfur signal was discernable by XPS prior to sulfonation (see Figure 2.3a). The sulfur-to-carbon ratio on these materials, measured in the S2p and C1s XP narrow scans, was found to be 0.021 and 0.036 for the polystyrene and polystyrene/DVB diamond powders, respectively. The increased sulfur-to-carbon ratio also suggests that thicker films are formed when the crosslinker (DVB) is used. The compositions of these diamond surfaces as measured by XPS are shown in Table 2.1.

The hydrogen-terminated diamond particles were functionalized using the same procedure and the similar results were obtained.

المنارة للاستشارات
www.manaraa.com

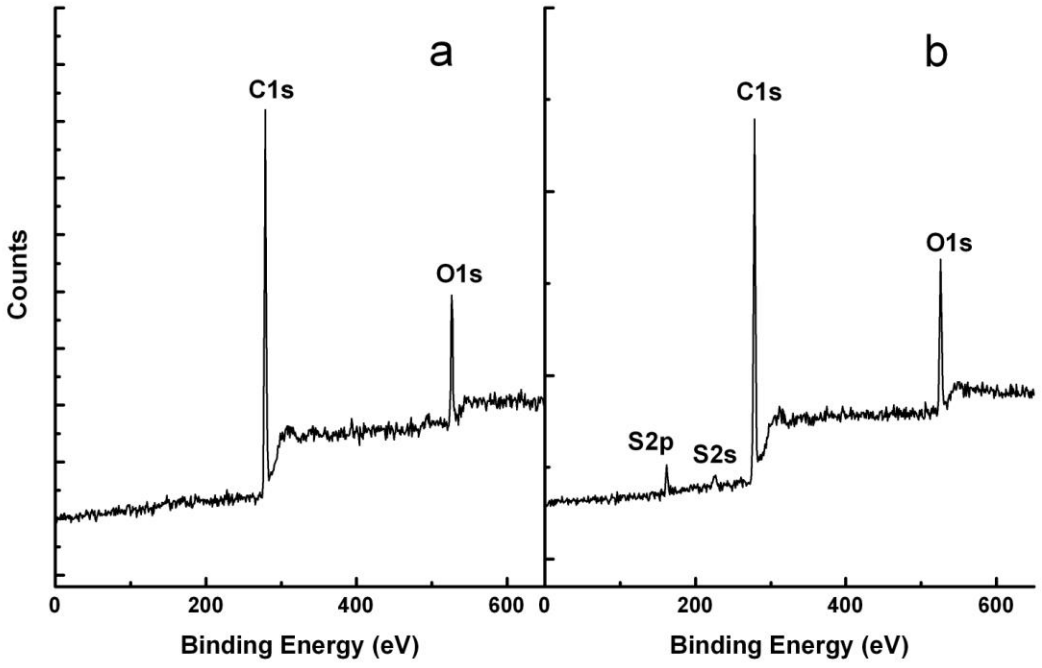

Figure 2.3. XPS survey spectra of diamond powders: (a) polystyrene-functionalized diamond powder and (b) sulfonated polystyrene/DVB-fuctionalized diamond powder.

المنارة للاستشارات
www.manaraa.com

Table 2.1. Compositions (atom percentage of elements detected by XPS) of the surfaces of diamond powders.

	C%	O%	S%
Polystyrene(PS)	86.7	13.3	
PS-sulfonation	86.7	11.5	1.8
PS-DVB-sulfonation	81.5	15.6	2.9

المنارة للاستشارات
www.manaraa.com

These polystyrene-modified and sulfonated polystyrene-modified diamonds can be used as reversed and strong cation exchange stationary phases, respectively for solid phase extraction (SPE) (See Chapter 4).

2.5 Conclusions

I have demonstrated a new method for effectively growing polymers in a direct fashion on deuterium-/hydrogen-terminated diamond powder using a simple, one-step procedure. The surface radicals that should be produced at the diamond surface appear to react with monomers, crosslinkers, and perhaps growing polymer chains in solution to tether them to the surface of the diamond power. The incorporation of some crosslinking in these adsorbed polymer films through crosslinking should increase both film thickness and chemical stability. Some non-specific adsorption of the polymer also seems to occur. The one-step method for growing polymers on deuterium-/hydrogen-terminated diamond powders shown here should provide a simple, inexpensive way to covalently modify diamond powder with tailored polymers produced from a variety of known monomers.

2.6 References

(1) Strother, T.; Knickerbocker, T.; Russell, J. N. J.; Butler, J. E.; Smith, L. M.; Hamers, R. J. *Langmuir* **2002**, *18*, 968-971.

(2) Wang, G. T.; Bent, S. F.; Russell, J. N. J.; Butler, J. E.; D'Evelyn, M. P. *Journal of the American Chemical Society* **2000**, *122*, 744-745.

(3) Tsubota, T.; Hirabayashi, O.; Ida, S.; Nagaoka, S.; Nagata, M.; Matsumoto, Y.

المنارة للاستشارات
www.manaraa.com

Diamond and Related Materials **2002**, *11*, 1374-1378.

(4) Tsubota, T.; Hirabayashi, O.; Ida, S.; Nagaoka, S.; Nagata, M.; Matsumoto, Y. *Physical Chemistry Chemical Physics* **2002**, *4*, 806-811.

(5) Ida, S.; Tsubota, T.; Hirabayashi, O.; Nagata, M.; Matsumoto, Y.; Fujishima, A. *Diamond and Related Materials* **2003**, *12*, 601-605.

(6) Tsubota, T.; Ida, S.; Hirabayashi, O.; Nagaoka, S.; Nagata, M.; Matsumoto, Y. *Physical Chemistry Chemical Physics* **2002**, *4*, 3881-3886.

(7) Ida, S.; Tsubota, T.; Tanii, S.; Nagata, M.; Matsumoto, Y. *Langmuir* **2003**, *19*, 9693-9698.

(8) Tsubota, T.; Tanii, S.; Ida, S.; Nagata, M.; Matsumoto, Y. *Diamond and Related Materials* **2004**, *13*, 1093-1097.

(9) Tsubota, T.; Tanii, S.; Ida, S.; Nagata, M.; Matsumoto, Y. *Physical Chemistry Chemical Physics* **2003**, *5*, 1474-1480.

(10) Gu, H.; Su, X. D.; Loh, K. P. *J. Phys. Chem. B.* **2005**, *109*, 13611-13618.

(11) Steenackers, M.; Lud, S. Q.; Niedermeier, M.; Bruno, P.; Gruen, D. M.; Feulner, P.; Stutzmann, M.; Garrido, J. A.; Jordan, R. *J. Am. Chem. Soc.* **2007**, *129*, 15655-15661.

(12) Cheng, J.; He, J.; Li, C.; Yang, Y. *Chem. Mater.* **2008**, *20*, 4224-4230.

(13) Saini, G.; Yang, L.; Lee, M. L.; Dadson, A.; Vail, M. A.; Linford, M. R. *Anal. Chem.* **2008**, *80*, 6253-6259.

(14) Kong, X. L.; Huang, L. C. L.; Liau, S.-C. V.; Han, C.-C.; Chang, H.-C. *Anal. Chem.* **2005**, *77*, 4273-4277.

(15) Blake, R. B.; Pei, L.; Yang, L.; Lee, M. V.; Conley, H. J.; Davis, R. C.; Shirahata, N.;

المنارة للاستشارات
www.manaraa.com

Linford, M. R. *Macromolecular rapid communications* **2008**, *29*, 638-644

(16) Ando, T.; Ishii, M.; Kamo, M.; Sato, Y. *J. Chem. Soc. Faraday Trans.* **1993**, *89*, 1783-1789.

(17) Jiang, T.; Xu, K.; Ji, S. *Journal of the Chemical Society, Faraday Transactions* **1996**, *92*, 3401-3406.

(18) *Handbook of Chemistry and Physics*, 81 ed.; CRC Press: Boca Raton, 2000.

(19) *Polymer Handbook*, 4th ed.; John Wiley & Sons: New York, 1999.

(20) Fritz, J. S.; Dumont, P. J.; Schmidt, L. W. *Journal of Chromatography, A* **1995**, *691*, 133-140.

(21) Dumont, P. J.; Fritz, J. S. *Journal of Chromatography, A* **1995**, *691*, 123-131.

المنارة للاستشارات
www.manaraa.com

Chapter 3 Direct Polymer Attachment and Growth on Hydrogen-Terminated Diamond Substrates with Atom Transfer Radical Polymerization (ATRP)

3.1 Abstract

Atom transfer radical polymerization (ATRP) is performed to grow polymer films on diamond surfaces. The ATRP initiator could be introduced in two ways, which are the reaction of hydrogen- or deuterium-terminated diamond with bromine under light and the reaction of piranha-treated diamond with 2-bromoisobutyryl bromide. Polystyrene (PS) or cross-linked polystyrene (PS-DVB) can be grown on both types of powders by ATRP. Thicker polymer layers are obtained when a crosslinking agent, such as divinylbenzene is employed as part of the monomer mixture. Sulfonation of these phenyl phases is demonstrated with a H_2SO_4/CH_3COOH mixture.

3.2 Introduction

Atom transfer radical polymerization (ATRP) is a well-developed, controlled, "living" radical polymerization, which has been applied to surfaces. Unlike other polymerization methods, it is easy with ATRP to control polymer thickness, composition, polydispersity, homogeneity and surface density. In addition, ATRP can be performed under ambient conditions and it does not require stringent experimental conditions. ATRP

المنارة للاستشارات
www.manaraa.com

has been previously used to modify various surfaces successfully, such as silica,[1] silicon,[2-8] gold,[9-11] and other porous substrates.[12, 13] However, there are only two reports of the functionalization of diamond (ultrananocrystalline diamond film and nanodiamond) by ATRP.[14-17] Matrab and his coworkers[14] modified an ultrananocrystalline diamond thin film by electrochemical reduction to introduce an ATRP initiator, followed by growth of poly(methyl methacrylate) and polystyrene brushes. Li, et al. reported synthesis of methacrylate polymers on both ultrananocrystalline diamond thin films and nanodiamond particles by ATRP.[16, 17]

Here, I report atom transfer radical polymerization (ATRP) to grow polystyrene from diamond particle surfaces. To do this, an ATRP initiator must first be immobilized on a diamond surface. I investigated two methods to immobilize the requisite initiators. One method is to immerse hydrogen-terminated diamond in bromine under illumination (visible and UV). The other method is to react piranha-cleaned diamond with 2-bromoisobutyryl bromide. Polystyrene (PS) can be grown on the resulting diamond powders by ATRP. Thicker polymer layers are obtained when a crosslinking agent, such as divinylbenzene is part of the monomer mixture. These materials have excellent stability in both highly acidic and highly basic media, and sulfonation is demonstrated with an H_2SO_4/CH_3COOH mixture. Surface characterization was performed by X-ray photoelectron spectroscopy (XPS), time-of-flight secondary ion mass spectrometry (ToF-SIMS) and diffuse reflectance Fourier transform infrared spectroscopy (DRIFT).

المنارة للاستشارات
www.manaraa.com

3.3 Experimental Section

3.3.1 Reagents

With the exception that all monomers were passed through an inhibitor-removing column prior to use, all chemicals were used as received as follows: tetrahydrofuran, methanol and glacial acetic acid (spectra grade, Mallinckrodt Chemicals, Phillipsburg, NJ); H_2SO_4 (95-98%, EMD, Gibbstown, NJ), HNO_3 (68-70%, EMD), H_2O_2 (30%, Fisher, Fair Lawn, NJ), 2-bromoisobutyryl bromide (98%, Aldrich, St. Louis, MO), copper (I) bromide (CuBr, 98% in purity, Aldrich), 2,2'-bipyridine (99% in purity, Aldrich), bromine (reagent, Aldrich), dry pyridine, styrene (spectrum grade, 99%, inhibited with 50 ppm p-*tert*-butylcatechol, Aldrich); divinylbenzene (DVB) (80%, remainder mostly 3- and 4-ethyl vinyl benzene, inhibited with 1000 ppm p-*tert*-butylcatechol, Aldrich): The inhibitor-removing sorbents for removing MEHQ and *tert*-butylcatechol were obtained from Aldrich. The mixture gases including 6% hydrogen in argon (99.999% pure) were purchased from Airgas (Radnor, PA). Diamond powder (70 μm) was provided by U.S. Synthetic (Orem, UT).

3.3.2 Surface Modification

Preparation of Hydrogen-Terminated Diamond Powder.

Diamond powder was used as substrate. The diamond powder was washed with mixed acid (90% H_2SO_4 + 10% HNO_3) at 80° C for 4 h and then rinsed with distilled water.[18] After drying, the diamond powder was treated in flowing 6% H_2 (in Ar) gas at 900° C (Mini-Mite tube furnace, model number is TF55030A-1, Thermo Electron, Waltham, MA) for 28 h. *6% hydrogen (in Ar) is not a flammable mixture, and therefore*

المنارة للاستشارات
www.manaraa.com

safer to work with than pure H_2 gas. During the reaction, the diamond powder was shaken twice to evenly hydrogenate the surface and it was then cooled in flowing 6% H_2 (in Ar). The resulting hydrogen-terminated diamond powder was used as a starting material.

ATRP Initiators Immobilized on Diamond Surfaces by Two Methods

I investigated two ways to immobilize the ATRP initiators. One is to immerse the hydrogen-terminated diamond in bromine under illumination (250－600 nm) and nitrogen gas. In the second way, the diamond powder was cleaned in piranha solution (70% H_2SO_4:30% conc. H_2O_2) at 100°C for 1 h, and then thoroughly washed with deionized water. Clean, dry, untreated diamond powder was then slurried in a dry THF solution containing 0.5 M 2-bromoisobutyryl bromide (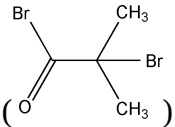) and 0.55 M pyridine. After 24 h, diamond powder was washed thoroughly with methanol and deionized water.

Polymerization on the Diamond Powder

Diamond particles terminated with ATRP initiator (3 g) and CuBr (0.26 g) were placed in a flask and degassed with nitrogen. Subsequently, degassed 2,2'-bipyridine (bipy) (0.58 g) in 10.0 g styrene (or 4 g styrene and 6 g divinylbenzene) and 10 mL 1,4-dioxane was added. The mixture was stirred with a magnetic stir bar, heated to 110° C under nitrogen, and the reaction was allowed to proceed for 19 h. The particles were washed and sonicated with THF and methanol/glacial acetic acid (95/5) until the solvent was colorless.

المنارة للاستشارات
www.manaraa.com

Sulfonation of Polystyrene-Functionalized Diamond Powder

The method of polystyrene-divinylbenzene resin sulfonation described by Dumont and Fritz was followed.[19, 20] Polystyrene-functionalized diamond powder (2 g) was slurried in 5 mL acetic acid, cooled with an ice water bath, after which concentrated sulfuric acid was added. The reaction temperature was then set to 90° C for 5 h, after which the reaction mixture was poured over ice to quench the reaction. The diamond powder was filtered and washed with water until the pH of the water was neutral.

Characterization of the Diamond Surfaces

X-ray photoelectron spectroscopy (XPS) was performed with an SSX-100 X-ray photoelectron spectrometer with a monochromatic Al K_{α} source and a hemispherical analyzer. An electron flood gun was employed for charge compensation. Survey scans as well as narrow scans were recorded with an 800×800 μm spot. Time-of-flight secondary ion mass spectrometry (ToF-SIMS) was performed with an ION-TOF ToF-SIMS Ⅳ instrument using monoisotopic 25 keV $^{69}Ga^{+}$ ions. The diamond surface was characterized with a Magna-IR 560 spectrometer from Nicolet (Madison, WI). DRIFT spectra were obtained from 400-4000 cm^{-1}. For each spectrum, 64 scans were collected at a resolution of 4 cm^{-1}. Spectra are presented with Kubelka-Munk units.

المنارة للاستشارات
www.manaraa.com

3.4 Results and Discussion

3.4.1 Overview of Atom Transfer Radical Polymerization (ATRP) on Diamond Followed by Sulfonation

Two methods have been considered for immobilizing an ATRP initiator on diamond surfaces. One is photoreaction under bromine; the other is nucleophilic addition/elimination to tether 2-bromoisobutyryl bromide, an acid bromide, which is performed according to the procedure of Carlmark and Malmstrom.[21, 22] Irradiation of bromine causes rupture of Br-Br bonds to produce two bromine radicals. Highly reactive bromine atoms should abstract hydrogen atoms from the diamond surface, especially tertiary hydrogens, to form HBr, thereby producing carbon-centered radicals at the diamond surface. This surface radical will then abstract a bromine atom from a bromine molecule to form the end product and a new bromine radical. For the nucleophilic addition/elimination reaction under 2-bromoisobutyryl bromide, there is nucleophilic attack on the fairly positive carbonyl carbon by a lone pair of electrons on an oxygen atom of a hydroxyl group on the diamond surface. To the best of my knowledge, a tertiary bromide is generally needed for ATRP.[23] Such a tertiary bromide (≡C-Br) should be obtained after both the photoreaction and chemisorption of 2-bromoisobutyryl bromide.

The resulting diamond powders react with styrene or styrene/DVB, Cu(I)Br and bipyridine at 110° C by ATRP. The mechanism of ATRP is shown in Figure 3.1. After this reaction, polystyrene or polystyrene-divinylbenzene functionalized diamond powders are sulfonated under concentrated sulfuric acid and acetic acid (Figure 3.2).

المنارة للاستشارات
www.manaraa.com

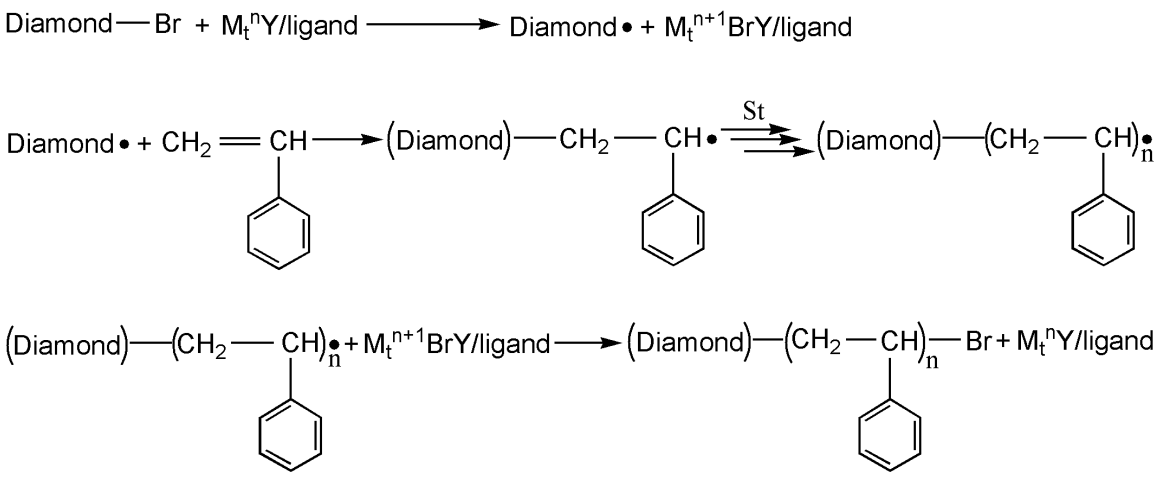

Figure 3.1. Mechanism of atom transfer radical polymerization (ATRP) on diamond.

المنارة للاستشارات
www.manaraa.com

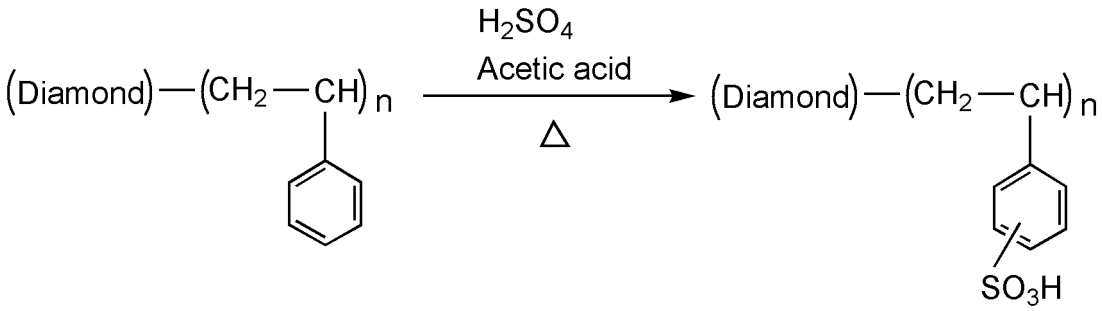

Figure 3.2. Sulfonation of polystyrene-modified diamond powder.

المنارة للاستشارات
www.manaraa.com

3.4.2 Immobilization of the ATRP Initiator on the Diamond Powder Surfaces

After modification of hydrogen- or oxide-terminated diamond with an ATRP initiator, XPS showed a bromine signal, which was not present before the reaction (See Figure 3.3). ToF-SIMS negative ion spectra also showed obvious signals from $^{79}Br^-$ and $^{80}Br^-$ after the reactions (See Figure 3.4). These two techniques confirm bromine immobilization via both the photoreaction and the two-electron chemistry. For the brominated diamond powder, which was obtained when the oxidized diamond reacted with 2-bromoisobutyryl bromide, XPS shows more oxygen (22.4% oxygen) compared to the brominated diamond powder after the photoreaction (8.8% oxygen). These results are consistent with the introduction of carbonyl groups from 2-bromoisobutyryl bromide. The oxygen signals in the negative ion ToF-SIMS spectra are also consistent with the XPS results. After the reaction with 2-bromoisobutyryl bromide, the signals due to O^- and OH^- in the negative ion spectra (See Figure 3.4b) are larger than the hydrocarbon peaks, *e.g.* C^-, CH^-, C_2^- and C_2H^-, compared to the diamond brominated via the photoreaction (See Figure 3.4a). 2-Bromoisobutyryl bromide introduces oxygen on the diamond surface while the photoreaction is under nitrogen gas, so (at least in theory) no oxygen can be introduced.

The compositions of the diamond surfaces are shown in Table 3.1. The bromine atom percent by photoreaction is 1% while the bromine atom percent after the nucleophilic addition/elimination reaction is 0.3%. The difference in bromine atom percent indicates that the photoreaction is more efficient than the nucleophilic addition/elimination reaction as a means of immobilizing an ATRP initiator. In the negative ion ToF-SIMS spectra, the ratios of the Br peaks (^{79}Br + ^{81}Br)/(all peaks) from 0-350 m/z for the diamond powders

المنارة للاستشارات
www.manaraa.com

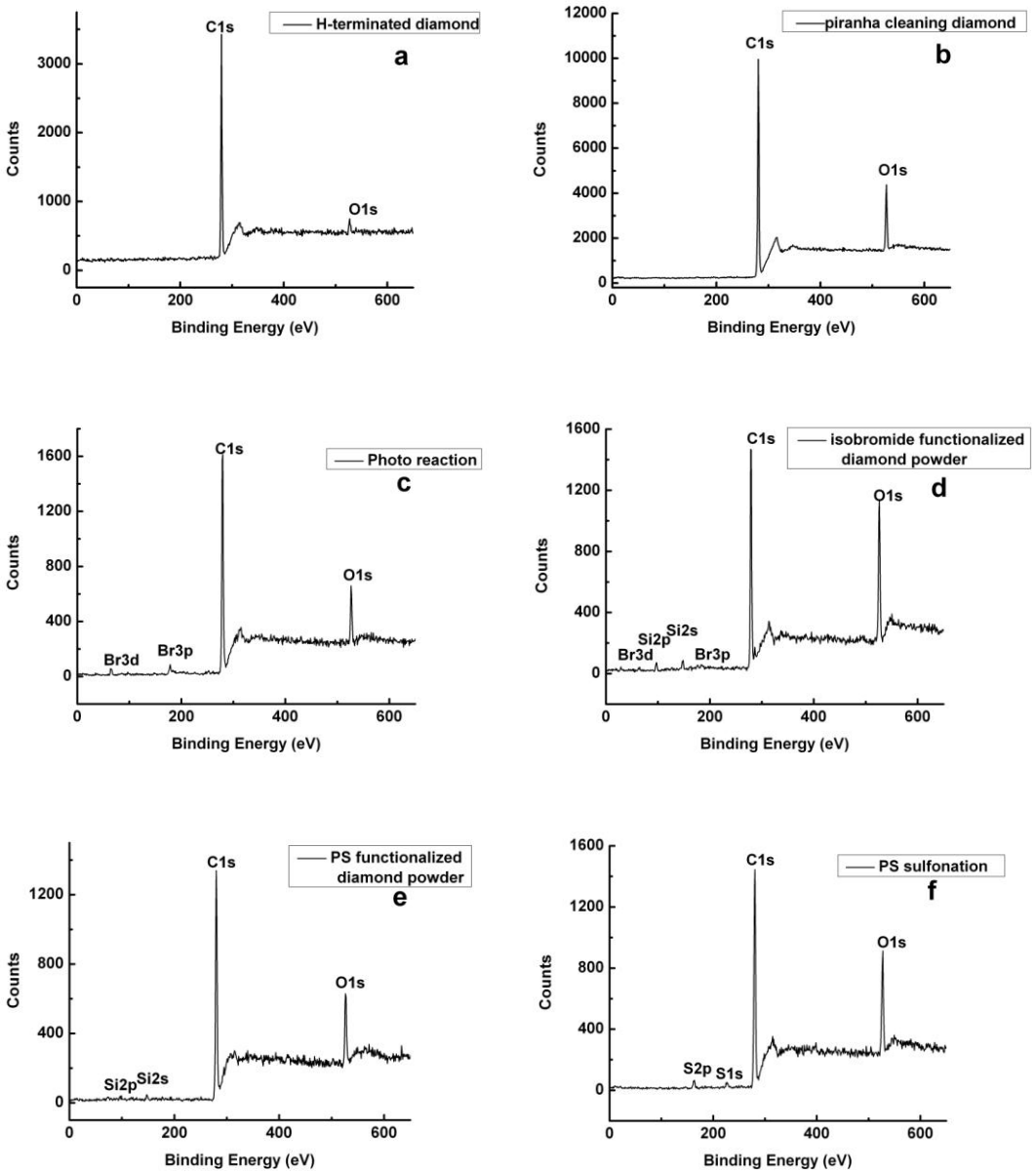

Figure 3.3. XPS of diamond powders. a) hydrogen-terminated diamond, b) piranha treated diamond, used as received diamond that had been cleaned, c) hydrogen-terminated diamond reacted with bromine under light, d) piranha treated diamond reacted with isobromide, e) brominated diamond functionalized with polystyrene by ATRP and f) sulfonated polystyrene diamond powder.

المنارة للاستشارات
www.manaraa.com

A:

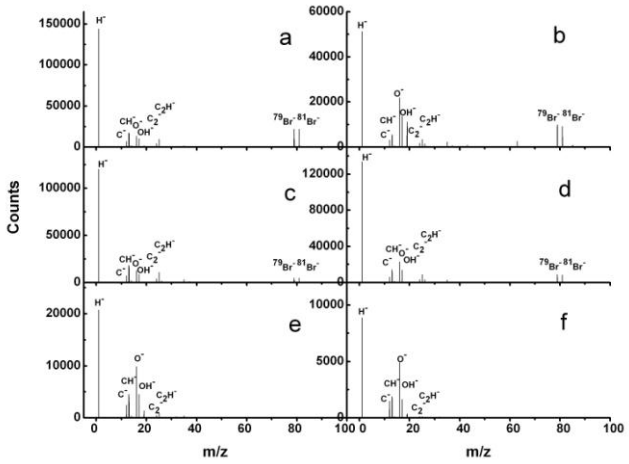

B:

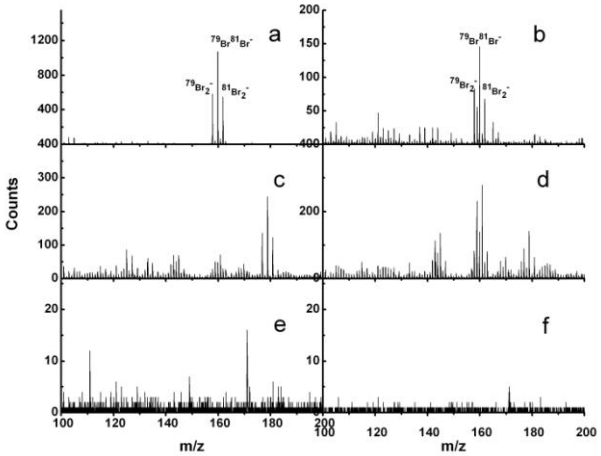

Figure 3.4. ToF-SIMS negative ion spectra. A: m/z 0-100 and B: m/z 100-200. a) diamond-brominated by photoreaction, b) diamond-brominated by the nucleophilic addition/elimination reaction, c) diamond functionalized with polystyrene by ATRP (on photoreacted/brominated diamond), d) diamond functionalized with polystyrene by ATRP on 2-bromoisobutyryl bromide modified diamond, e) sulfonated, polystyrene-functionalized diamond (on photoreacted/brominated diamond) and f) sulfonated, polystyrene functionalized diamond made by ATRP on 2-bromoisobutyryl bromide modified diamond.

المنارة للاستشارات
www.manaraa.com

Table 3.1. Compositions (atom percentage of elements detected by XPS) of the surfaces of diamond powders by XPS.

	C (%)	O (%)	Br (%)	S (%)	Si (%)
Raw diamond	87.5	12.5			
H-terminated diamond	97.2	2.8			
Brominated diamond (photoreaction)	90.2	8.8	1.0		
Piranha treated diamond	77.6	22.4			
Brominated diamond (isobromide)	74.4	21.8	0.3		3.5
Polystyrene functionalized diamond	86.7	11.8			1.5
Sulfonated diamond	82.5	15.7		1.8	

المنارة للاستشارات
www.manaraa.com

are consistent with XPS results. These ratios of photo reacted and nucleophilic addition/elimination reacted diamond are 0.31 and 0.24, respectively.

3.4.3 Polymerization on the Diamond Surface by ATRP

After the introduction of an ATRP initiator, both types of brominated diamond powders were treated with styrene or a mixture of styrene and DVB, Cu(I)Br and bipyridine at 110ºC. After the ATRP reaction, XPS of the diamond brominated with 2-bromoisobutyryl bromide showed a significant reduction in the oxygen signal (See Figures 3.3d and e), *i.e.*, the ratio of oxygen to carbon by XPS decreased from 0.29 to 0.14. This result is consistent with polystyrene growth on the diamond surface, which represents an increase in the fraction of carbon at the diamond surface and probably attenuation of O1s electrons from the oxidized diamond surface as well. The small silicon signal seen by XPS of polystyrene-functionalized diamond is probably a result of diamond particles scratching the glassware used in the reaction. Table 3.1 shows the compositions derived from XPS of all of the diamond surfaces.

ToF-SIMS positive ion spectra of polystyrene-functionalized diamond powders made by ATRP with both types brominated surfaces are very similar to the spectra of polystyrene-functionalized diamond obtained previously by peroxide activation and spin-coated polystyrene films on silcon (See Chapter 2). Numerous hydrocarbon peaks in the diamond modified with polystyrene by ATRP match the characteristic peaks of pure polystyrene, especially in the highly characteristic high mass region, *e.g.*, m/z 103, 105, 115, 117 and 128 (See Figures 3.5c and d). These results demonstrate that diamond brominated by both methods could be functionalized with polystyrene by ATRP. Prior to

المنارة للاستشارات
www.manaraa.com

A:

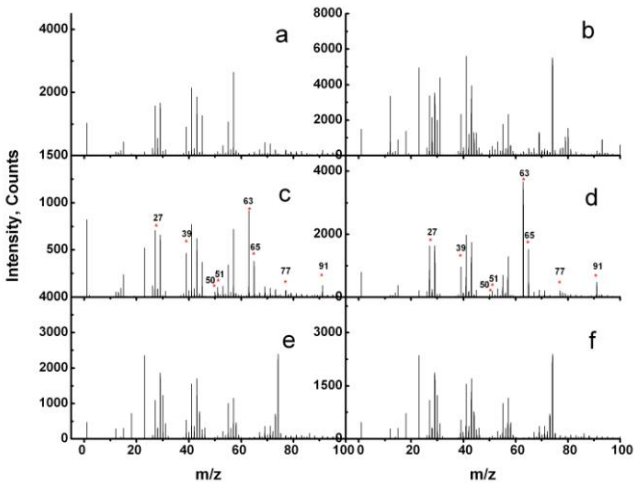

B:

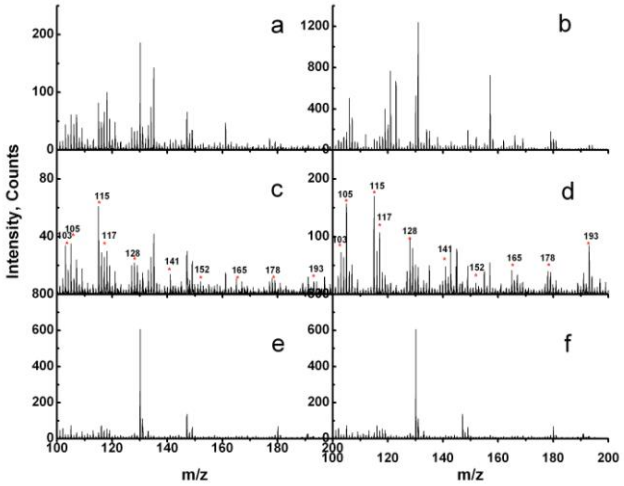

Figure 3.5. ToF-SIMS positive ion spectra. A: m/z 0-100 and B: m/z 100-200. a) diamond-brominated by photoreaction, b) diamond-brominated by nucleophilic addition/elimination reaction, c) polystyrene functionalized diamond made by ATRP on photoreacted Br_2/diamond, d) polystyrene functionalized diamond made by ATRP on 2-bromoisobutyryl bromide reacted diamond, e) sulfonated polystyrene-functionalized diamond (ATRP, photoreaction) and f) sulfonated polystyrene functionalized diamond (ATRP, 2-bromoisobutyryl bromide).

المنارة للاستشارات
www.manaraa.com

ATRP, characteristic polystyrene peaks, such as 103, 105, 115, 117 and 128, are not found in the ToF-SIMS spectra. Negative ion ToF-SIMS spectra also indicate that diamond surfaces can be functionalized using ATRP. After polystyrene growth from both types of brominated diamond, the ratio of the bromine peaks to the hydrocarbon peaks decreases significantly as there appears to be more hydrocarbon at the surfaces (See Figures 3.5a, b, c and d). This supposition is consistent with the increase in carbon in the ToF-SIMS spectra after ATRP (See Table 3.2). Since ToF-SIMS is more sensitive to halogens than XPS, especially in the negative ion mode, the bromine signal can still be seen in ToF-SIMS after ATRP, while it can no longer be observed by XPS. Both positive and negative ion ToF-SIMS spectra suggest polystyrene growth on diamond powder by ATRP.

The infrared spectra of both types of brominated diamond after ATRP showed C-H stretching peaks from aromatic rings (3000-3200 cm^{-1}) and alkyl chains (2800-3000 cm^{-1}) (See Figures 3.6d, e and f). Infrared spectra of unreacted hydrogen-terminated diamond powder and piranha-cleaned diamond powder (See Figures 4b and c) showed no C-H stretching peaks of aromatic rings (3000-3200 cm^{-1}), or other characteristic peaks of polystyrene. IR spectra of unreacted hydrogen-terminated diamond powder only showed the C-H stretches of this material. Compared to the standard IR spectrum of polystyrene (See Figure 3.6a), most of other peaks in the spectra matched very well, including the monobenzene peak at 700 cm^{-1} and the other characteristic peaks at 1450 cm^{-1}, 1500 cm^{-1} and 1600 cm^{-1} (See Figures 3.6a, d, e and f), which are assigned as combined ring vibrations. Polystyrene-DVB functionalized diamond powder made by ATRP has larger peaks at 1450 cm^{-1}, 1500 cm^{-1} and 1600 cm^{-1} than polystyrene functionalized diamond powder made without the crosslinker (See Figures 3.6e and f). These results suggest that

المنارة للاستشارات
www.manaraa.com

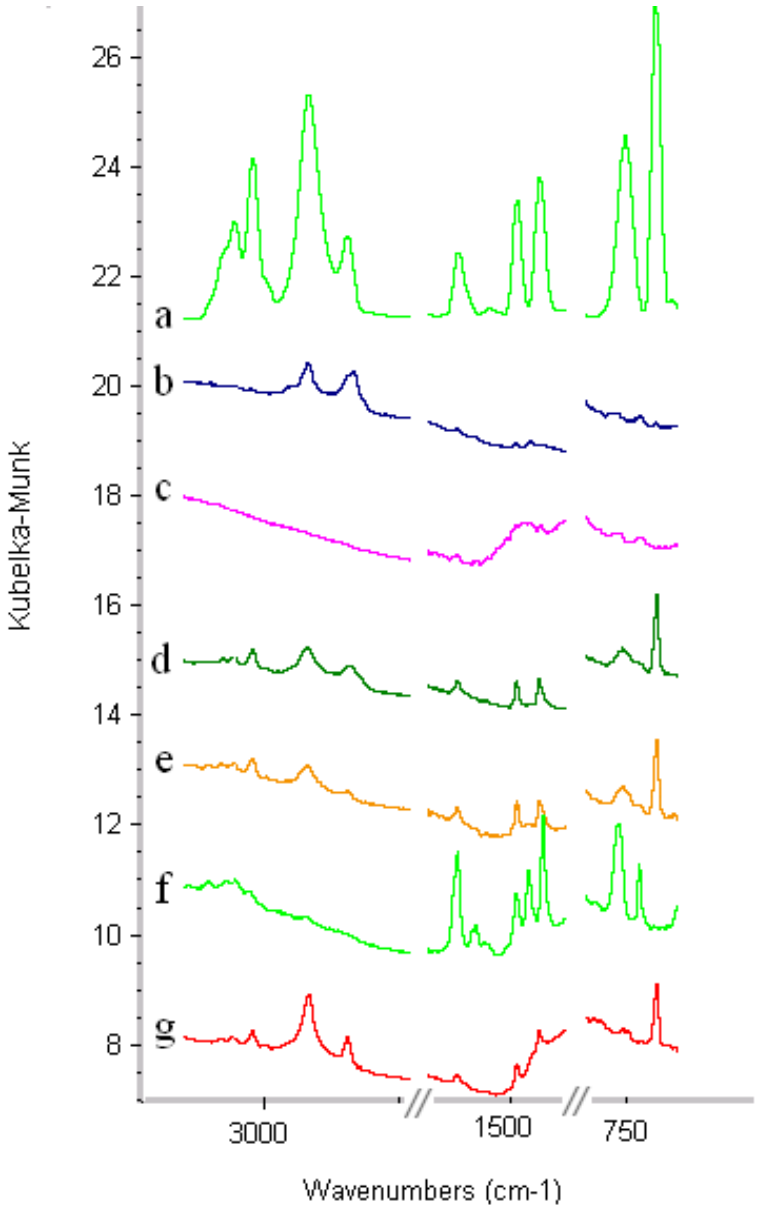

Figure 3.6. DRIFT-IR of diamond powders: a) infrared spectrum of neat polystyrene, b) hydrogen-terminated diamond, c) piranha-treated diamond, d) polystyrene functionalized diamond obtained by photoreaction and ATRP, e) polystyrene functionalized diamond obtained by reaction with 2-bromoisobutyryl bromide and ATRP, f) polystyrene-DVB functionalized diamond obtained by 2-bromoisobutyryl bromide and ATRP and g) polystyrene functionalized diamond obtained by di-tert-amyl peroxide and styrene.

المنارة للاستشارات
www.manaraa.com

the thicker polystyrene films could be obtained when a cross-linker is added.

3.4.4 Sulfonation of Polystyrene Functionalized Diamond Powder

Polystyrene (PS) functionalized diamond powder can be sulfonated with sulfuric acid in acetic acid. Sulfonated diamond particles were characterized by XPS and an obvious surfur signal appears (See Figure 3.3f) that was not discernable prior to sulfonation (see Figure 3.3e). The sulfur-to-carbon ratio on this material, measured by the S2p to the C1s XPS signals in the XPS narrow scans, was 0.022 (See Table 3.1). The sulfur signal in the negative ion ToF-SIMS spectra also appears after sulfonation (See Table 3.2). Interestingly, ToF-SIMS positive ion spectra show that the characteristic polystyrene peaks disappear, especially in the higher mass range, after sulfonation of polystyrene-functionalized diamond. After sulfonation, the bromine peaks also disappear in the negative ion SIMS spectra and the oxygen peaks increase significantly. For example, the ratio of oxygen main peaks to all the peaks increases from 0.16 to 0.37 after sulfonation.

Polystyrene and sulfonated diamonds can be used as reversed phase and ion-exchange stationary phase, respectively (See Chapter 4).

3.5 Conclusions

Atom transfer radical polymerization (ATRP) is applied to grow polystyrene on diamond surfaces. The necessary ATRP initiator could be immobilized in two ways. One is via the reaction of hydrogen-terminated diamond with bromine under light. The other method is the reaction of piranha-treated diamond with 2-bromoisobutyryl bromide.

المنارة للاستشارات
www.manaraa.com

Table 3.2. Ratios of areas of the main peaks (C, O, Br and S) to the sum of all areas of peaks in the negative ion ToF-SIMS spectra.

	C (%)	O (%)	Br (%)	S (%)
Brominated diamond (photoreaction)	0.16	0.09	0.31	0
Brominated diamond (isobromide)	0.09	0.21	0.24	0
Polystyrne functionalized diamond (photo reaction)	0.21	0.10	0.08	0
Polystyrene functionalized diamond (addition/elimination)	0.14	0.16	0.13	0
Sulfonated diamond	0.20	0.37	0.01	0.01

المنارة للاستشارات
www.manaraa.com

Polystyrene (PS) or cross-linked polystyrene (PS-DVB) was grown on the diamond powders by ATRP. Sulfonation of these phenyl phases was demonstrated with a H_2SO_4/CH_3COOH mixture. X-ray photoelectron spectroscopy (XPS), time of flight secondary ion mass spectrometry (ToF-SIMS) and diffuse reflectance Fourier transform infrared spectroscopy (DRIFT) were performed to follow surfaces changes and provide evidence of successful functionalization.

3.6 References

(1) von Werne, T.; Patten, T. E. *J. Am. Chem. Soc.* **1999**, *121*, 7409-7410.

(2) Kong, X.; Kawai, T.; Abe, J.; Iyoda, T. *Macromolecules* **2001**, *34*, 1837-1844.

(3) Yu, W. H.; Kang, E. T.; Neoh, K. G.; Zhu, S. *J. Phys. Chem. B.* **2003**, *107*, 10198-10205.

(4) Xu, F. J.; Yuan, Z. L.; Kang, E. T.; Neoh, K. G. *Langmuir* **2004**, *20*, 8200-8208.

(5) Zhao, B.; Brittain, W. J. *J. Am. Chem. Soc.* **1999**, *121*, 3557-3558.

(6) Hussemann, M.; Malmstro¨m, E.; McNamara, M.; Mate, M.; Mecerreyes, D.; Benoit, D. G.; Hedrick, J. L.; Mansky, P.; Huang, E.; Russel, T. P.; Hawker, C. J. *Macromolecules* **1999**, *32*, 1424-1431.

(7) Matyjaszewski, K.; Miller, P. J.; Shukla, N.; Immaraporn, B.; Gelman, A.; Luokala, B. B.; Siclovan, T. M.; Kickelbick, G.; Vallant, T.; Hoffman, H.; Pakula, T. *Macromolecules* **1999**, *32*, 8716-8724.

(8) Ejaz, M.; Yamamoto, S.; Ohno, K.; Tsuji, Y.; Fukuda, T. *Macromolecules* **1998**, *31*, 5934-5926.

(9) Shah, R. R.; Merreceyes, D.; Husemann, M.; Rees, I.; Abbott, N. L.; Hawker, C. J.;

المنارة للاستشارات
www.manaraa.com

Hedrick, J. L. *Macromolecules* **2000**, *33*, 597-605.

(10) Kim, J.-B.; Bruening, M. L.; Baker, G. L. *J. Am. Chem. Soc.* **2000**, *122*, 7616-7617.

(11) Huang, W.; Kim, J.-B.; Bruening, M. L.; Baker, G. L. *Macromolecules* **2001**, *35*, 1175-1179.

(12) Ejaz, M.; Tsuji, Y.; Fukuda, T. *Polymer* **2001**, *42*, 6811-6815.

(13) Huang, X.; Wirth, M. J. *Macromolecules* **1999**, *32*, 1694-1696.

(14) Matrab, T.; Chehimi, M. M.; Boudou, J. P.; Benedic, F.; Wang, J.; Naguib, N. N.; Carlisle, J. A. *Diamond and Related Materials* **2006**, *15*, 639-644.

(15) Li, L.; van der Ende, A. E.; Davidson, J. L.; Lukehart, C. M. In *231st ACS National Meeting*: Atlanta, GA, United States, 2006.

(16) Li, L., Vanderbilt University, 2007.

(17) Li, L.; Davidson, J. L.; Lukehart, C. M. *Carbon* **2006**, *44*, 2308-2315.

(18) Ando, T.; Ishii, M.; Kamo, M.; Sato, Y. *J. Chem. Soc. Faraday Trans.* **1993**, *89*, 1783-1789.

(19) Fritz, J. S.; Dumont, P. J.; Schmidt, L. W. *Journal of Chromatography, A* **1995**, *691*, 133-140.

(20) Dumont, P. J.; Fritz, J. S. *Journal of Chromatography, A* **1995**, *691*, 123-131.

(21) Carlmark, A.; Malmström, E. E. *Biomacromolecules* **2003**, *4*, 1740-1745.

(22) Carlmark, A.; Malmström, E. E. *J. Am. Chem. Soc.* **2002**, *124*, 900-901.

(23) Matyjaszewsli, K.; Xia, J. *Chem. Rev.* **2001**, *101*, 2921-2990.

المنارة للاستشارات
www.manaraa.com

Chapter 4 Phenyl and Sulfonic Acid Stationary Phases on Diamond Substrates for Solid Phase Extraction

4.1 Abstract

Both polystyrene-modified diamond and sulfonated polystyrene-modified diamond were used in solid phase extraction (SPE). These diamond-based stationary phases are stable under basic conditions, which is not the case for silica-based stationary phases. Solid phase extraction is performed on the resulting phenyl and strong cation exchange material using 1-naphthylamine. The stability, percent recovery and column capacity are provided for both phenyl (polystyrene) and sulfonic acid treated polystyrene SPE columns.

4.2 Introduction

Solid phase extraction (SPE) is a widely used sample preparation method in separation science.[1, 2] Numerous materials are potential candidates for stationary phases in solid phase extraction (SPE) or HPLC, such as silica, highly cross-linked polystyrene-divinylbenzene (PS-DVB) copolymer, carbon and other metal-containing sorbents.[3-9] However, few if any possess the full range of mechanical and chemical stability that one might desire. For example, polymer materials swell in organic solvents. Inorganic oxides (silica, zirconia and alumina) have low hydrolytic stability, especially at low and/or high pH. In contrast, diamond is an extraordinary material because of its

المنارة للاستشارات
www.manaraa.com

fascinating mechanical stability at high pressure, excellent stability over a very wide pH range, thermal stability, and remarkable chemical stability and inertness.[10-12] These properties make it an attractive material for many applications, including, perhaps, an ideal stationary phase for SPE[13], HPLC[14-18] and capillary ultrahigh pressure liquid chromatography.[19] There are a few recent examples of diamond being used in chromatography. Linford and coworkers[13] modified diamond with polyallylamine for solid phase extraction. Telepchak[16] used natural diamonds as a stationary phase for reverse phase HPLC. Patel et al.[17] investigated a column (100 mm×4.6 mm i.d.) packed with 3.8 μm diamonds for normal and reversed phase HPLC. These two latter studies were successful in spite of their very low column efficiencies. Nesterenko[14, 18] also studied sintered diamonds as a stationary phase for HPLC and obtained more efficient separations compared to the previous studies by Telepchak[16] and Patel.[17] In addition, he studied the oxidative treatment of diamond particles for a cation-exchange column.[15] Liu[19] attempted to use polybutadiene-modified, and alkylated diamond in capillary ultrahigh pressure liquid chromatography.

Diamond particles functionalized by the methods described in this thesis (unsaturated monomers/peroxide or ATRP) are expected to have excellent stability in both acids and bases. In particular, such diamond-based stationary phases should be stable under basic conditions, which is not the case for silica-based stationary phases. In this chapter, I demonstrate that both polystyrene-modified diamond and sulfonated, polystyrene-modified diamond can be used for solid phase extraction, which is an important technique for sample preparation, purification, concentration, and cleanup.[3, 7]

المنارة للاستشارات
www.manaraa.com

The stability, percent recovery and column capacity are provided for both phenyl and sulfonic acid SPE columns on diamond substrates.

4.3 Experimental Section

4.3.1 Reagents

All chemicals were used as received: methanol (spectra grade, Aldrich, St. Louis, MO); 1-naphthylamine (99%, Aldrich); NaCl (reagent grade, Fisher, Fair Lawn, NJ); phosphate buffer: H_3PO_4 (85%, EMD, Gibbstown, NJ) and $NaH_2PO_4 \cdot H_2O$ (reagent grade, EMD). Diamond powder (70 μm) was provided by U.S. Synthetic (Orem, UT). These diamonds were functionalized with polystyrene and sulfonated polystyrene using the procedure described in Chapters 2 and 3 of this dissertation.

4.3.2 Stability Test

Polystyrene and sulfonated polystyrene coated diamonds were immersed in 1 M NaOH and 1 M HCl solution for 72 h to evaluate their stability under strongly basic or acidic conditions. Methanol (10% by volume) was added to these solutions for the polystyrene-coated diamond so that the solution would better wet the particles. X-ray photoelectron spectroscopy (XPS), time-of-flight secondary ion mass spectrometry (ToF-SIMS) and diffuse reflectance Fourier transform infrared spectroscopy (DRIFT) were used to characterize these diamond powders (See Chapters 2 and 3 for experimental details).

المنارة للاستشارات
www.manaraa.com

4.3.3 Solid Phase Extraction (SPE)

Elution Procedure

SPE of 1-naphthylamine was performed with a cartridge prepared in my laboratory. In my experiments, the packing material from a commercially-available cartridge was replaced by my phenyl and sulfonated stationary phases. A control experiment showed that neither the plastic cartridges nor the frits retained 1-naphthylamine. The same volume (*ca*. 5.0 cm^3) of packing material was used in all of my experiments. To improve packing, the cartridges were washed with water or methanol, under reduced pressure from the house vacuum, during loading. Finally, the columns were dried using the house vacuum.

Prior to applying the analyte, the polystyrene-coated column was conditioned with 6 column volumes of methanol, followed by 6 column volumes of water. 50 μL of 1-naphthylamine (1 mg/mL) in water (~1% methanol) was loaded into the column. The column was then washed with water and finally eluted with methanol. This phenyl column could be reused multiple times in this fashion after washing with methanol.

For the sulfonated polystyrene-diamond stationary phase, the columns were first conditioned with 6 column volumes of methanol, and then with six column volumes of phosphate buffer (10 mM, pH=1.9). 50 μL of 1-naphthylamine (1 mg/mL) in phosphate buffer (10 mM, pH=1.9) was applied to the column. This analyte was used to test the sulfonation of polystyrene-coated diamond. After washing with phosphate buffer (10 mM, pH=1.9), the analyte was eluted with phosphate buffer (10 mM, pH=1.9, NaCl, ionic strength 0.2 M): methanol (v/v, 1:1).

المنارة للاستشارات
www.manaraa.com

In practice, sulfonated, polystyrene-modified diamond SPE sorbents could be repeatedly used without noticeable degradation. Before each reuse, the column was washed with phosphate buffer (10 mM, pH=1.9, NaCl, ionic strength 0.2 M): methanol (v/v, 1:1) several times to regenerate it.

Breakthrough Curves and Column Capacity

The columns, including the polystyrene-functionalized and sulfonated polystyrene-functionalized SPE columns, were first conditioned using the procedures mentioned above. After conditioning, the solution of 1-naphthylamine in water (1% methanol) (0.01 mg/mL) was passed through the polystyrene-functionalized SPE column, and the solution of 1-naphthylamine dissolved in phosphate buffer (pH=1.9) (0.02 mg/mL) was passed through the PS-sulfonated column, both at a constant flow rate. Equal volumes (fractions) eluting from the column were collected in separate vials. Finally, these fractions were analyzed by ESI-MS.

Breakthrough curves, which had sigmoidal shapes, are plots of solution volumes eluted from the column vs. the corresponding $[M+1]^+$ peak area of the analyte in each fraction. The breakthrough volume was calculated from the point on the curve corresponding to 5% of the average value at the maximum (the plateau region). The column capacity was calculated by multiplying the breakthrough volume by the corresponding concentration of analyte.

المنارة للاستشارات
www.manaraa.com

Percent Recovery

For phenyl SPE columns, 50 μL of 1-naphthylamine (1 mg/mL) in water (~1% methanol) was added to the column with a micropipette. The column was then extracted with methanol. A reference solution was created by adding 50 μL of 1-naphthylamine (1 mg/mL) in water (~1% methanol) directly to the extracted sample from a blank matrix. These two solutions were then analyzed by ESI-MS and the $[M+H]^+$ peak for each respective analyte was integrated. The division of these two peak areas multiplied by 100 gave the % SPE recovery.

For the sulfuric acid SPE column, 50 μL of 1-naphthylamine (1 mg/mL) in a phosphate buffer (10 mM, pH=1.9) was added to the column. The column was then extracted with phosphate buffer (10 mM, pH=1.9, NaCl, ionic strength 0.2 M): methanol (v/v, 1:1). A reference solution was created by adding the same amount of analyte directly to the extracted sample from a blank matrix. The remainder of the analysis and calculations were the same as above.

Electrospray MS (ESI-MS)

Electrospray MS (ESI-MS) was performed using an Agilent Technologies LC/MSD TOF system by direct infusion of several μLs of sample along with the mobile phase: 75% MeOH and 25% water, with 5 mM ammonium formate. A steel ES ionization needle was set in positive-ion mode, and the charging voltage and the capillary voltages were set at 900 V and 3500 V, respectively. The nebulizer was set at 35 psi, the gas temperature was 350ºC, and the skimmer was operated at 60 V. The flow rate of the

المنارة للاستشارات
www.manaraa.com

nitrogen drying gas was 12 L/min. One survey scan was collected per second over a mass range of m/z 100-1200.

4.4 Results

4.4.1 Solid Phase Extraction with Polystyrene-Modified and Sulfonated, Polystyrene-Modified Diamond

Polystyrene-coated diamond particles and sulfonated diamond particles were loaded into columns and used for solid phase extraction. Polystyrene-coated diamond particles were used as a reversed phase column packing and sulfonated diamond particles were used as an ion-exchange stationary phase. A demonstration of the retention and release of analyte was performed with 1-naphthylamine (see Figure 4.1). These polystyrene and sulfonated diamond columns were reusable; they could be used multiple times without any sign of degradation.

Polystyrene-coated columns were first conditioned and then 1-naphthylamine was loaded onto the column. The column was washed with water and the analyte was eluted with methanol. Electrospray ionization mass spectrometry (ESI/MS) was used to confirm the presence or absence of the analytes in the fractions that were taken. From the ESI-MS results, the $[M+1]^+$ peak at 144 amu of analyte (1-naphthylamine) appeared in the methanol fraction while nothing eluted in the pre-wash (See Figure 4.2a and b). The same procedure was applied to other SPE control columns, which were packed with hydrogen/deuterium-terminated diamond powder.[20] For these columns, the analyte (1-naphthylamine) was eluted directly by the first solvent (water). These results illustrate that 1-naphthylamine can be retained by a polystyrene-functionalized diamond stationary

المنارة للاستشارات
www.manaraa.com

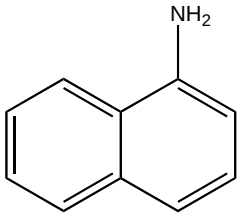

Figure 4.1. Structure of 1-naphthylamine.

المنارة للاستشارات
www.manaraa.com

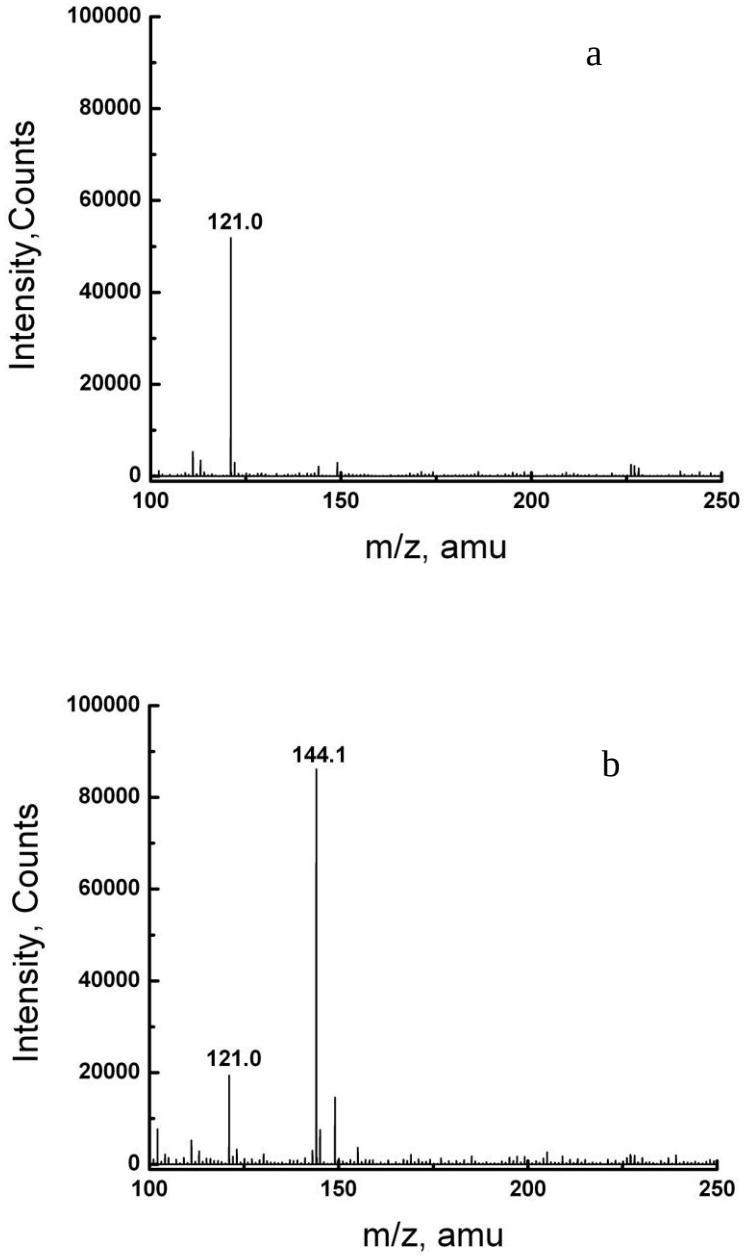

Figure 4.2. Positive ion ESI-MS spectra of SPE fractions from polystyrene-modified diamond stationary phases: (a) fraction eluted with water (no analyte present). (b) analyte (1-naphthylamine) eluted with methanol.

المنارة للاستشارات
www.manaraa.com

phase and not by a hydrogen/deuterium-terminated diamond SPE column, although it also possesses a non-polar (van der Waals type) interaction between the analyte and the column. Nevertheless, it should not allow for stacking of aromatic rings.

The sulfonated-styrene column was first conditioned with methanol, followed by phosphate buffer (10 mM, pH=1.9). 50 μL of 1-naphthylamine (1 mg/mL) in phosphate buffer (10 mM, pH=1.9) was loaded onto the column. The column was washed with phosphate buffer (10 mM, pH=1.9) and the analyte was finally eluted with phosphate buffer (10 mM, pH=1.9, NaCl, ionic strength 0.2 M): methanol (v/v, 1:1). For SPE columns made of polystyrene-coated diamond powder, or hydrogen/deuterium-terminated diamond powder, the analyte eluted directly in the very first fraction (phosphate buffer, 10 mM, pH=1.9) as shown by ESI-MS when this same procedure was employed. In contrast, 1-naphthylamine was eluted with phosphate buffer (10 mM, pH=1.9, NaCl, ionic strength 0.2 M): methanol (v/v, 1:1), but not in the first fraction (phosphate buffer, 10 mM, pH=1.9) for sulfonated, polystyrene-coated diamond SPE columns. These results indicate an ionic interaction between the analyte and the sulfonic acid group. Figure 4.3 show ESI/MS spectra of the corresponding eluted fractions from sulfonated-polystyrene coated diamond and the fraction eluted by phosphate buffer (10 mM, pH=1.9, NaCl, ionic strength 0.2 M): methanol (v/v, 1:1) that is dominated by one peak: the $[M + 1]^+$ peak for 1-naphthylamine at 144 amu. The peak at m/z 121 in Figures 4.2 and 4.3 is the reference peak added in the Agilent MS instrument.

المنارة للاستشارات
www.manaraa.com

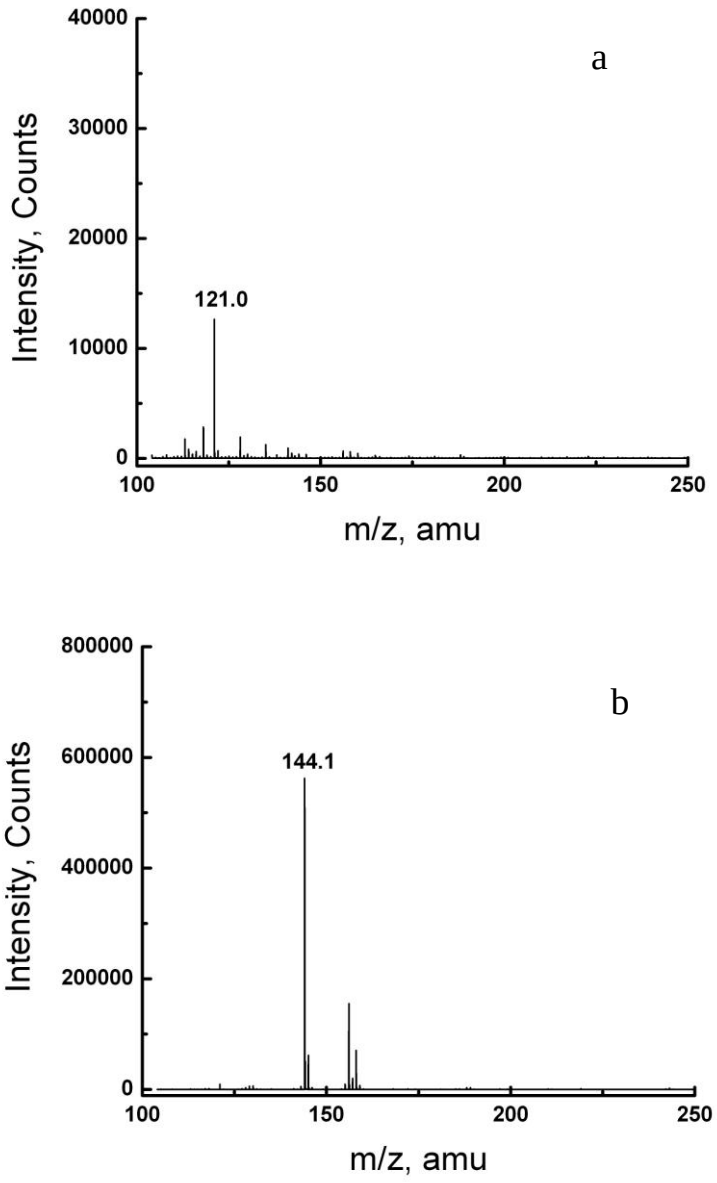

Figure 4.3. Positive ion ESI-MS spectra of SPE fractions from PS-sulfonated diamond phases: (a) fraction eluted with the phosphate buffer (10 mM, pH=1.9) showing no analyte, (b) the analyte 1-naphthylamine eluted with a higher ionic strength phosphate buffer, which also contained an organic solvent [10 mM, pH=1.9, NaCl, ionic strength 0.2 M): methanol (v/v, 1:1)].

المنارة للاستشارات
www.manaraa.com

4.4.2 Stability

Chemical stability tests were performed by immersing polystyrene-coated and sulfonated polystyrene-coated diamond particles [made by the peroxide method (Chapter 2) and ATRP (Chapter 3), respectively] into acid or base for 70 h. Following this

treatment, IR spectra of polystyrene-coated diamond particles (made by the peroxide method) showed little or no change in the intesities of the C-H stretches and the combined ring vibrations (See Figure 4.4). This result demonstrates that essentially, no polystyrene is removed by strong base or acid, *i.e.*, that polystyrene-coated diamond particles are stable to strong acid and base. For sulfonated polystyrene (made by the peroxide method), following this stability test in acid or base, the S2p-to-C1s ratio by XPS remained essentially constant, whether for polystyrene or polystyrene-DVB (See Table 4.1). These results were compared to the stability of a commercially-available SPE stationary phase (Phenomenex Strata SCX, 55 µM, 70 Å, silica based). Prior to stability tests, the S2p-to-C1s ratio of the commercial particles by XPS was 0.16± 0.03. Silica particles resist strongly acidic condition quite well, and the S2p-to-C1s ratio of the commercial particles after the immersion in acid was 0.15 ± 0.03. However, after immersion of these particles in 1.0 M NaOH for 8 h, the silica particles completely dissolved. To further verify the dissolution of these particles, the resulting clear solution was filtered. It easily passed through the filter, leaving no material behind. Polymer-based particles from Phenomenex were also immersed in 1 M HCl and 1 M NaOH for 70 h. Their S2p/C1s ratios stayed the same to within *ca*. 10%. Thus, sulfonated polystyrene on diamond has the same, or perhaps even slightly improved, stability in acid and base compared to a commercially-available polymer-based SCX SPE material, while being

المنارة للاستشارات
www.manaraa.com

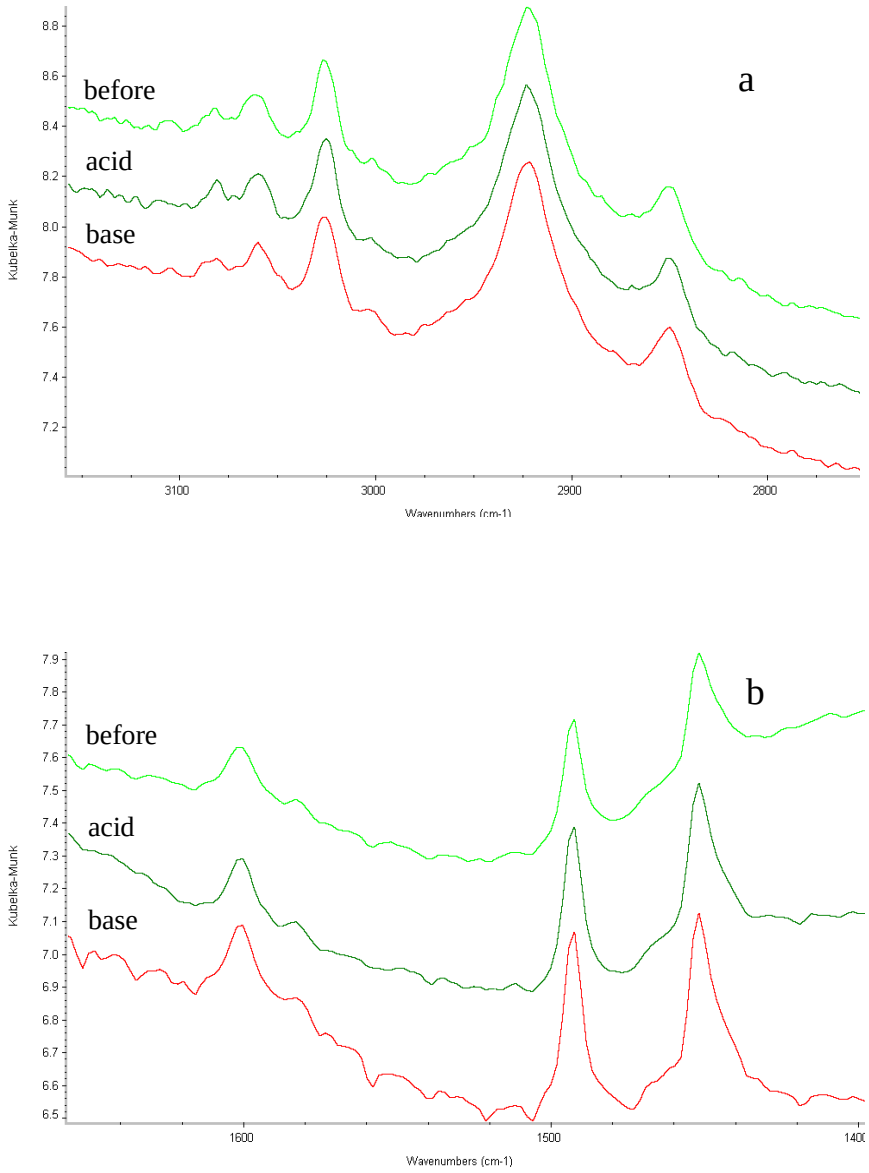

Figure 4.4. IR spectra of polystyrene-functionalized diamond a) before and b) after immersion in solutions of 1M HCl (acid) or 1M NaOH (base).

المنارة للاستشارات
www.manaraa.com

Table 4.1. Stability test results: S2p/C1s ratio from XPS of sulfonated polystyrene (PS) diamonds.

Type	Stationary Phase	Original	In 1 M HCl (70 h)	In 1 M NaOH (70 h)
ATRP (iso-bromide)	PS-sulfonated	0.0069±0.0009	0.0061±0.0004	0.0044±0.0000
Peroxide	PS-sulfonated	0.018± 0.000	0.019± 0.001	0.018± 0.002
	PS-DVB-sulfonated	0.036± 0.001	0.038± 0.001	0.038± 0.001
Commerial	Polymer SCX	0.017± 0.002	0.015± 0.00	0.016± 0.000
	Silica SCX	0.16± 0.03	0.15± 0.02	Dissolved

المنارة للاستشارات
www.manaraa.com

(overall) much more stable than the silica-based SPE material.

When polystyrene-coated diamond particles (made with the isobromide and ATRP) were immersed into 1.0 M HCl or 1.0 M NaOH for 70 h, IR results showed that the areas of the aromatic C-H stretches decreased 5.5% and 15%, respectively. In addition, the areas of the alkyl C-H stretches decreased 12.4% and 11.6%, respectively. Sulfonated polystyrene coated diamond particles (made by isobromide and ATRP) were also immersing into 1.0 M HCl or 1.0 M NaOH for 70 h. Following this treatment, approximately one-tenth and one-third of the sulfur was removed from the surface, respectively, which suggests that this fraction of the sulfur-containing coating on the particles had been lost. These results were compared to the stability of the particles functionalized with the peroxide. It is clear that particles functionalized using the peroxide/monomer mixture are considerally more stable than particles functionalized by ATRP, in both strong acid and base. These stability tests are consistent with hydrolysis of the carboxyl linkage of the isobromide between diamond and its polymer overlayers.

4.4.3 Column Capacity

Breakthrough curves were obtained for SPE columns using 1-naphthylamine as an analyte to determinate breakthrough volumes of the phenyl and the strong cation exchange SPE columns (diamonds functionalized by the peroxide method). The breakthrough curves are shown in Figure 4.5. The breakthrough volume was taken from the point on the breakthrough curve at 5% of the average value at the breakthrough curve plateau region. Figure 4.6 shows the dynamic ranges of the instrument for the different solutions of 1-naphythylamine as measured with the ESI-MS for both columns. This

المنارة للاستشارات
www.manaraa.com

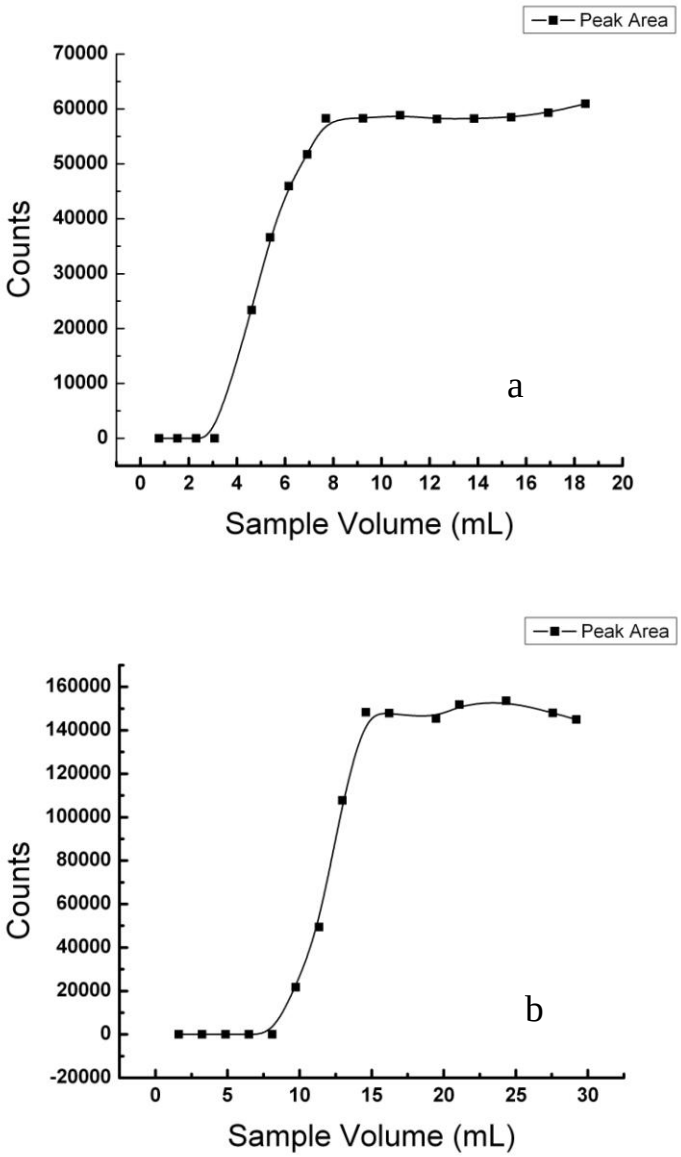

Figure 4.5. Breakthrough curves for 1-naphthylamine on polystyrene (a) and sulfonated polystyrene (b) coated 70 μm diamond particles. Each point represents the peak area of the analyte from the positive ESI-MS spectra.

www.manaraa.com

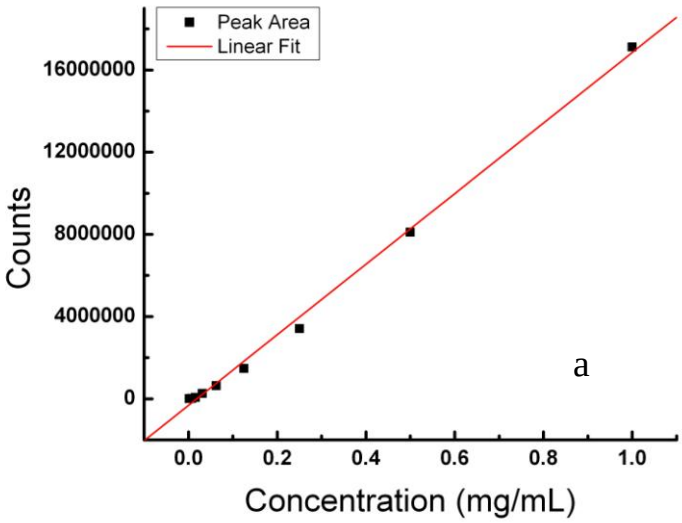

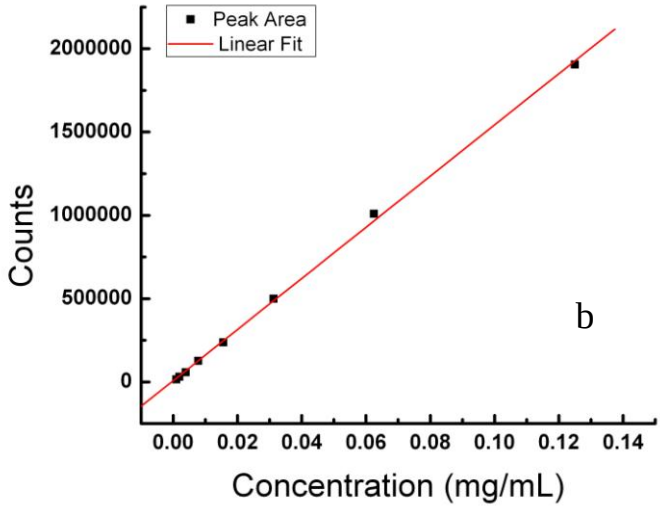

Figure 4.6. Linear relationship between signal and concentration for the analyte 1-naphthylamine in water (a) and phosphate buffer (pH=1.9) (b) from the positive ion ESI-MS spectra.

المنارة للاستشارات
www.manaraa.com

linear relationship shows that the breakthrough curve is under this range, and that while the plateau region of the breakthrough curve is at saturation for the phenyl and SCX SPE columns, it is not at the saturation of the ESI-MS detector. From these breakthrough curves, column capacities for phenyl and cation exchange SPE columns were found to be 31.5 and 80 μg, respectively. The capacities of phenyl and SCX SPE columns which were packed with diamond particles functionalized by ATRP were similar to those produced using the peroxide method.

4.4.4 Percent Recovery

The percent recoveries of the phenyl and cation exchange SPE columns (functionalized using the peroxide method) were 65.8% and 101% (my best retention measurements). These numbers indicate that much of the analyte (1-naphthylamine) can be recovered from phenyl SPE columns, and that all of the analyte can be recovered from the strong cation exchange column. The percent recoveries of the phenyl and SCX SPE columns packed with diamond particles functionalized with the ATRP method were similar to those found by the peroxide method.

I comment here on the elution of the analyte (1-naphthylamine) by phosphate buffer (pH=1.9) only, or with the mixture of the phosphate buffer (pH=1.9) and methanol (v/v 1:1). The percent recoveries after eluting with these buffers are around 60-70% and 101%, respectively. Thus, complete recovery of the analyte is found when 50% percent methanol is in the buffer. These results suggest that there are multiple interactions between the analyte and the stationary phase in the SCX SPE column, which include ionic interactions with the sulfonic acid groups and non-polar interactions with the

المنارة للاستشارات
www.manaraa.com

aromatic ring. When multiple mechanisms are active, disruption of more than one retention mechanism improves analyte recovery.

4.5 Conclusions

Diamond powder modified with phenyl and sulfonated phenyl moieties can be used as phenyl and strong cation ion exchange stationary phases, respectively. These phases have excellent stability in both highly acidic and highly basic media, especially the phase functionalized using my peroxide method. Solid phase extraction is performed on the resulting phenyl and strong cation exchange materials using 1-naphthylamine. Column capacity and percent recovery have been studied.

4.6 References

(1) Ruane, R. J.; Wilson, I. D. *Journal of Pharmaceutical and Biomedical Analysis* **1987**, *5*, 723-727

(2) Roberts, D. W.; Ruane, R. J.; Wilson, I. D. *Journal of Pharmaceutical and Biomedical Analysis* **1989**, *7*, 1077-1086

(3) Thurman, E. M.; Mills, M. S. *Solid-Phase Extraction*; John Wiley & Sons: New York, NY, 1998.

(4) Hennion, M. C. *Journal of Chromatography A* **1999**, *856*, 3-54.

(5) Pawliszyn, J. *Solid-Phase Microextraction: Theory and Practice*; Wiley-VCH: New York, 1997.

(6) Fritz, J. S. *Analytical Solid-Phase Extraction*; Wiley-VCH: New York, 1999.

المنارة للاستشارات
www.manaraa.com

(7) Simpson, N. J. K. *Solid-Phase Extraction: Principles, Strategies and Applications*; Marcel Dekker: New York 1998.

(8) Huck, C. W.; Bonn, G. K. *Journal of Chromatography A* **2000**, *885*, 51-72.

(9) Hennion, M. C. *Journal of Chromatography A* **2000**, *885*, 73-95.

(10) Wei, J.; Yates, J., J. T. *Crit. ReV. Surf. Chem.* **1995**, *5*, 1-71.

(11) Wilks, E.; Wilks, J. *Properties and Applications of Diamond*; Butterworth: Oxford, England 1997.

(12) Pierson, H. O. *Handbook of Carbon, Graphite, Diamond and Fullerenes* Noyes Publ.: Park Ridge, NJ, 1993.

(13) Saini, G.; Yang, L.; Lee, M. L.; Dadson, A.; Vail, M. A.; Linford, M. R. *Anal. Chem.* **2008**, *80*, 6253-6259.

(14) Nesterenko, P. N.; Fedyanina, O. N.; Volgin, Y. V. *Analyst* **2007**, *132*, 403-405.

(15) Nesterenko, P. N.; Fedyanina, O. N.; Volgin, Y. V. *J. Chromatogr.,A* **2007**, *1155*, 2-7.

(16) Telepchak, M. J. *Chromatographia* **1973**, *6*, 234-236.

(17) Patel, B. A.; Rutt, K. J.; Padalko, V. I.; Mikhalovsky, S. V. *J. Superhard Mater.* **2002**, *6*, 51-54.

(18) Nesterenko, P. N.; Fedyanina, O. N.; Volgin, Y. V., Moscow, 25-30 June 2006.

(19) Liu, Y. S., Brigham Young University, Provo, 2007.

(20) Tsubota, T.; Hirabayashi, O.; Ida, S.; Nagaoka, S.; Nagata, M.; Matsumoto, Y. *Diamond and Related Materials* **2002**, *11*, 1374-1378.

المنارة للاستشارات
www.manaraa.com

PART II. Silicon Functionalization

Chapter 5 The Chemistry of Olefin-Terminated Homogeneous and Mixed Monolayers on Scribed Silicon*

5.1 Abstract

I describe the preparation of homogeneous, olefin-terminated monolayers on scribed silicon made from 1,9-decadiene, and mixed monolayers that contain varying degrees of olefin termination, prepared from 1,9-decadiene and 1-decene or 1-octene, and their subsequent reactions with bromine, osmium tetroxide, dicholorocarbene, and Grubbs' catalyst. Each of these reagents contains a heteroatom, which allows straightforward monitoring of the surface reactions by X-ray photoelectron spectroscopy (XPS). Surface reactions are consistently more efficient in mixed monolayers made from 1-octene compared to 1-decene, presumably because of steric effects. After chemisorption of Grubbs' catalyst, ring-opening metathesis polymerization (ROMP) of norbornene is demonstrated. The kinetics of Grubbs' catalyst adsorption and of polynorbornene growth are monitored by XPS and time-of-flight secondary ion mass spectrometry (ToF-SIMS). A principal components analysis (PCA) of the ToF-SIMS data is presented. Autoscaling is shown to be a relatively ineffective preprocessing method for this data.

---

*This chapter is reproduced with pemission from *Chem. Mater.* **2007**, *19*, 1671-1678. Copyright 2007 American Chemical Society.

www.manaraa.com

5.2 Introduction

Silicon is arguably the most important material in the semiconductor and microelectronics industries. Because of its importance, numerous studies have been performed on its surface, including hydrogen-terminated, reconstructed, porous, and scribed.[1-4] Chemomechanical modification of silicon[4] is an effective and convenient method for functionalizing the surface of this material. In the chemomechanical method, a silicon surface is mechanically scribed in the presence of a reactive species. Scribing activates the surface so that it reacts immediately with the reagent it is in contact with. Scribed silicon reacts with 1-alkenes,[5-7] 1-alkynes,[5, 7] alkyl halides (chlorides, bromides, and iodides),[7, 8] alcohols,[6] epoxides,[9] aldehydes,[10] and acid chlorides[11] to produce hydrophobic, methyl-terminated monolayers. Scribed silicon also reacts with bifunctional compounds, including 1,2,7,8-diepoxyoctane[9] and suberoyl chloride,[11] to form amine-reactive epoxide and acid chloride monolayers, respectively. These papers were significant because of the rich and versatile chemistry of activated carboxyl and epoxy groups. The chemomechanical patterning method is straightforward, allowing both nanometer- and micron-sized features to be created.[12-15] It is similar to the nanografting method developed by Xu and coworkers[16, 17] and the micromachining/manipulation of surface wetting method developed by Abbott et al.[18]

The olefin group is found in numerous compounds and polymers of industrial, biological, and academic significance. It has important addition-reaction properties in organic chemistry and polymer science. Here I explore the chemistry of homogenous, olefin-terminated monolayers made with a neat dialkene,[13] along with mixed monolayers prepared with a mixture of a dialkene and a monoalkene. To demonstrate the preservation

المنارة للاستشارات
www.manaraa.com

of active carbon-carbon double bonds after monolayer formation, monolayers were exposed to three reagents that readily react with carbon-carbon double bonds: bromine (Br_2), osmium tertroxide (OsO_4) and dichlorocarbene ($:CCl_2$). A fourth reaction was also demonstrated: chemisorption of Grubbs' catalyst, followed by ring-opening metathesis polymerization (ROMP)[19-26] to form an adsorbed polymer film (See Figure 5.1). In ROMP, rings may be opened in a ruthenium carbene-catalyzed reaction, where the driving force is the relief of ring strain. ROMP on surfaces using Grubbs' catalyst has been demonstrated from olefin- or norbornenyl-terminated silicon oxide surfaces,[27-29] and porous silica[30] and from the surfaces of liposome.[31]

Wetting, X-ray photoelectron spectrometry (XPS), time of flight-secondary ion mass spectrometry (ToF-SIMS) and principal components analysis (PCA) of ToF-SIMS data are used to confirm monolayer formation and reactivity and polymer growth.

5.3 Experimental Section

5.3.1 Chemicals

All chemicals were reagent grade or the highest available commercial grade, unless otherwise specified, and used as received as follows: 1,9-decadiene (96%, Aldrich, St. Louis, MO), 1-decene (94%, Aldrich), 1-octene (97%, Aldrich), 1.0 M bromine in trimethyl phosphate (Aldrich), 2.5 wt % osmium tetroxide solution in 2-methyl-2-propanol (Aldrich), 1.0 M potassium *t*-butoxide solution in 2-methyl-2-propanol (Aldrich), $(Cy_3P)_2Cl_2Ru{=}CHPh$, Cy=cyclohexyl (Grubbs' catalyst 1st generation, Aldrich).

المنارة للاستشارات
www.manaraa.com

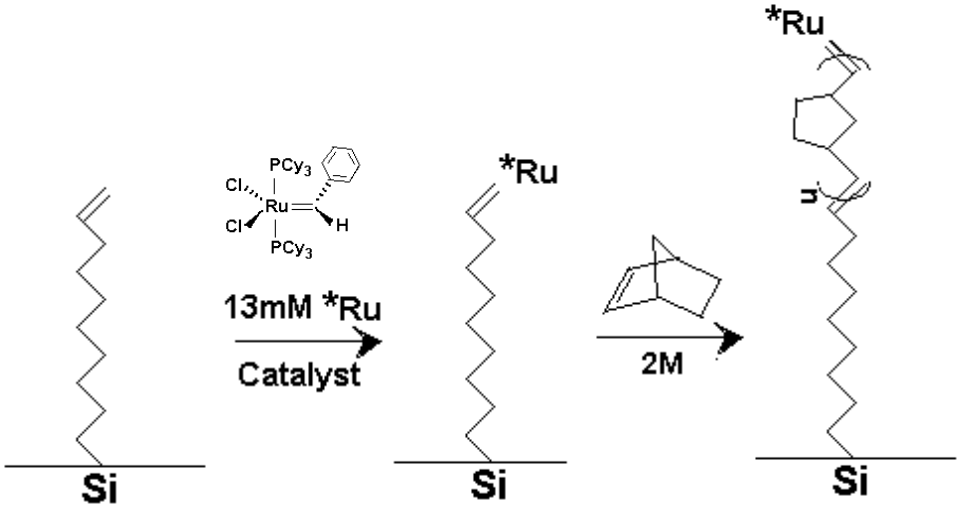

Figure 5.1. Schematic of growing polynorbornene chain on a patterned silicon surface.

(Cy = cyclohexyl)

المنارة للاستشارات
www.manaraa.com

5.3.2 Preparation for Patterning Silicon Surfaces

I employed scribing methods for chemomechanically patterning silicon. Native oxide-terminated silicon was scribed and patterned using a diamond-tipped rod.[5-11] All surfaces were cleaned with H_2O_2 (conc.)/NH_4OH (conc.) solution for 30-40 min, rinsed with water and dried with a stream of nitrogen. The cleaned silicon surfaces were wetted directly with reactive chemicals, and then scribing was performed on a 6 mm × 6 mm area of the surface. They were rinsed with acetone and water, and finally dried with a stream of nitrogen gas. Silicon samples with patterned monolayers on the surface were stored in nitrogen gas before the polymerization process.

5.3.3 Preparation of Monolayers

Mixed monolayers were prepared from solutions made from different proportions of 1-decene and 1,9-decadiene or from a mixture of 1-octene and 1,9-decadiene. No other solvent was employed. The compositions of these solutions are given in Table 5.1.

5.3.4 Reaction with Bromine

Monolayers (see Table 5.1) were placed in 1.0 M bromine in trimethyl phosphate for 12 h. After immersion they were washed with acetone and then with soap and water with agitation from a soft camel hair brush. Finally they were rinsed with DI water and Millipore water and dried with nitrogen gas.

5.3.5 Reaction with OsO_4

Scribed silicon surfaces (see Table 5.1) were immersed for 30 min in a 2.5 wt%

المنارة للاستشارات
www.manaraa.com

solution of osmium tetroxide in 2-methyl-2-propanol that had been diluted by the same solvent to 0.1 wt%. Finally, the surfaces were removed and washed with 2-methyl-2-propanol and then dried with nitrogen gas.

5.3.6 Reaction with Dichlorocarbene

Silicon surfaces, which had been scribed with the reagents shown in Table 5.1, were immersed in a stirred solution of 1.0 M potassium t-butoxide in 2-methyl-2-propanol that was diluted to 0.1 M with $CHCl_3$ for 3.5 h. The system was sealed and under nitrogen. After they were taken out, the surfaces were first washed with chloroform and then DI water. Finally they were rinsed with Millipore water and dried with nitrogen gas.

5.3.7 Reaction with Grubbs' Catalyst

Scribed silicon surfaces (see Table 5.1) were immersed in a 13 mM solution of an olefin metathesis catalyst (Grubbs' catalyst) in dichloromethane at room temperature for 30 min. After exposure to this catalyst the surfaces were rinsed in CH_2Cl_2.

5.3.8 Calculation of Reaction Yields

Yields of 1,9-decadiene monolayers with different reagents were calculated using the following formulas that employ the heteroatom/C ratio, which can be directly measured by XPS: percent yield of the Br_2 reaction = 500*(Br/C), percent yield of the OsO_4 reaction = 1000*(Os/C),

المنارة للاستشارات
www.manaraa.com

Table 5.1 Compositions in mole percent of the mixed solutions used to prepare the surfaces in Figure 5.4.

component	compositions				
1,9-decadiene	0%	25%	50%	75%	100%
1-octene or 1-decene	100%	75%	50%	25%	0%

المنارة للاستشارات
www.manaraa.com

percent yield of the CCl_2 Reaction = 1000 * (Cl/C)/(2-(Cl/C)) and percent yield of the Grubbs catalyst Reaction = 1000 * (Ru/C)/(35-(Ru/C)). In practice, the "yield" for the reaction of the given reagent with 1-decene (12%, 3%, 19%, and 0.68%, respectively) was subtracted from the yield for the reaction of the reagent with 1,9-decadiene to give the numbers reported in the text.

5.3.9 Polymerization

To grow polynorbornene on functionalized regions, the olefin-terminated/functionalized/patterned Si samples (prepared from 1,9-decadiene) were first immersed in a 13 mM solution of Grubbs' catalyst in dichloromethane at room temperature for 30 min. Samples were then removed from the solution, washed thoroughly with dichloromethane, and dried with a stream of dry nitrogen gas. The silicon samples were next immersed in a 2.0 M solution of norbornene monomer in toluene at room temperature for 40 min. Finally, the samples were removed from solution, washed thoroughly with dichloromethane, and dried with a stream of nitrogen gas. In order to study the kinetics of polymer growth, different reaction times were investigated.

5.3.10 Instrumentation

Time-of-flight secondary ion mass spectrometry (ToF-SIMS) was performed with an ION-TOF TOF-SIMS IV instrument with monoisotopic 25 keV $^{69}Ga^+$ primary ions in "bunched mode." The primary ion (target) current was typically 1.3 μA, with a pulse width of 20 ns before bunching, and the raster area of the beam was 500 x 500 μm^2. X-ray photoelectron spectroscopy was performed with an SSX-100 X-ray photoelectron

المنارة للاستشارات
www.manaraa.com

spectrometer with a monochromatic Al K_α source and a hemispherical analyzer. No electron flood gun was employed. Survey scans as well as narrow scans were recorded with an 800 x 800 μm^2 spot size.

5.3.11 PCA Analysis of ToF-SIMS Data

The "Peak List" feature in the instrument software was used to integrate (bin) spectral regions ± 0.3 mass units around each integer value along the abscissa. This operation effectively binned the data to unit mass resolution, and the positive and negative ion spectra were binned in this manner from 1 – 350 amu. The data were then exported into Microsoft Excel, normalized and arranged into data matrices where the spectra were in rows and the variables (integrated regions) were in columns. Normalization, a row operation, was done with the "1-Norm", which divides each mass in a spectrum by the sum of masses from the row. Two matrices consisting of the positive ion spectra, and the negative ion spectra were thus obtained. These matrices were then exported to the PLS_Toolbox 3.0 (Eigenvector Research, Wenatchee, WA) in Matlab. Four different processing methods were applied to these data. The first is normalization,[35] which may account for the differences between spectra collected under somewhat different instrumental conditions, *e.g.*, data collection times. Following normalization, which is a row operation, three other preprocessing methods were used for some of the analyses: mean centering, standardization and logarithmic scaling. In mean centering,[35] a column operation, the mean of the values that correspond to each variable is subtracted from each value in that column. In standardization,[35] also a column operation, each data point is mean centered and then divided by the standard deviation of all of the data points

المنارة للاستشارات
www.manaraa.com

in a column in the data matrix. Standardization has the effect of putting all of the variables on equal footing. This method may be disadvantageous for ToF-SIMS data, which has many regions containing mostly noise. In logarithmic scaling, data points were replaced by their base 10 logarithms.

5.4 Results and Discussion

5.4.1 Chemical Verification of Olefin-Termination at the Monolayer Surface

Based on previous results,[9, 11, 13] it was expected that olefin-terminated monolayers would be formed when scribing was performed in the presence of neat 1,9-decadiene (see Figure 5.2), and that in mixed monolayers the degree of olefin termination at the monolayer-air interface could be controlled by varying the proportions of 1,9-decediene and a 1-alkene in the liquid above the surface (see Figure 5.3). My first evidence for monolayer formation with 1,9-decadiene came from advancing water contact angle measurements of these surfaces. A silicon surface that has been scribed in the air has an advancing water contact angle of zero degrees – it is completely wetted by water. However, a silicon surface that has been scribed in the presence of 1,9-decadiene has a water contact angle of 107°. The advancing water contact angle of a densely-packed, vinyl-terminated monolayer (on mica) prepared from $CH_2{=}CH(CH_2)_{18}Si(OEt)_3$ has previously been reported to be 101°.[36] I attribute the higher water contact angle of my $CH_2{=}CH$- terminated monolayer to surface roughness. X-ray photoelectron spectroscopy (XPS), which is a valuable surface analytical technique that provides elemental analysis and oxidation states of species in near surface regions, showed that silicon scribed under

المنارة للاستشارات
www.manaraa.com

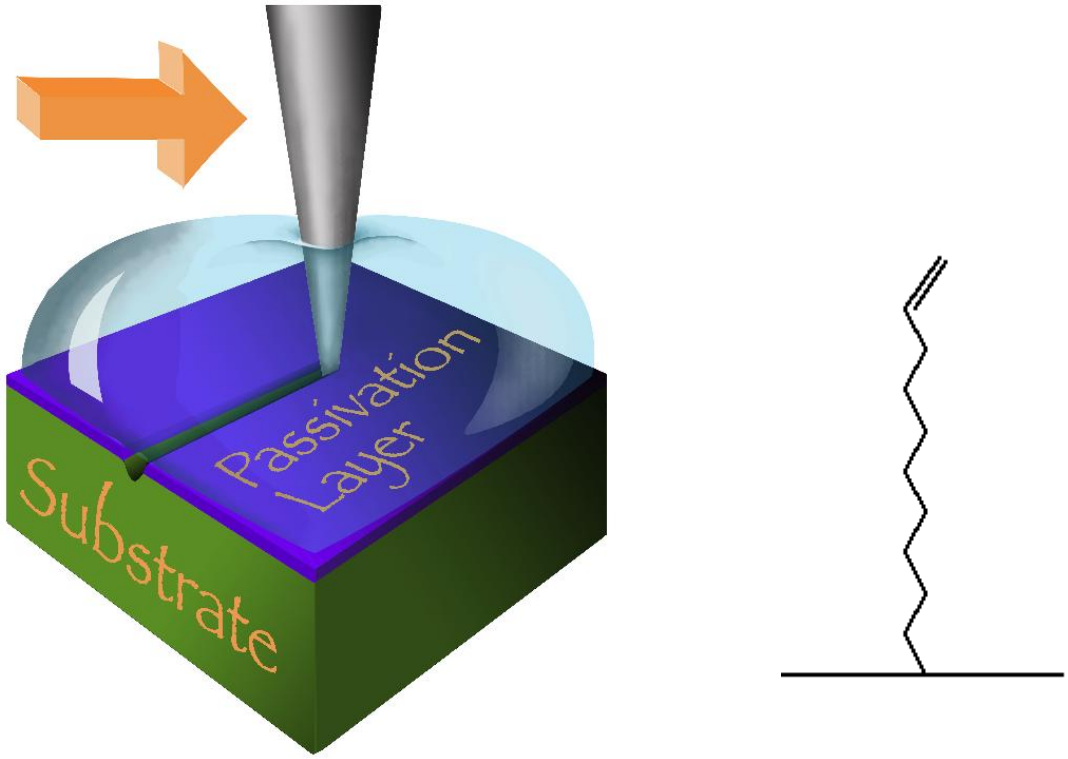

Figure 5.2. Schematic of scribing method and olefin-terminated monolayer on a patterned silicon surface.

المنارة للاستشارات
www.manaraa.com

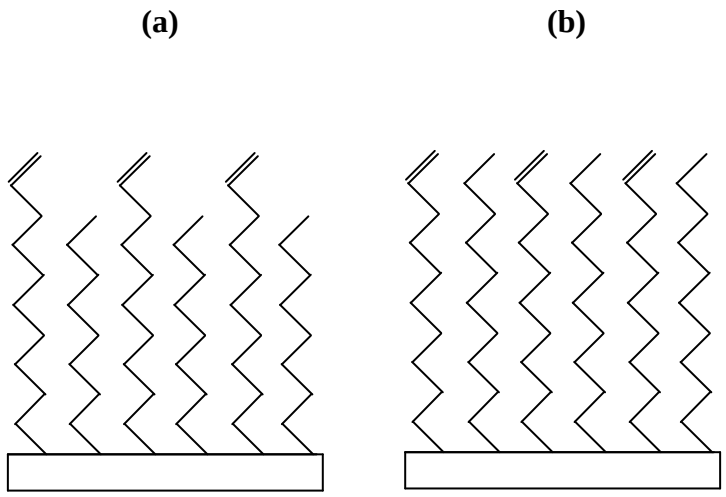

Figure 5.3. Possible arragment of alkyl chains in monolayers on a silicon surface scribed under (a) 50% 1-octene and 50% 1,9-decadiene and (b) 50% 1-decene and 50% 1,9-decadiene.

المنارة للاستشارات
www.manaraa.com

1,9-decadiene had monolayer quantities of carbon (vide infra).

In order to demonstrate the presence of a reactive double bond at the surface, homogeneous monolayers prepared from 1,9-decadiene and mixed monolayers made from 1,9-decadiene and 1-octene or 1-decene (see Table 5.1) were exposed to a variety of chemical reagents. That is, after scribing in the presence of these reactive liquids, the surfaces were allowed to react with bromine (Br_2), osmium tetroxide (OsO_4) and dichlorocarbene ($:CCl_2$). All of these reagents are known to react readily with carbon-carbon double bonds.[37] XPS proved particularly effective in monitoring these surface reactions, showing that when the fraction of 1,9-decadiene is increased in the scribing liquid, the corresponding Br/Si, Os/Si and Cl/Si ratios also increase (see Figure 5.4). It is noteworthy that for every pair of samples made from 1-octene and 1-decene, which employed the same fraction of 1,9-decadiene, the Br/Si, Os/Si and Cl/Si ratios were always slightly higher for 1-octene than that for 1-decene (See Figures 5.4a, 5.4b, 5.4c). No doubt these results reflect lower degrees of steric hindrance in mixed monolayers prepared with the shorter 1-alkene. The most reactive surfaces were made from 100% 1,9-decadiene. These results provide compelling evidence for formation of olefin-terminated mixed monolayers on scribed silicon. However, the data in Figure 5.4 also suggest that Br_2 and especially dichlorocarbene react both specifically with double bonds at monolayer surfaces and adsorb nonspecifically to these surfaces, presumably at the silicon-monolayer interface.

While the purpose of these studies was not to find optimal conditions for the reaction between these reagents and the double bonds at the surface, or to completely saturate the surface with these reagents, it was possible to use XPS to quantify the extent of reaction

المنارة للاستشارات
www.manaraa.com

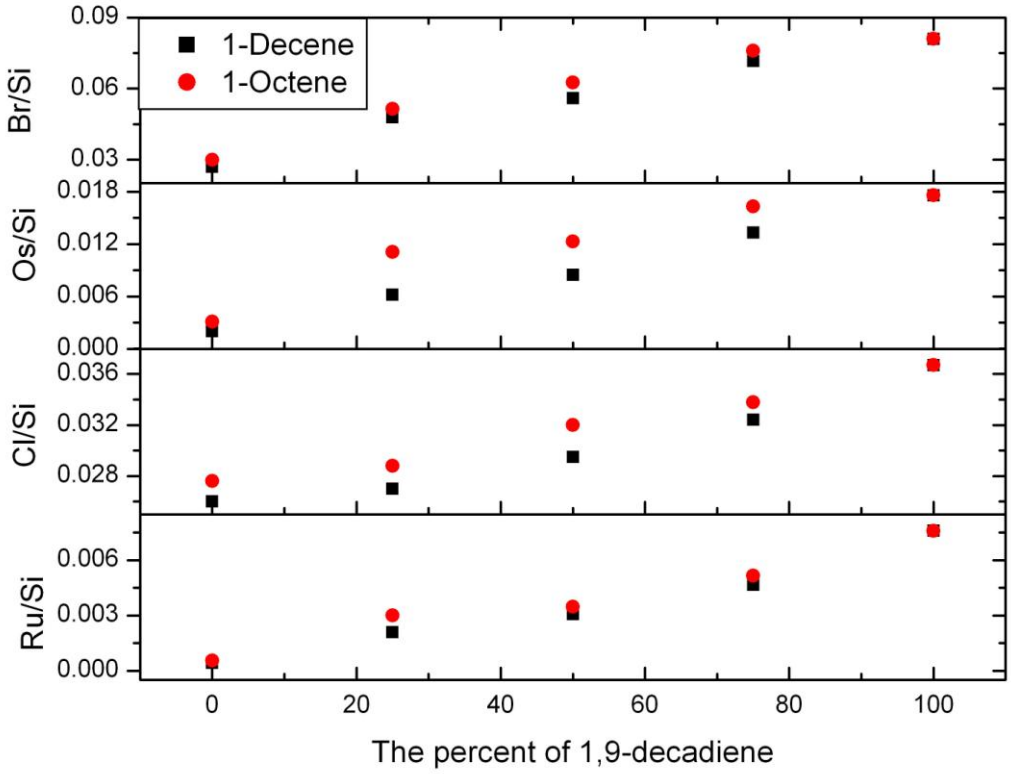

Figure 5.4. XPS (a) Br/Si ratio, (b) Os/Si ratio, (c) Cl /Si ratio and (d) Ru/Si ratio after exposure of monolayers scribed in Table 5.1 to Br_2, OsO_4, CCl_2 and Grubbs' catalyst, respectively.

المنارة للاستشارات
www.manaraa.com

of these reagents with the surface prepared from neat 1,9-decadiene. If attenuation of photoelectrons is ignored, which is a good approximation for my surfaces, I find that the yields (percentage of tethered alkyl chains that react) are 43%, 19%, and 11% for the reactions with Br_2, OsO_4, and CCl_2, respectively.

5.4.2 Reaction of Olefin-Terminated Monolayers with Grubbs' Catalyst

Another chemical verification of active carbon-carbon double bonds at the monolayer-air interface is their reaction with Grubbs' catalyst. Accordingly, the monolayers in Table 5.1 were immersed in a solution of Grubbs' catalyst for 30 min. XPS was then performed to verify that a reaction had occurred. It was not possible to use the more intense Ru 3d peaks to verify surface reaction because of their overlap with the C1s signal. However, the Ru $3p_{3/2}$ line was unobstructed and allowed determination of the yield of this surface reaction (19%). This calculation included subtracting the intensity of the Ru 3d peaks from the C1s peak. Clearly, the adsorption of Grubbs' catalyst follows the same trend as the chemisorption of Br_2, OsO_4, and CCl_2 on the mixed monolayers; as the fraction of 1,9-decadiene in the mixed monolayer increases, the corresponding Ru/Si ratio also increases. As was the case for the other adsorbates (see Figure 5.4), i) for every pair of samples made from 1-octene and 1-decene that had the same fraction of 1,9-decadiene, the Ru/Si ratio is always higher for octene than that for decene (See Figure 5.4d), presumably because of less steric hindrance around the tethered octyl chains, and ii) the homogeneous monolayer prepared from 1,9-decadiene adsorbed the largest amount of Grubbs' catalyst.

The kinetics of adsorption of Grubbs' catalyst to this monolayer was also studied.

المنارة للاستشارات
www.manaraa.com

XPS results of the Ru/Si ratio in Figure 5.5 shows that Grubbs' catalyst adsorption occurs most quickly during the first two hours of immersion in the catalyst solution and slower thereafter. It did not seem reasonable to continue this experiment for longer periods of time because after *ca*. 20 h. the Grubbs' catalyst solution began to darken, even if it was sealed under nitrogen gas and kept out of the light. Based on these results, I used a 30 min immersion time for the monolayers in the catalyst solution.

5.4.3 Polymerization

Silicon samples scribed in the presence 1,9-decadiene were immersed in a solution of Grubbs' catalyst for 30 min and rinsed well with solvent. They were then immersed in a 2.0 M solution of norbornene monomer in toluene at room temperature for 40 min to grow the polymer. XPS survey spectra (See Figure 5.6) showed that after the reaction with norbornene, the silicon and oxygen signals decreased dramatically and the carbon signal increased significantly compared to the spectrum before reaction. These results are consistent with growth of a polymer film that is on the order of 100 Å thick.

The following control experiment was performed to verify that carbon-carbon double bonds at the surface were responsible for binding Grubbs' catalyst and subsequent polynorbornene growth. A monolayer prepared from 1-decene, which should be terminated with methyl groups, was immersed in a solution of Grubbs' catalyst followed by immersion in a solution of norbornene, exactly as the surface that was prepared with 1,9-decadiene was treated. There is essentially no change in the XPS spectrum of this surface before exposure to catalyst and after exposure to Grubbs' catalyst and monomer. These spectra look essentially the same as the survey spectrum shown in Figure 5.6a, i.e.,

المنارة للاستشارات
www.manaraa.com

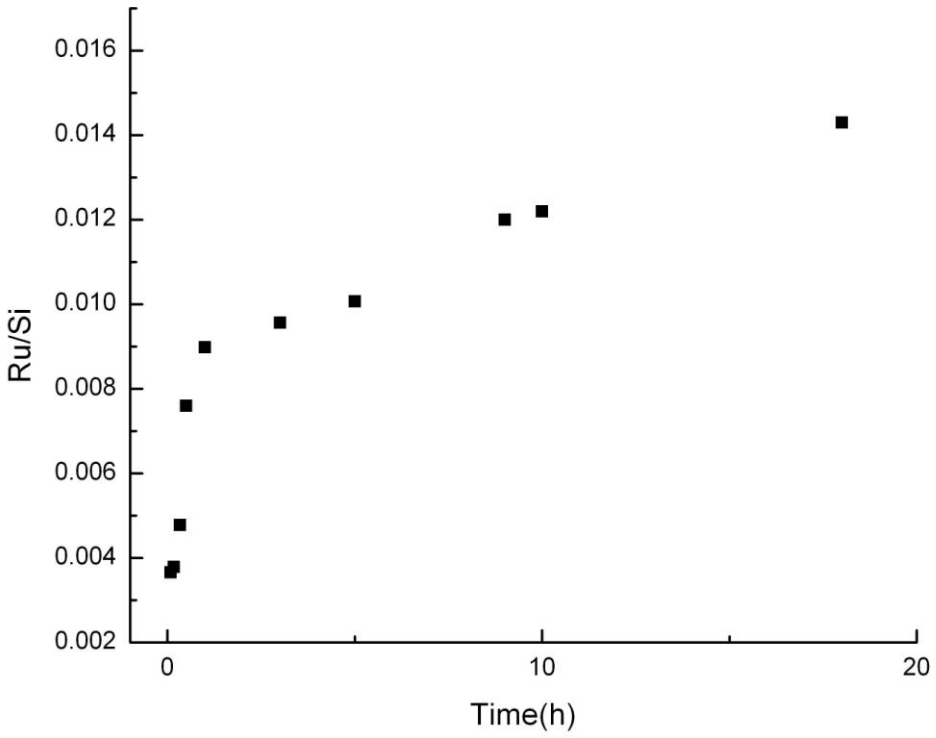

Figure 5.5. XPS Ru/Si ratio measured after adsorption of Grubbs' catalyst onto a homogenous 1,9-decadiene monolayer.

المنارة للاستشارات
www.manaraa.com

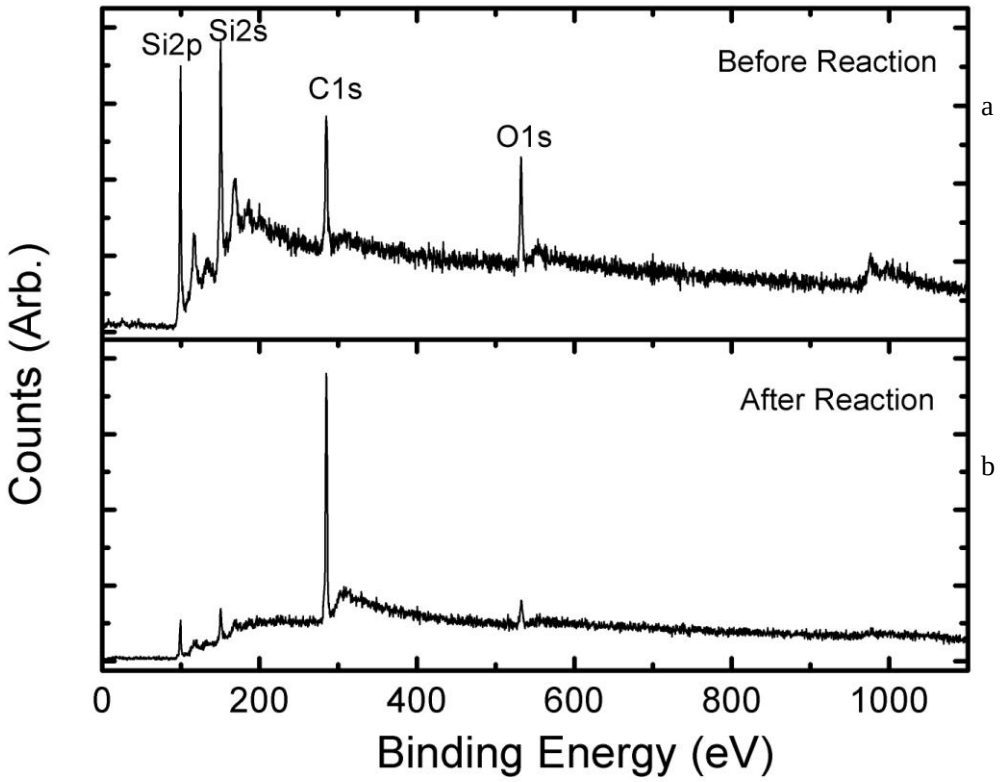

Figure 5.6. XPS of silicon scribed in the presence of 1,9-decadiene (functionalized area: 6 mm × 6 mm) before (a) and after (b) the growth of polynorbornene onto the functionalized region.

www.manaraa.com

the spectra consist of Si 2s and Si 2p peaks from the substrate, a C 1s peak that suggests monolayer quantities of alkyl chains, and a small O 1s peak, presumably due to mild oxidation of the silicon substrate, which is regularly observed in monolayers on scribed silicon.[4]

5.4.4 Kinetics of Polynorbornene Growth as Studied by XPS and ToF-SIMS

XPS and time-of-flight secondary ion mass spectrometry (ToF-SIMS) were used to study the kinetics of polynorbornene growth on 1,9-decadiene monolayers on scribed silicon surfaces. The C1s/Si2p XPS ratio showed that polymer growth was complete within *ca*. 10 min of exposure to monomer (see Figure 5.7).

ToF-SIMS provides complementary information to XPS in the form of hundreds of atomic and molecular fragments from surfaces. Because of the complexity of ToF-SIMS spectra, principal components analysis (PCA) was applied to the positive and negative ion spectra obtained from polynorbornene samples made with different exposure times to monomer. Chemometrics methods like PCA are increasingly used in ToF-SIMS data analysis to rapidly find the variation between spectra.[38] Four different preprocessing methods were applied to the data: normalization, mean centering, autoscaling, and log scaling. Figures 5.8a and 5.8b show the scores on the first principal component (PC1) using mean centering and autoscaling preprocessing of the data from the ToF-SIMS positive ion spectra from polynorbornene growth. The other two preprocessing methods used on the positive ion data (normalization and log scaling) show essentially the same trends. Figures 5.8c and 5.8d show the scores on PC1 of ToF-SIMS negative ion spectra using mean centering and autoscaling preprocessing, respectively, for the polymer growth

المنارة للاستشارات
www.manaraa.com

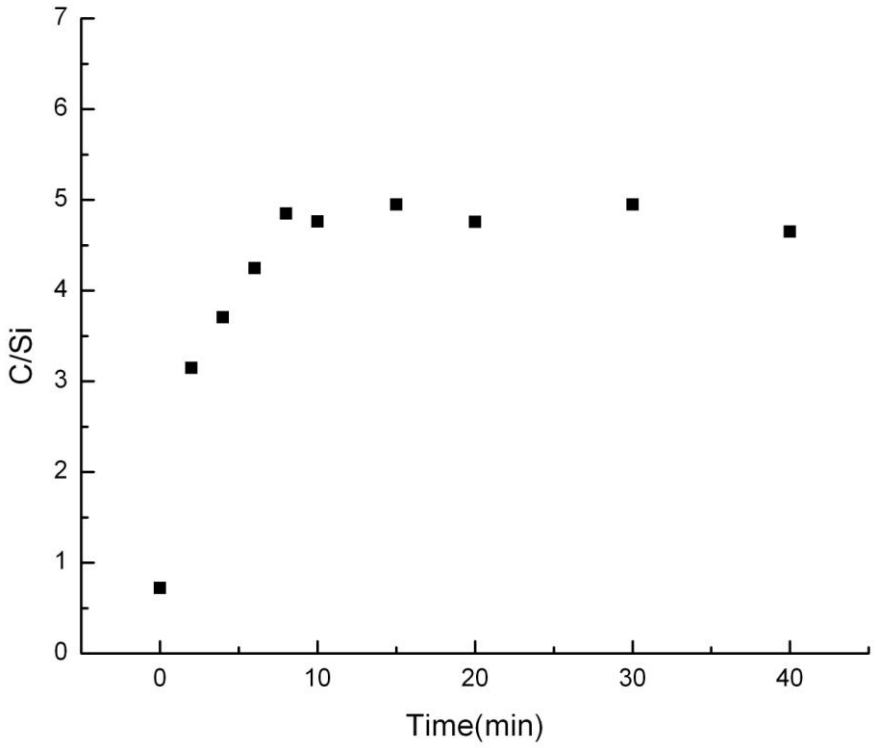

Figure 5.7. XPS C/Si ratio of samples prepared by varying the reaction time of norbornene with 1,9-decadiene monolayers after adsorption of Grubbs' catalyst. Each point represents a different experiment.

المنارة للاستشارات
www.manaraa.com

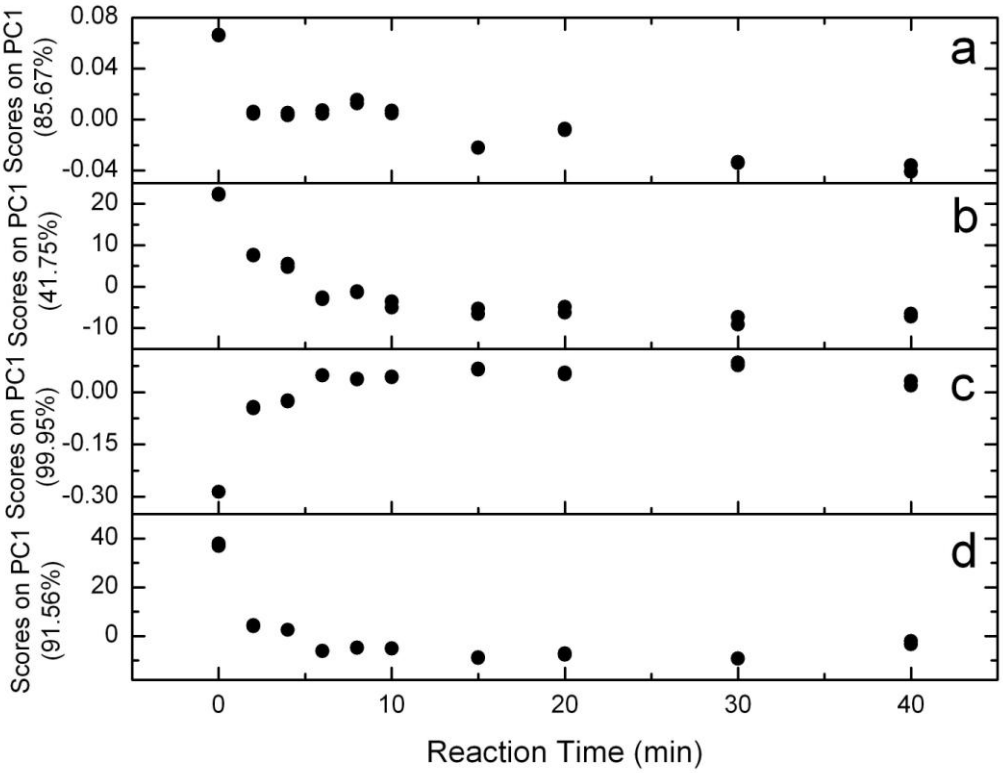

Figure 5.8. Scores on PC1 from a PCA analysis of TOF-SIMS data showing the combinations of positive and negative ion spectra with two different preprocessing methods (mean-centering and autoscaling): (a) positive ion spectra and mean centering (b) positive ion spectra and autoscaling (c) negative ion spectra and mean centering (d) negative ion spectra and autoscaling.

www.manaraa.com

samples. The negative ion spectra preprocessed with the other two processing methods again show essentially the same trends as those in Figures 5.8c and 5.8d. All of these ToF-SIMS results are similar to the XPS results shown in Figure 5.7. That is, after approximately 10 min, little if any change in the surface chemistry is observed.

Scores on principal components often show graphically the relationships between samples. Loadings, on the other hand, reveal the chemical base for these relationships. Table 5.2 shows the ten largest peaks from the loadings on PC1 of the positive ion data using mean centering and autoscaling. Here I see that the loadings of pure hydrocarbon fragments, such as $C_6H_5^+$, $C_5H_7^+$, $C_7H_7^+$, $C_3H_3^+$, $C_6H_7^+$, $C_4H_3^+$, $C_5H_5^+$, $C_6H_6^+$, $C_4H_4^+$, $C_4H_5^+$ and $C_7H_8^+$ are negative. These peaks are expected to come from the polynorbornene brushes. In contrast, the peaks that contain silicon, such as Si^+, SiH^+, $SiHO^+$ and $SiC_4H_7^+$, which are expected to come from the substrate, have the opposite polarity, i.e., they have positive values. These data, combined with the scores on PC1 in Figure 5.8, paint a consistent picture of polynorbornene growth on scribed silicon. That is, the data from surfaces with negative scores on PC1 (see Figures 5.8a-b), i.e., the surfaces with thicker polynorbornene layers, are richer in the peaks in the loadings plots with negative polarity, i.e., the hydrocarbon peaks. In contrast, the surfaces with positive scores on PC1 (see Figures 5.8a-b), i.e., the surfaces with thinner polynorbornene layers, are richer in the peaks in the loadings plots with positive polarity, i.e., the silicon-containing peaks that are expected from the substrate. It has previously been shown that ToF-SIMS data of alkyl monolayers of varying thickness on scribed silicon behave similarly, i.e., thicker monolayers were richer in hydrocarbon peaks and thinner monolayers were richer in silicon-containing substrate peaks.[35] Please note that the

المنارة للاستشارات
www.manaraa.com

Table 5.2. Ten largest peaks from the loadings plots of PC1 from a PCA analysis of positive ion spectra of samples after different reaction times with norbornene.

PC1					
Mean-centering			Autoscaling		
m/z	loadings	species	m/z	loadings	species
28	0.5911	Si	51	-0.109	C_4H_3
29	0.5288	SiH	65	-0.1084	C_5H_5
23	-0.4592	Na	78	-0.1082	C_6H_6
91	-0.1366	C_7H_7	77	-0.108	C_6H_5
67	-0.1361	C_5H_7	91	-0.108	C_7H_7
77	-0.1329	C_6H_5	52	-0.1078	C_4H_4
43	0.1206	$SiCH_3$,C_3H_7	53	-0.1078	C_4H_5
39	-0.1191	C_3H_3	92	-0.1069	C_7H_8
45	0.1059	SiHO	39	-0.1067	C_3H_3
79	-0.0989	C_6H_7	83	0.1065	Si C_4H_7

المنارة للاستشارات
www.manaraa.com

polarity (positive or negative) of the scores and loadings is completely arbitrary because of the sign ambiguity in PCA. That is, in PCA, a data matrix, **S**, is decomposed into a scores matrix, **T**, and a loadings matrix, **P**: $\mathbf{S} = \mathbf{TP}^T$. However, it is also true that $\mathbf{S} = (-\mathbf{T})(-\mathbf{P}^T)$.

Table 5.3 shows the loadings plots from PC1 of the ten largest peaks and their likely assignments from negative ion spectra (see Figures 5.8c-d) preprocessed by mean-centering and autoscaling. The results for mean centering are similar to those found in Table 5.2 and Figures 5.8a-b. That is, in Figure 5.8c, the thicker polynorbornene films show positive scores and these correspond to the peaks with positive loadings in Table 5.3, which include fragments expected from a hydrocarbon layer: H^-, CH^-, C_2H^-, C^-, and C_2^-, and CH_2^-. Conversely, the surfaces with thinner polymer layers have negative scores (Figure 5.8c) and loadings (Table 5.3) and these loadings peaks correspond to species that would be expected from the substrate: $^{35}Cl^-$, OH^-, $^{37}Cl^-$, and O^-.

The autoscaling results in Table 5.3 are more difficult to interpret. Autoscaling is a less than ideal method for preprocessing my data because a large fraction of my binned regions contain mostly noise, and autoscaling makes these regions as significant as those that contain real information. In addition, the large number of binned regions I analyze makes it increasingly likely that one or more of these noisy regions will correlate well with the data from real peaks, and that these regions will, by chance, emerge as being significant in the analysis. Thus, some of the loadings predicted by autoscaling should be unreliable. To check this hypothesis I examined the raw data at m/z 153, 168, 169, 170, 171, 186, and 193. The binned regions at m/z 153, 168, 169, 170, and 171 appear to contain only noise. Those at m/z 186 and 193 appear to contain small signals.

المنارة للاستشارات
www.manaraa.com

Table 5.3. Ten largest peaks from the loadings plots of PC1 from a PCA analysis of negative ion spectra of samples after different reaction times with norbornene.

PC1					
Mean-centering			Autoscaling		
m/z	loadings	species	m/z	loadings	species
1	0.8316	H	35	0.0738	Cl
35	-0.4732	Cl	37	0.0738	^{37}Cl
17	-0.159	OH	47	0.0738	CCl
37	-0.1492	^{37}Cl	153	0.0738	Unknown
16	-0.1261	O	168	0.0738	Unknown
13	0.113	CH	169	0.0738	Unknown
25	0.077	C_2H	170	0.0738	Unknown
12	0.033	C	171	0.0738	Unknown
24	0.0264	C_2	186	0.0738	Unknown
14	0.0111	CH_2	193	0.0738	Unknown

المنارة للاستشارات
www.manaraa.com

While the PCA results represent an important, total analysis of the data, it remains essential to stay close to the original data during data analysis. Figure 5.9 shows the normalized intensities of the ten largest peaks in the negative ion data (see Table 5.3). All of these peaks show the expected trends: as polynorbornene growth occurs, signals from ions expected from the substrate decrease in intensity ($^{35}Cl^-$, $^{37}Cl^-$, O^-, and OH^-), while signals from ions expected from the polynorbornene film increase in intensity (H^-, CH^-, C_2H^-, C^-, CH_2^-, C_2^-).

5.5 Conclusions

In summary, olefin-terminated monolayers and mixed monolayers with terminal olefin functionality have been prepared by chemomechanically modifying silicon. That a terminal double bond is present at the monolayer surfaces, and that this double bond remains reactive was demonstrated by reactions with bromine, osmium tetroxide, and dichlorocarbene. Grubbs' catalyst was also shown to bind to these surfaces, which then underwent polynorbornene growth by ROMP. The kinetics of Grubbs' catalyst adsorption and polynorbornene growth were investigated. ToF-SIMS gave additional chemical characterization and confirmation of polynorbornene growth as a function of time.

المنارة للاستشارات
www.manaraa.com

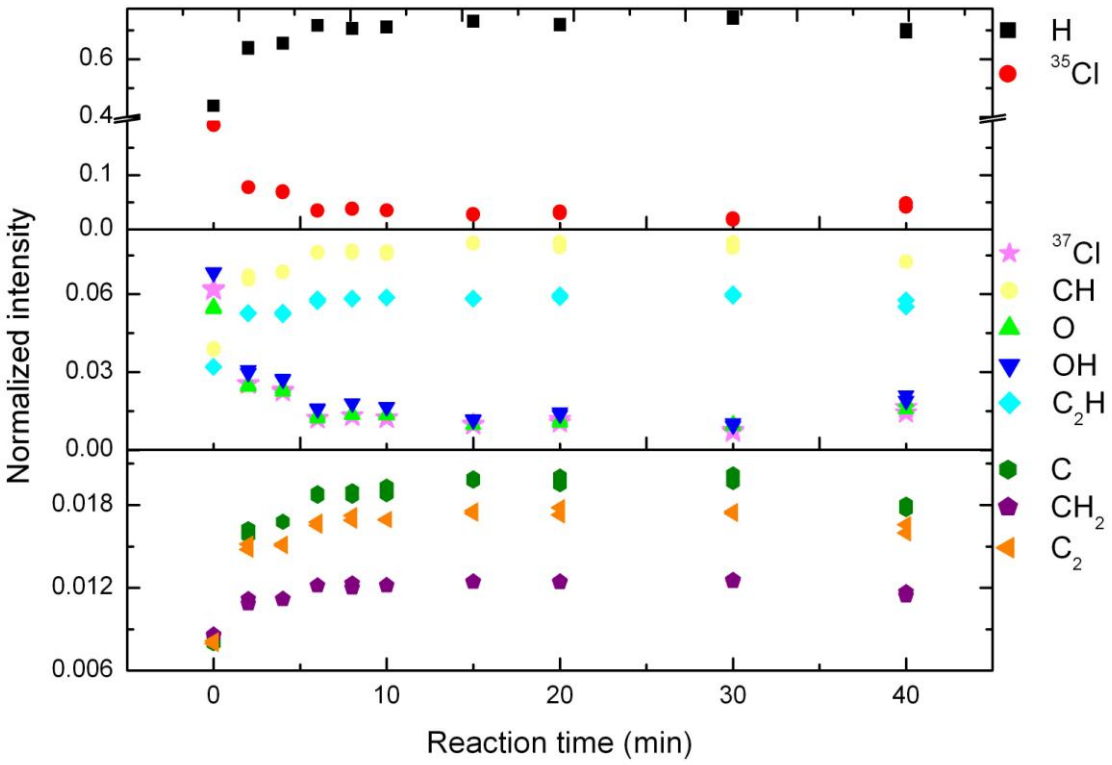

Figure 5.9. Normalized intensity of the ten largest peaks from PC1 loadings plot of a PCA analysis of TOF-SIMS negative ion spectra of samples, the same mean-centered data that were used to make Figure 5.8c.

المنارة للاستشارات
www.manaraa.com

5.6 References

(1) Buriak, J. M. *Chem.Rev.* **2002**, *102*, 1271-1308.

(2) Hamers, R. J.; Wang, Y. *Chemical Reviews* **1996**, *96*, 1261-1290.

(3) Bent, S. F. *Surface Science* **2002**, *500*, 879-903.

(4) Yang, L.; Lua, Y.-Y.; Lee, M. V.; Linford, M. R. *Acc.Chem.Res.* **2005**, *38*, 933-942.

(5) Niederhauser, T. L.; Jiang, G.; Lua, Y.-Y.; Dorff, M. J.; Woolley, A. T.; Asplund, M. C.; Berges, D. A.; Linford, M. R. *Langmuir* **2001**, *17*, 5889-5900.

(6) Niederhauser, T. L.; Lua, Y.-Y.; Jiang, G.; Davis, S. D.; Matheson, R.; Hess, D. A.; Mowat, I. A.; Linford, M. R. *Angew.Chem., Int.Ed.Engl.* **2002**, *41*, 2353-2356.

(7) Lua, Y.-Y.; Niederhauser, T. L.; Matheson, R.; Bristol, C.; Mowat, I. A.; Asplund, M. C.; Linford, M. R. *Langmuir* **2002**, *18*, 4840-4846.

(8) Niederhauser, T. L.; Lua, Y.-Y.; Sun, Y.; Jiang, G.; Strossman, G. S.; Pianetta, P.; Linford, M. R. *Chemistry of Materials* **2002**, *14*, 27-29.

(9) Lua, Y.-Y.; Lee, M. V.; Fillmore, W. J. J.; Matheson, R.; Sathyapalan, A.; Asplund, M. C.; Fleming, S. A.; Linford, M. R. *Angew.Chem.Int.Ed.Eng.* **2003**, *42*, 4046-4049.

(10) Lua, Y.-Y.; Fillmore, W. J. J.; Linford, M. R. *Applied Surface Science.* **2004**, *231-232*, 323-327.

(11) Lua, Y.-Y.; Fillmore, W. J. J.; Yang, L.; Lee, M. V.; Savage, P. B.; Asplund, M. C.; Linford, M. R. *Langmuir* **2005**, *21*, 2093-2097.

(12) Wacaser, B. A.; Maughan, M. J.; Mowat, I. A.; Niederhauser, T. L.; Linford, M. R.; Davis, R. C. *Applied Physics Letters* **2003**, *82*, 808-810.

(13) Lee, M. V.; Hoffman, M. T.; Barnett, K.; Geiss, J.-M.; Smentkowski, V. S.; Linford,

المنارة للاستشارات
www.manaraa.com

M. R.; Davis, R. C. *Journal of Nanoscience and Nanotechnology* **2006**, *6*, 1639-1643.

(14) Lua, Y.-Y.; Niederhauser, T. L.; Wacaser, B. A.; Mowat, I. A.; Woolley, A. T.; Davis, R. C.; Fishman, H. A.; Linford, M. R. *Langmuir* **2003**, *19*, 985-988.

(15) Zilch, L. W.; Husseini, G. A.; Lua, Y.-Y.; Lee, M. V.; Gertsch, K. R.; Cannon, B. R.; Perry, R. M.; Sevy, E. T.; Asplund, M. C.; Woolley, A. T.; Linford, M. R. *Rev. Sci. Instr.* **2004**, *75*, 3065-3067.

(16) Xu, S.; Liu, G.-Y. *Langmuir* **1997**, *13*, 127-129.

(17) Liu, G.-Y.; Xu, S.; Qian, Y. *Acc.Chem.Res.* **2000**, *33*, 457-466.

(18) Abbott, N. L.; Folkers, J. P.; Whitesides, G. M. *Science* **1992**, *257*, 1380-1382.

(19) Weck, M.; Jackiw, J. J.; Rossi, R. R.; Weiss, P. S.; Grubbs, R. H. *J.Am.Chem.Soc.* **1999**, *121*, 4088-4089.

(20) Kim, N. Y.; Jeon, N. L.; Choi, I. S.; Takami, S.; Harada, Y.; Finnie, K. R.; Girolami, G. S.; Nuzzo, R. G.; Whitesides, G. M.; Laibinis, P. E. *Macromolecules* **2000**, *33*, 2793-2975.

(21) Trnka, T. M.; Grubbs, R. H. *Acc. Chem. Res.* **2001**, *34*, 18-29.

(22) Sanford, M. S.; Love, J. A.; Grubbs, R. H. *J. Am. Chem. Soc.* **2001**, *123*, 6543-6554.

(23) Sanford, M. S.; Ulman, M.; Grubbs, R. H. *J. Am. Chem. Soc.* **2001**, *123*, 749-750.

(24) Bielawski, C.; Grubbs, R. H. *Macromolecules* **2001**, *34*, 8838-8840.

(25) Scherman, O. A.; Kim, H. M.; Grubbs, R. H. *Macromolecules* **2002**, *35*, 5366-5371.

(26) Choi, T.-L.; Grubbs, R. H. *Angew. Chem. Int. Ed. Engl.* **2003**, *42*, 1743-1746.

(27) Juang, A.; Scherman, O. A.; Grubbs, R. H.; Lewis, N. S. *Langmuir* **2001**, *17*, 1321-1323.

المنارة للاستشارات
www.manaraa.com

(28) Perring, M.; Dutta, S.; Arafat, S.; Mitchell, M.; Kenis, P. J. A.; Bowden, N. B. *Langmuir* **2005**, *21*, 10537-10544.

(29) Dutta, S.; Perring, M.; Barrett, S.; Mitchell, M.; Kenis, P. J. A.; Bowden, N. B. *Langmuir* **2006**, *22*, 2146-2155.

(30) Buchmeiser, M. R.; Sinner, F.; Mupa, M.; Wurst, K. *Macromolecules* **2000**, *33*, 32-39.

(31) Jarroux, N.; Keller, P.; Mingotaud, A.-F.; Mingotaud, C.; Sykes, C. *J. Am. Chem. Soc.* **2004**, *126*, 15958-15959.

(32) Magagnin, L.; Maboudian, R.; Carraro, C. *Electrochem. Solid-State Lett.* **2001**, *4*, C5-C7.

(33) Boontongkong, Y.; Cohen, R. E.; Rubner, M. F. *Chem. Mater* **2000**, *12*, 1628-1633.

(34) Yosi, Y.; Shacham-Diamandz *Electrochem. Solid-State Lett.* **2000**, *3*, 279-282.

(35) Yang, L.; Lua, Y.-Y.; Jiang, G.; Tyler, B. J.; Linford, M. R. *Anal. Chem.* **2005**, *77*, 4654-4661.

(36) Peanasky, J.; Schneider, H. M.; Granick, S.; Kessel, C. R. *Langmuir* **1995**, *11*, 953-962.

(37) March, J. *Advanced Organic Chemistry*, 4th Ed. ed.; John Wiley & Sons: New York, 1992.

(38) Wagner, M. S.; Graham, D. J.; Ratner, B. D.; Castner, D. G. *Surface Science* **2004**, *570*, 78-97.

(39) *Monolayers chemomechanically patterned onto silicon surfaces using 1-hexadecene and a tungsten carbide ball similarly functioned as resist layers for the electroless deposition of copper.*

المنارة للاستشارات
www.manaraa.com

PART III. PDMS Transfer in Microcontact Printing

Chapter 6 Effect of Surface Free Energy on PDMS Transfer in Microcontact Printing, and its Application to ToF-SIMS to Probe Surface Energies*

6.1 Abstract

Although polydimethylsiloxane (PDMS) transfer during microcontact printing (μCP) has been observed in previous reports, which generally focused on only one or a few different substrates, in this work, I investigate the extent of PDMS transfer onto different surfaces with a wide range of hydrophobicities, including clean silicon, clean titanium, clean gold, "dirty" silicon, polystyrene, Teflon™, and surfaces modified with polyethylene glycol (PEG), amino, dodecyl, and hexadecyl monolayers, using an uninked, unpatterned PDMS stamp. The PDMS transferred onto planar surfaces is easily detected by wetting and spectroscopic ellipsometry. More importantly, it is detected by time-of-flight secondary ion mass spectrometry (ToF-SIMS) because of the sensitivity of this technique to PDMS. The effect of surface free energy on PDMS transfer in microcontact printing is investigated and the relationship between the amount of PDMS in ToF-SIMS spectra and the surface tensions of initial surfaces is revealed. Therefore,

---

*This chapter is reproduced with pemission from *Langmuir*, in press. Copyright 2009 American Chemical Society.

المنارة للاستشارات
www.manaraa.com

PDMS transfer can be applied as a probe of surface free energies using ToF-SIMS, where PDMS preferentially transfers onto more hydrophilic surface features during stamping, with little transfer onto very hydrophobic surface features. Multivariate curve resolution (MCR) analysis of the ToF-SIMS image data further confirms and clarifies these results.

6.2 Introduction

Microcontact printing (μCP) is a well-recognized and important tool for selective patterning of surfaces at the micron and nanoscale with a wide variety of adsorbates.[1, 2] In μCP, a patterned elastomeric stamp, usually polydimethylsiloxane (PDMS), is "inked" with a molecule/species of interest and then brought into contact with a substrate. Ideally, transfer of the ink takes place only at the raised points of the stamp that make contact with the substrate. A current and important topic in μCP is the transfer of low molecular weight oligomers of PDMS that often accompanies ink transfer.[3] PDMS is a rather common contaminant of many surfaces and materials, and ToF-SIMS, even with the older Ga^+ guns is exquisitely sensitive to it, showing strong, characteristic signals.

A series of reports in the literature leave no doubt regarding the transfer of PDMS oligomers during μCP. In 1999, Böhm and coworkers used X-ray photoelectron spectroscopy (XPS) and infrared spectroscopy to show that a significant amount of PDMS contamination occurs during μCP of dodecanethiol on gold, where their printing was done at fairly high pressures. The only precleaning of their stamps was a rinse in ethanol.[4] In 2000, Yang and coworkers observed PDMS transfer in microcontact printing on functionalized poly(ethylene terephthalate). In a control experiment, fluorescence

المنارة للاستشارات
www.manaraa.com

microscopy of a microcontact printed surface suggested that PDMS transfer enhanced streptavidin chemisorption. The presence of PDMS after μCP was confirmed by imaging ToF-SIMS. Transferred PDMS could be partially removed by sonicating in ethanol.[5] In 2002, Graham and coworkers published a detailed study of the transfer of PDMS to gold surfaces during microcontact printing with dodecanethiol. Their study included an exhaustive cleaning of the stamps that took approximately one week (a series of extractions consisting of soaking or sonicating in different solvents). After this cleaning procedure, and a final blotting, PDMS could only be detected at the detection limit of XPS (ca. 1%) in a subset of their samples. However, a principal components analysis of ToF-SIMS data from a series of surfaces prepared with increasing concentrations of a dodecanethiol ink indicated that PDMS transfer consistently occurred during μCP, but decreased with increasing thiol concentration. Their work is a statement of the sensitivity of ToF-SIMS for PDMS, and its importance as one of the tools that provides conclusive identification of it.[6] A year later, Glasmästar and coworkers introduced a UV/ozone treatment of PDMS stamps as a method for reducing PDMS transfer during μCP. This procedure only took a few minutes and had the advantage (or disadvantage, depending on the need) of yielding a hydrophilic stamp. PDMS transfer during μCP was demonstrated using Milli-Q water as the ink.[7]

In 2004, Zhou and coworkers[8] studied conditions for μCP of various oligo(ethyleneglycol)-containing thiols using oxygen plasma treated stamps. In their work, infrared reflection-absorption spectroscopy clearly showed PDMS transfer to gold substrates during μCP, and suggested that i) the PDMS is located at the top of the monolayer and ii) it is easily removed by a short sonication in ethanol. A reduction in

المنارة للاستشارات
www.manaraa.com

water contact angle to a level similar to that obtained with solution-prepared monolayers accompanied PDMS extraction of printed surfaces with solvents. Vickerman and Briggs[9] have also reported that PDMS contamination of surfaces in general can be removed by sonication with hexane, acetone, and methanol. In 2005 Langowski and Uhrich[10] studied different oxygen plasma treatments of PDMS stamps to reduce PDMS transfer during μCP to oxidized polymethyl methacrylate (PMMA), where the "ink" was deionized water. After plasma treatment, X-ray photoelectron spectroscopy showed a large increase in the oxygen content of the stamps, a large decrease in the carbon content, and a substantial decrease in PDMS transfer under all plasma treatment conditions studied. In related work, Felmet and coworkers[11] reported nanotransfer printing of copper lines onto dithiol-modified GaAs. The copper lines were always nonconductive and found to be filled with PDMS, unless the stamp was first leached with toluene, which reduced PDMS contamination.

Tingey and coworkers attributed, at least in part, non-specific transfer of material observed by ellipsometry during affinity μCP to PDMS from the stamp.[12] Thomson and coworkers similarly hypothesized that material observed by SEM after μCP may have been due to impurities from the PDMS stamp.[13] Perl and coworkers studied a new dendrimer-based ink for positive microcontact printing on gold. They reported water contact angles of surfaces made by printing with their inks (79 ± 2) that were ca. 20 degrees higher than the corresponding surfaces prepared by solution assembly (59 ± 4). They attributed this difference in wetting to PDMS transfer from the stamp.[14] Zhao and coworkers used wetting to show transfer of PDMS oligomers from a PDMS mold in replica molding of polyimide.[15]

المنارة للاستشارات
www.manaraa.com

As noted above, the presence of low molecular weight oligomers of PDMS transferred during the μCP of proteins often enhances protein transfer from the stamp. This effect also appears to be operative for DNA (vide infra). However, Foley et al. studied antibody binding to a protein antigen that had been deposited on gold using μCP. They used surface plasmon resonance and XPS to show significant silicone (PDMS) oligomer transfer, noting that *less* protein was transferred by μCP than the amount of protein adsorbed from solution.[16] In contrast, Ross and coworkers studied μCP of bovine serum albumin (BSA) on polymerized lipid bilayers and glass. In their work, the amount of protein transferred by μCP was greater than that obtained by nonspecific adsorption from solution. In addition, much more protein transfer occurred from hydrophobic (unoxidized) PDMS stamps than from (air) plasma oxidized stamps. Low molecular weight oligomers of PDMS were transferred to surfaces from uninked stamps, and the adsorbed PDMS was found to increase subsequent BSA adsorption from solution. Their PDMS stamps were cured at fairly high temperature, compared to other researchers: 100°C for 2 h.[17] Thibault and coworkers found that DNA transfer, along with its subsequent hybridization, was much more effective for stamps that had *not* undergone Soxhlet extraction (vide infra), i.e., the transfer of PDMS oligomers during μCP enhanced DNA adsorption.[18]

There is some question as to the efficiency of the different extraction methods that have been employed to remove unbound PDMS from stamps. In general, most of the methods that have been described, such as solvent extraction (soaking), UV or plasma treatment, or long cure times, are not completely effective in eliminating transfer of low MW PDMS oligomers during μCP.[16] For example, Hale and coworkers showed that

المنارة للاستشارات
www.manaraa.com

baking the PDMS significantly reduced, but by no means eliminated, the amount of PDMS transfer in μCP of an amino silane, compared to PDMS transfer from the unbaked stamp.[19] However, of all the methods investigated, Soxhlet extraction may be the most promising. Although Sharpe and coworkers,[20] who may have been the first to apply this technique to clean PDMS stamps, reported that extraction did not diminish PDMS trasfer in μCP, Tan and coworkers showed that Soxhlet extraction of PDMS stamps prevented transfer of PDMS oligomers during affinity μCP of DNA,[21] and Thibault and coworkers[18] showed that Soxhlet extraction of PDMS stamps would similarly eliminate the transfer of low molecular weight oligomers of PDMS. Thus, there is at least some suggestion that Soxhlet extraction may be the most efficient extraction method contemplated to date.

PDMS transfer from uninked (and unextracted) stamps has also been employed as a useful surface patterning tool. In 2004 Wang and coworkers modified polymer surfaces by stamping with uninked PDMS stamps. PDMS transfer was confirmed by AFM and infrared spectroscopy, and the residual PDMS could be used to direct subsequent polymer deposition in spin- or dip-coating.[22] Briseno and coworkers employed the same technique to transfer PDMS as a resist for dip coating organic semiconductors. PDMS transfer was confirmed by quartz crystal microbalance (QCM), Fourier transform infrared spectroscopy (FTIR), XPS, wetting, and mass spectrometry. No effective resist layer was deposited when solvent extracted (soaked) PDMS stamps were employed.[23] Åsberg and coworkers also used the transfer of low molecular weight PDMS oligomers from patterned, uninked, PDMS stamps as a method for creating patterns with hydrophobic and hydrophilic areas, and then observed selective adsorption to the PDMS of biomolecules and biomolecule conjugates.[24] Wigenius and coworkers then used imaging

المنارة للاستشارات
www.manaraa.com

ellipsometry and AFM to study PDMS transfer from uninked stamps to SiO_2 and $SiCl_2(CH_3)_2$-treated substrates.[25] They found that the thickness of the transferred material increased with the contact time between the stamp and the substrate, and that the resulting patterns of PDMS were unstable with time, forming submicron droplets on the surfaces. Similar submicron features appear to be present in Sharpe's AFM images, and are attributed to contamination from the stamp.[20]

Sharpe and coworkers recently studied PDMS contamination during μCP on gold of both a hydrophilic (16-mercaptohexadecanoic acid, MHDA) and a hydrophobic ink (*n*-octadecanethiol, ODT).[20] They noted that significant PDMS contamination was observed when MHDA was printed, but little or no contamination was observed if ODT was printed. This same effect was observed whether uninked stamps, or stamps inked with MHDA or ODT, were brought into contact with preformed MHDA or ODT monolayers, respectively. They proposed that *hydrophilic* contaminants are adsorbed onto surfaces from PDMS stamps during μCP, which have a high affinity for hydrophilic inks and surfaces.[20] That is, they interpreted their results in terms of hydrophilic inks promoting adsorption of hydrophilic species. I will comment on their hypothesis in Section 6.5.

All of this earlier work sets the stage for my present study on PDMS transfer onto a variety of different surfaces. Indeed, to the best of my knowledge, this paper represents the first systematic study of PDMS transfer from uninked and unextracted stamps to a series of surfaces that exhibit a wide range of hydrophobicities. Furthermore, it appears to be the first detailed study that articulates that the surface wetting (free energy) of the substrate plays a critical role in determining the extent of PDMS oligomer transfer during

المنارة للاستشارات
www.manaraa.com

μCP. I then use this phenomenon to demonstrate that PDMS oligomer transfer in μCP can be used in conjunction with ToF-SIMS as an effective tool for probing surface free energies at the micron scale, where PDMS oligomer transfer occurs preferentially to hydrophilic surfaces or surface features, over more hydrophobic regions (see Figure 6.1).

Because PDMS contamination is a common problem in materials analysis by ToF-SIMS, and the deliberate introduction of PDMS into a SIMS system may seem a fairly strange proposition to many practitioners of this technique, I emphasize that the few Ångstroms or nanometers of PDMS that adsorb to my surfaces in this study have not caused *any* noticeable contamination of our ToF-SIMS instrument. I also wish to emphasize that my work is *not* a report of a new contrast agent for SIMS, which might improve the ion yields of our gallium source. Rather, a material's adsorption of PDMS oligomers (or lack thereof) from planar PDMS stamps is shown to be a useful surface probe that can reveal the hydrophobicity or hydrophilicity of surface features by ToF-SIMS, providing at least a relative measure of the wetting properties of microscopic surface features. Hence, the application of this technique should not be dependent on any particularly SIMS primary ion source.

6.3 Experimental

6.3.1 Reagents

Toluene and chloroform were spectral grade and purchased from Aldrich, St. Louis, MO. Buckminsterfullerene (99.5%) was obtained from SES Research (Houston, TX). Trihexadecyloxybenzaldehyde (THOB) was obtained from the Advanced Materials Laboratory, National Institute for Materials Science (Namiki, Tsukuba, Ibaraki, Japan)

المنارة للاستشارات
www.manaraa.com

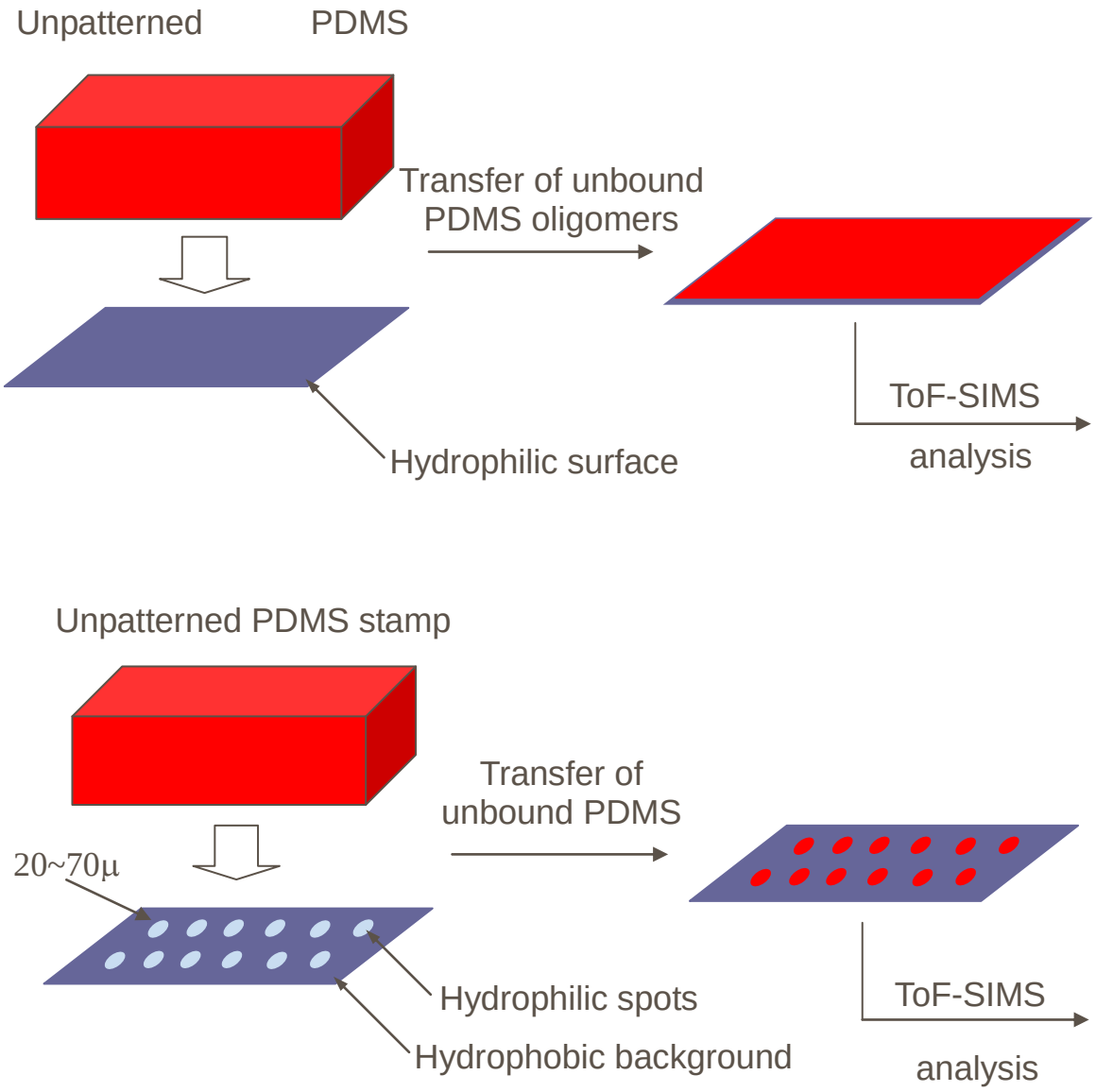

Figure 6.1. Illustration of the PDMS contrast stamping method. A planar PDMS stamp is pressed against a surface. Transfer of unbound PDMS oligomers in the stamp occurs preferentially at hydrophilic regions on the surface, over more hydrophobic regions.

المنارة للاستشارات
www.manaraa.com

and was used as received. Sylgard 184 silicone elastomer and curing reagent were purchased from Dow Corning, Midland, MI. 2-[methoxy(polyethylenoxy)propyl] trimethoxysilane [$(CH_3O)_3Si(CH_2)_3(OCH_2CH_2)_{6\text{-}9}OCH_3$, ≥ 90%, MW 460-590, 6-9 PEG units] was obtained from Gelest, Tullytown, PA. Trichloro(3,3,4,4,5,5,6,6,7,7,8,8,8-tridecafluorooctyl)silane [$CF_3(CF_2)_5CH_2CH_2SiCl_3$, ≥ 97%] was from Fluka, USA. 1-Hexadecene (~99%), 1-dodecene (≥ 99%) and polystyrene (average M_w ~192,000) were obtained from Aldrich. Fluoro Pcl™ PFC M1604V was obtained from Cytonix, Beltsville, MD.

6.3.2 Solid Surfaces

Silicon wafers (100) were obtained from Montco Silicon Technologies. Titanium and gold films on silicon wafers were obtained by electron beam evaporation at BYU. These surfaces were cleaned in a Harrick plasma cleaner (model number PDC-32G, Power: 18W) with an air plasma prior to stamping. “Dirty” silicon wafers are silicon surfaces that were used as received from the manufacturer, without any surface cleaning or rinsing.

6.3.3 Thin Film Preparation

Buckminsterfullerene was dissolved in toluene until the solution was saturated. Trihexadecyloxybenzaldehyde (THOB) was dissolved in chloroform at a concentration of 0.5% (w/w). These solutions were placed dropwise onto clean silicon shards and the solvents were allowed to evaporate leaving thin, molecular films of these compounds. THOB thin films were also obtained on silicon surfaces by spinning this solution. Polystyrene (average M_w ~192,000) was dissolved in toluene at a concentration of 0.5%

المنارة للاستشارات
www.manaraa.com

(w/w). Polystyrene thin films were obtained by spinning this solution. In order to create a hydrophobic, Teflon-like film ("Teflon surface"), a silicon wafer was spin coated with Fluoro Pcl™ PFC M1604V (Cytonix). After spinning, these wafers were cured on a hot plate at 90°C for 5 min and then at 180°C for 12 min.

6.3.4 Monolayer Preparation

Perfluoro monolayer surfaces were made through chemisorption of trichloro(3,3,4,4,5,5,6,6,7,7,8,8,8-tridecafluorooctyl)silane. Plasma cleaned silicon surfaces were placed in a dessicator and exposed to the vapor of this fluorinated silane overnight. The surfaces were then cured at 80°C for 1 h. 3-Aminopropyltriethoxysilane (APTES) surfaces were made by this same procedure using APTES. Polyethylene glycol (PEG) monolayer surfaces were made from $(CH_3O)_3Si(CH_2)_3(OCH_2CH_2)_{6\text{-}9}OCH_3$.[26] Plasma cleaned silicon surfaces were immersed in a 4-5 mM solution of this PEG silane in toluene with 0.8 mL/L HCl (conc) for 18 h at room temperature. The wafers were then washed with toluene, ethanol, and water. Hexadecyl and dodecyl monolayer surfaces were made from neat 1-hexadecene and 1-dodecene, respectively. The surfaces were hydrogen terminated with HF and then immersed into degassed 1-hexadecene or 1-dodecene at 150°C for 1 h under N_2. No particular attempt was made in this synthesis to produce surfaces with extremely high water contact angles, and the water contact angles observed on these surfaces were in the desired range for this particular study.

6.3.5 Hexadecyl and Dodecyl Monolayer Preparation (for UV Patterning)

A commercially available silicon wafer with a low resistance value was cleaved, and

المنارة للاستشارات
www.manaraa.com

then sonicated with acetone, dichloromethane, ethanol, and DI water in that order. Silicon shards were then photocleaned with a vacuum UV light. Photo-cleaned silicon was placed in a Teflon container, and then a sufficient quantity of 40% (vol.) NH_4F (used in commercial semicoductor processing) was added to the container. After 15 min, the sample was removed, and then washed immediately with DI water. The H-terminated sample was placed in a 10 vol% solution of 1-hexadecene or 1-dodecene in mesitylene, bubbled with Ar for several hours, and finally heated for at least 12 h at the boiling temperature of mesitylene.

6.3.6 Surface Patterning with the Microlens Array

A microlens array (MLA) with 100 μm spacing between microlenses (SUSS MicroOptics, Neuchatel, Switzerland) was placed approximately 200 μm over the PEG, perfluoro, APTES, or hexadecyl monolayer-coated silicon oxide substrates. A single ca. 4 ns pulse of 15 mJ 532 nm laser light (Coherent Infinity Nd:YAG laser) was then shot through this optical element to pattern the surface. The surface was not cleaned or rinsed in any way after MLA patterning.

6.3.7 Surface Patterning with UV Light

The surfaces terminated with hexadecyl and dodecyl monolayers were micropatterned by exposure to vacuum UV light generated from an excimer lamp (Ushio, UER20-172V; λ = 172 nm and 10 mW/cm^2) through a photomask in contact with their surfaces for 30 min at a reduced pressure of 10 Pa. A 10 mm-thick quartz glass plate (Asahi Glass, Synthetic silica glass AQX for Xe_2 172 nm excimer lamps) served as a top

المنارة للاستشارات
www.manaraa.com

weight on the photomask so as to obtain complete contact between the mask and the sample surface. The transparency of the photomask and the quartz plate at 172 nm was about 93% and 90%, respectively. The total light intensity at the sample surface was estimated at 8.4 mW/cm^2. The dose was about 15.1 J/cm^2.

6.3.8 PDMS Stamp Preparation

Stamps were fabricated from Sylgard 184 silicone elastomer (Dow Corning Corp.) mixed with curing agent at a 10:1 ratio. The mixture was placed in a flat-bottomed Petri dish and then in a vacuum desiccator for 1 h to remove bubbles from the elastomer. The elastomer was cured for 2 h at 80°C. After the stamp had cooled, the PDMS was carefully removed from the petri dish. Finally the round stamp was cut into several pieces. All results reported herein were obtained using freshly made PDMS stamps.

6.3.9 Surface Stamping

Silicon, titanium and gold surfaces, and the silicon surfaces that were modified with various monolayers, were contacted with the PDMS stamp for 2 s under light manual pressure.

6.3.10 Surface Characterization

Time-of-flight secondary ion mass spectrometry (ToF-SIMS) was performed with an ION-TOF ToF-SIMS Ⅳ instrument using monoisotopic 25 keV $^{69}Ga^+$ ions. ToF-SIMS spectra were collected over 100 s. ToF-SIMS images were collected after 150 scans at 2 shots/pixel. Raw data files of ToF-SIMS images were collected and saved for MCR.

المنارة للاستشارات
www.manaraa.com

Advancing water contact angle measurements were obtained with a Ramé-Hart model 100-00 contact angle goniometer. An advancing contact angle was measured when the sessile drop had the maximum volume allowable for the liquid-solid interfacial area and just moved across the surface. The contact angles on both sides of the drop were measured and averaged. To ensure reproducibility, at least three measurements were carried out on each solid surface. Spectroscopic ellipsometry was performed with an M-2000 instrument from J. A. Woollam (Lincoln, NE). The wavelength range of this instrument is *ca.* 200 nm-1000 nm.

6.3.11 Surface Tension Calculations

Young's equation ($\gamma_{lv}\cos\theta = \gamma_{sv} - \gamma_{sl}$) describes the thermodynamic equilibrium of the three surface tensions related to a droplet of liquid on a surface: γ_{sv}, γ_{sl}, and γ_{lv}, where the subscripts sv, sl and lv refer to the solid-vapor, solid-liquid, and liquid-vapor interfaces, respectively. Only two of the parameters in Young's equation (γ_{lv} and θ) are easily measured or obtained, which leaves one equation and two unknowns (γ_{sv} and γ_{sl}). To more easily determine solid-vapor surface tensions (γ_{sv}), an equation of state of interfacial tensions[27, 28] has been developed:

(1) $$\gamma_{sl} = \gamma_{lv} + \gamma_{sv} - 2\sqrt{\gamma_{lv}\gamma_{sv}}\,e^{-\beta(\gamma_{lv}-\gamma_{sv})^2}$$

When this equation is combined with Young's equation, the following equation[27-29] is obtained:

(2) $$\cos\theta = -1 + 2\sqrt{\frac{\gamma_{sv}}{\gamma_{lv}}}\,e^{-\beta(\gamma_{lv}-\gamma_{sv})^2}$$

Hence, if γ_{lv}, θ, and the empirically derived parameter β are known, γ_{sv} is also known. γ_{sv}

المنارة للاستشارات
www.manaraa.com

was determined using a short Matlab program I wrote that employed values of 0.0001247 $(mJ/m^2)^{-2}$ for β and 72.8mJ/m^2 for γ_{lv} of water.[27, 28] Note that this equation sets γ_{lv} equal to γ_{sv} when $\theta = 0$ (when a surface is wet by water), which may or may not be correct for a given surface.

6.3.12 Multivariate Statistical Analysis of the ToF-SIMS Data

The multivariate curve resolution (MCR) algorithm in the Automated eXpert Spectral Image Analysis (AXSIA) tool-kit developed at Sandia National Laboratories[30, 31] was used to perform multivariate statistical analysis of the ToF-SIMS raw data files. For MCR analysis, the mass range of 0 to 300 amu was binned to 1 amu and the data were properly scaled to account for Poisson statistics (noise in most ToF-SIMS studies is approximately Poisson-distributed), which affords maximum discrimination of chemical information from noise and allows small spectral features to be detected that would otherwise be overlooked.[32] MCR analysis required about 3 s of computational time on a Dell D400 Lattitude computer with a 1700 MHz processor and 1.046 GB RAM. The advantages of AXSIA have been summarized elsewhere.[33]

6.4 Results

6.4.1 Effect of Surface Free Energy on PDMS Transfer

I began my study by analyzing two molecular surfaces that were prepared by depositing small amounts of two different compounds from solution: buckminsterfullerene (C_{60}) and trihexadecyloxybenzaldehyde (THOB) (see Figure 6.2).

المنارة للاستشارات
www.manaraa.com

Figure 6.3 shows the ToF-SIMS spectra of a thin film of C_{60} before and after stamping with an unlinked, unpatterned PDMS stamp. While C_{60} is a rather hydrophobic material, it is not as hydrophobic as PDMS, which fact appears to facilitate PDMS transfer. Indeed, the obvious peaks at m/z 73 [$CH_3Si^+(CH_3)_2$], 147 [$CH_3Si(CH_3)_2OSi^+(CH_3)_2$], 207 (see Figure 6.2 for structure), and 221 [$CH_3Si(CH_3)_2OSi(CH_3)_2OSi^+(CH_3)_2$] make it clear that a measurable quantity of PDMS has transferred to this surface after stamping. This same technique was then applied to a thin film of THOB, but as shown in Figure 6.4, no PDMS transfer appears to have taken place. Indeed, the long alkyl chains of this molecule would be expected to align themselves perpendicular to the surface to create a very low free energy material. FTIR was performed on THOB (in KBr), which showed asymmetric [$\nu_a(CH_2)$] and symmetric [$\nu_s(CH_2)$] methylene stretches of 2916.8 and 2848.8 cm^{-1}, respectively. These values are consistent with a high degree of ordering (all-trans) of the alkyl chains in this compound. When this type of ordering of alkyl chains appears in monolayers, it generally accompanies high advancing water contact angles (110° or greater),[34-36] which appear to be in the range in which PDMS transfer would *not* be expected to occur. This same result (no PDMS transfer during stamping) was obtained whether the THOB film was relatively thick (deposited dropwise) or thin (deposited by spin coating).

المنارة للاستشارات
www.manaraa.com

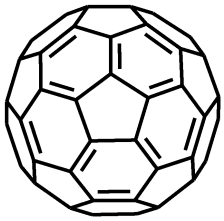

C_{60}

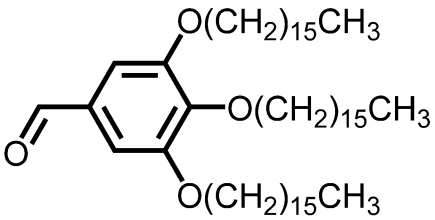

THOB

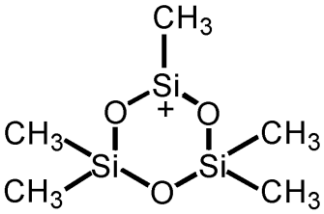

m/z 207

Figure 6.2. Structures of C_{60}, THOB and the m/z 207 peak from PDMS.

المنارة للاستشارات
www.manaraa.com

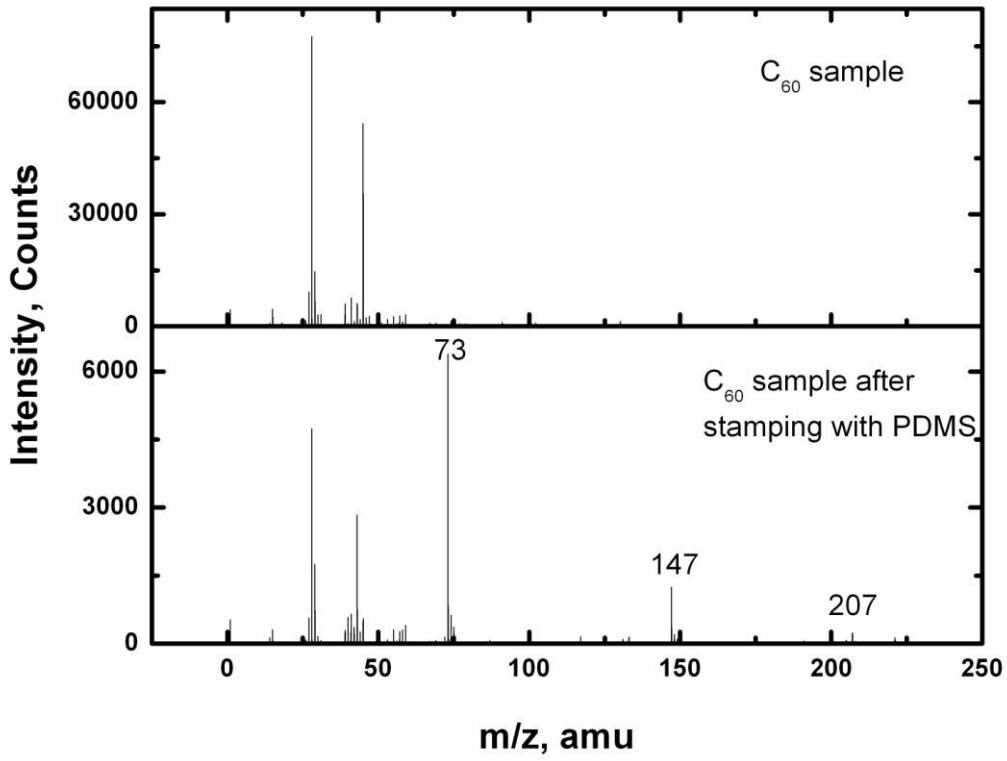

Figure 6.3. Positive ion ToF-SIMS spectra of a C_{60} film before and after stamping with PDMS.

المنارة للاستشارات
www.manaraa.com

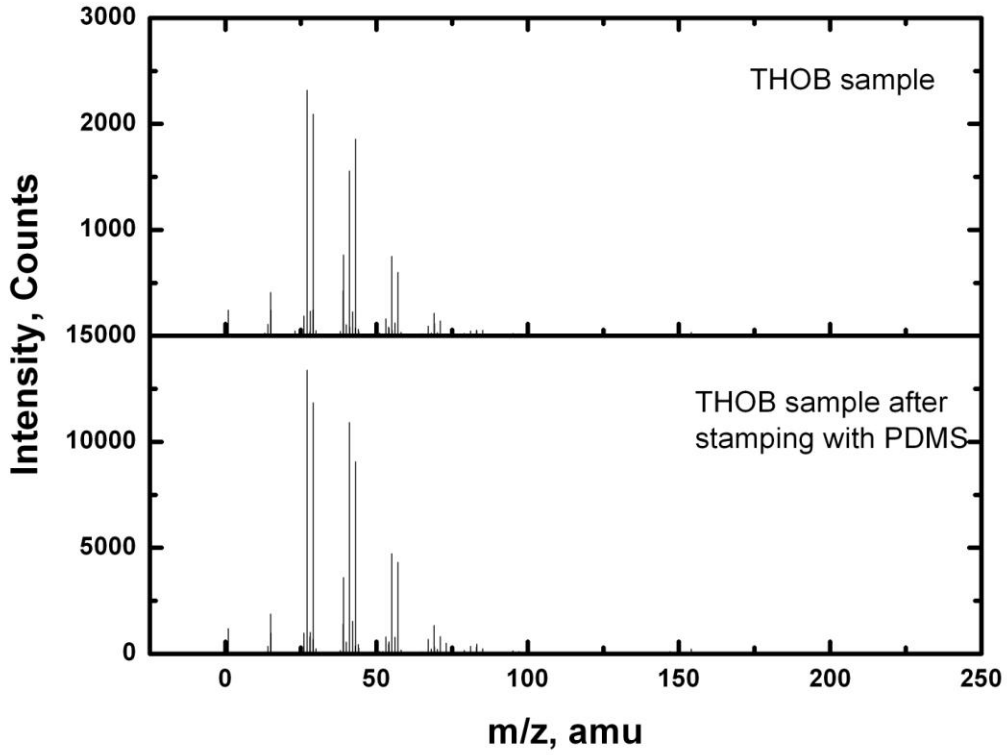

Figure 6.4. Positive ion ToF-SIMS spectra of a THOB film before and after stamping with PDMS.

المنارة للاستشارات
www.manaraa.com

In addition to ToF-SIMS, two important surface analytical methods for probing surface thicknesses and free energies are optical ellipsometry and contact angle goniometry. Unfortunately, these techniques could not be applied to thin films of C_{60} and THOB. The unbound molecules in these films were moved by water droplets in contact angle measurements giving unstable results, and the films were too rough for optical ellipsometry. Therefore, to study the transfer of PDMS during μCP with greater thoroughness and at a more fundamental level, a series of planar surfaces were stamped that did not contain loose molecular material, and that could be better probed with surface analytical techniques. These surfaces ranged from extremely hydrophilic to very hydrophobic, and included clean silicon, clean titanium, clean gold, "dirty" silicon, polystyrene, Teflon™, and surfaces modified with PEG, amino, dodecyl, hexadecyl and perfluoro monolayers. Representative ToF-SIMS spectra from these surfaces after stamping are shown in Figure 6.5. In particular, on two very hydrophilic surfaces (clean Ti and clean gold) stamped with PDMS, the m/z 73 and m/z 147 ions, which are characteristic of PDMS, are the dominant peaks in the spectra. For the APTES and PEG surfaces, which are still rather hydrophilic, these two ions from PDMS remain significant. For my hexadecyl monolayer on silicon, and again for polystyrene, which are more hydrophobic, the fraction of the peak area due to these ions from PDMS has decreased. Finally, for the perfluorinated materials, which are the most hydrophobic in my study, signals due to PDMS in the ToF-SIMS spectra are scarcely discernible.

More quantitative results from ToF-SIMS, contact angle goniometry, and spectroscopic ellipsometry before and after stamping with unpatterned stamps are shown in Table 6.1. It is clear from these data that the largest changes in water contact angles

المنارة للاستشارات
www.manaraa.com

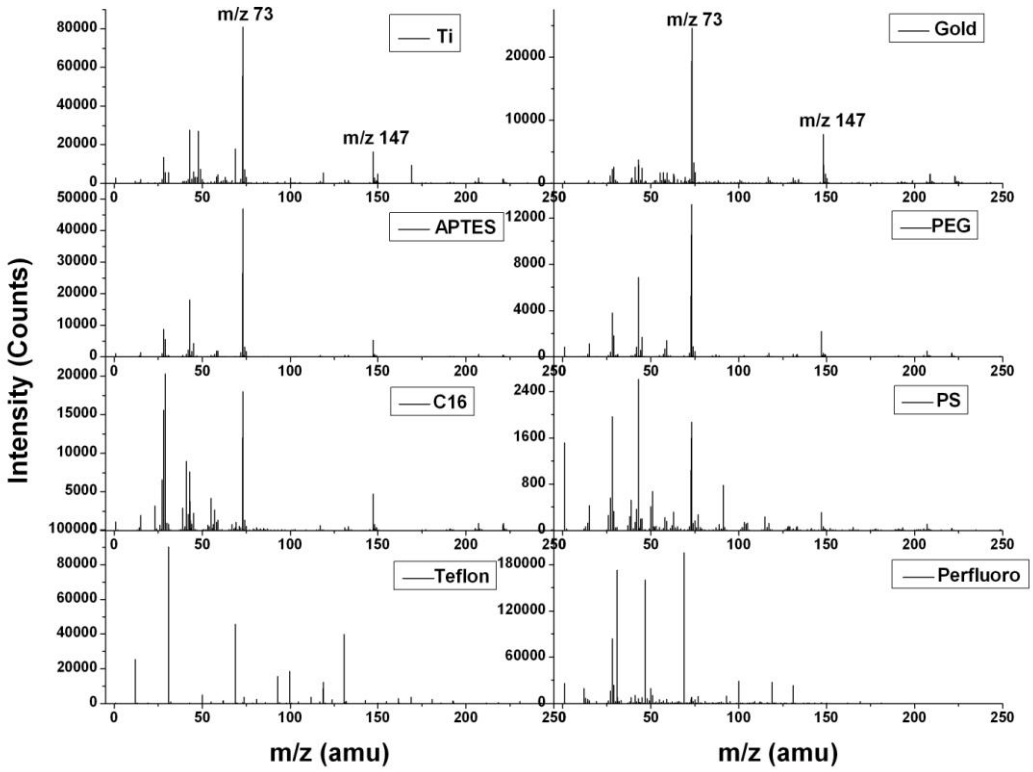

Figure 6.5. Positive ion ToF-SIMS spectra of different surfaces after contact with an uninked, unpatterned PDMS stamp. (PDMS is confirmed by the characteristic peaks at m/z 73, 147, 207, and 221.) "Ti" refers to electron beam evaporated titanium on silicon. "Gold" refers to electron beam evaporated Au on Ti on silicon. APTES refers to a layer of 3-aminopropyltriethoxysilane, PEG to a polyethylene glycol monolayer, C16 to a hexadecyl monolayer, PS to polystyrene, perfluoro to a layer of trichloro (3,3,4,4,5,5,6,6,7,7,8,8,8-tridecafluorooctyl)silane, and Teflon to Fluoro Pcl^{TM} PFC M1604V. The Fluoro Pcl^{TM} is a product of Cytonix.

المنارة للاستشارات
www.manaraa.com

Table 6.1. Physical properties of various surfaces before and after stamping.

	Before stamping		After stamping		$\Delta\theta_a(H_2O)_{stamped}$	$\Delta\gamma_{sv}$	$\Delta t_{stamped}$(Å)	PDMS
Surface	$\theta_a(H_2O)_{init}$	γ_{sv} (mJ/m^2)	$\theta_a(H_2O)_{stamped}$	γ_{sv}(mJ/m^2)				Peaks (%)
Clean Si/SiO_2	< 5°	72.5	28.2°±1.2°	65.3	23.2°±1.2°	-7.2	10.1±2.7	33.4±1.3
Clean Ti/TiO_2	< 5°	72.5	28.2°±1.8°	65.3	28.2°±1.8°	-7.2	10.0±3.3	36.1±0.8
Clean Au	< 5°	72.5	33.2°±3.0°	62.9	28.2°±3.0°	-9.6	14.1±4.0	48.0±13.6
Dirty Si/SiO_2	27.6°±1.7°	65.6	33.3°±1.8°	62.9	5.7°±2.5°	-2.7	9.4±2.9	31.5±0.2
SiO_2/PEG monolayer	30.6°±0.8°	64.2	38.9°±0.7°	60.0	8.3°±1.1°	-4.2	5.7±1.0	36.6±0.7
SiO_2/APTES monolayer	52.8°±2.7°	52.1	61.6°±1.7°	46.9	8.8°±3.2°	-5.2	8.1±1.7	39.1±7.7
SiO_2/Polystyrene	90.8°±1.0°	28.7	94.6°±3.5°	26.4	3.8°±3.6°	-2.3	4.7±0.5	20.7±6.6
PDMS stamp	89.0°±1.4°	29.8	--	--	--	--	--[a]	--
Si/Dodecyl monolayer	97.1°±4.0°	24.8	96.3°±3.4°	25.3	-0.8°± 4.2°	0.5	5.5±0.8	24.3±0.4
Si/Hexadecyl monolayer	98.2°±2.6°	24.1	97.3°±2.4°	24.7	-0.9°±3.5°	0.6	5.3±1.7	21.0±2.3
SiO_2/Perfluoro monolayer	107.7°±2.1°	18.4	107.3°±0.8°	18.7	-0.4°±2.3°	0.3	1.7±1.9	2.4±0.2
Teflon™ surface	118.1°±0.8°	12.6	117.2°±0.9°	13.1	-0.9°±1.2°	0.5	0.3±1.6	0.4±0.4

Note:

[a]Ellipsometry could not be performed on this surface

*Surface tension γ_{sv} of different surfaces before and after stamping calculated from mean advancing water contact angles (γ_{lv}=72.8 mJ/m^2 and β=0.0001247 (mJ/m^2)$^{-2}$).

المنارة للاستشارات
www.manaraa.com

after stamping occur with the surfaces that had the smallest water contact angles to begin with, *i.e.*, that were most hydrophilic. The same trend is observed in the changes in ellipsometric thicknesses; the largest changes in thickness after stamping occur for the samples that initially had the highest surface free energies. Likewise, the hydrophilic surfaces had the largest fraction of PDMS peaks in their ToF-SIMS spectra after stamping. Because surfaces with similar initial water contact angles responded similarly during stamping, the results from similar surfaces are grouped in the discussion of results below.

Air plasma cleaned silicon dioxide (Si/SiO_2), e-beam evaporated titanium (Ti/TiO_2), and e-beam evaporated gold were all wet with water (they had water contact angles less than 5°) just prior to stamping. The extremely low water contact angles of these surfaces are indicative of their high surface free energies. After stamping, the water contact angles of these surfaces increased substantially, and their ellipsometric thicknesses increased by *ca*. 10 Å. The presence of PDMS on these surfaces is confirmed by the highly characteristic m/z 73, 147, 207, and 221 ions in their ToF-SIMS spectra. These peaks were not present in the spectra prior to stamping.

The percentage of main PDMS peaks (m/z 73 and 147) in the total spectral area from 0 – 150 amu varies from 32% to 47% for the clean silicon, titanium, and gold surfaces after stamping. All of these results are consistent with significant PDMS transfer that lowers surface free energies by covering high free energy surfaces with a lower free energy molecule (PDMS).

Three surfaces with somewhat higher advancing water contact angles than this initial set were also studied: “dirty” silicon/silicon dioxide, which is silicon that is contaminated with adventitious hydrocarbons (used-as-received silicon), a PEG monolayer on Si/SiO_2,

المنارة للاستشارات
www.manaraa.com

and an APTES monolayer on Si/SiO_2. These surfaces had advancing water contact angles that were initially between *ca*. 30° and 50°. After stamping, the water contact angles of these surfaces increased by *ca*. 6° – 9°, their ellipsometric thicknesses also increased by *ca*. 6 – 9 Å, and the percentage of the m/z 73 and 147 PDMS peaks in their ToF-SIMS spectra was high: 32 - 40%. These changes in properties are generally less than those for the clean silicon, titanium, and gold surfaces, and are consistent with my hypothesis that PDMS transfer decreases as surface hydrophobicity increases.

The next group of surfaces (spin-coated polystyrene, and my dodecyl and hexadecyl monolayers) had initial water contact angles in the range of *ca*. 90° - 100°. These water contact angles are similar to that of the PDMS stamp. Consequently, PDMS transfer to these surfaces would not be expected to significantly change the water contact angles of these surfaces, as is observed. I noted, however, that *ca*. 5 Å of material does transfer to these surfaces after stamping. The percentage of main PDMS peaks in the ToF-SIMS spectra is also rather high: 21 – 24%. Overall, the changes in physical properties for this group of surfaces is smaller than the group with lower water contact angles that preceded it.

The final group (the perfluoro and Teflon™ materials) contained two very hydrophobic surfaces. Their advancing water contact angles were initially 108° and 118°, respectively. After stamping, the physical properties of these surfaces scarcely change. Their water contact angles and ellipsometric thicknesses remain essentially constant, and little or no PDMS is observed in their ToF-SIMS spectra. PDMS oligomers do not appear to transfer effectively to these hydrophobic surfaces, presumably because such a transfer would *raise* their surface free energies.

المنارة للاستشارات
www.manaraa.com

XPS was particularly useful in indicating chemisorption of PDMS on surfaces that did not initially contain silicon. The clean gold surface was 100% Au (no measurable Si) by XPS before stamping, but showed substantial contamination after stamping: 28.2 ± 2.6% C, 20.5 ± 0.6% O, 15.2 ± 2.4% Si, 36.1 ± 0.3% Au. The clean Ti/TiO_2 surface contained 20.9 ± 1.3% C, 59.0 ± 0.1% O, and 20.1 ± 1.3% Ti, and no measurable Si before stamping, but 31.3 ± 1.6% C, 46.0 ± 5.8% O, 4.6 ± 0.9% Si, and 14.8 ± 1.2% Ti after stamping. The spin-coated polystryrene surface was 100% C by XPS before stamping, but 95.6 ± 1.2% C, 2.8 ± 0.7% O, and 1.6 ± 0.5% Si after stamping. Finally, the Teflon™ surface, which was 29.3 ± 0.2% C, 11.0 ± 0.0% O, 0% Si, and 59.7 ± 0.3% F before stamping, showed essentially no change after stamping: 30.5 ± 0.2% C, 10.8 ± 0.0% O, 0% Si, and 58.7 ± 0.1% F.

Using Equation 2, the equation of state for interfacial tensions, solid-vapor surface tensions (γ_{sv}) were calculated for the surfaces in Table 6.1 from their water contact angles, from which the change in solid-vapor surface tension ($\Delta\gamma_{sv}$) after stamping was estimated. Table 6.1 clearly shows that the change in surface tension is greatest for the surfaces that initially were most hydrophilic, where stamping lowers their surface free energies. The degree to which the surface free energy is lowered decreases with increasing surface hydrophobicity until little change in this property is observed for the most hydrophobic surfaces. These results for $\Delta\gamma_{sv}$ are consistent with the other results in Table 6.1 for $\Delta\theta_a(H_2O)$, Δt, and the percentage of the ToF-SIMS spectra due to PDMS peaks. As an important graphical illustration of these trends, all of these properties, along with the percentage of the PDMS peaks in the ToF-SIMS spectra, are plotted in Figures 6.6 as a function of the cosine of the initial water contact angle of the surfaces.

المنارة للاستشارات
www.manaraa.com

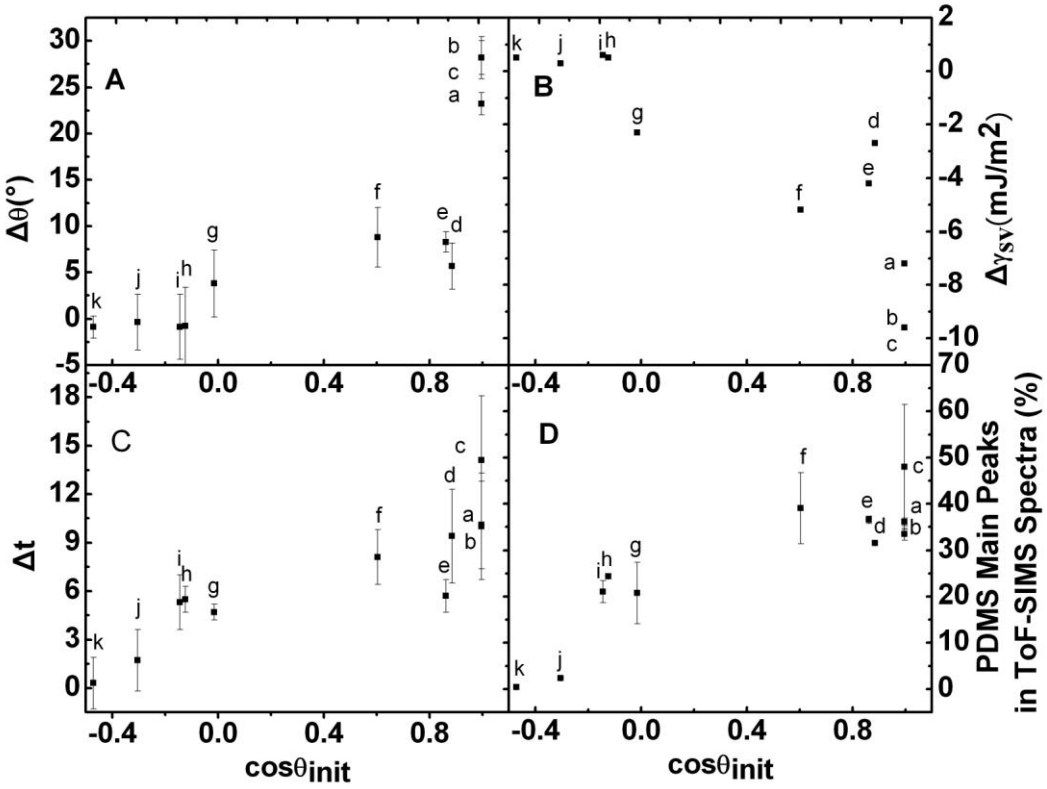

Figure 6.6. Change in water contact angle (A), surface tension (B), thickness (C), and percentage of PDMS main peaks in ToF-SIMS spectra (D) after stamping with PDMS for different surfaces. a-k represent clean Si/SiO_2 (a), clean Ti/TiO_2 (b), clean gold (c), dirty Si/SiO_2 (d), SiO_2/PEG monolayer (e), SiO_2/APTES monolayer (f), SiO_2/polystyrene (g), Si/dodecyl monolayer (h), Si/hexadecyl monolayer (i), SiO_2/perfluoro monolayer (j) and Teflon^{TM} (k).

المنارة للاستشارات
www.manaraa.com

These results point to a relationship between the surface tension of a material, γ_{sv}, and the percentage of the main PDMS peaks (%PDMS) in its ToF-SIMS spectrum. Figure 6.7 shows a plot of γ_{sv} vs. %PDMS. An approximate fit to this data is shown in Figure 6.7 and is given by $\gamma_{sv} = 0.0105*(\%PDMS)^2 + 0.961*(\%PDMS) + 11.0$, with $R^2 = 0.77$. Admittedly, this relationship would be of little worth for a large planar surface because of the ease with which water contact angles can be measured, and a different relationship would most likely need to be determined if a different primary ion source was employed. However, this relationship would allow one to estimate the surface free energies of microscopic features on patterned surfaces.

6.4.2 PDMS Transfer to Patterned Surfaces and Probing Surface Energies by Imaging ToF-SIMS

The fact that surface free energy influences PDMS transfer caused me to question whether this method could be used as a tool for probing surfaces in SIMS imaging. Accordingly, I analyzed six patterned surfaces. The first set consisted of hydrophobic monolayers on silicon that had been patterned with (presumably) hydrophilic spots. A perfluoro, hydrophobic monolayer of $Cl_3Si(CH_2)_2(CF_2)_5CF_3$ on Si/SiO_2, and a monolayer of 1-hexadecene on hydrogen-terminated silicon were patterned with a brief pulse of intense laser light through a microlens array to give a square pattern of ca. 40 μm spots spaced by 100 μm.[26] Monolayers of 1-dodecene and 1-hexadecene on hydrogen-terminated silicon were also patterned with vacuum UV light through a stencil mask to again prepare a series of spots that should be more hydrophilic than their hydrophobic backgrounds.

المنارة للاستشارات
www.manaraa.com

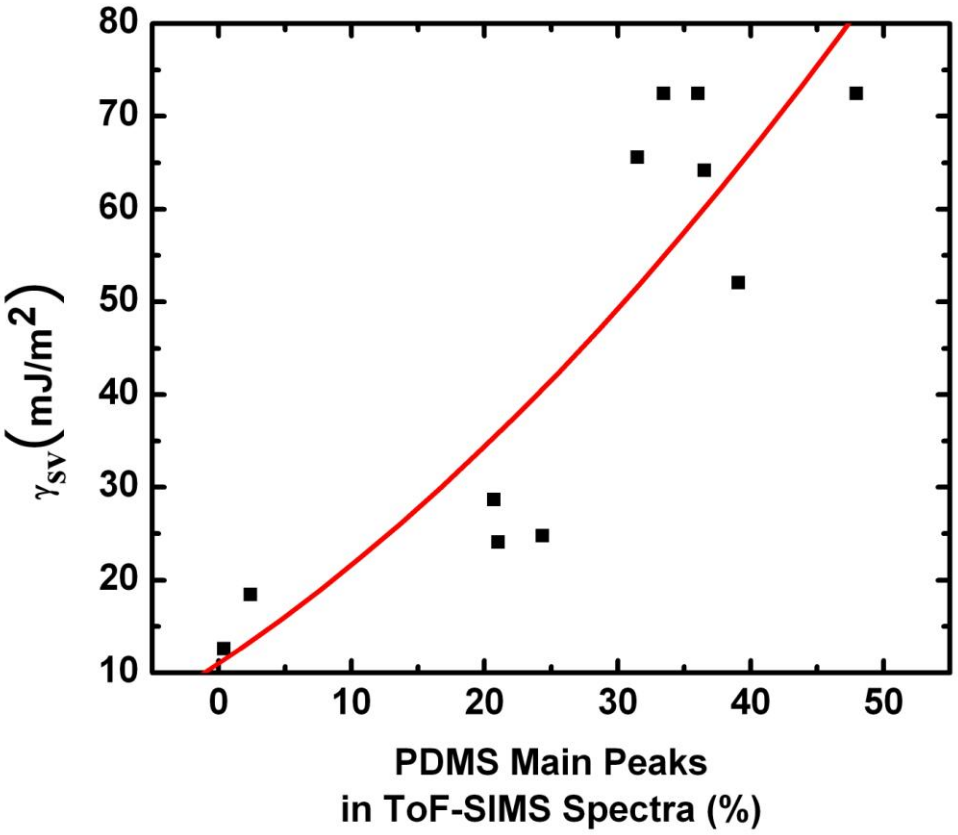

Figure 6.7. Relationship between the surface tension at the solid-vapor interface and the percentage of the PDMS main peaks in the ToF-SIMS spectra of various surfaces.

المنارة للاستشارات
www.manaraa.com

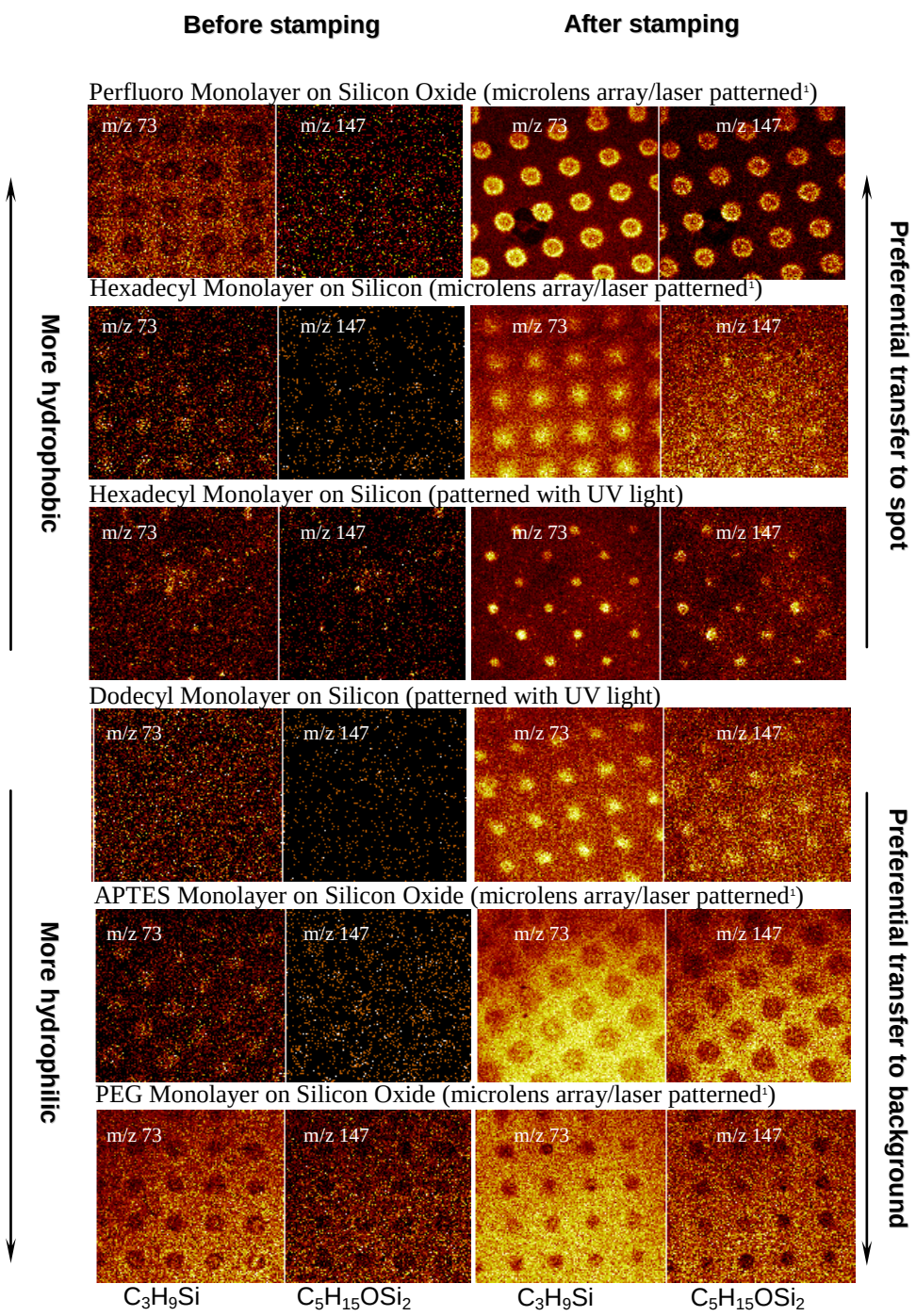

Figure 6.8. Positive ion ToF-SIMS images (500×500 μm) for various surfaces before and after stamping with PDMS. SIMS images were collected at m/z 73 and 147 by binning to ±0.3 amu around each integer mass value.

المنارة للاستشارات
www.manaraa.com

Figure 6.8 shows that, in general, little contrast is present in the SIMS images of the m/z 73 and 147 ions prior to stamping. The little contrast that is observed in a few of the cases may be a result of the data binning to ±0.3 amu around each integer mass value that was necessary for image creation, and which would possibly incorporate more than one signal within these ranges. There may also be a small amount of PDMS contamination in some cases, which is common in many materials. This open question, regarding PDMS contamination is answered below (vide infra); after a multivariate curve resolution analysis of the images taken before stamping, only the PEG monolayer on Si/SiO_2 appeared to have any real PDMS contamination.

After stamping, Figure 6.8 shows that the hydrophilic/hydrophobic pattern that was created by microlens array or UV patterning becomes apparent in the m/z 73 and 147 ion images. The contrast in the patterned perfluoro monolayer is especially stark, and is consistent with very low or nonexistent levels of PDMS transfer to these very hydrophobic background regions. A clear preference for PDMS transfer to the spots over the backgrounds is also present in the patterned hexadecyl and dodecyl surfaces, and this selective transfer is again consistent with rather hydrophobic backgrounds next to more hydrophilic spots. In particular, the two hexadecyl monolayers provide an effective graphical illustration of my results. These surfaces had water contact angles of 106° C and 98° C prior to UV and microlens array patterning, respectively. As would therefore be expected, the more hydrophobic surface has the lower background signal (improved contrast) in the ToF-SIMS image after stamping (See Figure 6.8).

An interesting and very significant change in PDMS transfer occurs with patterned APTES and PEG monolayers. In these cases, PDMS has a greater tendency to transfer to

المنارة للاستشارات
www.manaraa.com

the *backgrounds* over the spots. I regard these results as remarkable, in that they suggest that microlens array patterning of these important surfaces creates spots that are more hydrophobic than their background areas. These results on the PEG monolayer surface are consistent with a recently published study[26] that showed selective protein adsorption to the spots of a microlens array patterned PEG monolayer surface. The obvious implication of these later results is that microlens array patterning of PEG monolayers destroys, and/or even chars, PEG surfaces, producing hydrophobic spots, to which proteins selectively adsorb. Protein adsorption to hydrophobic surfaces is a well known phenomenon.

Multivariate curve resolution (MCR) is an important chemometrics tool for analyzing complicated data sets, including ToF-SIMS spectra. A priori, the MCR analysis of the ToF-SIMS data sets shown in Figure 6.9 was expected to reveal two main components, one associated with the spots and another with the background area. For all of the data sets except one, MCR analysis revealed 3 to 5 chemical components, where the number of components was determined using eigenvalue analysis.[37] Whatever the total number of components is that describe each image, they are grouped as background (Component A), spot (Component B) and general components (Component C). Figure 6.9 shows these grouped components with their percent variances for the perfluoro, dodecyl (UV) and APTES surfaces. Compared to the univariate analysis shown in Figure 6.8, MCR analysis often provides higher image contrast because the image is represented by a full spectral signature and not just one species.

Figure 6.9a shows all components of the MCR analysis of the images taken before stamping, where the perfluoro, dodecyl (UV) and APTES monolayers on Si/SiO_2 do not

المنارة للاستشارات
www.manaraa.com

(a)

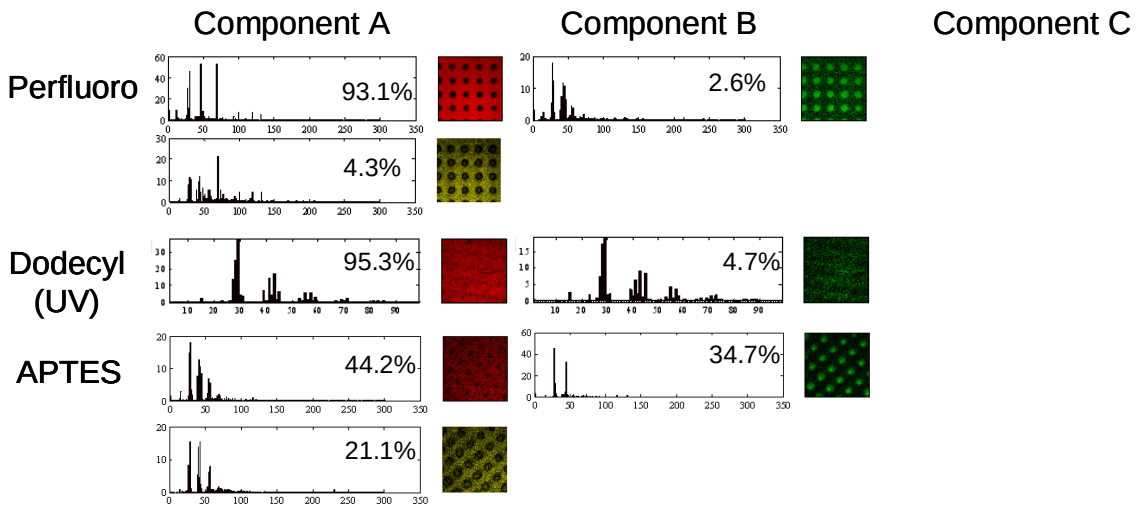

(b)

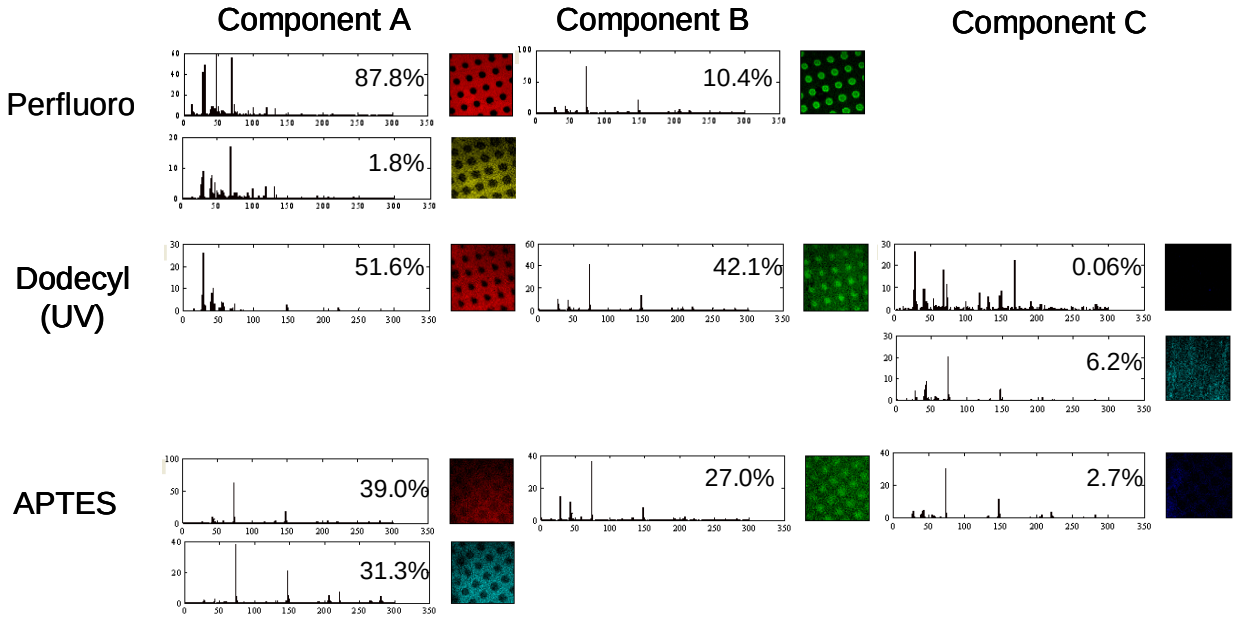

Figure 6.9. MCR spectra (loadings plots), associated images (scores plots) and the corresponding percentage of variance in each data set of three grouped MCR components corresponding to the background area, spots and overall area (a) before stamping and (b) after stamping.

المنارة للاستشارات
www.manaraa.com

have any noticeable PDMS contamination (no peaks at m/z 73 and 147; See components A and B), i.e., these results are consistent with the original ToF-SIMS spectra, which did not show PDMS contamination. For the APTES and perfluoro surfaces, contrast between spots and background is seen before stamping. It is significant that for the dodecyl surface (UV), essentially no contrast is observed before stamping, which is also consistent with the ion images shown in Figure 6.8.

Figure 6.9b shows the MCR components of the perfluoro, dodecyl (UV) and APTES surfaces after stamping. The perfluoro surface is primarily described by two MCR components, which like the raw data in Figure 6.9a show high contrast. The three largest peaks in the background component (A) are at m/z 31, 47, and 69, which correspond to CF^+, SiF^+, and CF_3^+, respectively. These peaks would be expected from a perfluorinated material. There is also a minor background component. Neither of the background components contains PDMS ions. In contrast, the spot component (B) is almost exclusively due to PDMS, which confirms PDMS transfer to the spot and not the background, and suggests that the spot created by microlens array patterning is more hydrophilic than its background. The dodecyl (UV) surface is described by 4 MCR components. There is a background component (A) that shows essentially no PDMS, a significant spot component (B) that contains strong PDMS signals, and one significant overall component that reveals PDMS. In contrast to the MCR results from the perfluoro surface, these results show focused PDMS transfer to hydrophilic spots along with some PDMS transfer over the entire surface, which is consistent with the greater PDMS transfer to these substrates suggested in Table 6.1 (See above). It is noteworthy that PDMS transfer revealed chemical contrast in this patterned surface that was not obvious

المنارة للاستشارات
www.manaraa.com

in the ToF-SIMS, or even MCR, images prior to stamping. The APTES surface is again described by background, spot, and overall components. However, all of these components contain PDMS signals. These loadings spectra appear to vary only in the degree to which they contain PDMS. This result and that in Figure 6.8 are consistent with a significant amount of PDMS transfer to the APTES surface (See Table 6.1), with the formation of a more hydrophobic surface that also imbibes some PDMS oligomers. This analysis clearly increases my understanding of the data in Figure 6.8.

6.5 Discussion

Perhaps the first mention of the possibility of contamination during μCP was in 1997 by Larsen and coworkers. They studied microcontact printed monolayers of dodecanethiol on Au(111) using scanning tunneling microscopy (STM) and wetting. They reported that there was no evidence for surface contamination from the PDMS stamp. There are two ways to view their conclusions. The first is that the techniques they used to analyze their surfaces, STM and wetting, lack, to some degree, chemical specificity so they may not have been able to see any contamination that may have been present. (Although it should be noted that the authors were able to obtain reasonably high resolution STM images of the monolayers, which suggests that the level of any surface contamination was low.) The other possibility, which I favor, is that little or no PDMS contamination was present on their surfaces because, as my results suggest, little or no PDMS contamination occurs on very hydrophobic surfaces. The results of Larsen and coworkers need to be weighed against the subsequent report of Böhm, who reported significant PDMS contamination in microncontant printed hexadecanethiol-on-gold

المنارة للاستشارات
www.manaraa.com

monolayers, even though the monolayers were quite hydrophobic. In order to explain why others had not previously observed PDMS contamination during μCP, Böhm and coworkers noted the rather high pressures they applied during printing. (Comparison of results between labs is somewhat challenging because different groups typically use different conditions to prepare PDMS stamps, and printing conditions may also vary from lab to lab.)

Sharpe and coworkers recently reported that: "the extent of the PDMS-contamination is dependent on the nature of the ink used." They arrived at this conclusion because much more PDMS contamination was observed when μCP on gold was performed with a hydrophilic ink (16-mecaptohexadecanoic acid, MHDA), than with a hydrophobic ink (*n*-octadecanethiol, ODT). They reported a control experiment consisting of μCP using MHDA and ODT on monolayers that were performed from MHDA and ODT, respectively. PDMS contamination was strong in the case of the MHDA monolayer, but none was observed on the ODT film. This latter result is consistent with the earlier report of Graham and coworkers.[6]

I wish to qualify the emphasis of Sharpe and coworkers that it is the hydrophilicity/hydrophobicity of the ink that primarily determines PDMS transfer during μCP. That is, my findings are consistent with their interpretations to the extent that hydrophilic inks produce hydrophilic surfaces, which adsorb PDMS, and that hydrophobic surfaces produce hydrophobic surfaces, which resist PDMS adsorption. That is, the ink itself in the stamp may have less to do with PDMS transfer to substrates than the surface free energies of the films produced by the inks. In the case of an ink that takes a significant amount of time to assemble at a surface, it may be the underlying substrate

المنارة للاستشارات
www.manaraa.com

that largely determines the degree of PDMS contamination, as least for short contact times between the stamps and the substrates.

I am also not entirely comfortable with Sharpe and coworker's proposal that it is primarily *hydrophilic* PDMS oligomers that are the contaminating species in μCP. While some of the material that is transferred from the stamp during μCP probably is hydrophilic, I believe that my results, and those of previous researchers, are more consistent with the idea that *hydrophobic* oligomers of PDMS are the primary contaminants that are observed in μCP. I give the following reasons. First, it has been repeatedly shown by other researchers (vide supra), and now by us, that PDMS contamination of surfaces during μCP generally makes them *more* hydrophobic, which is consistent with the transfer of a hydrophobic species. In addition, hydrophilic surfaces having high free energies are well known to spontaneously contaminate with less hydrophilic materials to reduce their surface free energies. A classic example of this phenomenon is the spontaneous contamination of clean, native oxide-terminated silicon wafers with adventitious hydrocarbons upon exposure to the laboratory environment. The resulting surfaces, which were originally wetted by water, became fairly hydrophobic. In addition, I note that NMR has shown that most of what is removed by Soxhlet extraction from PDMS stamps is silicones,[18] although in partial support of the Sharpe hypothesis a relatively small fraction of this material was thought to be hydrophilic. Finally, FTIR and ToF-SIMS have repeatedly shown the characteristic signals of poly(dimethylsiloxane) after μCP (vide supra), including those signals that confirm the presence of the (hydrophobic) methyl groups of this polymer.

The decomposition of transferred PDMS into submicron droplets[38] should not be an

المنارة للاستشارات
www.manaraa.com

issue for the relatively large (tens of microns) features studied in this work, especially since the practical resolution of our instrument for organic materials is on the order of a micron.

6.6 Conclusions

The transfer of polydimethylsiloxane (PDMS) to a series of patterned and unpatterned surfaces with different surface free energies has been observed by ToF-SIMS, wetting, and spectroscopic ellipsometry. PDMS transfers to hydrophilic surfaces or even moderately hydrophobic surfaces. However, hydrophobic surfaces, *e.g.*, Teflon™ or perfluoro monolayers with high advancing water contact angles, resist adsorption of PDMS. On patterned surfaces, PDMS transfers to hydrophilic spots patterned onto hydrophobic monolayers, but not onto the hydrophobic background, or it transfers preferentially onto more hydrophilic backgrounds. Surface free energy calculations from wetting results help explain PDMS transfer. MCR analysis of ToF-SIMS images on patterned surfaces reveals that PDMS transfers to different areas according to the properties of background monolayers and patterned features. My results strongly suggest that PDMS stamps can effectively probe these materials. In addition, this study provides a correlation between surface free energies based on the relationship between fraction of peaks due to PDMS in ToF-SIMS spectra and surface free energy. These results have obvious implications for traditional microcontact printing with PDMS stamps.

المنارة للاستشارات
www.manaraa.com

6.7 References

(1) Kumar, A.; Biebuyck, H. A.; Whitesides, G. M. *Langmuir* **1994**, *10*, 1498-1511.

(2) Xia, Y.; Whitesides, G. M. *Angewante Chemie International Edition* **1998**, *37*, 550-575.

(3) Quist, A. P.; Pavlovic, E.; Oscarsson, S. *Analytical and Bioanalytical Chemistry* **2005**, *381*, 591-600.

(4) Böhm, I.; Lampert, A.; Buck, M.; Eisert, F.; Grunze, M. *Applied Surface Science* **1999**, *141*, 237-243.

(5) Yang, Z.; Belu, A. M.; Liebmann-Vinson, A.; Sugg, H.; Chilkoti, A. *Langmuir* **2000**, *16*, 7482-7492.

(6) Graham, D. J.; Price, D. D.; Ratner, B. D. *Langmuir* **2002**, *18*, 1518-1527.

(7) Glasmastar, K.; Gold, J.; Andersson, A.-S.; Sutherland, D. S.; Kasemo, B. *Langmuir* **2003**, *19*, 5475-5483.

(8) Zhou, Y.; Valiokas, R.; Liedberg, B. *Langmuir* **2004**, *20*, 6206-6215.

(9) *ToF-SIMS. Surface Analysis by Mass Spectrometry*; IM Publications: Huddersfield, UK, 2001.

(10) Langowski, B. A.; Uhrich, K. E. *Langmuir* **2005**, *21*, 6366-6372.

(11) Felmet, K.; Loo, Y.-L.; Sun, Y. *Applied Physics Letters* **2004**, *85*, 3316-3318.

(12) Tingey, M. L.; Wilyana, S.; Snodgrass, E. J.; Abbott, N. L. *Langmuir* **2004**, *20*, 6818-6826.

(13) Thomson, N. R.; Bower, C. L.; McComb, D. W. *Materials Chemistry* **2008**, *18*, 2500-2505.

(14) Perl, A.; Peter, M.; Ravoo, B. J.; Reinhoudt, D. N.; Huskens, J. *Langmuir* **2006**, *22*,

المنارة للاستشارات
www.manaraa.com

7568-7573.

(15) Zhao, Y.; Li, M.; Lu, Q.; Shi, Z. *Langmuir* **2008**, *24*, 12651-12657.

(16) Foley, J. O.; Fu, E.; Gamble, L. J.; Yager, P. *Langmuir* **2008**, *24*, 3628-3635.

(17) Eric E. Ross, J. R. J., Ronald J. Wysocki, Jr., Ken Nebesny, Tony Spratt, David F. O'Brien, and S. Scott Saavedra *Biomacromolecules* **2006**, *7*, 1393-1398.

(18) Thibault, C.; Severac, C.; Mingotaud, A.-F.; Vieu, C.; Mauzac, M. *Langmuir* **2007**, *23*, 10706-10714.

(19) Hale, P. S.; Kappen, P.; Prissanaroon, W.; Brack, N.; Pigram, P. J.; Liesegang, J. *Applied Surface Science* **2007**, *253*, 3746-3750.

(20) Sharpe, R. B. A.; Burdinski, D.; van der Marel, C.; Jansen, J. A. J.; Huskens, J.; Zandvliet, H. J. W.; Reinhoudt, D. N. P., B. *Langmuir* **2006**, *22*, 5945-5951.

(21) Tan, H.; Huang, S.; Yang, K.-L. *Langmuir* **2007**, *23*, 8607-8613.

(22) Wang, X. J.; Ostblom, M.; Johansson, T.; Ingana¨s, O. *Thin Solid Films* **2004**, *449*, 125-132.

(23) Briseno, A. L.; Roberts, M.; Ling, M.-M.; Moon, H.; Nemanick, E. J.; Bao, Z. *Journal of the American Chemical Society* **2006**, *128*, 3880-3881.

(24) Asberg, P.; Nilsson, K. P. R.; Inganas, O. *Langmuir* **2006**, *22*, 2205-2211.

(25) Wigenius, J. A. H., Mahiar; Inganaes, Olle. *Advanced Functional Materials* **2008**, *18*, 2563-2571.

(26) Zhang, F.; Gates, R.; Smentkowski, V. S.; Watt, R.; Asplund, M. C.; Linford, M. R. *J. Am. Chem. Soc.* **2007**, *129*, 9252-9253.

(27) Tavana, H.; Simonb, F.; Grundke, K.; Kwok, D. Y.; Hair, M. L.; Neumann, A. W. *Journal of Colloid and Interface Science* **2005**, *291*, 497-506.

المنارة للاستشارات
www.manaraa.com

(28) Kwok, D. Y.; Neumann, A. W. *Advances in Colloid and Interface Science* **1999**, *81*, 167-249.

(29) Li, D.; Neumann, A. W. *J. Colloid Interface Sci.* **1992**, *148*, 190-200.

(30) Kotula, P. G.; Keenan, M. R. *Microsc. Microanal.* **2000**, *6*, 1052-1053.

(31) Keenan, M. R.; Kotula, P. G.: U.S. Patent 6,675,106, 2004.

(32) Keenan, M. R.; Kotula, P. G. *Surf. Interface Anal.* **2004**, *36*, 203–212.

(33) Smentkowski, V. S.; Ostrowski, S. G.; Kollmer, F.; Schnieders, A.; Keenan, M. R.; Ohlhausen, J. A.; Kotula, P. G. *surface and interface analysis* **2008**,*40*, 1176-1182.

(34) Linford, M. R.; Chidsey, C. E. D. *Journal of the American Chemical Society* **1993**, *115*, 12631-12632.

(35) Linford, M. R.; Fenter, P.; Eisenberger, P. M.; Chidsey, C. E. D. *Journal of the American Chemical Society* **1995**, *117*, 3145-3155.

(36) Porter, M. D.; Bright, T. B.; Allara, D. L.; Chidsey, C. E. D. *J.Am.Chem.Soc.* **1987**, *109*, 3559-3568.

(37) Keenan, M. R. In *Techniques and Applications of Hyperspectral Image Analysis*; Grahn, H., Geladi, P., Eds.; John Wiley & Sons, Ltd.: Chinchester, 2007.

(38) Hui, C. Y.; Jagota, A.; Lin, Y. Y.; Kramer, E. J. *Langmuir* **2002**, *18*, 1394-1407.

المنارة للاستشارات
www.manaraa.com

PART IV. Chemometrics

Chapter 7 Multivariate Analysis of ToF-SIMS Spectra of Monolayers on Scribed Silicon*

7.1 Abstract

Static time-of-flight secondary ion mass spectrometry (ToF-SIMS) was performed on monolayers on scribed silicon (Si_{scr}) derived from 1-alkenes, 1-alkynes, 1-holoalkanes, aldehydes and acid chlorides. In order to rapidly determine the variation in the data without introducing user bias, a multivariate analysis was performed. First, principal components analysis (PCA) was done on data obtained from silicon scribed with homologous series of aldehydes and acid chlorides. For this study, the positive ion spectra, the negative ion spectra, and the concatentated (linked) positive and negative ion spectra were preprocessed by normalization, mean centering, and autoscaling. The mean centered data consistently showed the best correlations between the scores on PC1 and the number of carbon atoms in the adsorbate. These correlations were not as strong for the normalized and autoscaled data. After reviewing these methods, it was concluded that mean centering is the best preprocessing method for ToF-SIMS spectra of monolayers on Si_{scr}. A PCA analysis of all of the positive ion spectra revealed a good correlation between the number of carbon atoms in all of the adsorbates and the scores on PC1. PCA of all of

*This chapter is reproduced with pemission from *Anal. Chem.* **2005**, *77*, 4654-4661. Copyright 2005 American Chemical Society.

المنارة للاستشارات
www.manaraa.com

the negative ion spectra and the concatenated positive and negative ion spectra showed a correlation based on the number of carbon atoms in the adsorbate *and* the class of the adsorbate. These results imply that the positive ion spectra are most sensitive to monolayer thickness, while the negative ion spectra are sensitive to the nature of the substrate-monolayer interface *and* the monolayer thickness. Loadings show an inverse relationship between (inorganic) fragments that are expected from the substrate and (organic) fragments expected from the monolayer. Multivariate peak intensity ratios were derived. It is also suggested that PCA can be used to detect outlier surfaces. Partial least squares showed a strong correlation between the number of carbon atoms in the adsorbate and the number it predicted.

7.2 Introduction

In time-of-flight secondary ion mass spectrometry (ToF-SIMS)[1] a beam of energetic ions (the primary ions) is directed onto a surface. As a result of their collisions with the surface, positive and negative secondary ions are ejected from the very near surface region (about the upper 25 Å). The secondary ions are then mass analyzed. The resulting mass spectra are usually highly characteristic of the material from which they come, being very rich in chemical information. It is not unusual for a ToF-SIMS spectrum to contain hundreds or even thousands of peaks. The enormous quantities of information that are generated with ToF-SIMS actually create a problem for the user. It would be an arduous task to carefully analyze and compare every peak from the ToF-SIMS spectra of even a moderately large series of samples.

One approach to dealing with the huge quantities of data that are obtained with

المنارة للاستشارات
www.manaraa.com

ToF-SIMS is to employ one's knowledge of one's samples to select and analyze a few of the peaks that may be most important. While this univariate approach is often valid and even very useful, it may miss or ignore much of the information that is present in the data. A second approach is to perform a multivariate analysis so as to better consider all of the variation in the data simultaneously. Principal components analysis (PCA) has been recognized as one of the most powerful methods for performing such multivariate analyses of multiple spectra.[2, 3]

In PCA of ToF-SIMS data, each peak or spectral region in the mass spectrum is considered to be a unique variable. Each spectrum is then "plotted" as a single point in a hyperspace of these variables. The axes of the coordinate system are then rotated to capture the maximal variation in the data. The axis that captures the largest fraction of this variation, as measured by the projections of the data points onto the axes, is termed the first principal component (PC1). The projections of the data points are termed scores. The axis that captures the next largest fraction of the variation, and which must be perpendicular to PC1, is denoted PC2. PC3 and the higher principal components are obtained in a similar fashion. The contributions (projections) of the old axes onto the new ones (principal components) are termed loadings. From the perspective of the mathematician, PCA is a calculation of the eigenvectors (new axes) and eigenvalues (projections of the data points onto the new axes, *i.e.*, scores) of a data matrix.

Principal components analysis is being increasingly used to analyze ToF-SIMS data from series of related samples. Recent examples include PCA of ToF-SIMS spectra of i) dodecanethiol monolayers on gold during different stages of their formation,[4] ii) poly(L-lysine)-graft-poly(ethylene glycol) monolayers on niobium pentoxide,[5]

المنارة للاستشارات
www.manaraa.com

immunoglobulin G immobilized on monolayers with different end groups,[6] and monolayers of thiols on gold made by immersion[7] and by microcontact printing.[8]

A central issue in PCA is how the raw data (the mass spectra) are converted into a data matrix. In general, the first step in preprocessing ToF-SIMS data is to calculate the areas of a relatively large number of peaks, or spectral regions. It is then advisable to normalize (row scale) the data to allow spectra that may have been collected under somewhat different conditions, *e.g.*, collection times, to be directly compared. After row scaling, the data might be used directly for PCA, although they typically undergo further preprocessing. In this work, I primarily consider data that have been mean centered and autoscaled.[2] In mean centering, the mean of the values in each column of variables in the data matrix is subtracted from each value in that column. Thus, mean centering centers the values corresponding to each variable about zero. In autoscaling, each data point is mean centered and then divided by the standard deviation of all of the data points for that variable. The result of autoscaling is that all of the variables are put on equal footing.

In 2001, Linford and coworkers described a new method for simultaneously functionalizing and patterning silicon by chemomechanically scribing it in the presence of reactive liquids.[9] In that original work and those that followed it has been shown that 1-alkenes,[9] 1-alkynes,[9] alkyl halides,[10] alcohols,[11] epoxides,[12] aldehydes,[13] and acid chlorides[14] chemomechanically react with scribed silicon (Si_{scr}) to form monolayers. It is remarkable that monolayer formation takes place in an open laboratory with compounds that have not been degassed. Both micron-[15, 16] and nanometer-sized[17] features have been chemomechanically patterned onto silicon. A variety of tools, including ToF-SIMS

المنارة للاستشارات
www.manaraa.com

(univariate analyses), X-ray photoelectron spectroscopy (XPS or ESCA), wetting, atomic force microscopy (AFM), and scanning electron microscopy (SEM) have been used to characterize these new materials. Alkyl chain length has been shown to be a key parameter in determining the physical properties of alkyl monolayers on Si_{scr} as measured by XPS, wetting, and ToF-SIMS.[13, 18]

Here I show a PCA analysis of the positive ion, negative ion, and combined positive and negative ion ToF-SIMS spectra from monolayers on Si_{scr}. Three preprocessing conditions were considered for each of the three data sets: normalization, mean centering, and autoscaling. (It is the author's experience that, when first studied, data from each new system should be preprocessed with different methods.) PCA was performed on a large data set of 66 ToF-SIMS spectra of monolayers on Si_{scr}. Two subsets of this data were also analyzed individually: the spectra from the homologous series of the aldehydes and the acid chlorides.

The fundamental objective of this study was to determine whether PCA and another multivariate analysis method (partial least squares, or PLS) can effectively analyze ToF-SIMS spectra of monolayers on scribed silicon. For example, it is of interest to know whether the PCA analyses are strongly correlated to alkyl chain length. I also wish to determine which preprocessing method is most effective in these analyses. Monolayer thickness is another issue of importance because it has not been possible to use optical ellipsometry or X-ray reflectivity to measure monolayer thicknesses because of scribed silicon's roughness. If monolayer thicknesses increase with adsorbate length as I believe they do, PCA should show hydrocarbon peaks increasing in intensity and substrate peaks decreasing in intensity with adsorbate chain length. Along these lines, it is of interest to

المنارة للاستشارات
www.manaraa.com

know whether different reactive adsorbates with the same number of carbon atoms produce surfaces with approximately the same thicknesses. If these multivariate analyses prove fruitful, they should also help one to rapidly identify outlier surfaces using multivariate peak intensity ratios, PCA, and PLS.

7.3 Experimental

7.3.1 Time-of-flight secondary ion mass spectrometry

ToF-SIMS was performed with an ION-TOF TOF-SIMS IV instrument with $^{69}Ga^{+}$ primary ions. The raster area of the beam was 51.8 x 51.8 μm^2.

7.3.2 Data Processing

Spectral regions were integrated using the "Peak List" feature in the instrument software. The following spectral regions were integrated in the positive ion spectra over a range of ± 0.2 amu at unit mass increments, unless otherwise indicated by a decimal: 1, 12 – 19, 23 – 27, 30 – 33, 36 - 121, 123, 128.1, 130.1, 131.1, 133, 146.1, 147.1, 148.1, 149.0, 177, 191, 205, 207, 208, 221.1, 281.1. The following four regions were also included: 27.8 to 27.995, 27.995 to 28.2, 28.8 to 28.995, and 28.995 to 29.2. The following spectral regions were integrated in the negative ion spectra over a range ± 0.2 amu at unit mass increments, unless otherwise indicated by a decimal: 1, 12 – 17, 24 - 129, 131, 133, 135 - 139, 141, 143 - 145, 147, 149, 151 – 153, 155 – 158, 160, 161, 161.9, 162.9, 165 – 167, 171, 172, 172.9, 179, 181, 181.9, 183, 184, 185.2, 185.9, 186.9, 187.8, 188.8, 189.8, 190.9, 193, 194.8, 196.8, 197.9, 199, 200.2, 207, 209, 211, 221, 225, 227.2, 229, 235, 239, 241.2, 249.1, 253.8, 254.8, 255.2, 263.1, 265.1, 266.7, 267.1, 268.7, 270.7,

المنارة للاستشارات
www.manaraa.com

277.1, 281.1, 281.8, 282.8, 291.1, 293.2, 294.2, 295.1, 297.1, 305.2, 307.1, 309.1, 311.1, 316.7, 321.2, 322.2, 323.2, 325.1, 335.2, 337.2, 339.1, 349.2, 380.7, 408.7.

After integration with the instrument software, the data were exported into Microsoft Excel where they were normalized and arranged into data matrices. Three n×m type matrices of the positive ion spectra, negative ion spectra and combined positive and negative spectra were thus obtained. The rows contained different samples and the columns corresponded to different spectral regions (variables). The matrix of the combined positive and negative ion spectra was made by normalizing the positive ion and negative ion data sets individually, and then concatenating them (linking them together). These matrices were then exported to the PLS_Toolbox 3.0 in Matlab. The PLS_Toolbox mean centered, autoscaled, and performed PCA and PLS on the data. Preprocessing for PLS included normalization and mean centering.

7.3.3 Material

Monolayers on Si_{scr} made from the following reactive adsorbates were studied: 1-pentene, 1-octene, 1-dodecene, 1-pentyne, 1-octyne, 1-dodecyne, 1-iodomethane, 1-iodoethane, 1-iodopropanol, 1-iodopentane, 1-iodooctane, 1-iodododecane, 1-bromopentane, 1-bromooctane, 1-bromododecane, 1-chloropentane, 1-chlorooctane, 1-chlorodecane, butyryl chloride, hexanoyl chloride, octanoyl chloride, decanoyl chloride, dodecanoyl chloride, tetradecanoyl chloride, hexadecanoyl chloride, butyraldehyde, pentaldehyde, hexaldehyde, heptaldehyde, octyl aldehyde, nonyl aldehyde, decyl aldehyde, and undecylic aldehyde. Monolayer preparation and characterization have been described previously.[9-14]

المنارة للاستشارات
www.manaraa.com

7.4 Results and Discussion

7.4.1 PCA of ToF-SIMS of Homologous Series of Aldehydes and Acid Chlorides on Si_{scr} to Determine the Best Preprocessing Method

In an effort to determine the best preprocessing method for my data set, the data from two homologous series of adsorbates were analyzed individually before considering the entire set of ToF-SIMS data. That is, PCA was performed on the positive ion, negative ion, and concatenated positive and negative ion data from surfaces prepared from eight aldehydes [$CH_3(CH_2)_{n-2}CHO$] (n = 4 - 11) and seven acid chlorides [$CH_3(CH_2)_{m-2}COCl$] (m = 4, 6, 8, 10, 12, 14, 16). Three different preprocessing conditions (normalization alone, mean centering, and autoscaling) were employed on each of the three types of data making a total of nine analyses for each adsorbate.

Table 7.1 shows R^2 values for plots of scores on PC1 vs. the number of carbon atoms for the aldehyde and acid chloride adsorbates. While autoscaling or normalization are sometimes a little more effective than mean centering in elucidating this correlation, it is clear, based on the average R^2 value for the three types of data that mean centering is the most effective preprocessing method. It is also clear from Table 7.1 that normalization alone is the weakest method. Figures 7.1 and 7.2 show these trends in the scores on PC1 of normalized, mean centered and autoscaled data for the positive ion data from the aldehydes and the negative ion data for the acid chlorides, respectively.

Because the results above are relevant to the remainder of this paper, it is valuable to discuss here why normalization and autoscaling are less effective than mean centering in preprocessing my data. First, a glance at the regions that were integrated over in the original spectra reveals that many of them contain mostly noise. Autoscaling makes these

المنارة للاستشارات
www.manaraa.com

Table 7.1. R^2 values for plots of scores on the PC's vs. the number of carbon atoms in the adsorbate.

Aldehydes				
PC1	positive	negative	concatenated	average
Mean Centering	**0.95**	**0.96**	**0.97**	**0.96**
Autoscaling	0.80	**0.96**	0.94	0.90
Normalization	0.25	0.90	0.71	0.62
PC2				
Mean Centering	0.04	0.02	0.00	0.02
Autoscaling	0.20	0.02	0.05	0.09
Normalization	0.98	0.96	0.97	0.97
Acid Chlorides				
PC1	positive	negative	concatenated	average
Mean Centering	0.92	0.97	**0.96**	**0.95**
Autoscaling	**0.97**	0.50	0.94	0.80
Normalization	0.78	**0.99**	0.92	0.89
PC2				
Mean Centering	0.02	0.01	0.02	0.02
Autoscaling	0.01	0.47	0.04	0.17
Normalization	0.94	0.96	0.96	0.95

المنارة للاستشارات
www.manaraa.com

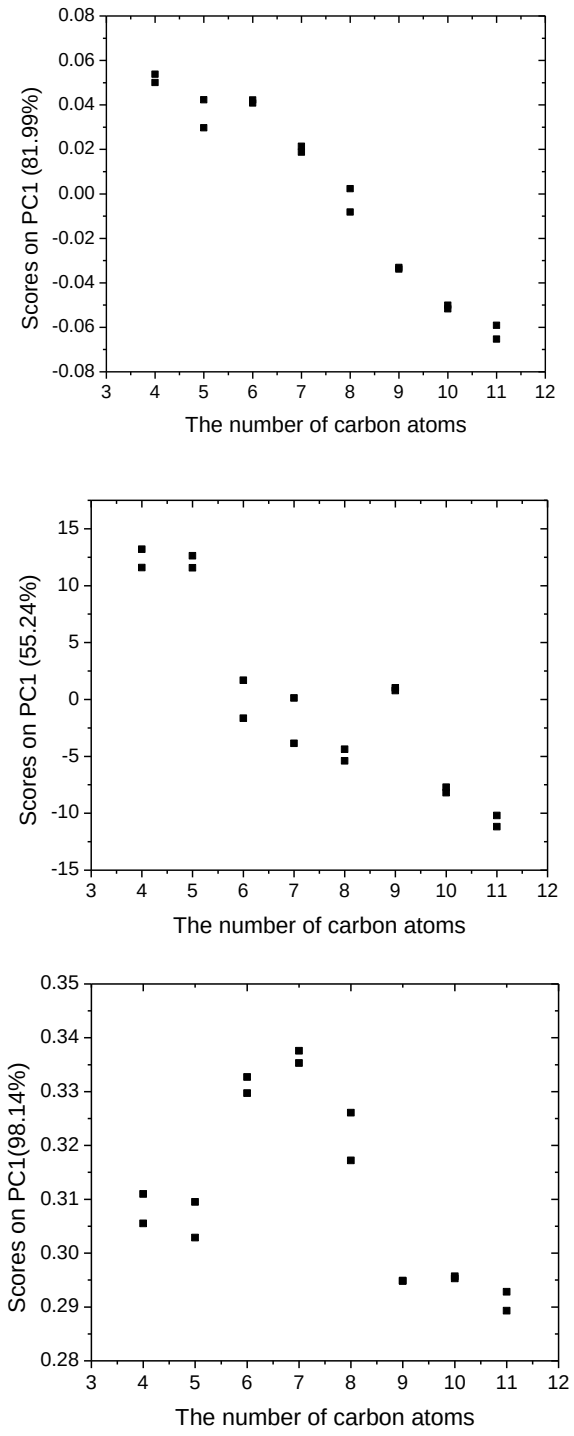

Figure 7.1. Scores on PC1 of ToF-SIMS positive ion spectra of silicon scribed under aldehydes containing 4 – 11 carbon atoms. Three preprocessing methods were used: a) mean centering, b) autoscaling and c) normalization.

المنارة للاستشارات
www.manaraa.com

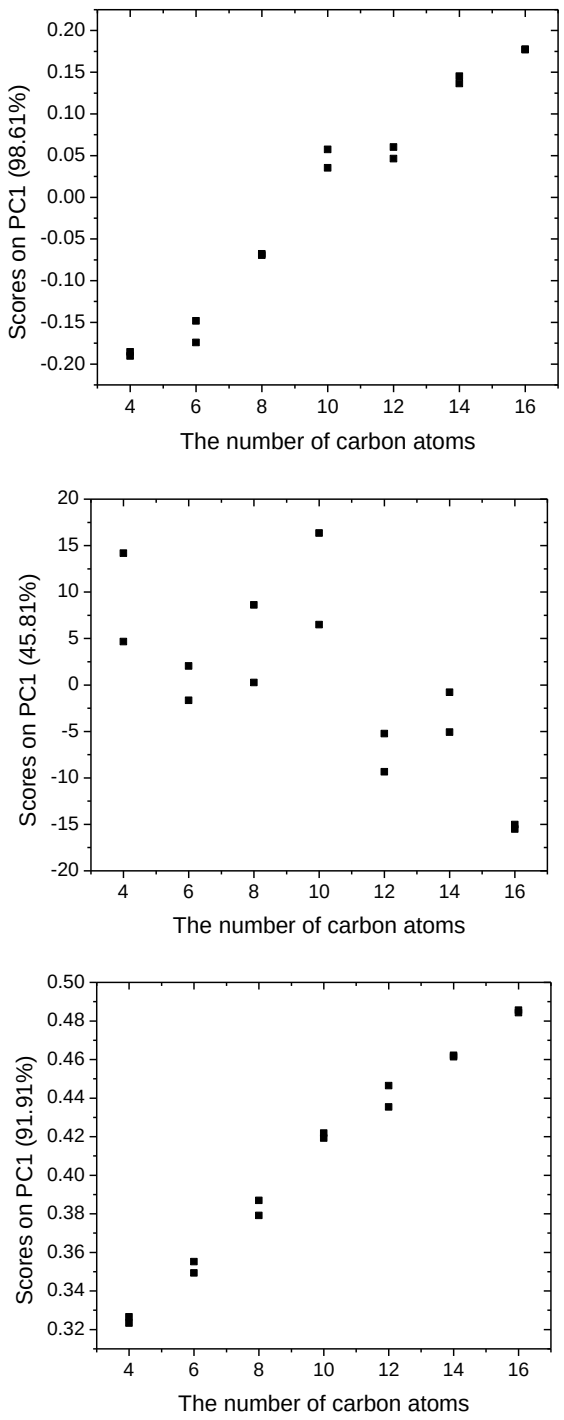

Figure 7.2. Scores on PC1 of ToF-SIMS negative ion spectra of silicon scribed under acid chlorides containing 4 – 16 carbon atoms. Three preprocessing methods were used: a) mean centering, b) autoscaling and c) normalization.

المنارة للاستشارات
www.manaraa.com

less important variables as important as the larger, highly characteristic peaks in the spectra. As a result, it should come as no surprise that PCA using autoscaling sometimes struggles to establish the desired correlation.

The normalized data present a different problem, the crux of which lies in the fact that their scores on PC1 do not center about zero, as do those from the data that are mean centered and autoscaled. That is, because the spectra, which are "plotted" as single points in a hyperspace, are not clustered about the origin when the data is only normalized, the first principal component must do its best to account for both the distance from the origin to the cluster of data points, as well as the chemical variation between the data points. PC1 is limited in its ability to accomplish this task because it is constrained to pass through the origin. A good portion of PC1 may thus be "wasted" when the data are not mean centered. For example, even though PC1 from the normalized data nominally accounts for more than 98% of the variation in the data, the scores on PC1 and the number of carbon atoms in the aldehyde do not correlate well.

As a consequence of the fact that PC1 from normalized data struggles to account for the variation in the data, PC2 from normalized data is meaningful, *i.e.*, the scores on PC2 correlate well with the number of carbon atoms in the adsorbate (see R^2 values in Table 7.1 and Figures 7.3c). In contrast, the scores on PC2 in the mean centered and autoscaled data do not show this correlation, although PC2 "accounts" for much larger fractions of the variation in these data sets (*ca.* 16% and 24%, respectively) compared to the normalized data (1.6%) (see again R^2 values in Table 7.1 and Figures 7.3). In the nine analyses of the scores on PC2 performed for the aldehydes (three different data sets and three different preprocessing methods), as well as the nine analyses performed for the

المنارة للاستشارات
www.manaraa.com

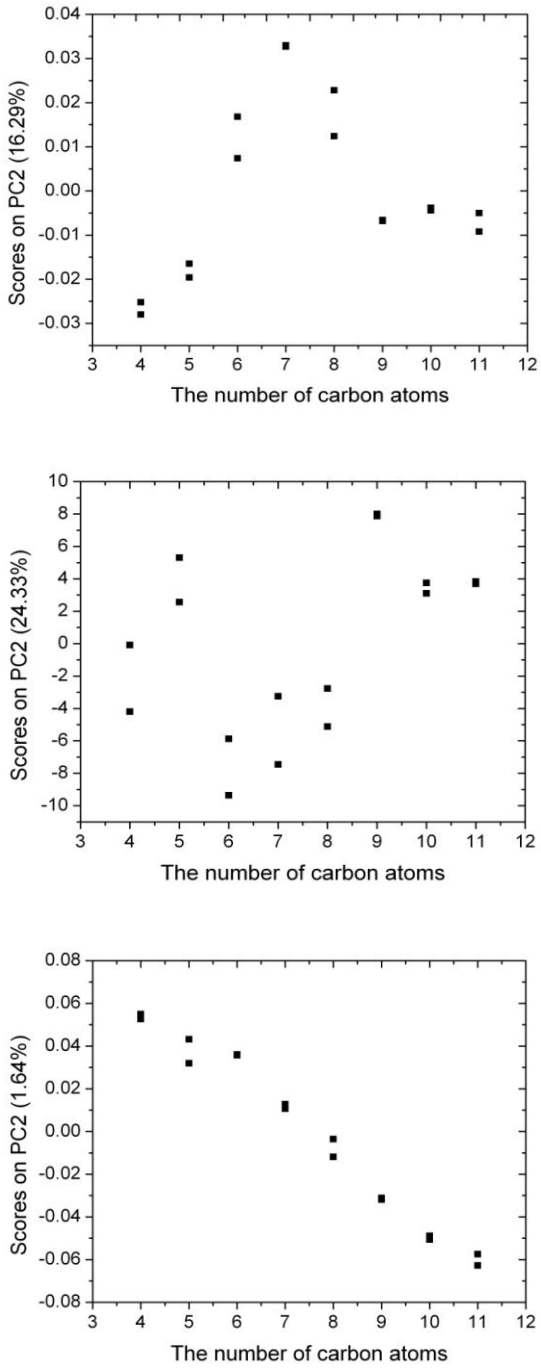

Figure 7.3. Scores on PC2 of ToF-SIMS positive ion spectra of silicon scribed under aldehydes containing 4 – 11 carbon atoms. Three preprocessing methods were used: a) mean centering, b) autoscaling and c) normalization.

المنارة للاستشارات
www.manaraa.com

acid chlorides, the scores on PC2 from the normalized data always correlate well with the number of carbon atoms in the adsorbate, while none of those from the mean centered or autoscaled data do. None of the 18 analyses for PC3 shows any correlation with the number of carbon atoms in the adsorbate.

It is my experience that it is valuable to consider more than one preprocessing method when performing a multivariate analysis on a new set of data. Based on the arguments in the three previous paragraphs and the results for the homologous series of the aldehydes and acid chlorides, I conclude that mean centering is the most appropriate preprocessing method for PCA of monolayers on Si_{scr}. Indeed, the four papers on multivariate analysis of ToF-SIMS data cited above[4-6, 8] also use mean centering, but without considering other preprocessing techniques. They also consider positive and negative ion spectra, but not combinations of the two.

While scores plots show trends and groupings of data, loadings reveal the chemical basis of variation. Table 7.2 lists the largest peaks and their likely assignments from mean centered positive ion, negative ion, and concatenated positive and negative ion spectra for silicon scribed under the aldehydes. It is of significance that in each of the data sets peaks of one polarity (positive or negative) are expected to come from the silicon-monolayer interface (inorganic ions), while peaks of the other polarity would be expected to come from the monolayer itself (organic ions). That is, monolayers prepared from aldehydes with 4 – 8 carbon atoms (see Figure 1a) show larger substrate peaks, e.g., Si^+, and smaller hydrocarbon peaks, e.g., $C_3H_5^+$, while those prepared from aldehydes with 8 – 11 carbon atoms show smaller substrate peaks and larger hydrocarbon peaks. The loadings from the

المنارة للاستشارات
www.manaraa.com

Table 7.2. The largest peaks from the loadings plots from mean centered positive ion, negative ion, and concatenated positive and negative ion spectra from silicon scribed under different aldehydes.

	Positive			**Negative**	
	PC1			PC1	
m/z	Loadings	species	m/z	Loadings	species
27.9	0.616	Si	1	0.7936	H^-
45	0.5979	SiHO	13	0.2834	CH^-
57	-0.0858	SiC_2H_5, C_4H_9	14	0.0892	CH_2^-
29.1	-0.0914	C_2H_5	25	0.0598	C_2H^-
39	-0.1058	C_3H_3	45	-0.0682	$^{30}SiCH_3^-$, $SiHO^-$
55	-0.111	SiC_2H_3, C_4H_7	60	-0.108	SiO_2^-
28.9	-0.132	SiH	77	-0.1175	$SiHO_3^-$
27	-0.1412	C_2H_3	61	-0.1371	$SiHO_2^-$
43	-0.2112	$SiCH_3$, C_3H_7	17	-0.2126	OH^-
41	-0.3577	C_3H_5	16	-0.4196	O^-
		Concatenated			
	PC1			PC1	
m/z	Loadings	species	m/z	Loadings	species
1	0.6869	H^-	39	0.0508	C_3H_3
13	0.2496	CH^-	29.1	0.0436	C_2H_5
41	0.1785	C_3H_5	45	-0.0592	$^{30}SiCH_3^-$, $SiHO^-$
43	0.1028	$SiCH_3$, C_3H_7	60	-0.0941	SiO_2^-
28.9	0.0952	SiH	77	-0.1024	$SiHO_3^-$
14	0.0786	CH_2^-	61	-0.1195	$SiHO_2^-$
27	0.0702	C_2H_3	17	-0.1867	OH^-
55	0.0542	SiC_2H_3, C_4H_7	27.9	-0.2792	Si
25	0.0535	C_2H^-	45	-0.3102	$^{30}SiCH_3^-$, $SiHO^-$
12	0.0519	C^-	16	-0.3674	O^-

المنارة للاستشارات
www.manaraa.com

PCA analysis of monolayers prepared from the acid chlorides show similar trends. These results are evidence for increasingly thick alkyl monolayers on Si_{scr} made from increasingly long aldehyde and acid chloride precursors. As noted, this type of analysis is useful because optical ellipsometry and X-ray reflectivity are not possible on our rough surfaces. Loadings of monolayers of dodecanethiol on gold made with different immersion times similarly showed that certain peaks were more intense for thinner monolayers than for more complete monolayers.[4]

7.4.2 PCA of ToF-SIMS of 66 Adsorbates on Si_{scr}

PCA was also performed on a matrix of data from 66 monolayers prepared on Si_{scr} from 1-alkenes, 1-alkynes, alkyl halides (chlorides, bromides, and iodides), acid chlorides, and aldehydes. Figure 7.4 shows the scores of these spectra on PC1 for the (mean centered) positive ion, negative ion, and concatenated positive and negative ion scans. In these plots the abscissa corresponds to the number of carbons in the adsorbate, regardless of its type. Figure 7.4a shows a good correlation between the number of carbon atoms in the adsorbate and the scores on PC1 for the positive ion spectra. This simple correlation is not as apparent in Figures 7.4b (negative ion spectra) and 7.4c (concatentated positive and negative ion spectra), which show a separation based on the number of carbon atoms in the adsorbate *and* the class of adsorbate. The significant conclusion from the three panels in Figure 7.4 is that the positive ion spectra are primarily sensitive to the length of the alkyl chains in the monolayer, while the negative ion and concatenated positive and negative ion scans seem to be sensitive to both the number of carbon atoms in the adsorbate *and* the class of adsorbate. Because the different types of adsorbates are

المنارة للاستشارات
www.manaraa.com

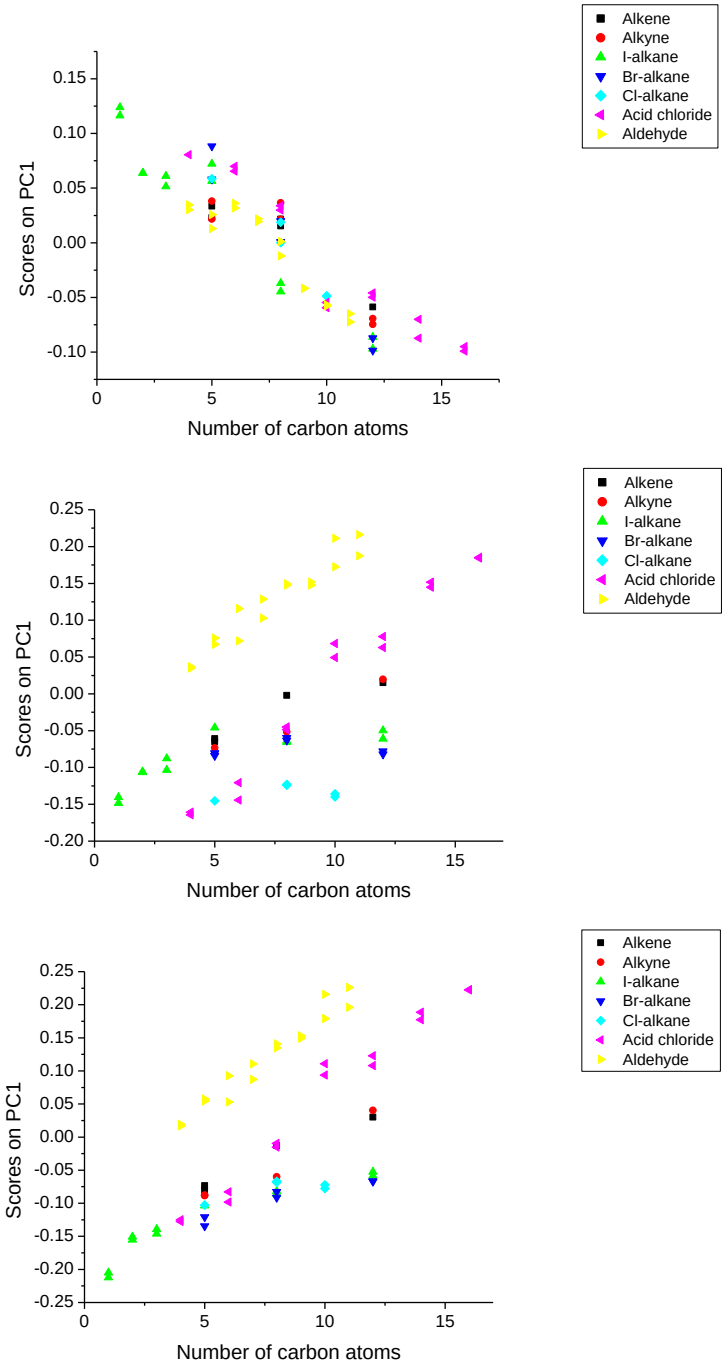

Figure 7.4. Plot of the scores on PC1 vs. the number of carbon atoms in the adsorbate. PCA of mean centered a) positive ion scans, b) negative ion scans, and c) combined positive and negative ion scans.

المنارة للاستشارات
www.manaraa.com

expected to adsorb differently to the surface,[9, 10, 13, 14] these results imply that the negative and concatenated positive and negative spectra are sensitive to changes in the substrate-monolayer interface. The correlation in Figure 7.4a is confirmed in its loadings (see Table 7.3), which, as in Table 7.2, demonstrates that peaks from the silicon-monolayer interface (inorganic ions) are inversely correlated to organic ions, or organic containing ions, that are expected to come from the monolayers.

The correlation between scores on PC1 and the number of carbon atoms in the adsorbate in Figure 7.4a also suggests that multivariate peak intensity ratios[5] could be found. I tried three such ratios. The first is the ratio of the mass 28 (Si^+) and 29 (SiH^+) regions to the total integrated regions (see Experimental), which I denote Φ_{Si}. The number of carbon atoms in the adsorbates ($^{\#}C$) was plotted as a function of Φ_{Si}.

The least squares linear fit to the data is $^{\#}C = -38.69\ \Phi_{Si} + 25.39$ with $R^2 = 0.766$. I next took the ratio of four hydrocarbon peaks centered about 27 ($C_2H_3^+$), 29.1 ($C_2H_5^+$), 39 ($C_3H_3^+$), and 41 ($C_3H_5^+$) to the total integrated regions, which I denote Φ_C. The fit to this data gives $^{\#}C = 62.43\ \Phi_C - 4.93$ with $R^2 = 0.812$. An even better fit was found by using the information in Table 7.3, taking the ratio of the regions with negative loadings to the regions with positive loadings. I denote this ratio Φ_{CSi}. The linear fit to this data gives $^{\#}C = 10.536\ \Phi_{CSi} - 0.159$, $R^2 = 0.829$ (see Figure 7.5). The value of Φ_{CSi} is that it allows one to perform a quick check on monolayer quality without running a full PCA analysis.

PCA is probably the most extensively used exploratory data analysis method. That is, PCA finds wide application as a tool for categorizing and grouping data. Recognizing that it is the negative ion spectra that appear to be most sensitive to differences in adsorbates, a three-dimensional plot of the scores on PC's 1, 2, and 3 for all of the negative ion

المنارة للاستشارات
www.manaraa.com

Table 7.3. The largest peaks from the loadings plot of mean centered, positive ion spectra from 66 monolayers.

positive		
m/z	PC1 loadings	species
27.9	0.6946	Si
45	0.4652	SiHO
28.9	0.163	SiH
42	-0.0679	$SiCH_2$, C_3H_6
57	-0.0863	SiC_2H_5, C_4H_9
55	-0.129	SiC_2H_3, C_4H_7
39	-0.1663	C_3H_3
43	-0.1824	$SiCH_3$, C_3H_7
27	-0.2323	C_2H_3
41	-0.3398	C_3H_5

المنارة للاستشارات
www.manaraa.com

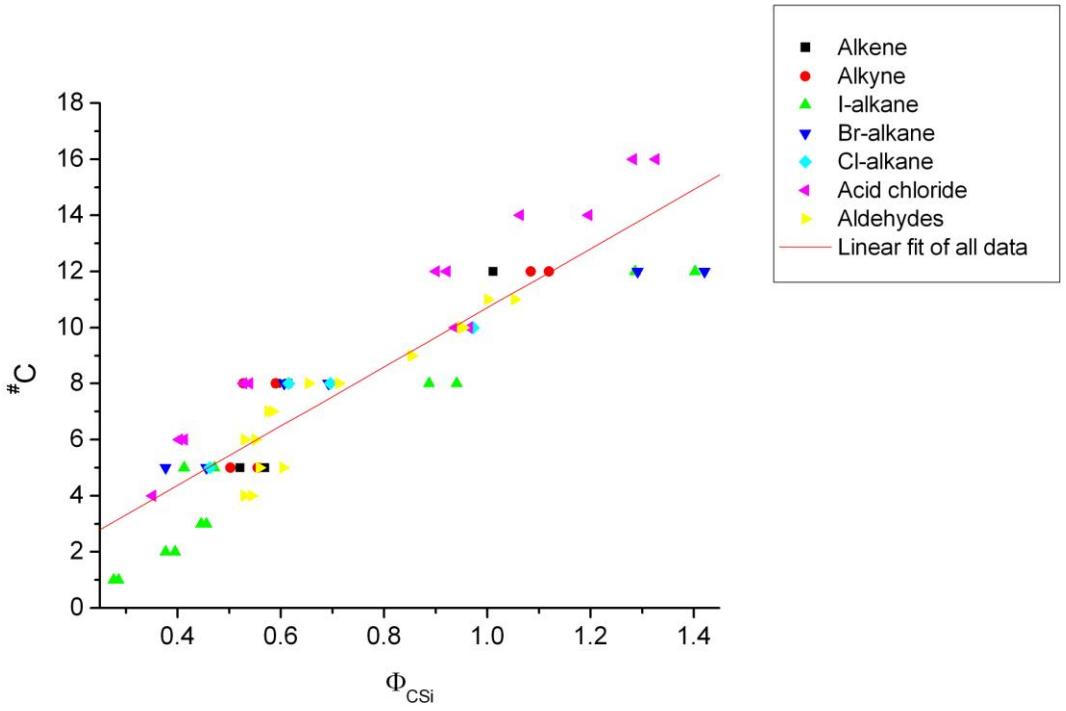

Figure 7.5. Plots derived from the positive ion ToF-SIMS spectra of 66 monolayers on Si_{scr}. Φ_{CSi} is the ratio of the area of the spectral regions: 42 ($C_3H_6^+$), 57 ($C_4H_9^+$), 55 ($C_4H_7^+$), 39 ($C_3H_3^+$), 43 ($C_3H_7^+$), 27 ($C_2H_3^+$), 41 ($C_3H_5^+$) by the area of 28 (Si^+), 29 (SiH^+) and 45 ($SiHO^+$).

المنارة للاستشارات
www.manaraa.com

spectra was generated (see Figure 7.6). It is clear from this plot that most of the different types of adsorbates separate well in this space. For example, the surfaces made from the three different haloalkanes are easily distinguished from each other. A similar three-dimensional plot made from the positive ion spectra did not show nice groupings of data points as revealed in Figure 7.6.

PCA provides another check on monolayer quality. Figure 7.7 shows the scores on PC1 from all 66 monolayers that were plotted as a function of number of carbons in the adsorbate and according to the class of the adsorbate. All of the data points from the positive ion spectra in Figure 7.7a follow the expected trends. However, for the negative ion spectra (Figure 7.7b) and the concatenated positive and negative ion spectra (Figure 7.7c) two outliers appear. Because it has been shown that the negative ion spectra and the concatenated negative and positive ion spectra are sensitive to the substrate-monolayer interface (*vide supra*), the results from Figure 7.7 imply that the two surfaces in question have monolayers of reasonable thicknesses, but that their interfaces are in some way different from others made with the same class of adsorbate.

A regression method, partial least squares (PLS), was also used on the positive and negative ion spectra from the 66 monolayers (see Figure 7.8). Figures 7.8a and b both show excellent correlations between the number of carbon atoms in the adsorbate and the number predicted by PLS from the positive and negative ion spectra. Thus, PLS of the positive and negative ion spectra could serve as another check on monolayer quality.

I end with a short comment on the concatenated positive and negative ion spectra. As shown in Figures 7.4 and 7.7, the negative ion and concatenated positive and negative ion spectra appear to behave similarly during PCA. Furthermore, when there is a difference

المنارة للاستشارات
www.manaraa.com

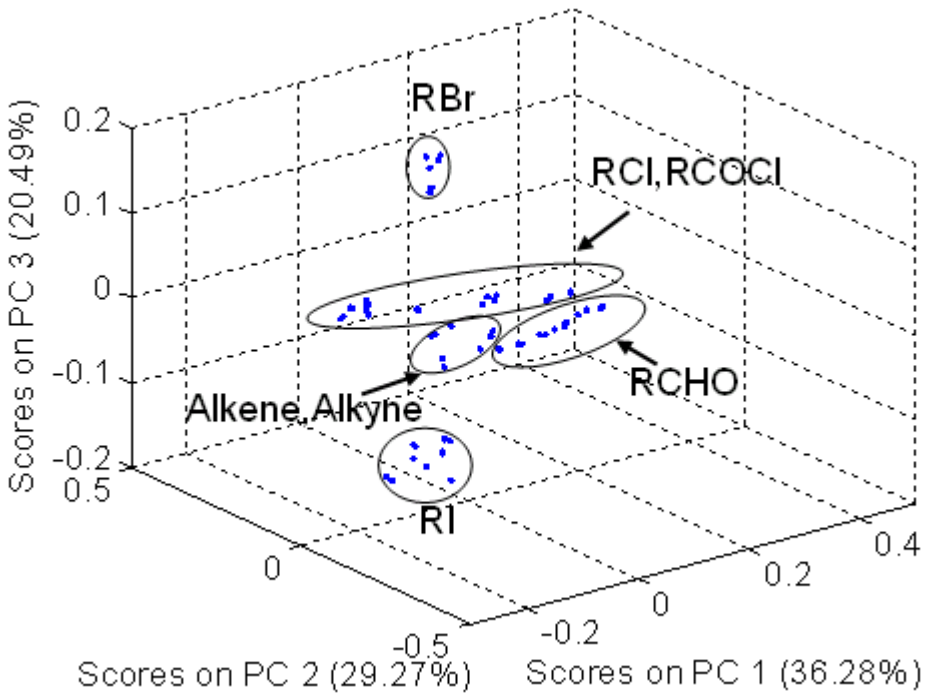

Figure 7.6. Three dimensional plot of scores on PC1, PC2, and PC3 from (mean centered) negative ion data taken from alkyl chloride (RCl), alkyl bromide (RBr), alkyl iodide (RI), acid chloride (RCOCl), aldehyde (RCHO), alkene, and alkyne adsorbates. Ovals are guides to the eye.

المنارة للاستشارات
www.manaraa.com

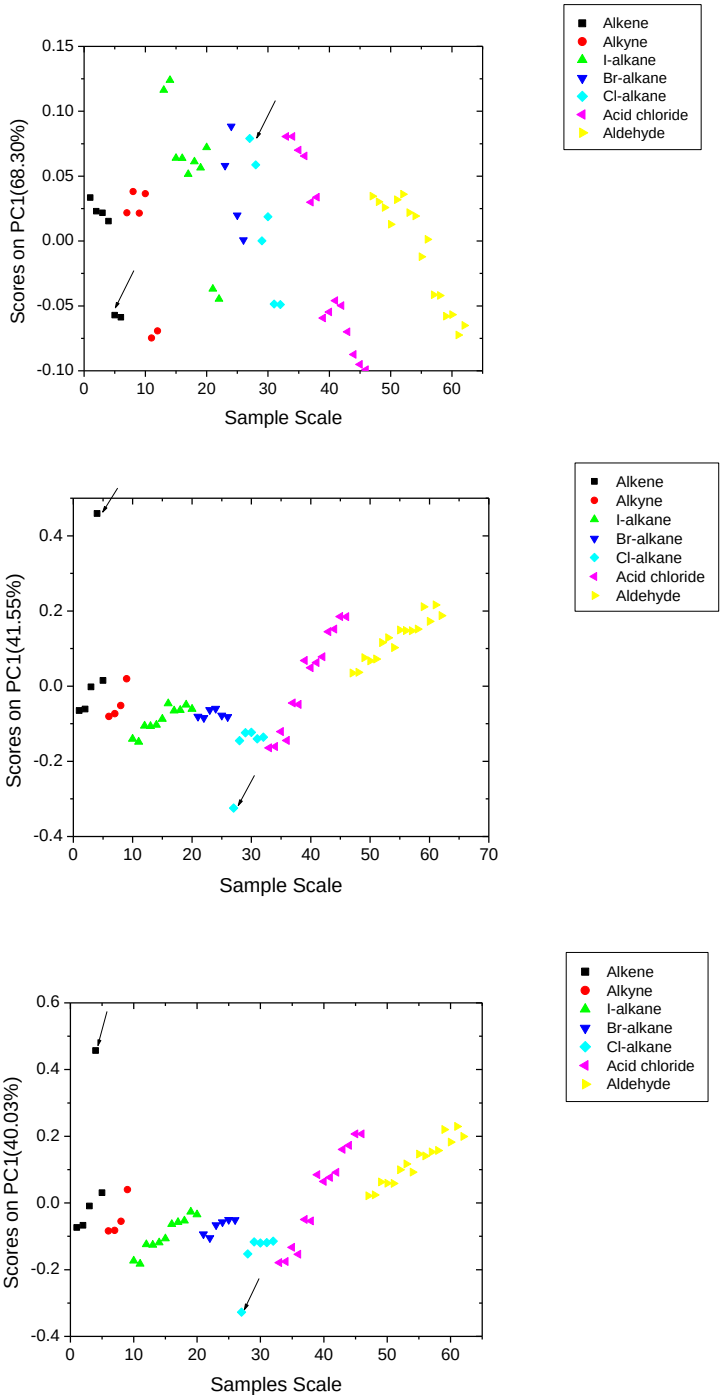

Figure 7.7. Scores on PC1 for 66 monolayers on silicon from normalized, mean centered a) positive ion scans, b) negative ion scans, and c) combined positive and negative ion scans.

المنارة للاستشارات
www.manaraa.com

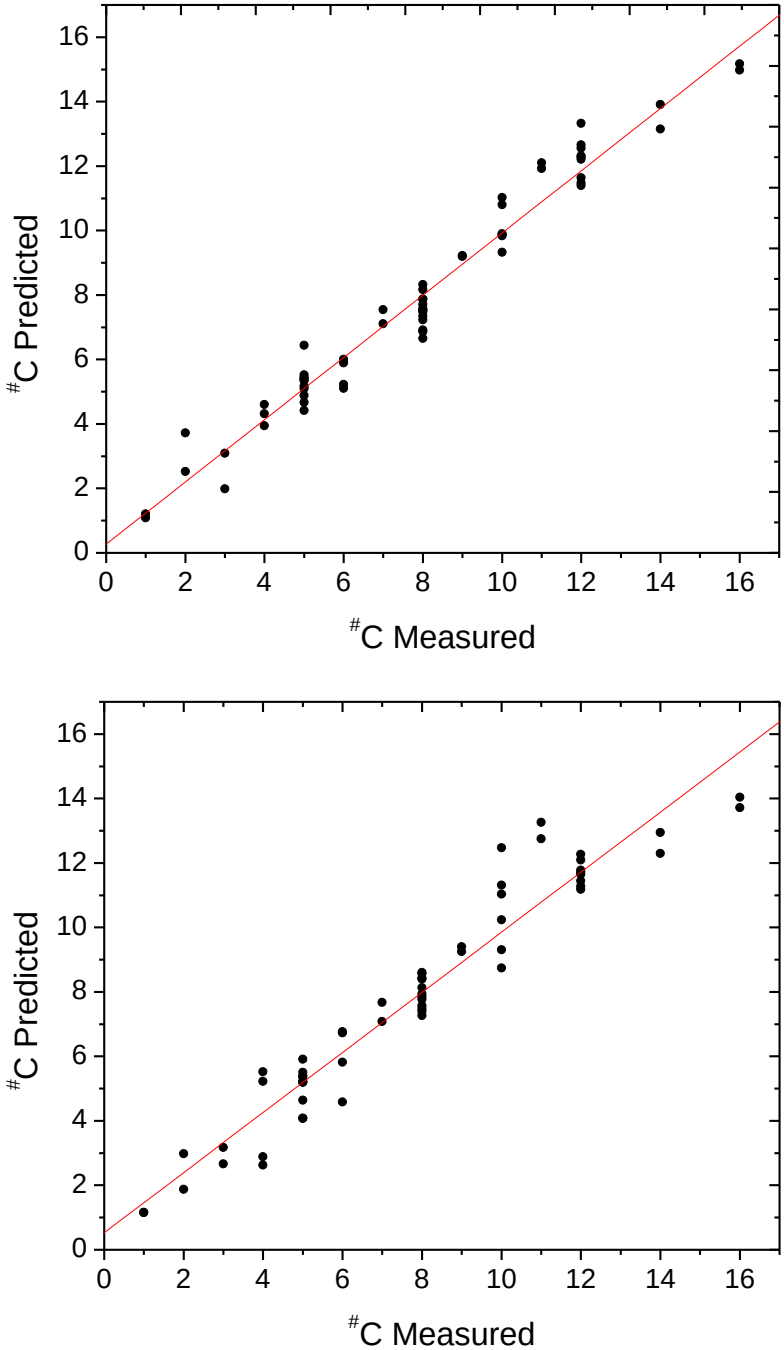

Figure 7.8. Partial least squares (with six latent variables) of 66 different monolayers showing the actual and predicted number of carbon atoms in the reactive adsorbates for a) the positive ion spectra, and b) the negative ion spectra.

المنارة للاستشارات
www.manaraa.com

between the R^2 values from negative ion and positive ion spectra in Table 7.1, the concatenated spectra usually have a value that is closer to that of the corresponding negative ion spectrum, although there are two exceptions to this statement in the table. Overall, I did not find any obvious advantage to concatenating the spectra that could not be obtained from analyzing either the set of positive or negative ion spectra alone. It is recommended that data be preprocessed by mean centering, and that both the positive and negative ion spectra, which contain valuable and complementary information, be analyzed.

7.5 Conclusions

Multivariate analysis methods such as principal components analysis (PCA) and partial least squares (PLS) are both efficient methods to rapidly determine the variation in ToF-SIMS data of monolayers on scribed silicon. In this study, mean-centering is the best preprocessing method among three preprocessing methods (normalization, mean-centering and autoscaling) for TOF-SIMS positive ion, negative ion and the concatenated positive and negative ion spectra spectra of monolayers on scribed silicon. In addition, PCA analysis shows that the relationship in positive ion spectra is based on alkyl chain length and the relationship in the negative ion and the concatenated positive and negative ion spectra are based on both the nature of the adsorbate and the monolayer chain length. PCA loadings revealed the chemical base of this relationship. The stong relationships between the number of carbon atoms in the adsorbate and the number it predicted from positive and negative ion sprctra are shown by PLS.

المنارة للاستشارات
www.manaraa.com

7.6 References

(1) Niehuis, E.; Grehl, T. In *ToF-SIMS, Surface Analysis by Mass Spectrometry*; Vickerman, J. C., Briggs, D., Eds.; IMPublications: Chichester, UK, 2001, pp 753-778.

(2) Brereton, R. G. *Chemometrics Data Analysis for the Laboratory and Chemical Plant.*; John Wiley & Sons, Ltd.: Chichester, 2003.

(3) Jackson, J. E. *A User's Guide to Principal Components*; John Wiley & Sons: New York, 1991.

(4) Graham, D. J.; Ratner, B. D. *Langmuir* **2002**, *18*, 5861-5868.

(5) Wagner, M. S.; Pasche, S.; Castner, D. G.; Textor, M. *Anal Chem.* **2004**, *76*, 1483-1492.

(6) Wang, H.; Castner, D. G.; Ratner, B. D.; Jiang, S. *Langmuir* **2004**, *20*, 1877-1887.

(7) Ulman, A. *An Introduction to Ultrathin Organic Films: from Langmuir-Blodgett to Self-Assembly*; Academic Press: Boston, 1991.

(8) Graham, D. J.; Price, D. D.; Ratner, B. D. *Langmuir* **2002**, *18*, 1518-1527.

(9) Niederhauser, T. L.; Jiang, G.; Lua, Y.-Y.; Dorff, M. J.; Woolley, A. T.; Asplund, M. C.; Berges, D. A.; Linford, M. R. *Langmuir* **2001**, *17*, 5889-5900.

(10) Niederhauser, T. L.; Lua, Y.-Y.; Sun, Y.; Jiang, G.; Strossman, G. S.; Pianetta, P.; Linford, M. R. *Chemistry of Materials* **2002**, *14*, 27-29.

(11) Niederhauser, T. L.; Lua, Y.-Y.; Jiang, G.; Davis, S. D.; Matheson, R.; Hess, D. A.; Mowat, I. A.; Linford, M. R. *Angew.Chem., Int.Ed.Engl.* **2002**, *41*, 2353-2356.

(12) Lua, Y.-Y.; Lee, M. V.; Fillmore, W. J. J.; Matheson, R.; Sathyapalan, A.; Asplund, M. C.; Fleming, S. A.; Linford, M. R. *Angew.Chem.Int.Ed.Eng.* **2003**, *42*,

المنارة للاستشارات
www.manaraa.com

4046-4049.

(13) Lua, Y.-Y.; Fillmore, W. J. J.; Linford, M. R. *Applied Surface Science.* **2004**, *231-232*, 323-327.

(14) Lua, Y.-Y.; Fillmore, W. J. J.; Yang, L.; Lee, M. V.; Savage, P. B.; Asplund, M. C.; Linford, M. R. *Langmuir* **2005**, *21*, 2093-2097.

(15) Cannon, B. R.; Lillian, T. D.; Howell, L. L.; Magleby, S. P.; Niederhauser, T. L.; Linford, M. R. *In Press Precision Engineering.* **2003**.

(16) Cannon, B. R.; Magleby, S. P.; Howell, L. L.; Jiang, G.; Niederhauser, T. L.; Linford, M. R. In *Influence of Scribe Speed and Force on Chemomechanical Nanofunctionalized Features*, ASME International Mechanical Engineering Congress and Exposition, New Orleans, LA, November 17-22, 2002, 2002; New Orleans, LA.

(17) Wacaser, B. A.; Maughan, M. J.; Mowat, I. A.; Niederhauser, T. L.; Linford, M. R.; Davis, R. C. *Applied Physics Letters* **2003**, *82*, 808-810.

(18) Lua, Y.-Y.; Niederhauser, T. L.; Matheson, R.; Bristol, C.; Mowat, I. A.; Asplund, M. C.; Linford, M. R. *Langmuir* **2002**, *18*, 4840-4846.

المنارة للاستشارات
www.manaraa.com

Chapter 8 Screening Phosphatidylcholine Biomarkers in Mouse Liver Extracts from a Hypercholesterolemia Study using ESI/MS and Chemometrics*

8.1 Abstract

When fed a high-fat, high-cholesterol diet (HFD), homozygous LDL receptor knockout mice exhibit extremely high levels of plasma cholesterol that are expected to influence liver metabolism. One step in the investigation of potential hepatic alterations was the analysis of organic extracts of livers from these and control mice by electrospray mass spectrometry (ESI/MS). Chemometrics (bioinformatics) analysis shows that the sample spectra cluster into two groups: one from mice with plasma cholesterol levels in excess of 900 mg/dL and one from animals with cholesterol levels of 60 – 250 mg/dL. The loadings plot of the first PC in the principal components analysis (PCA) reveals the chemical basis for clustering, i.e., biomarkers present at different concentrations in the different groups. The exact masses of the key peaks in this loadings plot indicate these species are phosphatidylcholines (PtdChos). This assignment is confirmed by tandem MS. Partial least squares (PLS) with variable selection shows that the spectra are well correlated with plasma total cholesterol, HDL cholesterol, and triglyceride (TG) levels.

---

*This chapter is reproduced with pemission from *Anal. Bioanal Chem.* **2009**, *393*, 643-654. Copyright 2009 Springer.

المنارة للاستشارات
www.manaraa.com

8.2 Introduction

As a class of biomolecules, the phosphatidylcholines (PtdChos) are the predominant phospholipids in cell membranes and circulating plasma lipoproteins.[1] Differences in the nature and quantity of PtdChos can influence membrane fluidity, membrane function and interaction of PtdCho with enzymes in lipid metabolism. With regards to these lipids, long-term exposure to a high-cholesterol diet (HFD) in mice has been shown to induce nonalcoholic fatty liver disease. Indeed, feeding low density lipoprotein receptor-deficient (LDLR-/-) mice a high-fat, high-cholesterol diet (HFD) for as little as 12 weeks is sufficient to induce measurable aortic atherosclerotic lesions.[2] Preliminary data (Patel and Banka, unpublished) suggest that the diet causes an inflammatory response, and others have shown that long-term exposure to HFD in mice leads to nonalcoholic fatty liver disease,[3] a common feature of the metabolic syndrome in humans. To determine if the inflammatory effects and potential hepatic lipid changes could be reversed by discontinuing the high-cholesterol diet, we fed one group of LDLR-/- mice HFD for 21 weeks followed by 7 weeks of normal chow and compared them with chow-fed wild type (C57BL/6) mice and LDLR-/- mice fed either HFD or chow for the entire 28-week study. I then examined the liver lipid profiles of all groups in an untargeted fashion by electrospray mass spectrometry. Because of their ease of ionization and concentrations, which led to ion suppression of other species in solution, the predominant signals from our instrument were the PtdChos. Thus, my experimental conditions allow for an unbiased analysis of the PtdChos in biological tissue.

A number of methods have been used to analyze lipids in biological tissues. However, because of lack of volatility, gas chromatography (GC) often lacks the ability to profile

المنارة للاستشارات
www.manaraa.com

complex, intact polar lipids, and high performance liquid chromatography (HPLC) lacks sensitivity and/or specificity, although for a targeted approach it can be invaluable when coupled to a mass spectrometer.[4-10] In addition, these separation methods identify compounds primarily through their retention times, a criterion of limited utility for analyzing complicated samples of unknown composition. In contrast, high resolution mass spectrometry (MS) is one of the most valuable tools for lipid analysis because it can provide exact molecular weights and unique spectra to aid in identification of unknown compounds.[11-13] MS is particularly important as a detector for chromatographic separations. Electrospray ionization (ESI) is a widely used ionization technique for analysis of polar and less polar compounds that has the advantage of being a soft ionization method. Therefore, ESI/MS has emerged as a powerful means of analyzing animal and plant tissues for molecular species such as erythromycin A,[14] phenolic compounds,[15] and plant hormones,[16] and is recognized as the best current method for analyzing phospholipids.[17] As a soft ionization method, ESI often only provides the mass-to-charge ratio of a molecular ion or protonated molecule. While extremely valuable, this information is not usually sufficient for identification of complex molecular species. To supplement this information it is often possible to perform tandem mass spectrometry (MS/MS) of analytes. Mass analysis of the resulting daughter ions can shed considerable light on molecular structure.

ESI/MS spectra of extracts of biological materials can be very complex, and the high degree of complexity of these mass spectra is both an advantage and a disadvantage. The many peaks in the spectra, especially the abundant signals in the mass region due to phosphatidylcholines, usually contain a wealth of chemical information about the sample

المنارة للاستشارات
www.manaraa.com

they came from. However, this complexity presents a challenge to the analyst who may be faced with more information than can be studied in a reasonable amount of time in a univariate fashion. In order to more rapidly determine the chemical variation between spectra, biomarkers, and even the covariance between individual peaks, a variety of advanced statistical methods, known as chemometrics tools in chemistry or bioinformatics tools in biology,[18-22] have been applied to mass spectrometric data. These include multivariate analyses such as principal components analysis (PCA),[23-26] K-means cluster analysis,[27-29] multivariate curve resolution (MCR) [30, 31] and partial least squares (PLS).[32-34] A brief review of these techniques is provided in this chapter (vide infra). These techniques help reveal the relationships between samples without peak choice bias and without neglecting a significant amount of the information in the spectra. The loadings of the factors in PCA, MCR and PLS are invaluable for showing which biomarker peaks are responsible for the chemical differences between the different samples. Recently this approach, mass spectrometry coupled with chemometrics, has been successfully applied to lipid analysis.[25, 26]

In this chapter I show an untargeted, top down, lipidomics approach to tissue analysis that includes the following steps: 1) tissue extraction with an appropriate organic solvent, 2) extract analysis by high resolution ESI/MS under conditions that favor the PtdChos, 3) MS data analysis by chemometrics, separating the spectra into two groups, corresponding to high and low cholesterol animals, which provides a chemical rationale for the identification of biomarkers and 4) identification of biomarkers based on exact molecular weights, isotope patterns, tandem MS results and literature precedent.[35] The goal of this study is to develop a quick and simple method for analysis of tissue extracts that is

المنارة للاستشارات
www.manaraa.com

focused on the PtdChos and based on ESI/MS spectra and chemometrics. This method is used to discriminate different samples. It also reveals the similarities and differences between samples. PLS is then used to build a model to predict the concentrations of specific compounds in unknown samples.

8.3 Experimental

8.3.1 Materials

All solvents (hexane, isopropanol, chloroform, methanol, and formic acid) were spectrophotometry grade or the highest available commercial grade and were used as received unless otherwise specified.

8.3.2 Instrumentation

All electrospray spectra were collected by an Agilent Technologies LC/MSD TOF system. No liquid chromatography was used in these experiments. Several µLs of extract solution were infused into the ESI source along with the mobile phase (75% MeOH and 25% water with 5 mM ammonium formate). A steel ES ionization needle was set in the positive-ion mode. The charging voltage and the capillary voltages were 900 V and 3500 V, respectively. The nebulizer was at 35 psi and the gas temperature was 350° C. The skimmer was operated at 60 V. The flow rate of the nitrogen drying gas was 12L/min. One survey scan was collected per second over a mass range of m/z 100-1200.

Product ion mass spectra were collected with an AB Applied Biosystems API QSTAR Pulsar i LC/MS/MS instrument. No liquid chromatography was used in these experiments. Diluted extract solutions were infused at 3 µL/min (continuous mode) through a Harvard

المنارة للاستشارات
www.manaraa.com

model 22 syringe pump (Harvard Apparatus, South Natick, MA). The ion source and ion optical parameters were optimized with respect to the positive ions of phosphatidylcholine standards. For each spectrum, 120 scans (2-min duration) were averaged. The curtain gas was set at 18 psi. Ions of interest were selected in the first quadrupole and accelerated (collision energy 35 eV) into a collision cell containing argon to induce CAD (collisionally activated dissociation). Fragment ions produced by CAD were then analyzed in the TOF analyzer.

8.3.3 Animals

LDLR-/- mice backcrossed to a C57BL/6 background were purchased from Jackson Laboratories (Bar Harbor, ME) and a breeding colony was established at the La Jolla Institute for Molecular Medicine. All husbandry and experimental procedures were conducted in accordance with the Institutional Animal Care and Use Committee of the La Jolla Institute and adhered to NIH guidelines. The experimental diet (HFD) was designed as a synthetic, casein-based diet containing 6% fat and 1.25% cholesterol, the minimum dietary requirement of vitamin E, and no other antioxidants (Harlan Teklad, diet # TD96335). The three treatment groups of female LDLR-/- mice included chow-fed (four mice with numbers 614, 641, 642 and 643), HFD-fed (four mice with numbers 254, 255, 256 and 278), and a group that received HFD for the first 21 weeks followed by chow feeding for the final seven weeks (three mice with numbers 249, 250 and 251). C57BL/6 (wild type) female mice (three mice with numbers 637, 639 and 640) were maintained on a chow diet throughout. The mice were entered into the feeding study at three months of age.

المنارة للاستشارات
www.manaraa.com

8.3.4 Plasma and Tissue Collection

Venous blood was collected from each mouse into heparinized capillary tubes from the retro-orbital sinus under isoflurane inhalant anesthesia one week before termination of the experiment. Plasma for cholesterol determination was collected after centrifugation and stored at –20º C. Plasma cholesterol levels were determined using an enzymatic colorimetric kit (Sigma Chemical, St. Louis, MO). At termination of the experiment, livers were collected following perfusion with ice-cold phosphate-buffered saline, snap frozen in liquid nitrogen, and pulverized while frozen prior to storage at –70º C.

8.3.5 Extraction Procedure

The frozen liver tissue was homogenized in 16 volumes of a hexane/isopropanol (3:2 v/v) for 5 min.[36] The resulting suspension was filtered and the glass filter (VWR) was rinsed with a small volume of hexane-isopropanol mixture. The resulting combined filtrate and rinse were suitable for direct injection into the electrospray mass spectrometer (ESI-MS).

8.3.6 Solution Preparation for Tandem MS

To avoid detector saturation, mouse liver extract solutions were diluted by a factor of 10 with 3:2 (v/v) hexane/isopropanol. To increase tandem MS signals, a small amount of 0.1 M formic acid in 50:50 (v/v) methanol/H_2O was added (10% of the solution volume).

8.3.7 Data Processing

For principal components analysis (PCA), hierarchical cluster analysis (HCA),

المنارة للاستشارات
www.manaraa.com

multivariate curve resolution (MCR), and partial least squares (PLS) the MS data representing 53 spectra from 14 different animal liver samples were first simplified by binning to unit mass resolution from m/z 101 to 1199. The total number of binned regions is 1099. Each liver extract solution was analyzed at least three times. I have previously employed this approach (binning to unit mass or half unit mass resolution) in chemometrics analyses of mass spectral data.[37] Binning greatly simplifies the formation of data matrices from raw data (spectral) files. It also avoids user bias (peak choice bias) because all spectral regions are treated (binned) equally. In addition, binning is relatively insensitive to minor calibration errors and/or small day-to-day instrumental variations in peak positions and separations. While binning facilitates exploratory data analysis, the original high resolution data remain extremely important for identifying the chemical components of sample mixtures.

Binned data were exported into Microsoft Excel to form spectral data matrices. To facilitate direct comparison of the individual spectra, the data were normalized with the "1-Norm", which divides each mass in a spectrum by the sum of all masses, making allowance for spectra that may have been collected under somewhat different conditions and times. The normalized data were then exported into MATLAB 7.0 (The MathWorks, Natick, MA) for PCA, HCA, MCR and PLS analysis using the PLS_Toolbox 4.0 for MATLAB (Eigenvector Research, Wenatchee, WA). Prior to PCA and HCA analysis, the data were mean centered. The PLS_Toolbox genetic algorithm was employed for variable selection. HCA was performed on mean centered data using the Euclidian distance measure.

Mean centering is favored over autoscaling when mass spectra contain large amounts

المنارة للاستشارات
www.manaraa.com

of noise.[37] For MCR, normalized data were used without additional mathematical treatment because mean centering and autoscaling are incompatible with the non-negativity constraints imposed by MCR. For PCA, HCA and MCR, only a single block of data is needed (the X-block), which is composed of the spectra of all the samples. A second block is also needed for PLS. In this work, this Y-block is composed of the concentrations of cholesterol, HDL cholesterol, and triglycerides (TG) as measured in the blood plasma of the mice, where PLS was applied individually to these columns in the Y-block, and not to the entire block, *i.e.*, I performed so-called "PLS1" and not "PLS2".[22] Mean-centering is applied to this Y-block. For PLS, contiguous blocks of data (9 data splits) were removed during cross validation to assure that all replicates from a sample were removed during this analysis. Because cross-validation was performed, a method for obtaining the internal predictive capability of a model was employed, where the cross-validated correlation coefficient (q^2) is defined as:

$$q^2 = 1.0 - \frac{\sum_Y \left(Y_{pred} - Y_{actual}\right)^2}{\sum_Y \left(Y_{actual} - Y_{mean}\right)^2}$$

8.3.8 A Brief Overview of Chemometrics Data Analysis Methods

The first step in preparing data for a chemometrics analysis is assembly of the data into a data matrix and subsequent preprocessing.[22, 37] In a typical data matrix, each row represents one sample, and each column represents a variable, e.g., a region over which the mass spectrum has been integrated. In the case where the ratios between peaks should remain constant, but the overall counts in the spectrum vary, it is common to row scale, or

المنارة للاستشارات
www.manaraa.com

normalize, the data using the so-called 1-Norm in a row operation: $^{rs}x_{ij} = \frac{x_{ij}}{\sum_{j=1}^{J} x_{ij}}$. The two most common preprocessing methods that might next be considered are column operations: mean centering and autoscaling. In mean centering, the mean of the values in each column is subtracted from each value in that column: $^{cen}x_{ij} = x_{ij} - \bar{x}_j$. Mean centering is important in principal components analysis (PCA) because otherwise the first PC may be largely wasted as it accounts for the distance between the origin and a set of data points of interest. Autoscaling includes mean centering of the data, followed by division of the data in a column by its standard deviation. Autoscaling makes each variable of equal importance. Thus, autoscaling may not be useful when a large number of integrated spectral regions contain mostly noise.

In chemometrics analyses it is often valuable to view spectra as vectors, i.e., as single points in a hyperspace. In PCA, the axes of the coordinate system are then rotated to capture the maximal variation in the data. The axis that captures the largest fraction of this variation is the first principal component (PC1). Unfortunately, acceptable abbreviations for “phosphatidylcholine” and for “principal component” are both “PC”. In this work, “PC” will refer to principal component, and “PtdCho,” which is also an acceptable abbreviation for “phosphatidylcholine,” will be used. The projections of the data points onto the PCs are termed scores. Scores plots show relationships between spectra. The axis that captures the next largest fraction of the variance after PC1, and which is of necessity perpendicular to PC1, is PC2. Other PC’s are obtained in a similar fashion. The contributions (projections) of the old axes (variables) onto the principal components are called loadings.[37, 38] Loadings plots show the contributions of the original

المنارة للاستشارات
www.manaraa.com

variables to the PCs, i.e., they provide the chemical basis for separations seen by PCA. In PCA, the Hotelling T^2 measures the variance within the model, and the Q Residuals provides the variance outside the model. A plot of Hotelling T^2 vs. Q Residuals often reveals outliers.

Cluster analysis has been widely employed as a categorization tool in the biological sciences. Like PCA, cluster analysis may determine the degree of similarity, or lack thereof, between objects in a data set. Two common cluster methods are the K-nearest neighbors (KNN) algorithm and the K-means algorithm.[27-29] Various distance measures between data points may be employed, which include the Euclidean distance and the Manhattan distance.[39] The results of a cluster analysis are usually represented by a two-dimensional plot called a dendrogram because of its tree-like appearance. Dendrograms show the connections found at each level of the clustering algorithm. The length of each horizontal line in the dendrogram is proportional to the distance between the objects. It is valuable to use cluster analysis in conjunction with PCA. Unlike a PCA model, which will often neglect a fraction of the variance in the data, cluster analysis is usually used as a whole spectrum analytical method. In addition, the mathematics of PCA and cluster analysis are very different so that if nearly the same separation of data points is obtained with both methods one can have greater confidence in the chemometrics/bioinformatics analysis.

Multivariate curve resolution (MCR) has also been applied to mass spectrometry data. MCR is of great value because the factors it provides have only positive peaks, i.e., they look like spectra. They can thus be interpreted with greater ease by the non-expert, and are more ‘natural’ in their appearance. MCR can be viewed as an interesting variant of

المنارة للاستشارات
www.manaraa.com

classical least squares (CLS) in which the only known quantity in the problem is the data matrix **S**. The basic equation **S** = **C***P is then right and left multiplied by the pseudoinverses of **P** and **C**, respectively, to get:

i) $\mathbf{C} = \mathbf{S}\mathbf{P}^T(\mathbf{P}\mathbf{P}^T)^{-1}$

ii) $\mathbf{P} = (\mathbf{C}^T\mathbf{C})^{-1}\mathbf{C}^T\mathbf{S}$

In these equations, **S** is a data matrix that contains the spectra in rows, **P** is a matrix that contains the pure spectra in rows, and **C** is a matrix that contains the contributions of the pure component spectra to the spectra in **S**. After an initial guess is contructed for **P**, equations i) and ii) are iterated until convergence is obtained, subject to the nonnegativity constraints that all the values in **C** and **P** are greater than or equal to zero, and that $\mathbf{P}_i\mathbf{P}_i^T = 1$, i.e., the pure component spectra have unit length.

The basic idea of partial least squares (PLS) is that it is a linear model, $Y = b_0 + b_1X_1 + b_2X_2 + b_3X_3 + \ldots + bpXp$, that relates two sets of data. This equation allows a predicted property of a system, Y, to be estimated by the function of the other properties of the experiment, X. That is, I can use the mass spectral data I obtain in a set of experiments to predict new observations by a linear regression model.

8.4 Results

8.4.1 MS Data Collection

This work is focused on the analysis of phosphatidylcholine (PtdCho) biomarkers. Hence, it would be advantageous to have mass spectra that would emphasize the

المنارة للاستشارات
www.manaraa.com

molecular ions of the phosphatidylcholines, while deemphasizing those of other species. To this end, I observed that the ratios of the phosphatidylcholine quasi-molecular ions remained essentially constant over a wide range of concentrations, *even beyond the linear limit*. For example, I chose six key peaks in my data: the five identified peaks in Figure 8.5, along with the m/z 835 ion in this spectrum (vide infra). Figure 8.1a shows the plot of instrument signal of these peak areas as a function of the relative concentration of the organic extract of a mouse liver tissue sample that contains both a linear region at low concentration and a saturated region at high concentration. Figure 8.1b shows the ratio of each of these peak areas to the total peak area in its spectrum as a function of solution concentration. It is of great significance for this work that the relative peak areas remain essentially constant over this very wide range of concentrations. Based on these results, it was possible to work at high lipid concentrations, which resulted in ion suppression of other lipid signals. This resulted in the clean spectra illustrated in Figure 8.2, which greatly facilitated my analysis.

8.4.2 Electrospray MS Analysis of Homogenized Mouse Liver Tissues

Mouse livers were homogenized and filtrates analyzed by ESI/MS. Figure 8.2 contains a representative ESI/MS spectrum that reveals a series of intense peaks at *ca*. m/z 750 – 850. The more than 50 such mass spectra that were collected represent the liver lipid profiles of all the various animal feeding groups.

المنارة للاستشارات
www.manaraa.com

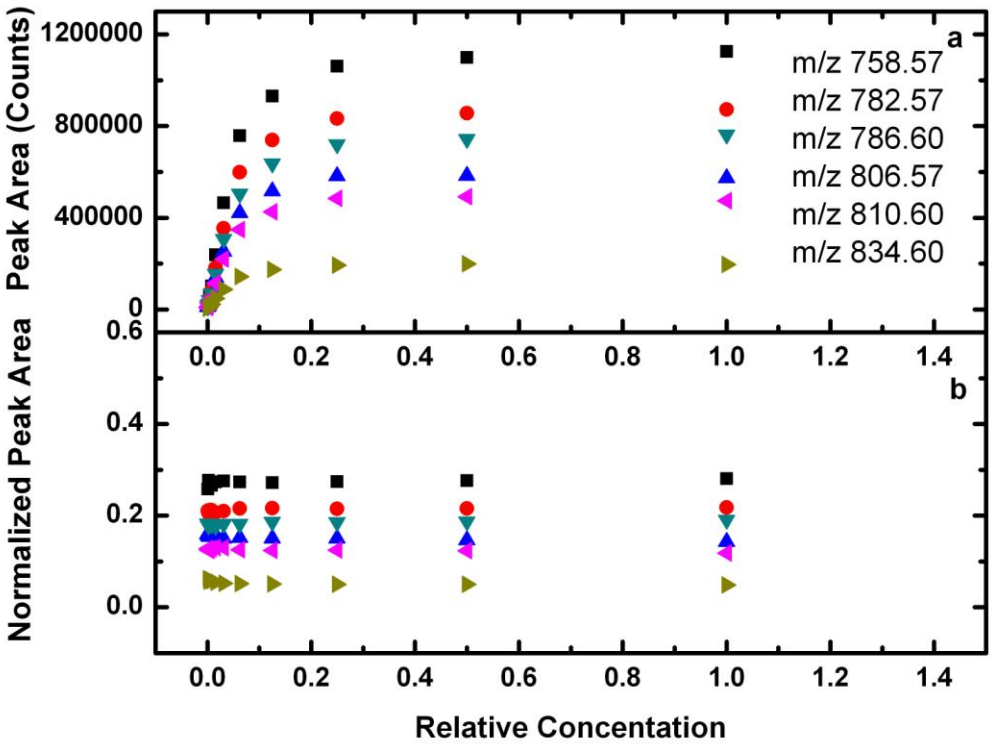

Figure 8.1. Peak areas (a) and normalized peak areas (b) of six peaks of significance from Figure 8.5, showing results from ten dilutions of 50%. [The mouse liver used was obtained at Brigham Young University (BYU). The analysis shown in this Figure was also performed on beef liver (obtained from a local grocery store), which again showed that the ratio of the peak areas of the most significant phosphatidylcholines to the sum of areas remained essentially constant over the same wide range of concentrations.]

المنارة للاستشارات
www.manaraa.com

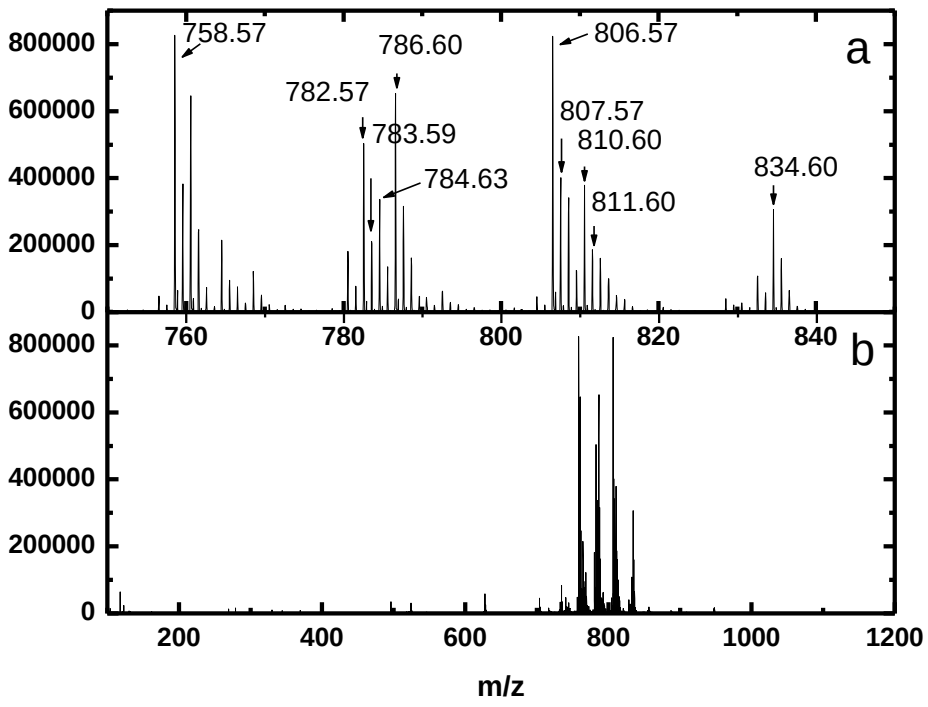

Figure 8.2. Livers from hypercholesterolemic and normocholesterolemic mice were extracted and analyzed by electrospray mass spectrometry. Shown are representative mass spectra for a normocholesterolemic mouse. (a) Electrospray mass spectrum of mouse 249 in the range from 750 to 850 (b) Whole electrospray mass spectrum of mouse 249 in the range from 100 to 1200.

المنارة للاستشارات
www.manaraa.com

8.4.3 Principal Components Analysis

It is usually difficult to compare large numbers of spectra in a univariate fashion. Accordingly, principal components analysis (PCA) has been successfully applied to mass spectral data.[23-26, 37-40] Figure 8.3 shows the PCA analysis of my ESI/MS data as a plot of PC1 vs. PC2. The first principal component, PC1, showed an excellent separation of the data into two groups, and accounted for ca. 62% of the variance in the data. No such clustering was observed on the second PC, or higher PCs. The plot of "percent variance captured per PC" suggested that a minimum of two PCs should be retained in a model, and that four or possibly five PCs would fully describe the data. The cross validation results, either "Leave One Out" or "Venetian Blinds (with seven data splits)," showed a minimum error at five PCs. However, because separation of the data points (spectra) into two main clusters appears only on PC1, I focused my attention on the scores and loadings of this principal component.

The ESI/MS and PCA were done as blinded studies. After these analyses, it was revealed that the samples on the left of Figure 8.3 came from mice with high plasma choloesterol levels (900 – 1450 mg/dL) and the samples on the right came from mice with low plasma cholesterol levels (60 – 250 mg/dL). PCA did a remarkable job of segregating the mice according to their measured plasma cholesterol levels, and strongly suggested that there was a significant chemical variation between the liver samples of the two groups.

PCA was also used to look for outliers in the data. Using a five PC model, a Hotelling T^2 vs. Q Residuals plot was constructed. In this plot, two of the spectra were found to be significant outliers (beyond 99% confidence limits), while all of the

المنارة للاستشارات
www.manaraa.com

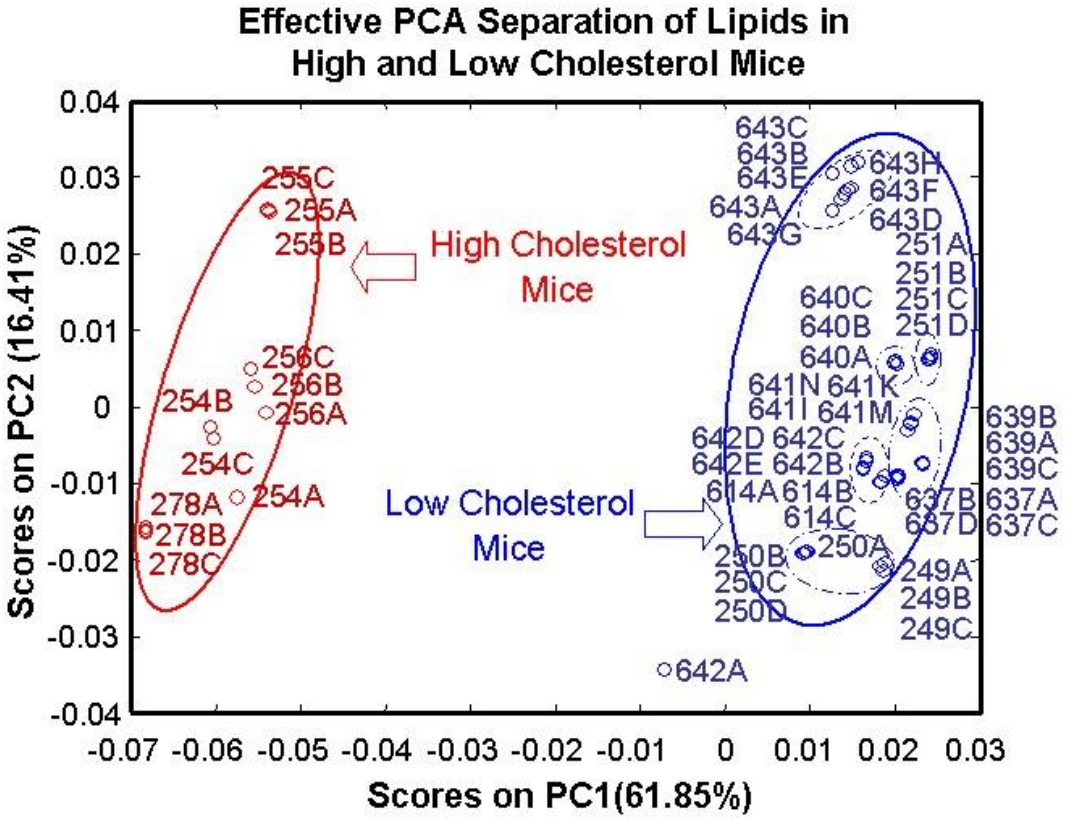

Figure 8.3. PCA analysis of infusion mass spectrometry data from organic extracts of mouse livers. Samples (red circles) in the red line oval on the left are LDLR-/- mice fed a high fat, high cholesterol diet (HFD) for the entire period. These mice had plasma cholesterol levels between 900 and 1450 mg/dL. Samples in the small dash line ovals on the right are LDLR-/- mice fed chow for the entire period. These mice had plasma cholesterol levels of ca. 250 mg/dL. Samples in the dash-dot line ovals on the right are LDLR-/- mice fed HFD for 21 weeks and then returned to a chow diet. Samples in the dash-dot-dot line oval are C57BL/6 mice fed a chow diet. These are controls in that they are normal mice with the same genetic background as the LDLR-/- mice. Their cholesterol levels were ca. 80 mg/dL. (The samples on the right had plasma cholesterol levels between 60 and 250 mg/dL.) The label numbers indicate individual mice.

المنارة للاستشارات
www.manaraa.com

remaining points were well within these limits. These outlying spectra were from the first runs of the day, which could have been contaminated by solutions injected by previous users of the instrument. Repeat analyses of these liver extracts produced spectra that were well within 99% confidence limits. For the remaining multivariate analyses considered herein (HCA, MCR, and PLS), these two data points were removed.

8.4.4 Hierarchical Cluster Analysis (HCA)

Because PCA only separated the data on one principal component, it seemed reasonable to analyze my data using a chemometrics method based on different mathematics that would account for all the variance in the data. Therefore, K-means and K-nearest neighbors (KNN) clustering were applied to my data. Both of these clustering methods segregated the data into two main groups which were in excellent agreement with the PCA results, i.e., one group contained all of the samples from the high cholesterol mice, and the other contained all of the samples from the low cholesterol mice. Figure 8.4 shows the dendrogram for the KNN analysis. Interestingly, when the two outliers from the PCA analysis were included in the cluster analyses, they were also observed to be outliers, i.e., they were their own clusters, or they were at the extreme end of a cluster. These results serve as a mathematically independent confirmation of the PCA results.

8.4.5 Examining the PCA Loadings

Scores plots in PCA, *e.g.*, Figure 8.3, reveal relationships between spectra (samples), while loadings plots reveal the chemical variation in biomarkers responsible for the

المنارة للاستشارات
www.manaraa.com

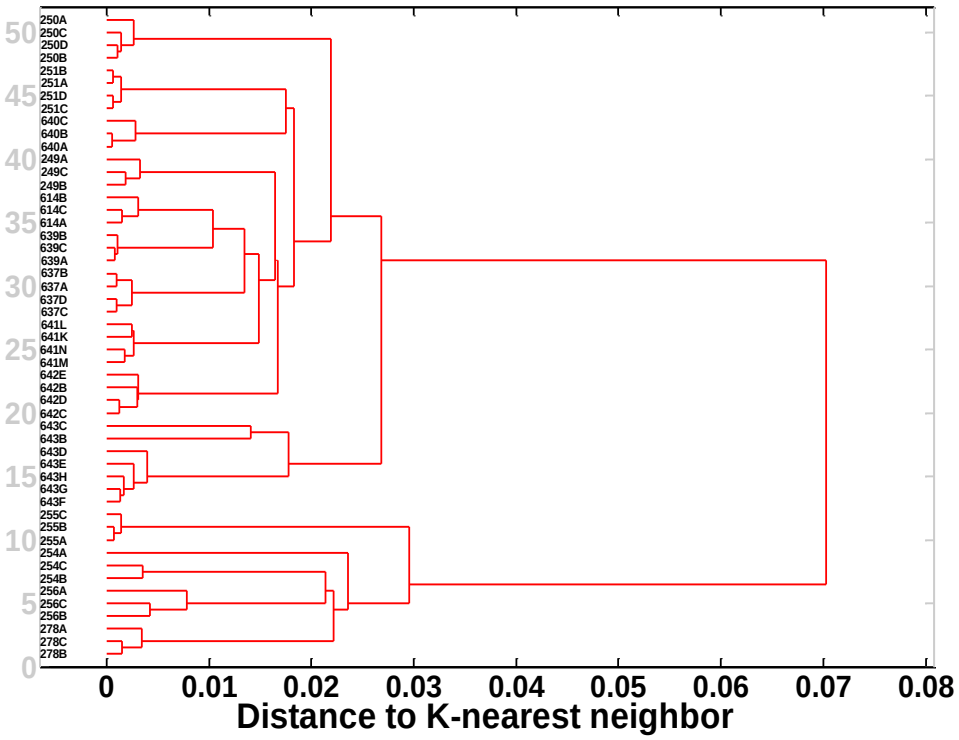

Figure 8.4. Dendrogram of the K-nearest neighbor (KNN) cluster analysis of all of the electrospray MS data from the mouse liver extracts. The top cluster comes from livers of normocholesterolemic mice and the bottom cluster comes from livers of hypercholesterolemic mice. The y-axis labels are the identification numbers for the original samples.

المنارة للاستشارات
www.manaraa.com

relationships in scores plots. Figure 8.5 shows the region of the loadings plot of PC1 that contains the largest observable peaks in the ESI/MS spectra. Table 8.1 contains a list of the ten largest peaks (biomarkers) in the loadings plot and the corresponding peaks in the original ESI/MS spectra. The positive peaks in the loadings plot (Figure 8.5) are correlated to each other and are more intense in samples that have positive scores on PC1 (the low cholesterol mice). Similarly, the negative peaks in Figure 8.5 are correlated to each other and are more intense in samples that have negative scores on PC1 (the high cholesterol mice). Accordingly, the biomarkers shown in Table 8.1 reveal the chemical differences in the organic extracts of the high and low cholesterol mouse livers. Due to mean centering, the differences between the high and low cholesterol animals are characterized by differences in the quantities of different PtdChos and not by the presence or absence of different PtdChos.

8.4.6 Identifying the Key Peaks in the Loadings Plots

PCA clearly shows that the high and low cholesterol mice have different profiles of the same PtdChos. To identify these PtdChos biomarkers, I return to the original spectra, which had been binned for the chemometrics analysis (see Figure 8.2), to examine the precise masses of the peaks. A search of a lipid database [41] showed an exact match between the masses of many of these peaks and those of a series of PtdChos. In many cases, there was also an excellent match between the theoretical and observed isotope patterns for the suggested PtdChos. These analyses further suggested that only some of the biomarkers in Table 8.1 are unique, e.g., m/z 759, 783, 787, 807, 811, and 835, and that others, e.g., m/z 784, 785, 808, 812, etc., are secondary, i.e., simply part of the isotope patterns of the main peaks. Note that all of these secondary peaks are correlated

المنارة للاستشارات
www.manaraa.com

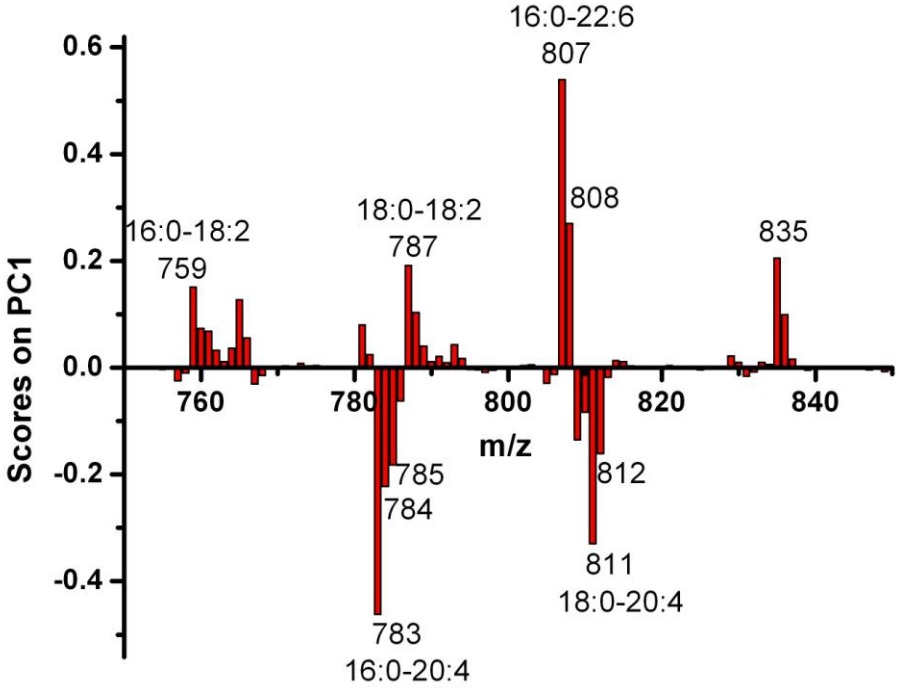

Figure 8.5. Loadings plot of PC1 from the electrospray MS data, where the data were mean-centered. Positive peaks in this loadings plot are more intense in spectra that have positive scores on PC1 (in Figure 8.3), and negative peaks are more intense in spectra that have negative scores on PC1.

المنارة للاستشارات
www.manaraa.com

Table 8.1. The ten largest peaks from the loading plot of PC1 in Figure 8.5.

Exact Mass	Mass in PCA	PC1
806.57	807	0.5395
782.57	783	-0.462
810.60	811	-0.3294
807.57	808	0.2702
783.59	784	-0.222
834.60	835	0.2055
786.60	787	0.1914
784.63	785	-0.182
811.60	812	-0.1609
758.57	759	0.1511

المنارة للاستشارات
www.manaraa.com

to their primary peaks, i.e., they have the same sign in the loadings plot, and they are less intense than their primary peaks. Two representative examples of this data that show excellent agreement between theoretical and observed masses and good agreement between the theoretical and observed isotope patterns are shown in Figure 8.6.

8.4.7 Tandem Mass Spectrometry (MS/MS) and a Literature-Based Identification of the Primary Phosphatidylcholine Biomarkers in the Loadings Plot

The results in the previous section suggest that the peaks in the loadings plot in Figure 8.5 are PtdChos. Additional evidence for this premise was provided by MS/MS. Figure 8.7 shows a representative MS/MS spectrum of one of the main peaks in Table 8.1. This spectrum shows the expected protonated parent ion, and more significantly the m/z 184.1 peak, which is characteristic of the PtdCho head group. The six main peaks in Table 8.1 and their accompanying isotope peaks were likewise conclusively identified as PtdChos. The ratio of the area of the head group ion to the area of the protonated parent ion is essentially the same for each PtdCho in the different samples. However, this ratio varies from PtdCho to PtdCho, which confirms that the same PhtChos are in the different samples. The PtdChos in Table 8.1 and Figure 8.5 could have a variety of different side chains, i.e., the carbon atoms and any double bonds in the alkyl side chains could be distributed in many ways between the two positions on the glycerol backbone. The main PtdChos in mouse liver are known.[35] A comparison of these known species and the peaks in Figure 8.5 allows me to make the tentative assignments that are given in Figure 8.5 (I do not yet have a suggested assignment for the m/z 835 peak). These results suggest that PtdChos with side chains 16:0-18:2, 18:0-18:2, and 16:0-22:6 are more abundant in mice

المنارة للاستشارات
www.manaraa.com

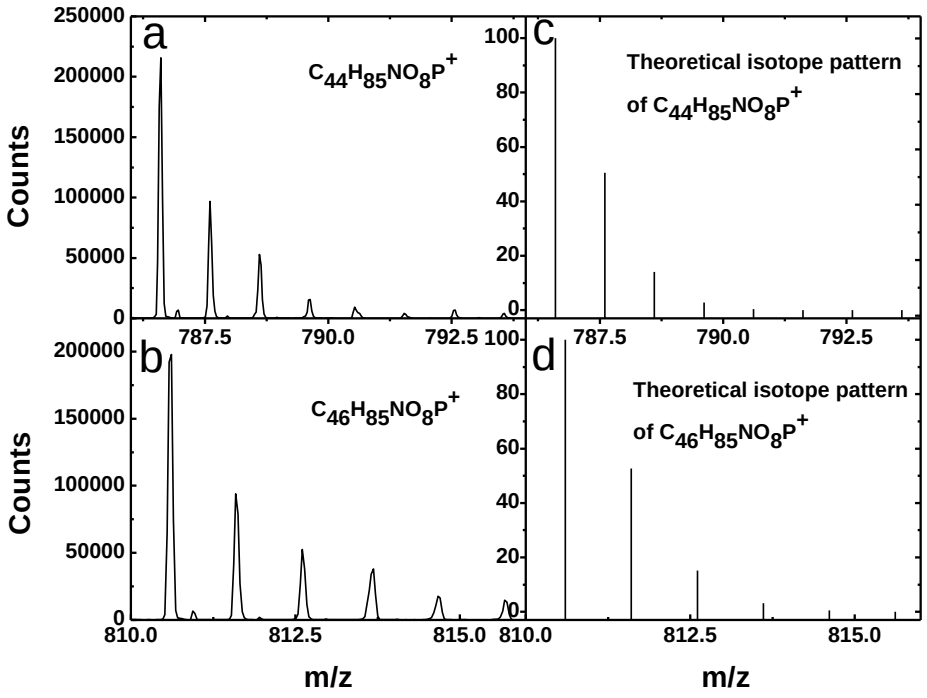

Figure 8.6. Experimental data and theoretical isotope patterns for two phosphatidylcholines: a) and c) correspond to the m/z 786.60 peak and b) and d) correspond to the m/z 810.60 peak.

المنارة للاستشارات
www.manaraa.com

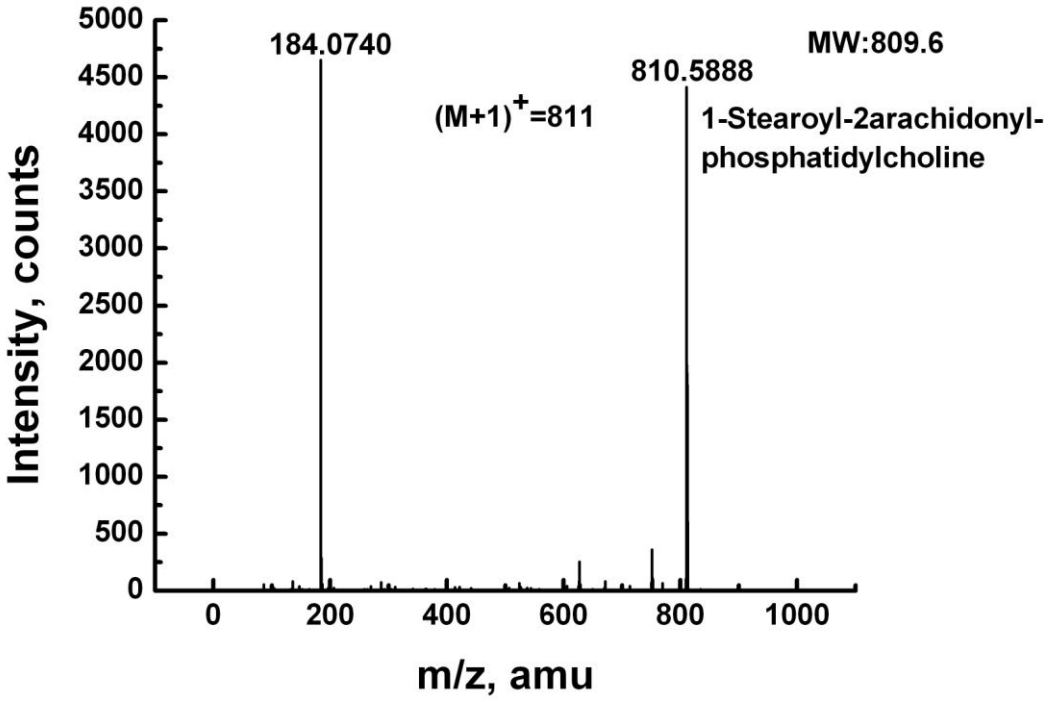

Figure 8.7. Representative daughter ion spectrum of a phosphatidylcholine. This particular daughter ion spectrum is of the mouse 643 liver tissue extract showing the phosphatidylcholine head group at 184 amu as well as the $(M+1)^+$ ion at 811 amu.

المنارة للاستشارات
www.manaraa.com

with low cholesterol levels, and that PtdChos with side chains 16:0-20:4 and 18:0-20:4 are more abundant in mice with high cholesterol levels, where 20:4 is arachidonate.

8.4.8 Multivariate Curve Resolution (MCR)

MCR was also applied to the data. An advantage of MCR over PCA is that MCR does not allow negative peaks in scores or loadings plots, so the results are easier for the non-expert to interpret. A disadvantage of MCR is that because the data cannot be mean centered, the correlation of peaks in the loadings plots and their relationships to the scores plots is not immediately obvious, as it is with PCA. When MCR was performed on the mass spectral data of all of the mouse liver extracts, two components (factors or loadings) best describe the data. Unlike PCA, which only showed good separation between samples in the scores on PC1, the scores on both of the MCR components efficiently separate the high and low cholesterol samples into two clusters. Figure 8.8 shows a comparison between the loadings plots on the first two factors of the MCR analysis and the average spectra from all of the high cholesterol or low cholesterol samples. It is clear that the loadings and the spectra are in excellent agreement. It is remarkable that the MCR analysis has performed this well, especially considering that no initial guesses for these MCR components were provided to the algorithm by the user. The fact that multiple statistical techniques, which rely on different mathematics, produce the same answer is a confirmation of the results presented herein.

8.4.9 Partial Least Squares (PLS)

PLS was used to weigh the possibility of using the mass spectral data to predict the

المنارة للاستشارات
www.manaraa.com

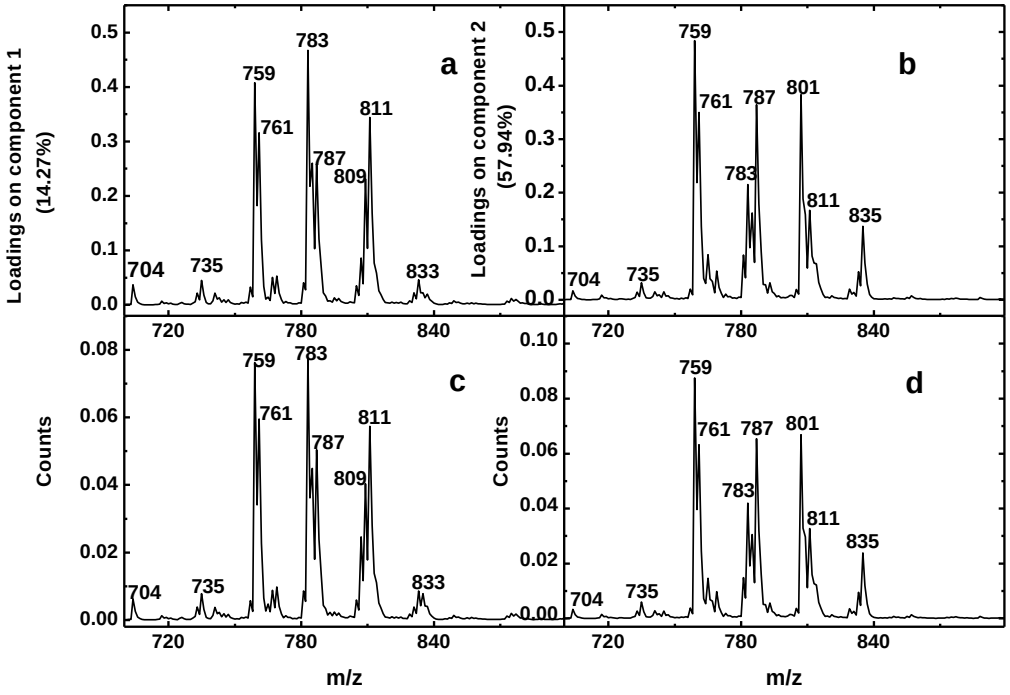

Figure 8.8 (a) and (b): Loadings on component 1 and 2 of MCR from the electrospray MS spectra at 700-900 amu, respectively. (c) and (d): Average, normalized electrospray MS spectra of all of the high and low cholesterol mice at 700-900 amu, respectively.

المنارة للاستشارات
www.manaraa.com

plasma concentrations of cholesterol, HDL cholesterol, and triglycerides in mice. It is well known that the PLS algorithm is challenged when only a relatively small fraction of the variables in the X-block correlate with those in the Y-block. To overcome this problem, a variety of variable selection methods were considered. One of the simplest of these is elimination of noisy regions of a spectrum. It is clear from Figure 8.2 that most of the regions in the mass spectra contain mostly noise. My first approach to variable selection, which greatly improved the PLS results, was to eliminate all of the spectral regions, except m/z 350 - 400 and m/z 600 – 850. The m/z 350 – 400 region was retained because the cholesterol peak is at 369 amu ($[M + H - H_2O]^+$).[42] In contrast, in all of the other chemometrics work in this paper (PCA, HCA and MCR) the entire mass range of the spectra was employed (m/z 101 – 1199). The order of the spectra in the X-block is another consideration for PLS, especially when contiguous blocks are used in the cross validation, as they should be for my data. Accordingly, the X-block was arranged for PLS to assure that when any block of data was removed during cross validation, other samples that were similar to those removed were present in the remaining data. When this rough form of variable selection and spectral ordering was employed, relatively good R^2 values between the X-block and the cholesterol and HDL cholesterol could be obtained: 0.877 for one latent variable and 0.840 for four latent variables, respectively. However, essentially no correlation between the X-block and the TG values could be found.[43]

Genetic algorithms are a more sophisticated approach to variable selection in PLS.[44, 45] When this approach was taken, the PLS prediction of the plasma cholesterol level was outstanding, with R^2 at 0.995 and q2 at 0.993 for five latent variables (see Figure 8.9). The PLS predictions of HDL cholesterol and triglycerides are also very respectable (data

المنارة للاستشارات
www.manaraa.com

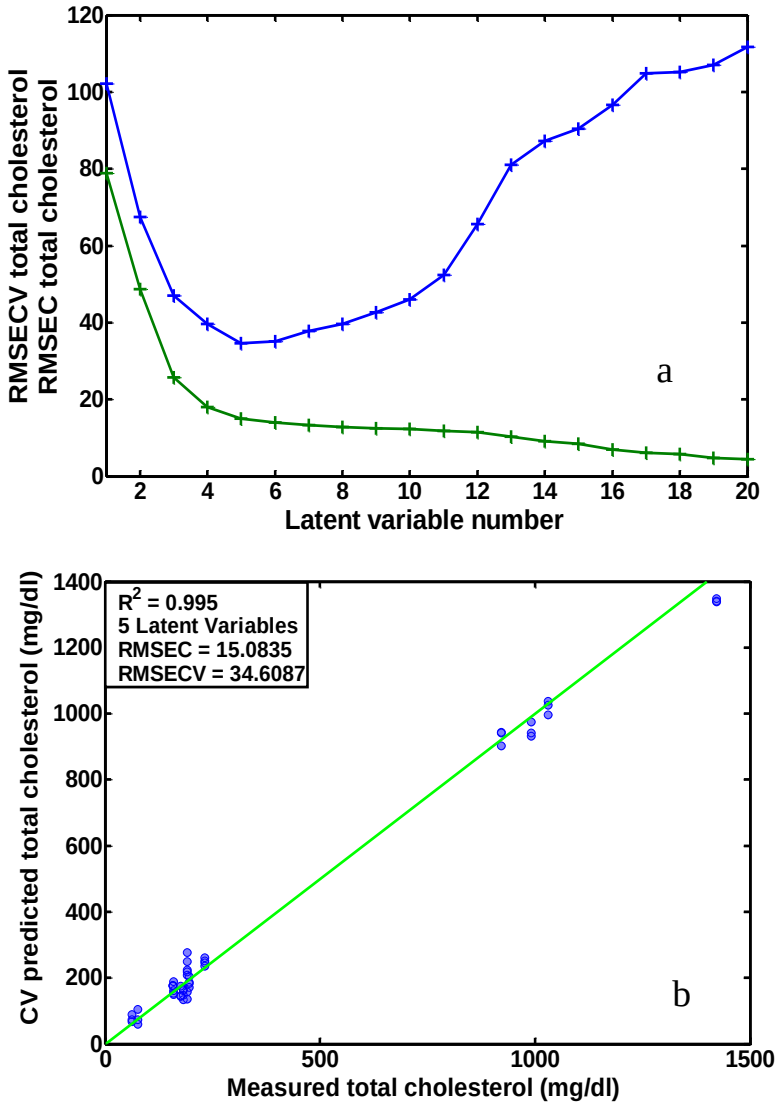

Figure 8.9. (a) Root mean square error of the cross validation (RMSECV) and the root mean square error of the calibration (RMSEC) for a partial least squares (PLS) analysis relating plasma cholesterol levels (the Y-block) to mass spectra (the X-block). The RMSECV plot has a minimum at five latent variables. (b) PLS (with five latent variables) of the ESI mass spectra showing the actual and predicted CV total cholesterol levels.

المنارة للاستشارات
www.manaraa.com

not shown), where the R^2 values were 0.996 for 10 latent variables and 0.700 for 11 latent variables, respectively. These results show a good correlation between total cholesterol, HDL cholesterol or triglycerides and the ESI/MS data, and that reasonable predictive models of these, and perhaps other species in the plasma, could be built using only mass spectral data.

8.5 Discussion

All mammalian cells use lipids including cholesterol and phosphatidylcholines (PtdChos) for membrane synthesis, cell signaling, energy storage and a variety of other requisite functions. All mammalian cells can synthesize cholesterol. Hepatocytes (liver cells) are exceptional in that they are the only cells in the body that can convert cholesterol to bile acids, thereby removing it from the body through the intestines. This clearance is dramatically impaired in mice lacking low density lipoprotein receptors (LDLR-/-) due to the lack of receptors to internalize LDL cholesterol for disposal. Hepatocytes are also unique in that they use cholesterol, phospholipids and triglycerides to synthesize plasma lipoproteins.

PtdChos are the predominant phospholipid in mammalian cell membranes and in lipoproteins. In addition, PtdChos are critical precursors in signal transduction as substrates for diacylglycerol (DAG) and phosphatidic acid and they serve as precursors for biologically active leukotrienes and prostaglandins. Therefore, alterations in the quantities and ratios of PtdChos such as those demonstrated in the HFD-fed LDLR-/- mice may have significant consequences for cellular and organismal metabolism. For example, changes in molecular species of PtdCho markedly alter hepatocyte biliary lipid

المنارة للاستشارات
www.manaraa.com

secretion[46] and alter the affinity of PtdCho for its intracellular transfer protein.[47] In both cases, changes in fatty acids at both the sn-1 and sn-2 positions within the PtdCho are responsible for altered function. Furthermore, the ratio of PtdCho to other phospholipids is critical to membrane integrity and severe decreases in PtdCho can lead to liver failure.[48] In mice, it has been shown that long-term ingestion of an HFD leads to nonalcoholic fatty liver disease,[3] a recently recognized component of the metabolic syndrome in humans. Finally, although postprandial hyperlipidemia in humans does not alter the total lipoprotein phospholipid content,[49] it is possible that hyperlipidemia-induced changes in PtdCho species in the lipoproteins may contribute to their atherogenic potential. The use of PtdCho biomarkers in hypercholesterolemia studies is important in human health issues. PtdCho biomarkers can be used to probe and predict cholesterol levels with high sensitivity and specificity.

Whether the changes in hepatic PtdCho species in livers from HFD-fed LDLR-/- mice represent a "passive" reflection of the fatty acid content of the diet or a selective synthesis or retention of specific PtdChos remains to be determined. There are two pathways for PtdChos synthesis in hepatocytes, one of which is unique to these cells, and the two pathways result in profoundly different phospholipids.[50] It would be of interest to determine if the enzyme systems responsible for synthesis and for biliary secretion are altered in mass or activity in the HFD-fed LDLR-/- livers. In any case, the altered phospholipid patterns revealed in this study may have marked consequences for cellular lipid metabolism and lipoprotein synthesis and may contribute to fatty liver disease. Therefore, it may be significant that the HFD-induced changes in phospholipid profiles can be reversed by returning mice to a low-fat diet even after atherosclerosis is

المنارة للاستشارات
www.manaraa.com

established in the vasculature.

8.6 Conclusions

Livers from hypercholesterolemic and normocholesterolemic mice were extracted with an organic solvent mixture, and the extracts were analyzed by electrospray MS. The resulting spectra are fairly complicated and are analyzed accordingly by chemometrics/bioinformatics methods. PCA and cluster analysis show that the data naturally segregate into two principal clusters – a high plasma cholesterol cluster and a low plasma cholesterol cluster. The loadings plot of PC1 reveals the chemical variation in the samples, which aids biomarker discovery. Two MCR components also efficiently separate the high and low cholesterol samples. PLS predicts cholesterol, HDL cholesterol and triglycerides using mass spectral data. The exact masses, isotope patterns and tandem MS results of the main biomarkers in this loadings plot indicate that they are phosphatidylcholines. I have conditionally identified the side chains on five of these compounds. My results allow me to conclude that when the plasma cholesterol level of a mouse is altered, certain hepatic PtdChos are upregulated and others are downregulated to compensate for the change in cholesterol levels. The changes in PtdCho biomarkers in livers of hyperlipidemic mice may alter hepatocyte and whole-body lipid metabolism and contribute to the atherogenic potential of the lipoproteins. As the field of lipidomics becomes more essential for the study of biological systems[51] my model paradigm for multi-computational lipid analyses should be considered as an important mechanism for rapidly and accurately assessing tissue lipids.

المنارة للاستشارات
www.manaraa.com

8.7 References

(1) Nelson, D. L.; Cox, M. M. *Lehninger Principles of Biochemistry*, Fourth Edition ed.; W. H. Freeman and Company: New York, 2004.

(2) Marsh, M. M.; Walker, V. R.; Curtiss, L. K.; Banka, C. L. *J. Lipid Res.* **1999**, *40*, 893-900.

(3) Yoshimatsu, M.; Terasaki, Y.; Sakashita, N.; Kiyota, E.; Sato, H.; van der Laan, L. J. W.; Takeya., M. *Int. J. Exp. Pathol.* **2004**, *85*, 335-343.

(4) Antonopoulou, S.; Demopoulos, C. A.; Andrikopoulos, N. K. *J. Agric. Food Chem.* **1996**, *44*, 3052-3056.

(5) Brouwers, J. F. H. M.; Gadella, B. M.; van Golde, L. M. G.; Tielens, A. G. M. *J. Lipid Res.* **1998**, *39*, 344-353.

(6) Fragopoulou, E.; Nomikos, T.; Antonopoulou, N. K.; Christiana A. Mitsopoulou, a. C. A. D. *J. Agric. Food Chem.* **2000**, *48*, 1234-1238.

(7) Schulzki, G.; Spiegelberg, A.; Bögl, K. W.; Schreiber, G. A. *J. Agric. Food Chem.* **1997**, *45*, 3921-3927.

(8) Lim, S. Y.; Park, W. K.; Suzuki, H. *J. Agric. Food Chem.* **1999**, *47*, 960-963.

(9) Patton, G. M.; Fasulo, J. M.; Robins, S. J. *Journal of Lipid Research* **1982**, *23*, 190-196.

(10) Hurst, W. J.; Tarka, S. M.; Dobson, G.; Reid, C. M. *J. Agric. Food Chem.* **2001**, *49*, 1264-1265.

(11) Basile, F.; Beverly, M. B.; Abbas-Hawks, C.; Mowry, C. D.; Voorhees, K. J.; Hadfield, T. L. *Anal. Chem.* **1998**, *70*, 1555-1562.

(12) Dailey, O. D.; Severson, R. F.; Arrendale, R. F. *J. Agric. Food Chem.* **1997**, *45*,

المنارة للاستشارات
www.manaraa.com

3914-3920.

(13) Lemaire, R.; Wisztorski, M.; Desmons, A.; Tabet, J. C.; Day, R.; Salzet, M.; Fournier, I. *Anal. Chem.* **2006**, *78*, 7145-7153.

(14) Billedeau, S. M.; Heinze, T. M.; Siitonen, P. H. *J. Agric. Food Chem.* **2003**, *51*, 1534-1538.

(15) Ryan, D.; Antolovich, M.; Herlt, T.; Prenzler, P. D.; Lavee, S.; Robards, K. *J. Agric. Food Chem.* **2002**, *50*, 6716-6724.

(16) Durgbanshi, A.; Arbona, V.; Pozo, O.; Miersch, O.; Sancho, J. V.; Gomez-Cadenas, A. *J. Agric. Food Chem.* **2005**, *53*, 8437-8442.

(17) Pulfer, M.; Murphy, R. C. *Mass Spectrometry Reviews* **2003**, *22*, 332-364.

(18) Otto, M. *Chemometrics: Statistics and Computer Application in Analytical Chemistry*; Wiley-VCH: Weiheim, 1999.

(19) Beebe, K. R.; Pell, R. J.; Seasholtz, M. B. *Chemometrics: A Practical Guide*; John Wiley & Sons: New York, NY, 1998.

(20) Kramer, R. *Chemometric Techniques for Quantitative Analysis*; Marcel Dekker: New York, 1998.

(21) Chau, F. T.; Liang, Y. Z.; Gao, J.; Shao, X. G. *Chemometrics From Basics to Wavelet Transform*; John Wiley & Sons, Ltd., 2004.

(22) Brereton, R. G. *Chemometrics Data Analysis for the Laboratory and Chemical Plant.*; John Wiley & Sons, Ltd.: Chichester, 2003.

(23) Catharino, R. R.; Haddad, R.; Cabrini, L. G.; Cunha, I. B. S.; Sawaya, A. C. H. F.; Eberlin, M. N. *Anal. Chem.* **2005**, *77*, 7429-7433.

(24) Eide, I.; Zahlsen, K.; Kummernes, H.; Neverdal, G. *Energy & Fuels* **2006**, *20*,

المنارة للاستشارات
www.manaraa.com

1161-1164.

(25) Wang, C.; Kong, H.; Guan, Y.; Yang, J.; Gu, J.; Yang, S.; Xu, G. *Anal. Chem.* **2005**, *77*, 4108-4116.

(26) Schwudke, D.; Hannich, J. T.; Surendranath, V.; Grimard, V.; Moehring, T.; Burton, L.; Kurzchalia, T.; Shevchenko, A. *Anal. Chem.* **2007**, *79*, 4083-4093.

(27) Du, Z.; Yang, R.; Guo, Z.; Song, Y.; Wang, J. *Anal. Chem.* **2002**, *74*, 5487-5491.

(28) Boernsen, K. O.; Gatzek, S.; Imbert, G. *Anal. Chem.* **2005**, *77*, 7255-7264.

(29) Zhang, B.; VerBerkmoes, N. C.; Langston, M. A.; Uberbacher, E.; Hettich, R. L.; Samatova, N. F. *J. Proteome Res.* **2006**, *5*, 2909-2918.

(30) Navea, S.; Tauler, R.; de Juan, A. *Anal. Chem.* **2006**, *78*, 4768-4778.

(31) Ruckebusch, C.; Duponchel, L.; Sombret, B.; Huvenne, J. P.; Saurina, J. *J. Chem. Inf. Comput. Sci.* **2003**, *43*, 1966-1973.

(32) Lutz, U.; Lutz, R. W.; Lutz, W. K. *Anal. Chem.* **2006**, *78*, 4564-4571.

(33) Eide, I.; Neverdal, G.; Thorvaldsen, B.; Shen, H. G., B.; Kvalheim, O. *Environ. Sci. Technol.* **2001**, *35*, 2314-2318.

(34) Jonsson, P.; Johansson, A. I.; Gullberg, J.; Trygg, J.; A, J.; Grung, B.; Marklund, S.; Sjostrom, M.; Antti, H.; Moritz, T. *Anal. Chem.* **2005**, *77*, 5635-5642.

(35) Amigo, L.; Zanlungo, S.; Miquel, J. F.; Glick, J. M.; Hyogo, H.; Cohen, D. E.; Rigotti, A.; Nervi, F. *Journal of Lipid Research* **2003**, *44*, 399-407.

(36) Eder, K.; Reichlmayr-Lais, A. M.; Kirchgessner, M. *Clin. Chim. Acta* **1993**, *219*, 93-104.

(37) Yang, L.; Lua, Y.-Y.; Jiang, G.; Tyler, B. J.; Linford, M. R. *Anal. Chem.* **2005**, *77*, 4654-4661.

المنارة للاستشارات
www.manaraa.com

(38) Eide, I.; Zahlsen, K. *Energy & Fuels* **2005**, *19*, 964-967.

(39) Johnson, K. J.; Rose-Pehrsson, S. L.; Morris, R. E. *Energy & Fuels* **2004**, *18*, 844-850.

(40) Zahlsen, K.; Eide, I. *Energy & Fuels* **2006**, *20*, 265-270.

(41) http://www.lipidmaps.org/data/structure/text_search.php

(42) Nagy, K.; Jakab, A.; Pollreisz, F.; Bongiorno, D.; Ceraulo, L.; Averna, M. R.; Noto, D.; Vékey, K. *Rapid Commun. Mass Spectrom.* **2006**, *20*, 2433-2440.

(43) Note that all of the R^2 values cited in this section on PLS are obtained from plots of the measured property vs. the CV predicted property, where the CV predicted property is the property predicted by the PLS model that leaves out the data it is predicting. Note also that the number of latent variables that were kept was determined by the minimum in the cross validation plot.

(44) Leardi, R. *Journal of Chemometrics* **1994**, *8*, 65-79.

(45) Leardi, R.; Boggia, R.; Terrile, M. *Journal of Chemometrics* **1992**, *6*, 267-281.

(46) Robins, S. J.; Fasulo, J. M.; Robins, V. F.; Patton, G. M. *J. Lipid Res.* **1991**, *32*, 985-992.

(47) Kasurinen, J.; van Paridon, P. A.; Wirtz, K. W.; Somerharju, P. *Biochemistry* **1990**, *29*, 8548-8554.

(48) Li, Z.; Agellon, L. B.; Allen, T. M.; Uneda, M.; Jewell, L.; Mason, A.; Vance, D. E. *Cell Metab.* **2006**, *3*, 321-331.

(49) Björkegren, J.; Hamsten, A.; Milne, R. W.; Karpe, F. *J. Lipid Res.* **1997**, *38*, 301-314.

(50) DeLong, C. J.; Shen, Y.-J.; Thomas, M. J.; Cui, Z. J. *Biol.Chem.* **1999**, *274*,

المنارة للاستشارات
www.manaraa.com

29683-29688.

(51) Watson, A. D. *J. Lipid Res.* **2006**, *47*, 2101-2111.

المنارة للاستشارات
www.manaraa.com

PART V. Future work

Future Work

Diamond is extremely stable and in many ways an ideal stationary phase for separations. In this dissertation I have successfully functionalized diamond surfaces with di-tert-amyl peroxide, polystyrene and sulfonated polystyrene and applied these materials to solid phase extraction.

There are only a few separation studies that show the use of diamond. Nesterenko studied sintered diamonds as a stationary phase for HPLC and oxidized diamond in a cation-exchange column[1] and obtained more efficient separation[2, 3] compared to the previous studies by Telepchak[4] and Patel.[5] Therefore, a future direction for this work is functionalized diamond as a stationary phase for HPLC. Different kinds of functionalized diamond particles (including alkyl, polystyrene and solfonated polystyrene functionalized diamond particles) might be used in HPLC, where these materials should bear harsh acidic and basic conditions, beyond that seen for silica. Furthermore, unlike polymeric stationary phases diamond columns will not swell in organic solvents.

In tissue analysis, given the heterogeneous nature of biological tissue, I had anticipated that there would be peaks of significance like free fatty acids, diglycerides and triglycerides etc. over most of the mass range that was studied. The fact that intense peaks are only present over a relatively small mass range (from ca. 750 – 850 m/z) of the positive ion mode spectrum suggests ion suppression by the phosphatidylcholines. This is most likely because the phosphatidylcholines bear a permanent charge. In order to obtain

المنارة للاستشارات
www.manaraa.com

comprehensive information from the extracts, solid phase extraction (SPE) will be applied to separate the different kinds of lipids. After loading the SPE column, all aliquots will be collected by washing the SPE column with different solvents. ESI/MS spectra (including positive and negative mode) of these aliquots will show many additional peaks, in addition to the phosphatidylcholines. These peaks should represent free fatty acids, diglycerides and triglycerides etc. which are rather common in tissue extracts. GC-MS and LC-MS will be also used to analyze the extracts to get more information like the side chains of the lipids and separate the different species at same mass. Finally, multivariate analysis will be used in these data sets to reveal differences between samples and explore the chemical variation between the samples.

References

(1) Nesterenko, P. N.; Fedyanina, O. N.; Volgin, Y. V. *J. Chromatogr.,A* **2007**, *1155*, 2-7.

(2) Nesterenko, P. N.; Fedyanina, O. N.; Volgin, Y. V. *Analyst* **2007**, *132*, 403-405.

(3) Nesterenko, P. N.; Fedyanina, O. N.; Volgin, Y. V., Moscow, 25-30 June 2006.

(4) Telepchak, M. J. *Chromatographia* **1973**, *6*, 234-236.

(5) Patel, B. A.; Rutt, K. J.; Padalko, V. I.; Mikhalovsky, S. V. *J. Superhard Mater.* **2002**, *6*, 51-54.

المنارة للاستشارات
www.manaraa.com